LUND UNIVERSITY

ISSN 1101-9824
ISBN 978-91-7473-047-0
Printed by ***MEDIA-TRYCK***, Lund 2010

Pham Thanh Nam

Numerical Model of Beach Topography Evolution due to Waves and Currents

Report No 1051

WATER RESOURCES ENGINEERING
Lund University, Sweden

Numerical Model of Beach Topography Evolution due to Waves and Currents

Special Emphasis on Coastal Structures

Pham Thanh Nam

Report No. 1051
Lund, Sweden, 2010

Numerical Model of Beach Topography Evolution due to Waves and Currents

Special Emphasis on Coastal Structures

Pham Thanh Nam

Akademisk avhandling som för avläggande av teknologie doktorsexamen vid tekniska fakulteten vid Lunds Universitet kommer att offentligen försvaras vid Institutionen för Bygg- och Miljöteknologi, John Ericssons väg 1, Lund, hörsal V:B, fredagen den 17 december 2010, kl. 10:15.

Academic thesis submitted to Lund University in partial fulfillment of the requirements for the Degree of Doctor of Philosophy (Ph.D. Engineering) will be publicly defended at the Department of Building and Environmental Technology, John Ericssons väg 1, lecture hall V:B, Friday, December 17, 2010, at 10.15 a.m.

Fakultetsopponent/Faculty Opponent: Prof. Theofanis V Karambas, Dept. of Marine Sciences, University of Aegean, Greece.

Organization: LUND UNIVERSITY Water Resources Engineering Box 118, SE-221 00, Lund, Sweden	**Document name:** DOCTORAL DISSERTATION
	Date of issue: November 8, 2010
	Coden: LUTVDG/TVVR-1051 (2010)
Author: Pham Thanh Nam	**Sponsoring organization**

Title:
Numerical Model of Beach Topography Evolution due to Waves and Currents:
Special Emphasis on Coastal Structures

Abstract

The beach topography change in the nearshore zone may be induced by natural phenomena such as wind, wave, storm, tsunami, and sea level rise. However, it can also be caused by man-made structures and activities, for example, groins, detached breakwaters, seawalls, dredging, and beach nourishment. Therefore, understanding the beach topography evolution in this zone is necessary and important for coastal engineering projects, *e.g.*, constructing harbors, maintaining navigation channels, and protecting the beach against erosion.

During the latest decade, advanced numerical models have been used as useful tools for simulating the beach morphological evolution. A number of such numerical models have been developed and applied through the years in many practical applications. However, the hydrodynamical and morphological processes are extremely complex in the nearshore zone and still beyond our current knowledge to describe in detail. Thus, these numerical models often include a limited set of processes characterized by certain time and space scales. Furthermore, high-quality and synchronized data sets from laboratories and the field are also limited, making model validation difficult.

The overall objective of this study was to develop a robust and reliable numerical model of beach topography evolution due to waves and currents with the emphasis on the impact of coastal structures. Such a model should describe the effects of both longshore and cross-shore sediment transport over time scales from individual storms to seasonal variations. In order to facilitate this, a number of sub-models were developed and improved, including (i) a random wave transformation model, (ii) a surface roller model, (iii) a nearshore wave-induced current model, (iv) a sediment transport model, and (v) a morphological evolution model. These sub-models were coupled together and validated against detailed, high-quality data from the Large-scale Sediment Transport Facility (LSTF) of the Coastal and Hydraulics Laboratory in Vicksburg, Mississippi, United States.

The obtained results predicted by the numerical model were satisfactory and in good agreement with measurements. The simulations showed that the calculated wave conditions and longshore current were well reproduced for all investigated test cases with and without structures. The calculated cross-shore current somewhat underestimated the measurements, however, it was in good agreement with observations in the lee of structures. Although the calculated wave setup overestimated observations, the absolute differences between calculations and measurements were relatively small. The predictions of beach morphological evolution under waves and currents in the vicinity of a detached breakwater and a T-head groin agreed rather well with measurements. Both salient and tombolo formation behind these structures were well reproduced by the numerical model. In the future, the model will be further validated against available data from the laboratory and the field. However, already in its current state it is expected that the model can be applied in coastal engineering projects for predicting the beach evolution in the vicinity of coastal structures with some confidence.

Key words: morphodynamics, sediment transport, random waves, wave-induced currents, surface roller, coastal structures

Classification system and/or index terms (if any):

Supplementary bibliographical information — Language: English

ISSN and key title: 1101-9824 — ISBN: 978-91-7473-047-0

Recipient´s notes — Number of pages: 200 — Price:

Security classification:

Distribution by Division of Water Resources Engineering, Lund University, Box 118, SE-221 00, Lund, Sweden.

Signature  Date 2010-11-08

WATER RESOURCES ENGINEERING, FACULTY OF ENGINEERING,
LUND UNIVERSITY
CODEN: LUTVDG/TVVR-1051 (2010)

Doctoral Thesis

Numerical Model of Beach Topography Evolution due to Waves and Currents

Special Emphasis on Coastal Structures

By Pham Thanh Nam

November, 2010

Numerical Model of Beach Topography Evolution due to Waves and Currents:
Special Emphasis on Coastal Structures

Doktorsavhandling
Teknisk Vattenresurslära
Institutionen för Bygg-och Miljöteknologi
Lunds Universitet

Doctoral Thesis
Water Resources Engineering
Department of Building & Environmental Technology
Faculty of Engineering
Lund University

Box 118
SE-221 00 Lund
Sweden

http://www.tvrl.lth.se

Cover: Salient development in the lee of a detached breakwater, the Large-scale Sediment Transport Facility (LSTF), Coastal and Hydraulics Laboratory, US Army Engineer Research and Development Center, Vicksburg, Mississippi, United States (from Gravens and Wang, 2003)

CODEN: LUTVDG/(TVVR-1051) (2010)
ISBN: 978-91-7473-047-0
ISSN: 1101-9824
Report No. 1051

Printed in Sweden by Media-Tryck, Lund, Sweden, 2010

ACKNOWLEDGMENTS

First of all I would like to thank my supervisor Professor Magnus Larson, not only for his advice, novel ideas, and reviews, but also for his generous guidance, patience, and encouragement. I would also like to thank my co-supervisor Professor Hans Hanson for valuable advice, ideas, and helpful support. In addition, I would like to thank Dr. Nguyen Manh Hung, my external supervisor, and the late Professor Pham Van Ninh for their great support and contributions through the Project VS/RDE/03 "*The evolution and sustainable management in the coastal areas of Vietnam*". Thanks to all of you for giving me the opportunity to become a PhD student at Water Resources Engineering in Lund University.

Furthermore, I am grateful to Professor Hajime Mase at Kyoto University for kindly providing the source code of the EBED model, and for helping me to use his model when I was beginning to study random wave transformation. I also appreciate the support from Dr. Ping Wang at the University of South Florida and Mr. Mark Gravens at the Coastal and Hydraulics Laboratory, US Army Engineer Research and Development Center, in providing the high-quality experimental data from their tests in the Large-scale Sediment Transport Facility. Without these data, I would have had difficulties to validate my numerical model. Thanks for helping me to dig into the data. I would also like to thank several anonymous reviewers for their valuable comments, which improved the quality of the published articles.

This research was mainly funded by the Swedish International Development Cooperation Agency (SIDA), Lars Erik Lundberg Scholarship Foundation, and J. Gust. Richert Foundation. Their sponsorships are gratefully acknowledged. The financial support granted by Carl Swartz Foundation for the presentation at the International Workshop on Environmental Hydraulics in Valencia (2009), and by Åforsk Foundation for the paper presented in the International Conference on Coastal Engineering in Shanghai (2010), is also much appreciated.

I am very grateful to all my friends and colleagues at the Center for Marine Environment, Research, Survey, and Consultation, Institute of Mechanics, Hanoi, Vietnam, especially to Ass. Prof. Tran Gia Lich, Dr. Phan Ngoc Vinh, Dr. Dang Huu Chung, Dr. Le Xuan Hoan, Dr. Dinh Van Manh, Dr. Nguyen Thi Viet Lien, and Mrs. Tran Thi Ngoc Duyet who gave me a lot experience in numerical modeling. I would also like to thank all my friends and colleagues at Department of Water Resources Engineering, Lund University, and all Vietnamese friends in Lund for sharing valuable experiences about studying as well as living in Lund. Thanks Mr. Tony Brady for his proof reading this manuscript.

Finally, I would like to thank my parents, my wife, and all my siblings for their great support, assistance, inspiration, and encouragement. I love you all very much.

Lund, Sweden, November, 2010

Pham Thanh Nam

ABSTRACT

The beach topography change in the nearshore zone may be induced by natural phenomena such as wind, wave, storm, tsunami, and sea level rise. However, it can also be caused by man-made structures and activities, for example, groins, detached breakwaters, seawalls, dredging, and beach nourishment. Therefore, understanding the beach topography evolution in this zone is necessary and important for coastal engineering projects, *e.g.,* constructing harbors, maintaining navigation channels, and protecting the beach against erosion.

During the latest decade, advanced numerical models have been used as useful tools for simulating the beach morphological evolution. A number of such numerical models have been developed and applied through the years in many practical applications. However, the hydrodynamical and morphological processes are extremely complex in the nearshore zone and still beyond our current knowledge to describe in detail. Thus, these numerical models often include a limited set of processes characterized by certain time and space scales. Furthermore, high-quality and synchronized data sets from laboratories and the field are also limited, making model validation difficult.

The overall objective of this study was to develop a robust and reliable numerical model of beach topography evolution due to waves and currents with the emphasis on the impact of coastal structures. Such a model should describe the effects of both longshore and cross-shore sediment transport over time scales from individual storms to seasonal variations. In order to facilitate this, a number of sub-models were developed and improved, including (i) a random wave transformation model, (ii) a surface roller model, (iii) a nearshore wave-induced current model, (iv) a sediment transport model, and (v) a morphological evolution model. These sub-models were coupled together and validated against detailed, high-quality data from the Large-scale Sediment Transport Facility (LSTF) of the Coastal and Hydraulics Laboratory in Vicksburg, Mississippi, United States.

The obtained results predicted by the numerical model were satisfactory and in good agreement with measurements. The simulations showed that the calculated wave conditions and longshore current were well reproduced for all investigated test cases with and without structures. The calculated cross-shore current somewhat underestimated the measurements, however, it was in good agreement with observations in the lee of structures. Although the calculated wave setup overestimated observations, the absolute differences between calculations and measurements were relatively small. The predictions of beach morphological evolution under waves and currents in the vicinity of a detached breakwater and a T-head groin agreed rather well with measurements. Both salient and tombolo formation behind these structures were well reproduced by the numerical model. In the future, the model will be further validated against available data from the laboratory and the field. However, already in its current state it is expected that the model can be applied in coastal engineering projects for predicting the beach evolution in the vicinity of coastal structures with some confidence.

APPENDED PAPERS

This thesis is submitted with the support of the following papers that will be referred to by their numerals in the body of the text.

I. Nam, P.T., Larson, M., Hanson, H., Hoan, L.X., 2009. A numerical model of nearshore waves, currents, and sediment transport. *Coastal Engineering* 56, 1084-1096.

II. Nam, P.T., Larson, M., 2010. Model of nearshore waves and wave-induced currents around a detached breakwater. *Journal of Waterway, Port, Coastal, and Ocean Engineering* 136(3), 156-176.

III. Larson, M., Camenen, B., Nam, P.T., 2010. A unified sediment transport model for inlet application. *Journal of Coastal Research* (in press).

IV. Nam, P.T., Larson, M., Hanson, H., Hoan, L.X., 2010. A numerical model of beach morphological evolution due to waves and currents in the vicinity of coastal structures. *Coastal Engineering* (submitted).

V. Hoan, L.X., Hanson, H., Larson, M., Donnelly, C., Nam, P.T., 2010. Modeling shoreline evolution at Hai Hau Beach, Vietnam. *Journal of Coastal Research* 26(1), 31-43.

VI. Hoan, L.X., Hanson, H., Larson, M., Nam, P.T., 2010. Modeling regional sediment transport and shoreline response in the vicinity of tidal inlets on the Long Island coast, United States. *Coastal Engineering* (submitted).

CONTRIBUTION TO CO-AUTHORED PAPERS

Paper I The author developed the study work plan, modified the random transformation model, developed the surface roller, nearshore current, and sediment transport models, validated the model against data from laboratory, and wrote all sections of the papers. The co-authors participated in discussions and revised the paper.

Paper II The author developed the numerical model, validated the model against data from laboratory, and wrote all sections of the papers. The co-author participated in discussions and revised the paper.

Paper III The author provided the material for the section "*Validation of sediment transport in the swash zone and inner surf zone*", and participated in the review and discussion of the paper.

Paper IV The author developed the numerical model, validated the model against data from the laboratory, and wrote all sections of the papers. The co-authors participated in discussions and revised the paper.

Paper V The author set up the random wave model, participated in the review and discussion of the paper.

Paper VI The author participated in the discussion of the paper.

RELATED PUBLICATIONS

1. Nam, P.T., Larson, M., Hanson, H., 2010. Modeling morphological evolution in the vicinity of coastal structure. *Proceedings of the 32nd International Conference on Coastal Engineering*, Shanghai, ISSN: 2156-1028.

2. Nam, P.T., Larson, M., 2009. A model of wave and current fields around coastal structures. *Proceedings of Coastal Dynamics 2009*, Tokyo, World Scientific, ISBN: 13-978-981-4282-46-8.

3. Nam, P.T., Larson, M., Hanson, H., Hoan, L.X., 2009. Numerical modeling of nearshore waves, currents, and sediment transport: validation with laboratory data. *International Workshop on Environmental Hydraulics*, Valencia, CRC/Balkema Press, ISBN: 978-0-415-56697-1.

4. Nam, P.T., Larson, M., Hanson, H., Hoan, L.X., 2010. Modeling beach topographical evolution due to waves and currents. *Proceedings of the 3rd Scientific Workshop of VS/RDE/03 – Coastline Evolution*, Vietnam-Sweden Research Cooperation Program, Ha Long, Vietnam.

5. Nam, P.T., Larson, M., Hung, N.M., Hanson, H., 2007. A numerical model of waves, currents, and sediment transport in the nearshore. *Proceedings of the 2nd Scientific Workshop of VS/RDE/03 – Coastline Evolution*, Vietnam-Sweden Research Cooperation Program, Thinh Long, Vietnam.

6. Nam, P.T., Larson, M., Hung, N.M., Hanson, H., Ninh, P.V., 2007. A model of nearshore currents generated by waves. *Proceedings of the 1st Scientific Workshop of VS/RDE/03*, Vietnam-Sweden Research Cooperation Program, Thinh Long, Vietnam.

ABBREVIATIONS AND SYMBOLS

The list of abbreviations used in the thesis:

AD	advection-diffusion
CHL	coastal and hydraulics laboratory
EBED	random wave transformation model based on the energy balance equation with diffraction term
FTBS	forward in time, backward in space
FTCS	forward in time, center in space
LSTF	large-scale sediment transport facility
Lund-CIRP	formulas for bed load and suspended load
Lund-CIRP-AD	total load combining the bed load by Lund-CIRP and the suspended load derived from AD equation
Modified-EBED	EBED model with modification of energy dissipation term

The list of symbols used in the thesis:

Roman letters:

a_c, b_c	empirical coefficient in Lund-CIRP for bed load
c_R	reference concentration at bottom
d	total depth
d_{50}	median grain size
d_*	dimensionless grain size
f	Coriolis parameter
f_c, f_w	friction factors due to current and wave
g	acceleration due to gravity
h	still-water depth
k	wave number
k_b, k_c, k_w	coefficients in formula for sediment diffusivity
k_s	total roughness
k_{sd}, k_{sf}, k_{ss}	grain-related roughness, form-drag roughness, sediment related roughness
m	bottom slope
n	wave index
n_p	porosity parameter
$q_{bc,net}, q_{bl,net}$	net transport rates in cross-shore and longshore directions

q_{bc}	bed load
q_s	suspended load
q_{sx}, q_{sy}	suspended load in x and y directions
$q_{tot,x}, q_{tot,y}$	total load in x and y directions
q_x, q_y	flow per unit width parallel to x and y axes
r	relative roughness
s	relative density between sediment and water
t	time
t_0	scaling time in swash zone computation
$t_{\max}$	maximum duration when maximum runup height is attained
u, v	depth-averaged velocity components in the x and y directions
u_0, v_0	scaling velocities in swash zone computation
u_s, v_s	wave front speeds at the start of the uprush
u_{c*}, u_{w*}	shear velocities due to current and waves
v_x, v_y, v_θ	propagation velocities in the energy balance equation
w_s	sediment fall velocity
x, y	horizontal coordinates
x_0, y_0	position of wave front
$x_{\max}$	maximum uprush location
x_s, y_s	location at the start of swash zone
z_0	vertical distance from the reference level to x_0
A_w	semi-orbital excursion
$A_{c1}, A_{c2}, A_{w1}, A_{w2}$	coefficients for determining Schmidt number
A_{cR}	coefficient for determining reference concentration
C	phase speed
C_b	bottom friction coefficient
C_g	group speed
C_r	roller speed
C_z	Chezy roughness coefficient
$\overline{C}$	depth-averaged suspended sediment concentration
D	deposition rate in AD equation
$\overline{D}$	modification of deposition rate

D_0, D_1, D_2, D_x, D_y	eddy viscosity coefficients
D_b	energy dissipation due to wave breaking
D_c, D_w	energy dissipation from bottom friction due to current and wave
E	wave energy
H_{rms}	root-mean-square wave height
H_s	significant wave height
H_{stab}	stable wave height
K	decay coefficient
K_c, K_l	coefficients in swash zone computation
K_x, K_y	diffusion coefficients in x and y directions
M	wave-averaged-period mass flux
P	pick-up rate in AD equation
$\overline{P}$	modified pick-up rate
P_D	energy dissipation due to wave breaking
R	runup height
R_{xx}, R_{xy}, R_{yy}	radiation stresses due to roller
S	angular-frequency spectrum density
S_{stab}	stable wave spectrum density
S_{xx}, S_{xy}, S_{yy}	wave-driven radiation stresses
T	swash duration
T_s	significant wave period
U_c	magnitude of current vector
U_w	wave orbital velocity at the bottom
U_{wc}	combined wave and mean current in calculation of bottom stresses
$\overline{V}$	mean velocity across the profile

Greek letters:

α	weighting parameter
β	foreshore slope
β_d	coefficient in calculation of deposition rate
β_D	roller dissipation coefficient
β_e	foreshore equilibrium slope

ε	sediment diffusivity
ε_b	energy dissipation coefficient in EBED model
ϕ_m	friction angle for a moving grain
η	water elevation
θ	angle measured counter clockwise from x axis
$\overline{\theta}$	mean wave direction
θ_c	Shields parameter due to current
θ_{cr}	critical Shields parameter
θ_{cw}	maximum Shields parameter due to wave-current interaction
$\theta_{cw,m}$	mean Shields parameter due to wave-current interaction
θ_w	Shields parameter due to wave
$\theta_{w,m}$	mean wave Shields parameter
κ	free parameter in calculation of wave diffraction
λ_r	ripple length
μ, ϑ	coefficients in modified formulas of pick-up and deposition rates
ν	kinematic viscosity of water
ρ_s, ρ_w	densities of sediment and water
σ	peak wave frequency
σ_i	Schmidt number
τ_{bx}, τ_{by}	bottom stresses
τ_c, τ_w	shear stresses due to current and wave
τ_{Sx}, τ_{Sy}	wave stresses
φ	angle between the wave and current directions
ω	angular frequency
ω_b	coefficient in calculation of bottom stresses
Δ_r	ripple height
Γ	stable coefficient
Λ	coefficient in calculation of eddy viscosity
Ψ	particle mobility parameter

CONTENTS

1 Introduction

1.1 Background

The nearshore zone is a very dynamic area, and the bed material in this area is almost in constant motion due to external forces such as wind, tide, waves, and currents. Gradients in the transport rate can cause deposition or erosion of sediment, affecting the local topography. Such gradients in transport rate may occur naturally in the nearshore zone, for example, when there are changes in the wave and/or wind conditions. Currents induced by waves and wind may change, resulting in changing sediment transport rates and evolution of the local beach topography. However, gradients in the transport rate can also be induced by man-made structures and activities, for example, groins, detached breakwaters, sea walls, dredging, and beach nourishment. For many purposes, such as protection of the shoreline against erosion, construction of harbors, and implementation of navigation channels (see Figs. 1a and b), human activities have changed the beach topography at many locations around the world. Therefore, the study of beach evolution in order to gain knowledge for application in coastal engineering projects is necessary.

Fig. 1a. Tombolo formation behind the detached breakwaters at Maumee Bay State Park, Ohio, USA (Ken Winters, U.S. Army Corp. Eng., 1992)

Fig. 1b. Jetty layout at the mouth of the Rogue River, Golden Beach, Oregon, USA (Bob Heims, U.S. Army Corp. Eng., 1990)

Numerical models of beach evolution have been useful tools in engineering projects. The first advantage of numerical models is that they are often less expensive than physical models. With numerical models, one can easily simulate the beach topography evolution under various scenarios of wave and current conditions that are difficult to carry out in the laboratory because of the high costs required. Furthermore, advanced and robust algorithms, as well as the capabilities of computers, are being developed and enhanced very quickly, enabling the improvement of numerical models for efficiently predicting the beach topography evolution.

A number of numerical models have been developed though the years for simulating beach topography evolution. These models can be classified into six groups as (Watanabe, 1988; De Vriend, 1993; Hanson *et al*., 2003): (i) conceptual models, (ii) shoreline evolution models, (iii) profile evolution models, (iv) 2D horizontal morphological evolutions models, (v) fully 3D morphological models, and (vi) quasi-3D morphological models. The conceptual models (*e.g.* De Vriend *et al.*, 1994; Gravens, 1996; Kana *et al.*, 1999; Kraus, 2000; Ruessink and Terwindt, 2000), which are often based on the empirical formulations obtained from experiences and observations, are effective for qualitative assessment of beach evolution. Shoreline evolution models (*e.g.* Pelnard-Considere, 1956; Hanson and Kraus, 1989; Steetzel *et al.*, 2000) describe changes in the shoreline evolution due to gradients in the longshore transport rate. These models typically simulate shoreline evolution over decades with limited resolution of the response on the intra-annual scale. Profile evolution models compute changes in the profile shape due to cross-shore transport only (Larson and Kraus, 1989; Larson *et al.*, 1989; Nairn and Southgate, 1993). Such models have traditionally been used to estimate the impact of storms, implying a characteristic scale of the processes on the order of days. 2D horizontal morphological models employ the depth-averaged wave and current equations, neglecting the vertical variations of waves and current (Latteux, 1980; Watanabe, 1987; Andersen *et al.*, 1988; Maruyama and Takagi, 1988; Johnson, 1994; Johnson *et al.*, 1994; Nicholson *et al.*, 1997, Roelvink *et al.*, 2010). These models can simulate the morphological evolution over a coastal area with a rather wide range of spatial scales and over time scales from individual storms to seasonal variations. Fully 3D morphological model includes both the horizontal and vertical variations of waves and currents (*e.g.* Roelvink and Banning, 1994; Lesser *et al.*, 2004). These models include various processes of hydrodynamics such as wind shear, wave forces, tidal forces, density-driven flows and stratification due to salinity and/or temperature gradients, atmospheric pressure changes, drying and flooding of intertidal flats, etc. However, the applications of these models for practical problems are still limited because a long time computation is required. Quasi-3D models (*e.g.* Zyserman and Johnson, 2002; Ding *et al.*, 2006; Drønen and Deigaard, 2007) enhances the 2D horizontal models in which the vertical current velocity at given location is determined by the local forcing and the depth integrated flow. The computational effort required by quasi-3D models is similar to that by 2D horizontal models. Therefore, presently, they are expected to be a feasible tool for simulating the long-term beach topographical evolution in the large-scale coastal engineering projects.

According to Houston (2003), coastal structures have been used since antiquity for reducing the shoaling in navigation channels and protecting harbors against wave action. Although there have been many debates about the advantages and disadvantages of coastal structures, they are still frequently utilized in coastal engineering projects to prevent beach erosion. Therefore, understanding the morphological evolution in the vicinity of coastal structure is necessary to achieve an optimal functional design. There have been many attempts to develop and apply numerical models for simulating beach topography change around structures (see brief review of previous relevant studies in the *Section 2.5*). However, the nearshore hydrodynamics and sediment transport processes are highly complex in the vicinity of coastal structures. Moreover, the validation of numerical models against high-quality data sets is still limited. Thus, the development of models that accurately predict the morphological evolution around structures remains a challenge.

1.2 Objectives, Scope, and Appended Papers

The overall objective of this study is to develop a robust and reliable numerical model to simulate beach morphological evolution under waves and currents. The model should describe the effects of both longshore and cross-shore sediment transport over time scales from individual storms to seasonal variations. The focus of this study is to investigate and simulate the beach morphological evolution due to the impact of coastal structures such as detached breakwaters and T-head groins.

In order to achieve this aim, the following necessary tasks were undertaken:

1) Compilation of the existing literature on beach change modeling with focus on simulating the bed evolution in two spatial dimensions and time.

2) Compilation of available high-quality data sets on beach topography change in the open literature with focus on hydrodynamics, sediment transport, and morphological change.

3) Formulation of governing equations concerning hydrodynamics, sediment transport, and morphological evolution.

4) Numerical implementation of the governing equations and validation of individual model components (waves, currents, sediment transport) towards data (laboratory and/or field data).

5) Development of methods to reduce calculation time by investigating coupling between hydrodynamics, sediment transport, and morphological response.

6) Simulation of topographic evolution with the complete model for the compiled data sets (focus on structures).

The above tasks are addressed in a series of journal articles which are appended to this thesis. Tasks 1-4 were addressed in **Paper I**. This paper firstly reviewed the relevant previous studies on numerical models for nearshore waves, currents, and sediment transport; discussed the modification of the random wave transformation model to achieve improved simulation of wave conditions in the surf zone; enhanced the energy balance equation for the surface roller equation; employed a new unified sediment transport model; calculated sediment transport rates in the swash zone and combined them with the sediment transport rates in the inner surf zone; and validated the individual sub-models against high-quality data sets from the LSTF basin without structures. The author carried out all tasks and wrote all sections of the paper.

Paper II presented the numerical model of nearshore wave and wave-induced currents, focused on the model validation regarding the wave conditions and current fields in the

vicinity of a detached breakwater against LSTF data sets, addressing tasks 3 and 4. The author carried out all tasks and wrote all sections of the paper.

Paper III also addressed tasks 3 and 4. This paper presented a unified sediment transport model for coastal applications. The author's contribution was to provide the material for the section on validation of the sediment transport model for the swash zone and inner surf zone; and to review and participate in the discussion of the paper content.

In general, all tasks were addressed in **Paper IV**. This paper summarized the relevant studies on modeling morphological evolution in the vicinity of coastal structures; coupled hydrodynamics, sediment transport, and morphological change; and validated the model against the measurements obtained from LSTF basin including a detached breakwater and a T-head groin. The author undertook all tasks and wrote all sections of the paper.

Paper V presented the application of a model to simulate the long-term coastal evolution to Hai Hau beach, Vietnam. In this case, the calculated wave field from EBED was employed to simulate the shoreline evolution. The author's contribution was to set up the random wave model, review the papers, and to participate in the general discussions of the paper.

Paper VI presented the shoreline evolution in the vicinity of tidal inlets on the Long Island coast, United States. The author's contribution was to participate in the general discussions of this paper.

The summary consists of six sections. Section 1 describes the background and the objectives of the study. Section 2 presents the state-of-art regarding relevant studies on hydrodynamics, sediment transport, and morphological change with emphasis on the impact of coastal structures. The model description is given in detail in Section 3. A brief description of the laboratory experiments from the LSTF basin is presented in Section 4. Selected model results and discussions regarding the nearshore wave conditions, wave-induced currents, sediment transport, and morphological evolution, are given in Section 5. Finally, the concluding remarks are presented in Section 6.

2 Literature Review

2.1 Modeling Random Wave Transformation

Waves in coastal areas display random characteristics; thus, random wave models are needed to properly assess the wave environment. Random wave transformation models can be classified into (i) phase-resolving models, and (ii) phase-averaging models. The first type of model, for example the ones based on the Boussinesq equations, is expressed through the conservation equations of mass and momentum (Madsen and Warren, 1984; Madsen *et al.*, 1991, 1997; Nwogu, 1993; Wei *et al.*, 1995; Gobbi *et al.,* 2000). These models describe the main physical processes in the coastal area (*e.g.* shoaling, diffraction, refraction, and dissipation) at the intra-wave scale. Thus, they require fine resolution in space and time and, therefore, their applications are often only suitable for small coastal areas and short-term simulations.

On the other hand, phase-averaging models, commonly based on the energy balance equation, describe slowly varying wave quantities (*e.g.* wave amplitude and wave energy) on the scale of a wavelength. Thus, they can be applied for the prediction of multi-directional random wave transformation over large coastal areas. Originally, the non-stationary wave models WAM (WAMDI group, 1988) and SWAN (Booij *et al.*, 1996) were based on phase-averaged equations including source terms. However, diffraction was not included in these models. Then, several attempts have been made in order to include diffraction effects in the phase-averaging wave model. For example, diffraction effects were included into the characteristic velocities through the wave number containing the second derivative of wave amplitude with respect to the spatial coordinates (Booij *et al.*, 1997; Rivero *et al.*, 1997; Holthuijsen *et al.*, 2003). Although these models can be applied in the coastal zone containing structures, the numerical schemes seem to be unstable, especially for the discontinuities and singularities occurring (see Holthuijsen *et al.*, 2003).

Mase (2001) developed a random wave transformation model called EBED in which diffraction effects were included. The diffraction term was derived from a parabolic approximation of the wave equation (Radder, 1979). The numerical scheme is stable and the model can be applied for complex coastal areas with structures. Mase *et al.* (2005) applied a high-order numerical scheme for the convective term in the extended energy balance equation in order to reduce the numerical diffusion. Lin *et al.* (2008) modeled the wave-current interaction based on Mase (2001) to simulate the wave and current fields at coastal inlets. In the present study, the EBED model was employed to calculate wave transformation after modifications to more accurately predict the wave conditions in the surf zone. However, the wave-current interaction was not modeled in this study.

2.2 Modeling Nearshore Wave-induced Currents and Surface Roller

There have been a number of numerical models for wave-driven currents after the concept of radiation stress was introduced by Longuet-Higgins and Stewart (1964). Early

simulations of longshore current induced by regular waves, for a simple plan form beach, were carried out by Bowen (1969), Longuet-Higgins (1970), and Thornton (1970). The disadvantage of these semi-analytic models is the occurrence of an abrupt change in longshore current at the break point. By introducing an eddy viscosity term (*i.e*., lateral mixing) in the momentum equation for the longshore current, the physically unrealistic current distribution at the breaker-line was eliminated.

Since the early models, significant progress has been made concerning nearshore currents generated by random waves. The pioneering work of Battjes (1972) illustrated that the longshore current generated by random waves is smooth in the surf zone, even though the lateral mixing term is not included. Thornton and Guza (1986) presented a model for the longshore current based on their random wave breaking model (Thornton and Guza, 1983). Van Dongeren *et al*. (1994, 2000, 2003) developed a quasi-3D nearshore hydrodynamic model named SHORECIRC, which is capable of describing several phenomena such as edge waves, surf beats, infragravity waves, and longshore current. Kraus and Larson (1991) and Larson and Kraus (2002) developed the NMLong model for computing the longshore current focusing on barred beaches. Militello *et al*. (2004) developed the M2D model for simulating the nearshore current due to tide, waves, wind, and rivers. Recently, Goda (2006) examined the influence of several factors on the longshore current under random waves. He demonstrated that significant differences in wave height and longshore velocity resulted depending on the employed random wave-breaking model. Thus, selecting a wave model that can accurately simulate surf-zone conditions is important when computing wave-induced nearshore currents.

Much research has demonstrated that the surface roller plays an important role in generating nearshore currents. The roller was initially investigated in the laboratory by Duncan (1981) and first applied theoretically by Svendsen (1984a, b) to improve the modeling of wave setup and undertow in the surf zone. Then, the roller model, including the roller energy gradients in the energy flux balance based on the roller theory of Svendsen (1984a, b), was employed in many studies related to wave-induced currents (*e.g.* Nairn *et al*., 1990; Deigaard *et al*., 1991; Stive and De Vriend, 1994; Lippmann *et al*., 1996; Reniers and Battjes, 1997; Ruessink *et al*., 2001; Tajima and Madsen, 2006; Roelvink *et al.*, 2010). Van Dongeren *et al*. (2003) extended the roller energy flux balance equation derived by Nairn *et al*. (1990), and they obtained calculations of longshore current that were in good agreement with data from the DELILAH field experiment.

Based on the depth-integrated and period-averaged energy balance equation, Dally and Osiecki (1994), and Dally and Brown (1995) developed a roller model for the evolution of the roller itself. Larson and Kraus (2002) applied this model in NMLong to improve longshore current simulations. In the energy balance equation, the energy dissipation per unit area after Dally *et al*. (1985) was used instead of the gradient in the depth-integrated time-averaged wave-induced energy flux in the *x*-direction. In almost all previous studies, the roller energy flux is only considered in the cross-shore direction in the balance equation. In the present study, the approaches by Dally and Brown (1995) and Larson and Kraus (2002) were followed, and the energy flux term in alongshore direction was included in the energy balance equation for the evolution of the roller itself.

2.3 Modeling Sediment Transport

Calculating sediment transport rate in the nearshore zone is a challenge because of the complexity of the hydrodynamics and the variety of governing phenomena. There are a number of nearshore sediment transport formulas that have been developed through the years for different types of applications in coastal engineering. For example, several formulas were examined and evaluated by Bayram *et al*. (2001), and Camenen and Larroude (2003). However, these formulas have typically described a specific set of physical processes and been validated with limited data. Recently, Camenen and Larson (2005, 2007, and 2008) developed a unified sediment transport formulation, which has been validated for a large set data on longshore and cross-shore sediment transport rate from the laboratory and field. Performance of the new sediment transport formulation was compared to several popular existing formulas, and the new formulation yielded the overall best predictions among investigated formulations, and therefore, it was employed in this study.

The mechanics of sediment transport in the swash zone have received less attention than the surf zone. However, the swash zone is important for the sediment exchange between land and sea, which in turn affects both the sub-aerial and sub-aqueous evolution of the beach. The limited number of studies, as well as lack of measurement data on net transport in the swash, has made it difficult to formulate mathematical models based on a detailed understanding of the governing physics. In spite of these difficulties, significant progress has been made in the last decade concerning the hydrodynamics and sediment transport conditions in the swash zone (see Elfrink and Baldock, 2002; Larson *et al*., 2004; Larson and Wamsley, 2007; Roelvink *et al.*, 2010). In this study, the formulas of hydrodynamics and sediment transport rates in swash zone of Larson and Wamsley (2007) were employed. The obtained sediment transport rate at the still-water shoreline was used as boundary condition for computing the suspended load in the inner surf zone, which was derived from the advection-diffusion equation.

2.4 Modeling Beach Morphological Evolution

Numerical models for simulating coastal morphological evolution have developed quickly during the recent decades. Development efforts have resulted in a wide range of models at different scales, including 1D, 2D, 3D, and quasi-3D models (*e.g.* Hanson and Larson, 1992; De Vriend *et al*., 1993; Hanson *et al*., 2003; Kobayashi, 2003; Roelvink *et al.*, 2010; Zyserman and Johnson, 2002; Lesser *et al*., 2004) and several of the models have been applied in coastal engineering projects. However, here we focus our review of numerical models that have been used for coastal morphological evolution in two dimensions with the emphasis on the response of the beach topography to coastal structures, such as breakwaters, jetties, and groins.

In their pioneering work, Watanabe *et al*. (1986) investigated the beach evolution in response to a detached breakwater. The wave, current, and sediment transport fields were

computed from which the topographic evolution was determined. Calculations showed that the model could reproduce small-scale laboratory measurements regarding the wave height and nearshore wave-induced current around a detached breakwater rather well, but the agreement with the measured beach evolution was mainly qualitative.

Nicholson *et al*. (1997) investigated and inter-compared five numerical models for simulating the development of a salient and a tombolo in the lee of a detached breakwater. In general, the output from these models regarding the hydrodynamics and morphological evolution was in qualitative agreement between the models (no data were employed), but differences were observed. Seven factors were identified as causing the different outputs obtained from the five numerical models, including wave type, bed roughness, eddy viscosity, wave-current interaction, refraction, smoothing, and sediment transport formula.

Steijn *et al*. (1998) applied the Delft3D model to simulate the morphological change in the vicinity of a long dam constructed at the northern end of the Texel coast. The predictions by the model were in quantitative agreement with some of the observations. A scour hole that developed in front of the tip of the dam was rather well reproduced. Nevertheless, there were large differences between the observations and computations of the morphological evolution in other areas.

Denot and Aelbrecht (1999) modeled the seabed evolution around a groin system. Two hypothetical test cases with different groin spacing and incident waves were investigated. The calculated wave and current fields around the groins were in good qualitative agreement. However, the simulated seabed evolution for both cases did not show clear areas of accumulation and erosion in the vicinity of the two groins, as expected.

Roelvink *et al*. (1999) investigated the morphological response adjacent to harbor moles and groins by using a depth-averaged morphodynamic model. Different grid sizes were applied to evaluate differences in the scour hole development around the structures. However, the wave-induced current was not considered, so the longshore transport rate may not have been calculated accurately.

Leont'yev (1999) developed a numerical model to simulate morphological changes due to coastal structures. Several hypothetical test cases involving groins and detached breakwaters were simulated. The model was also validated based on small-scale laboratory data and the computed result of the bed level evolution was in good agreement with the measurements.

Zyserman and Johnson (2002) applied a quasi-3D model of flow, sediment transport, and bed level evolution to simulate the beach morphological evolution in the vicinity of detached breakwaters. Selected results for three test cases with different locations and sizes of the breakwater showed that the model could produce reasonable results with respect to the wave, current, and sediment transport fields, although the calculations were not compared against measurements. However, when plotting their results, the resolution in the depth contours close to the shoreline was limited; for example, only contours deeper

than -2 m were shown. Thus, the topographical change near the shoreline might not have been considered in detail.

Gelfenbaum *et al*. (2003) simulated long-term morphological evolution for Grays Harbor inlet by using the Delft3D model. Filtering techniques for wave and tidal inputs were employed to reduce the number of wave conditions and flow simulations. Both the cases with and without jetties were investigated, and the model results showed quantitative agreement with observations, which indicated erosion in the inlet channel and accretion on the flood and ebb deltas. However, the simulations were only carried out for one year, whereas the measured topographic change was determined for an interval of thirty years. Thus, the comparison between the calculated and measured bed changes was not synchronized. Furthermore, the model was not successful in simulating the accumulation observed at the North Jetty.

Johnson (2004) simulated the coastal morphological evolution in the vicinity of groins by using the DHI Coastal Area Morphological Modelling System (MIKE 21 CAMS). Several important aspects of the modeling system were investigated including the effects of the sediment transport model, offshore wave height, offshore wave direction, tidal level variation, and groin spacing.

Saied and Tsanis (2005) developed a morphological model that was called the Integrated Coastal Engineering Model (ICEM). This model was tested against some hypothetical cases including detached breakwaters and groin systems. The computations for the hypothetical test cases produced results in good qualitative agreement with the expected response. Furthermore, a case study in Ras El-Bar in Egypt was employed to validate the model, and the computed shorelines were in quite good agreement with the measurements. However, detailed comparisons between calculations and measurements of the hydrodynamics and morphological evolution in the vicinity of the groins and detached breakwaters were not presented.

Johnson *et al*. (2005) validated the MIKE 21 CAMS model based on field data from the Dubai Coast. The wave transmission, overtopping, quasi-3D sediment transport, bed friction, and a global scale factor were manipulated to achieve reasonable calibration parameter values. The calculations of the bed evolution showed quite good agreement with the measurements.

Zyserman *et al*. (2005) and Zanuttigh (2007) modeled and analyzed the morphological response induced by low-crested structures on the adjacent seabed. These studies focused on the far-field erosion in the vicinity of roundheads and gaps between structures. The model was investigated by application at two field sites, Pellestrina and Lido di Dante in Italy, where groins and low-crested breakwaters were constructed to protect against beach erosion. The obtained simulation results were in good qualitative agreement with the measurements, especially the erosion near the roundheads of the breakwaters.

Ding *et al*. (2006), and Ding and Wang (2008), developed a quasi-3D morphological model that can be applied to coastal and estuarine morphological processes. The model was validated for a complex coastal area, which included detached breakwaters and a harbor. The calculated morphological change in the lee of the breakwaters was somewhat underestimated compared to the measurements. This was possibly because the sediment transport in the swash zone was not included in the model.

Brøker *et al*. (2007) also used MIKE 21 CAMS to optimize a new layout of the main breakwaters for the entrance of Thorsminde Harbor in Denmark. The recommended layout was constructed in 2004. However, the validation of the model was limited. The long-term beach evolution in the vicinity of new layout was not modeled, but only short simulations for selected storm conditions were carried out.

In summary, the development of numerical models of morphological evolution around coastal structures has encompassed significant improvements through the years. However, the morphodynamical processes are extremely complex and some are beyond our current state of knowledge. Furthermore, available high-quality data for validation are limited. Therefore, many of the previous modeling efforts neither included all relevant morphodynamical processes nor were validated against high-quality data from laboratories and field surveys.

3 Model Description

3.1 Random Wave Transformation Model

The random wave transformation model in the present study was originally developed by Mase (2001) based on the Energy Balance Equation with a Diffraction term and an energy dissipation term (EBED). The governing equation, for steady state, is expressed as follows (**Papers I and II**),

$$\frac{\partial\left(v_x S\right)}{\partial x}+\frac{\partial\left(v_y S\right)}{\partial y}+\frac{\partial\left(v_\theta S\right)}{\partial \theta} = \frac{\kappa}{2\omega}\left\{\left(CC_g\cos^2\theta S_y\right)_y-\frac{1}{2}CC_g\cos^2\theta S_{yy}\right\}-\varepsilon_b S \tag{1}$$

where $S=$ angular-frequency spectrum density; $(x,y)=$ horizontal coordinates; $\theta=$ angle measured counter clockwise from x axis; v_x , v_y , and $v_\theta=$ propagation velocities in their respective coordinate direction; $\omega=$ angular frequency; $C=$ phase speed; $C_g=$ group speed; $\kappa=$ free parameter that can be optimized to change the influence of the diffraction effects; and $\varepsilon_b=$ energy dissipation coefficient.

The propagation velocities are given as,

$$\left\{v_x, v_y, v_\theta\right\}=\left\{C_g\cos\theta,\ C_g\sin\theta,\ \frac{C_g}{C}\left(\sin\theta\frac{\partial C}{\partial x}-\cos\theta\frac{\partial C}{\partial y}\right)\right\} \tag{2}$$

The first term on the right hand of Eq. (1) was introduced by Mase (2001) in order to represent the diffraction effects. The second term represents the energy dissipation due to wave breaking. The output of the random wave transformation model includes three main wave parameters: significant wave height H_s , significant wave period T_s, and mean wave direction $\bar{\theta}$.

The original EBED model is stable and can be applied to the complex beach topography of coastal zones containing structures. However, it often overpredicts the wave conditions in the surf zone compared to measurements. The overestimation is mainly due to the algorithm describing wave energy dissipation caused by wave breaking. In the EBED model, the energy dissipation coefficient was determined by the Takayama *et al.* (1991) model. The calculation of this coefficient is rather complex and the coefficient does not easily lend itself to calibration.

In this study, the energy dissipation term based on the Dally *et al.* (1985) model was modified in order to improve the predictive capability of the wave model in the surf zone. The model is referred to as Modified-EBED model hereafter. The modified energy balance equation proposed is as follows (**Papers I, II, and IV**),

$$\frac{\partial\left(v_x S\right)}{\partial x}+\frac{\partial\left(v_y S\right)}{\partial y}+\frac{\partial\left(v_\theta S\right)}{\partial \theta} = \frac{\kappa}{2\omega}\left\{\left(CC_g\cos^2\theta S_y\right)_y-\frac{1}{2}CC_g\cos^2\theta S_{yy}\right\}-\frac{K}{h}C_g\left(S-S_{stab}\right) \tag{3}$$

where $h=$ still-water depth; $K=$ dimensionless decay coefficient; and $S_{stab}=$ stable wave spectrum density, which is determined based upon the stable wave height $H_{stab}\left(=\Gamma h\right)$, with Γ being a dimensionless empirical coefficient.

Assuming that the spectrum density S and the stable spectrum density S_{stab} are functions of H_s^2 and H_{stab}^2, respectively, Eq. (3) can be rewritten as,

$$\frac{\partial\left(v_x S\right)}{\partial x}+\frac{\partial\left(v_y S\right)}{\partial y}+\frac{\partial\left(v_\theta S\right)}{\partial \theta} = \frac{\kappa}{2\omega}\left\{\left(CC_g\cos^2\theta S_y\right)_y-\frac{1}{2}CC_g\cos^2\theta S_{yy}\right\}-\frac{K}{h}C_g S\left\{1-\left(\frac{\Gamma h}{H_s}\right)^2\right\} \tag{4}$$

Several previous studies have dealt with the empirical coefficients K and Γ. The values of these coefficients can be given by constants, *e.g.*, $\Gamma=0.4$, and $K=0.15$ (Dally *et al.*, 1985), or empirical expressions containing the bottom slope (see Goda, 2006; Tajima and Madsen, 2006). In the Modified-EBED model, a good description was obtained of wave conditions in the surf zone for LSTF data by modifying the expressions for the coefficients proposed by Goda (2006) as follows,

$$\begin{cases}\Gamma=0.45,\ K=\dfrac{3}{8}\left(0.3-19.2\,m\right) & :m<0\\ \Gamma=0.45+1.5\,m,\ K=\dfrac{3}{8}\left(0.3-0.5\,m\right) & :0\le m\le 0.6\end{cases} \tag{5}$$

where $m=$ bottom slope.

The wave radiation-driven stresses were determined by the output from the wave transformation model as,

$$S_{xx} = \frac{E}{2}\left[2n\left(1+\cos^2\bar{\theta}\right)-1\right] \tag{6}$$

$$S_{yy} = \frac{E}{2}\left[2n\left(1+\sin^2\bar{\theta}\right)-1\right] \tag{7}$$

$$S_{xy} = S_{yx} = \frac{E}{2}n\sin 2\bar{\theta} \tag{8}$$

where $E = \rho_w g H_{rms}^2 / 8 =$ wave energy per unit area, with $\rho_w =$ density of water, $g =$ acceleration due to gravity; and $n = C_g / C =$ the wave index.

3.2 Surface Roller Model

The wave energy balance equation for the surface roller in two dimensions is expressed as (Dally and Brown, 1995; Larson and Kraus, 2002; **Papers I, II, and IV**),

$$\frac{\partial\left(MC_r\right)}{\partial t} + \frac{\partial}{\partial x}\left(\frac{1}{2}MC_r^2\cos^2\bar{\theta}\right) + \frac{\partial}{\partial y}\left(\frac{1}{2}MC_r^2\sin^2\bar{\theta}\right) = g\beta_D M - P_D \tag{9}$$

where $P_D =$ wave energy dissipation; $M =$ wave-period-averaged mass flux; $C_r =$ roller speed; and $\beta_D =$ roller dissipation coefficient.

The wave energy dissipation is determined as,

$$P_D = \frac{KC_g\rho_w g}{8h}\left[H_{rms}^2 - \left(\Gamma h\right)^2\right] \tag{10}$$

where $H_{rms} =$ root-mean-square wave height, which can be derived from the output of the random wave transformation model.

The stresses due to the rollers are determined as follows,

$$R_{xx} = MC_r\cos^2\bar{\theta} \tag{11}$$

$$R_{yy} = MC_r\sin^2\bar{\theta} \tag{12}$$

$$R_{xy} = R_{yx} = MC_r\sin 2\bar{\theta} \tag{13}$$

3.3 Nearshore Current Model

The governing equations for the nearshore currents are written as (Militello *et al.*, 2004; **Papers I, II, and IV**),

$$\frac{\partial(h+\eta)}{\partial t}+\frac{\partial q_x}{\partial x}+\frac{\partial q_y}{\partial y}=0 \tag{14}$$

$$\frac{\partial q_x}{\partial t}+\frac{\partial uq_x}{\partial x}+\frac{\partial vq_x}{\partial y}+g(h+\eta)\frac{\partial \eta}{\partial x}=\frac{\partial}{\partial x}D_x\frac{\partial q_x}{\partial x}+\frac{\partial}{\partial y}D_y\frac{\partial q_x}{\partial y}+fq_y-\tau_{bx}+\tau_{Sx} \tag{15}$$

$$\frac{\partial q_y}{\partial t}+\frac{\partial uq_y}{\partial x}+\frac{\partial vq_y}{\partial y}+g(h+\eta)\frac{\partial \eta}{\partial y}=\frac{\partial}{\partial x}D_x\frac{\partial q_y}{\partial x}+\frac{\partial}{\partial y}D_y\frac{\partial q_y}{\partial y}-fq_x-\tau_{by}+\tau_{Sy} \tag{16}$$

where η = water elevation; t = time; q_x and q_y = flow per unit width parallel to the x and y axes, respectively; u and v = depth-averaged velocity components in the x and y directions, respectively; f = Coriolis parameter; D_x and D_y = eddy viscosity coefficients; τ_{bx} and τ_{by} = bottom stresses; and τ_{Sx}, τ_{Sy} = wave stresses (the latter variables are all in the x- and y-directions, respectively).

Outside the surf zone, the depth-averaged horizontal eddy viscosity coefficient can be calculated as a function of the total water depth, current speed, and bottom roughness according to Falconer (1980),

$$D_0=1.154g(h+\eta)\frac{\sqrt{u^2+v^2}}{C_z^2} \tag{17}$$

where C_z = Chezy roughness coefficient.

In the surf zone, the eddy viscosity was taken to be a function of the wave properties following Kraus and Larson (1991) as,

$$D_1=\Lambda U_w H_{rms} \tag{18}$$

where Λ = empirical coefficient; and $U_w=\pi H_{rms}/(T_s\sinh(kd))$ = wave orbital velocity at the bottom, in which $d=(h+\eta)$ = total depth, and k = wave number.

In the transition zone, the eddy viscosity is calculated as,

$$D_2 = (1-\alpha) D_0 + \alpha D_1 \tag{19}$$

where $\alpha = (H_{rms}/d)^3 =$ weighting parameter (see Militello *et al.*, 2004).

The bottom stresses under combined current and waves are determined following (Nishimura, 1988),

$$\tau_{bx} = C_b \left[\left(U_{wc} + \frac{\omega_b^2}{U_{wc}} \cos^2 \overline{\theta} \right) u + \left(\frac{\omega_b^2}{U_{wc}} \cos\overline{\theta} \sin\overline{\theta} \right) v \right] \tag{20}$$

$$\tau_{by} = C_b \left[\left(U_{wc} + \frac{\omega_b^2}{U_{wc}} \sin^2 \overline{\theta} \right) v + \left(\frac{\omega_b^2}{U_{wc}} \cos\overline{\theta} \sin\overline{\theta} \right) u \right] \tag{21}$$

in which C_b = bottom friction coefficient,

$$U_{wc} = \frac{1}{2} \left\{ \sqrt{\left| u^2 + v^2 + \omega_b^2 + 2\left(u\cos\overline{\theta} + v\sin\overline{\theta} \right) \omega_b \right|} + \sqrt{\left| u^2 + v^2 + \omega_b^2 - 2\left(u\cos\overline{\theta} + v\sin\overline{\theta} \right) \omega_b \right|} \right\} \tag{22}$$

$$\omega_b = \frac{\sigma H_{rms}}{\pi \sinh(kd)} \tag{23}$$

where $\sigma =$ peak wave frequency.

The wave stresses are derived from the wave transformation model and the surface roller model. They are expressed by the following formulas,

$$\tau_{Sx} = -\frac{1}{\rho_w} \left[\frac{\partial}{\partial x} \left(S_{xx} + R_{xx} \right) + \frac{\partial}{\partial y} \left(S_{xy} + R_{xy} \right) \right] \tag{24}$$

$$\tau_{Sy} = -\frac{1}{\rho_w} \left[\frac{\partial}{\partial x} \left(S_{xy} + R_{xy} \right) + \frac{\partial}{\partial y} \left(S_{yy} + R_{yy} \right) \right] \tag{25}$$

In the present study, the Coriolis force due to rotation of the earth is neglected. Thus, the value of Coriolis parameter *f* is set to 0.

3.4 Sediment Transport Model

3.4.1 Swash Transport

The net transport rates in the cross-shore and longshore directions can be calculated based on the study of Larson and Wamsley (2007) as (**Papers I, III, and IV**),

$$q_{bc,net} = K_c \frac{\tan\phi_m}{\tan^2\phi_m - \left(dh/dx\right)^2} \frac{u_0^3}{g}\left(\frac{dh}{dx} - \tan\beta_e\right)\frac{t_0}{T} \tag{26}$$

$$q_{bl,net} = K_l \frac{\tan\phi_m}{\tan^2\phi_m - \left(dh/dx\right)^2} \frac{u_0^2 v_0}{g}\frac{t_0}{T} \tag{27}$$

where $q_{bc,net}$, $q_{bl,net}$ = net transport rates in the cross-shore and longshore directions, respectively; K_c and K_l = empirical coefficients, ϕ_m = friction angle for a moving grain ($\approx 30\,\text{deg.}$); β_e = foreshore equilibrium slope; u_0, v_0 and t_0 = scaling velocities and time, respectively; and T = swash duration (assumed that T is equal to the incident wave period).

Based on the ballistics theory, and assuming that the friction on the foreshore is zero, Larson and Wamsley (2007) derived the hydrodynamics in the swash zone as,

$$x_0 = x_s - \frac{1}{2}gt^2\sin\beta + u_s t \tag{28}$$

$$u_0 = u_s - gt\sin\beta \tag{29}$$

$$y_0 = y_s + v_s t \tag{30}$$

$$v_0 = v_s \tag{31}$$

where x_0 = position of the wave front that travels along foreshore; y_0 = longshore direction of the front; u_s, v_s = wave front speeds at the start of the uprush; x_s, y_s = location at the start of the swash zone, $x_s = 0$ at the still-water shoreline; β = foreshore slope set to a constant.

The maximum uprush is attained at the time when the velocity is zero, as given by $t_{\max} = u_s/(g\sin\beta)$ and the corresponding location is $x_{\max} = u_s^2/(2g\sin\beta)$. Based on the geometry, one can derive the runup height $R = x_{\max}/\sin\beta = u_s^2/(2g)$. The value of u_s might be difficult to determine, so the runup height can be used in calculations instead of

this velocity. The runup height can be obtained by using various empirical formulas (*e.g.* Hunt, 1959; Holman, 1986; Mase, 1988; Mayer and Kribel, 1994; Hedges and Mase, 2004; Stockdon *et al.*, 2006). In this study, the Hunt (1959) formula was employed for calculating the runup height.

The duration (t_0) at any location on the foreshore can be related to the swash duration and runup height (Larson and Wamsley, 2007) as,

$$\frac{t_0}{T} = \sqrt{1 - \frac{z_0}{R}} \tag{32}$$

where $z_0 =$ vertical distance from the reference level to x_0.

3.4.2 Nearshore and Offshore Transport

3.4.2.1 Bed load

Camenen and Larson (2005, 2007, and 2008) developed a unified transport formulation for bed load and suspended load under combined waves and currents. It can be used for both sinusoidal and asymmetric waves, and is referred to as the Lund-CIRP formula hereafter. To simplify calculations, the waves are assumed to be sinusoidal, having no asymmetry. Therefore, the contribution to the transporting velocity from waves is negligible, implying that only current moves the material. In such case, the bed load can be expressed as (**Papers I, III, and IV**),

$$\frac{q_{bc}}{\sqrt{(s-1)\,g d_{50}^3}} = a_c \sqrt{\theta_c}\; \theta_{cw,m} \exp\left(-b_c \frac{\theta_{cr}}{\theta_{cw}}\right) \tag{33}$$

where $q_{bc} =$ transport rate obtained in the direction of the current, the transport normal to current is zero; $s =$ relative density between sediment and water $(= \rho_s / \rho_w)$, in which $\rho_s =$ density of sediment; $d_{50} =$ median grain size; a_c, and $b_c =$ empirical parameters; $\theta_{cr} =$ critical Shields parameter for initiation of motion; $\theta_{cw,m}$ and $\theta_{cw} =$ mean and maximum Shields parameters due to wave-current interaction, respectively.

The critical Shields parameter is calculated based on the formula proposed by Soulsby and Whitehouse (1997) as,

$$\theta_{cr} = \frac{0.24}{d_*} + 0.055\left[1 - \exp\left(-0.02\, d_*\right)\right] \tag{34}$$

where $d_* = \sqrt[3]{g(s-1)/\nu^2}\ d_{50}$ = dimensionless grain size, with ν = kinematic viscosity of water.

The mean and maximum Shields parameters due to wave-current interaction can be calculated by vector addition as,

$$\theta_{cw,m} = \left(\theta_c^2 + \theta_{w,m}^2 + 2\theta_{w,m}\theta_c \cos\varphi\right)^{1/2} \tag{35}$$

$$\theta_{cw} = \left(\theta_c^2 + \theta_w^2 + 2\theta_w\theta_c \cos\varphi\right)^{1/2} \tag{36}$$

where θ_c and θ_w = Shields parameters due to current and wave, respectively; $\theta_{w,m}$ = mean wave Shields parameter, $\theta_{w,m} = \theta_w / 2$ for a sinusoidal wave profile; and φ = angle between the wave and the current directions.

The Shields parameters for current and wave can be determined as follows,

$$\theta_c = \frac{\tau_c}{\rho_w (s-1) d_{50}} \tag{37}$$

$$\theta_w = \frac{\tau_w}{\rho_w (s-1) d_{50}} \tag{38}$$

where τ_c and τ_w = shear stresses due to current and wave, respectively. These stresses can be calculated by the following formulas:

$$\tau_c = \frac{1}{2}\rho_w f_c U_c^2 \tag{39}$$

$$\tau_w = \frac{1}{2}\rho_w f_w U_w^2 \tag{40}$$

in which f_c and f_w = friction factors due to current and wave, respectively; $U_c = \sqrt{u^2 + v^2}$ = magnitude of current vector.

Based on the roughness calculations, the friction factors due to current and wave are calculated after Soulsby (1997) and Swart (1974), respectively, as,

$$f_c = 2\left(\frac{0.4}{1+(k_s/30d)}\right)^2 \tag{41}$$

$$f_w = \begin{cases} \exp(5.21 r^{-0.19} - 6.0) & r > 1.57 \\ 0.3 & r \le 1.57 \end{cases} \tag{42}$$

where $k_s =$ total roughness; $r = A_w / k_s =$ relative roughness, with $A_w = U_w T_s / 2\pi =$ semi-orbital excursion.

The total roughness is assumed to include three components: grain-related roughness k_{sd}, form-drag roughness k_{sf}, and sediment-related roughness k_{ss} (Soulsby, 1997). The total roughness is calculated by the linear sum of these components as,

$$k_s = k_{sd} + k_{sf} + k_{ss} \tag{43}$$

The grain related roughness is determined based on the median grain size as,

$$k_{sd} = 2.5 d_{50} \tag{44}$$

The form-drag roughness can be related to the height Δ_r and wavelength λ_r of the ripples (Soulsby, 1997) as,

$$k_{sf} = 7.5 \frac{\Delta_r^2}{\lambda_r} \tag{45}$$

For current, the wavelength and height of the ripples can be calculated based on the median grain size by the following formulas (Soulsby, 1997),

$$\lambda_r = 1000 d_{50} \tag{46}$$

$$\Delta_r = \frac{\lambda_r}{7} \tag{47}$$

For wave, the ripple height and ripple length can be determined based on the following formulas (Van Rijn, 1993):

$$\begin{cases} \begin{bmatrix} \Delta_r = 0.22\, A_w \\ \lambda_r = 1.25 A_w \end{bmatrix} & \Psi \le 10 \\ \begin{bmatrix} \Delta_r = 2.8\times10^{-13}(250-\Psi)^{5}\, A_w \\ \lambda_r = 1.4\times10^{-6}(250-\Psi)^{2.5} A_w \end{bmatrix} & 10 < \Psi \le 250 \\ \begin{bmatrix} \Delta_r = 0 \\ \lambda_r = 0 \end{bmatrix} & \Psi \ge 250 \end{cases} \tag{48}$$

where $\Psi = U_w^2/((s-1)d_{50})$ = particle mobility parameter.

The sediment-related roughness is determined based on the formula proposed by Wilson (1966, 1989) as,

$$k_{ss} = 5 d_{50} \theta_i \tag{49}$$

where θ_i = Shields parameter for current or wave (i=c, w, respectively, for current and wave).

Eq. (49) is of implicit type and therefore, an iterative method needs to be employed to solve the equation. In this study, the Newton-Raphson method was employed for solving the non-linear equation for sediment-related roughness.

3.4.2.2 Suspended load

The suspended load can be calculated based on either the Lund-CIRP formula or the Advection-Diffusion (AD) equation (**Papers I, III, and IV**).

Assuming that the suspended concentration is in equilibrium and current velocity is constant over the water column, Camenen and Larson (2007, 2008) derived the Lund-CIRP formula for suspended load as,

$$q_s = U_c c_R \frac{\varepsilon}{w_s}\left[1 - \exp\left(-\frac{w_s d}{\varepsilon}\right)\right] \tag{50}$$

where c_R = reference concentration at the bottom; w_s = sediment fall velocity; ε = sediment diffusivity.

The bed reference concentration is obtained from,

$$c_R = A_{cR}\theta_{cw,m}\exp\left(-4.5\frac{\theta_{cr}}{\theta_{cw}}\right) \tag{51}$$

where the coefficient A_{cR} is written as,

$$A_{cR} = 3.5\times10^{-3}\exp(-0.3d_*) \tag{52}$$

The sediment fall velocity is calculated from Soulsby (1997) as,

$$w_s = \frac{\nu}{d_{50}}\left[\left(10.36^2 + 1.049d_*^3\right)^{1/2} - 10.36\right] \tag{53}$$

The sediment diffusivity is related to the energy dissipation as (Battjes, 1975; Camenen and Larson, 2008),

$$\varepsilon = \left(\frac{k_b^3 D_b + k_c^3 D_c + k_w^3 D_w}{\rho}\right)^{1/3} d \tag{54}$$

where $k_b, k_c,$ and k_w = empirical coefficients; D_b = energy dissipation due to wave breaking $(= P_D)$; $D_c,$ and D_w = energy dissipations from bottom friction due to current and waves, respectively, expressed as,

$$D_c = \tau_c u_{c*} \tag{55}$$

$$D_w = \tau_w u_{w*} \tag{56}$$

in which u_{c*}, and u_{w*} = shear velocities due to current and wave, respectively.

The empirical coefficient k_b is set to 0.017. The coefficients $k_w,$ and k_c are calculated based on the Schmidt number,

$$k_i = 0.067\sigma_i \tag{57}$$

where σ_i = Schmidt number; *i=c, w* denotes current and wave, respectively.

The Schmidt number is determined by the following empirical formulas (Camenen and Larson, 2007; Militello *et al.*, 2006),

$$\sigma_i = \begin{cases} A_{i1} + A_{i2}\sin^2\left(\dfrac{\pi}{2}\dfrac{w_s}{u_{i*}}\right) & \dfrac{w_s}{u_{i*}} \le 1 \\ 1 + (A_{i1} + A_{i2} - 1)\sin^2\left(\dfrac{\pi}{2}\dfrac{w_s}{u_{i*}}\right) & \dfrac{w_s}{u_{i*}} > 1 \end{cases} \tag{58}$$

where i = subscript equal to *c* or *w*; $A_{c1} = 0.7, A_{c2} = 3.6, A_{w1} = 0.09,$ and $A_{w2} = 1.4$.

Alternatively, the suspended load can be obtained by solving the AD equation. The two-dimensional time- and depth-averaged AD equation is expressed as (**Papers I, III, and IV**),

$$\frac{\partial\left(\overline{C}d\right)}{\partial t} + \frac{\partial\left(\overline{C}q_x\right)}{\partial x} + \frac{\partial\left(\overline{C}q_y\right)}{\partial y} = \frac{\partial}{\partial x}\left(K_x d\frac{\partial\overline{C}}{\partial x}\right) + \frac{\partial}{\partial y}\left(K_y d\frac{\partial\overline{C}}{\partial y}\right) + P - D \tag{59}$$

where $\overline{C}$ = depth-averaged sediment concentration; K_x, and K_y = sediment diffusion coefficients in *x* and *y* directions, respectively; P = sediment pick-up rate, and D = sediment deposition rate.

The sediment diffusion coefficient can be calculated by Elder (1959) as,

$$K_x = K_y = 5.93u_{c*}d \tag{60}$$

The sediment pick-up and deposition rates are given as,

$$P = c_R w_s \tag{61}$$

$$D = \frac{\overline{\mathrm{C}}}{\beta_d} w_s \tag{62}$$

where β_d = coefficient calculated based on Camenen and Larson (2008; see also Militello *et al*., 2006) as,

$$\beta_d = \frac{\varepsilon}{w_s d}\left[1 - \exp\left(-\frac{w_s d}{\varepsilon}\right)\right] \tag{63}$$

The concentration $\overline{C}$ is calculated in the AD equation until a steady condition is attained. The sediment transport rates in the *x* and *y* direction can be calculated as,

$$q_{sx} = \overline{C} q_x - K_x d \frac{\partial \overline{C}}{\partial x} \tag{64}$$

$$q_{sy} = \overline{C} q_y - K_y d \frac{\partial \overline{C}}{\partial y} \tag{65}$$

The sediment transport rate is often large near the shoreline due to the swash uprush and backwash processes. The observations from LSTF showed a peak in the sediment transport rate close to shoreline that was larger than the transport rate in the inner surf zone. The sediment transport rates in the swash zone can be well reproduced by the swash zone computation; the calculated transport rates increases in the seaward direction along the foreshore to the still-water shoreline. However, in the inner surf zone, the calculated sediment transport rates obtained by the currently available formulas often tend to decrease from offshore towards the still-water shoreline. Therefore, there is a significant difference between the calculated sediment transport rates near the still-water shoreline, since the interaction between the swash and inner surf zone is not well described in most models.

In this study, the sediment transport rate at the still-water shoreline obtained from the swash zone computation is employed to determine the suspended sediment concentration at the boundary for solving the AD equation. The pick-up and deposition rates those were described in the Eqs. (61) and (62), respectively, were also modified as follows,

$$\overline{P} = P\left[1 + \vartheta \frac{\overline{V}}{v_0} \exp\left(-\mu \frac{d}{R}\right)\right] \tag{66}$$

$$\overline{D} = \frac{D}{\left[1 + \vartheta \frac{\overline{V}}{v_0} \exp\left(-\mu \frac{d}{R}\right)\right]} \tag{67}$$

where ϑ and μ = free non-negative coefficients, $\overline{V}$ = mean velocity across the profile. The velocity $\overline{V}$ is determined as the average longshore current across the surf zone, v_0 is obtained from swash zone computation, and R is calculated by the Hunt (1959) formula.

The total load, which combines the bed load from the Lund-CIRP formula and the suspended load from the AD equation with the above modifications, is referred to as Lund-CIRP-AD hereafter. Calibration showed that $\vartheta = 9.3$ and $\mu = 2.4$ were the most suitable values for all experiment cases studied (**Papers I and III**). Although the modifications are somewhat *ad hoc*, the model reproduced well the sediment transport rates near the still-water shoreline, in agreement with the data from the LSTF measurements.

3.5 Morphological Evolution Model

The morphological evolution is based on the sediment volume conservation equation,

$$\frac{\partial h}{\partial t} = \frac{1}{1-n_p}\left(\frac{\partial q_{tot,x}}{\partial x} + \frac{\partial q_{tot,y}}{\partial y}\right) \tag{68}$$

where n_p = porosity parameter; and $q_{tot,x}, q_{tot,y}$ = total load in x and y directions, respectively.

In the offshore and surf zones, the total load is the sum of bed load and suspended load, which are calculated based on Eqs. (33) and (59). In the swash zone, it is based on the net transport rates obtained from Eqs. (26) and (27).

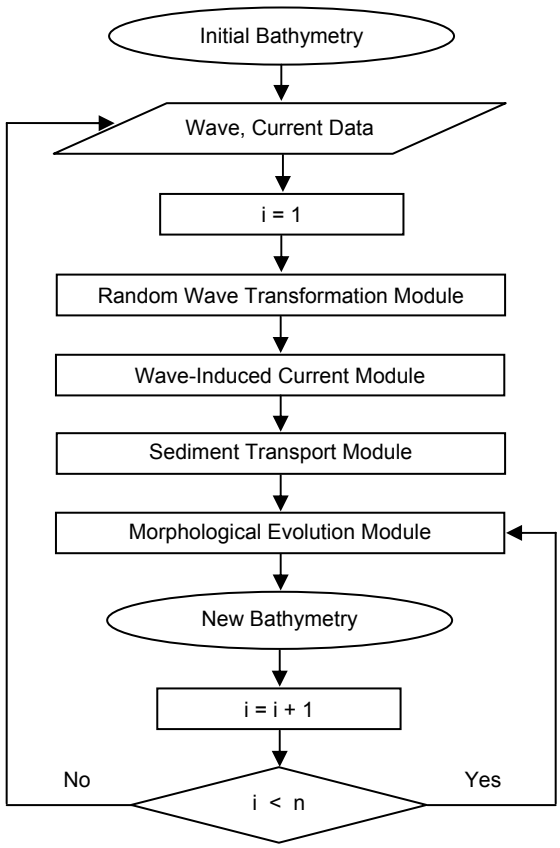

Fig. 2. Calculation procedure in the morphological evolution model

Fig. 2 presents a flowchart for the calculation of beach topography evolution, including the feedback loops. Based on the input data (offshore wave conditions), the Modified-EBED model is employed to calculate the wave field in the nearshore zone. The mass flux due to the roller is determined through the roller model. Thus, the wave stresses are calculated based on the random wave transformation model and the roller model. After that, the wave-induced current field at steady state is determined from the nearshore current model. The output from the wave and current models is used to compute the Shields parameter values that are employed for determining the bed load in the offshore and surf zone. The coupling between the sediment transport in the swash and the inner surf zone is included. When solving the advection-diffusion equation for the offshore and surf zones, the suspended sediment concentration at the still-water shoreline (boundary between swash and surf zones) is calculated based on the sediment transport rates obtained by the swash zone computations. The beach morphological change is determined from the volume conservation equation. In order to save time in the computations, the wave, current, and sediment transport fields are only re-calculated every n-th morphological time step (n=5 in the present study). The bed level is smoothed at an interval corresponding to 15 times the morphological time step, and the smoothing coefficient is 0.25 (Johnson and Zyserman, 2002).

3.6 Boundary conditions

The wave energy at offshore boundary is based on theoretical spectrums such as JONSWAP or TMA (Hasselmann *et al.*, 1973; Bouws *et al.*, 1985; Goda, 2000). At the lateral boundaries, the wave energy gradient in alongshore direction is set to zero (*Neumann boundary condition*). At the solid boundary (structures, land), wave energy flux is set to zero (*Dirichlet boundary condition*).

At the offshore and solid boundaries, the mass flux due to roller is assumed to be zero (*Dirichlet boundary condition*). The alongshore mass flux gradient is given as zero at the lateral boundaries (*Neumann boundary condition*).

The radiation boundary condition is employed to determine the currents at the offshore boundary (Reid and Bodine, 1968). At the lateral boundaries, the water fluxes were given based on the measurement data of nearshore currents (*Dirichlet boundary condition*, applied for this study). Alternatively, the alongshore water level gradient or gradient of cross-shore and longshore currents in the alongshore direction is set to zero at the lateral boundaries (*Neumann boundary condition*). No flow is assumed at the solid boundary.

The gradient of suspended concentration in alongshore direction is assumed to be zero at the offshore and lateral boundaries (*Neumann boundary condition*). At the boundary between the swash zone and inner surf zone, the suspended concentration is calculated based on the swash zone computation (*Dirichlet boundary condition*). The suspended concentration is given as zero at the location where the structures are placed (*Dirichlet boundary condition*). The alongshore bed level gradient is given as zero at the offshore and lateral boundary (*Neumann boundary condition*).

3.7 Numerical Implementation

A first-order upwind scheme and Gauss-Seidel method are employed to solve the energy balance equation (for detail see Mase, 2001). The mass flux due to the roller is calculated explicitly based on the FTCS (forward in time, center in space) scheme (Hoffman, 2001). The nearshore current is calculated based on the explicit scheme of Koutitas (1988). The Newton-Raphson method is used to solve the non-linear equation for the sediment-related roughness. The suspended sediment concentration is obtained by solving the AD equation using the Crank-Nicolson scheme (Hoffman, 2001). Finally, the explicit first-order upwind scheme FTBS (forward in time, backward in space) is employed to solve the sediment volume conservation equation (Long *et al.*, 2008).

4 Data Employed

Five series of physical model experiments were undertaken in the basin of the LSTF at the Coastal and Hydraulics Laboratory (CHL) in Vicksburg, Mississippi (Gravens *et al.*, 2006; Gravens and Wang, 2007; Hamilton and Ebersole, 2001; Wang *et al.*, 2002a, b). The main aim of these experiments was to obtain high-quality data sets for validating formulas for sediment transport, as well as investigating the beach evolution in the vicinity of coastal structures. The first series of experiments, referred to as "Base Case", consisted of four runs approximately 160 min each that were performed on a natural beach without structures. The second and third series of experiments, referred to as "Test 1" and "Test 2", were carried out with a detached breakwater in the basin that was located between profile Y22 and Y26, at four meter distance from the initial still water shoreline (see Fig. 3). The currents in Test 1 were generated by waves only, whereas in Test 2 the currents were a combination of wave-induced currents and external currents. Both Test 1 and Test 2 included eight runs approximately 190 min each. The fourth series, referred to as "Test 3", included six runs 180 min each, performed on the natural beach with a T-head groin (see Fig. 4). The last series of experiments, referred to as "Test 4", were conducted in the basin with a detached breakwater, but its length was shorter and its location was closer to the shoreline than those in Test 1 and Test 2.

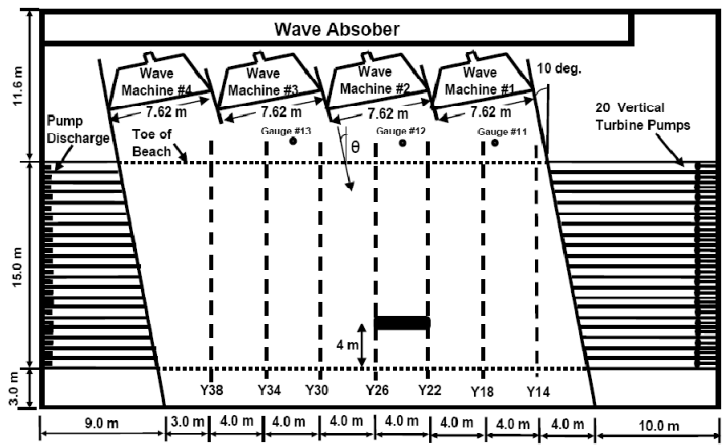

Fig. 3. Detached breakwater layout in the LSTF for Test 1 and 2 (Gravens and Wang, 2007)

In all experimental runs, spilling breaking waves were generated by four wave-makers and the water was re-circulated by the pumping systems located up- and downstream of the basin (see Figs. 5a and b). Wave gages and acoustic doppler velocimeters were co-located at ten cross-shore positions on the instrument bridge (see Fig. 6). These locations are presented in the Table 1. The instrument bridge moved in the alongshore direction, thus the wave conditions and currents could be observed at specific cross-shore profiles. Three wave gages (#11, #12, and #13) were located at three alongshore positions, 18.43 m seaward of the initial shoreline, to measure the wave conditions seaward of the toe of the

movable beach (see Figs. 3 and 4). The sand transport rate in alongshore direction can be measured based on 20 gravity-feed sediment traps which were located from offshore to swash zone at the downdrift end of the movable beach. A rod and acoustic survey techniques were employed to measure the beach profiles after each experimental run. The beach in the basin consisted of well-sorted sand with a median grain size of 0.15 mm.

Table 1. Measurement locations on the instrument bridge, distance from shoreline (m)

Measurement locations	ADV1	ADV2	ADV3	ADV4	ADV5	ADV6	ADV7	ADV8	ADV9	ADV10
Base Case	1.125	2.725	4.125	5.73	7.125	8.525	10.125	11.625	13.125	15.625
Test 1, 2, 3, and 4	1.125	2.2	3.3	4.125	5.73	7.125	8.525	10.125	11.625	13.125

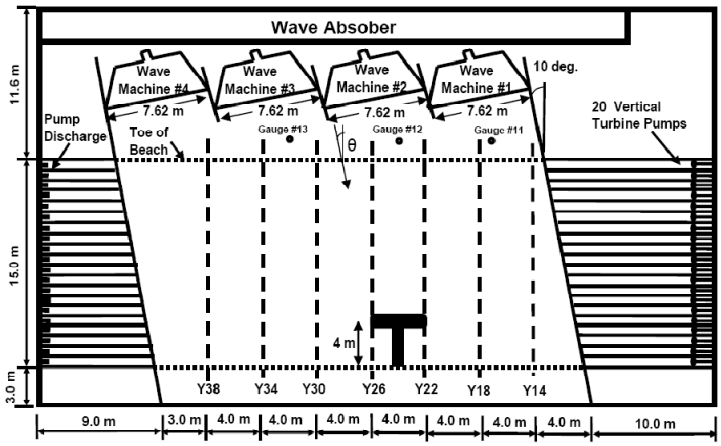

Fig. 4. T-head groin layout in the LSTF for Test 3 (Gravens and Wang, 2007)

Fig. 5a. Wave-maker layout in LSTF basin (from CHL official website)

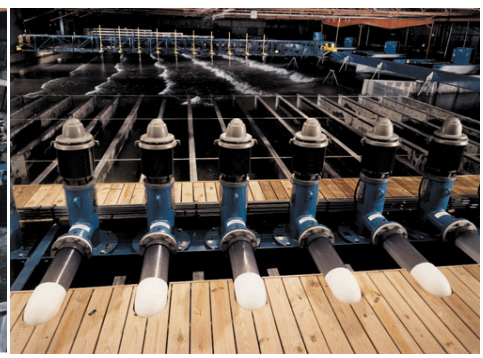

Fig. 5b. Pumping system at downstream end (from CHL official website)

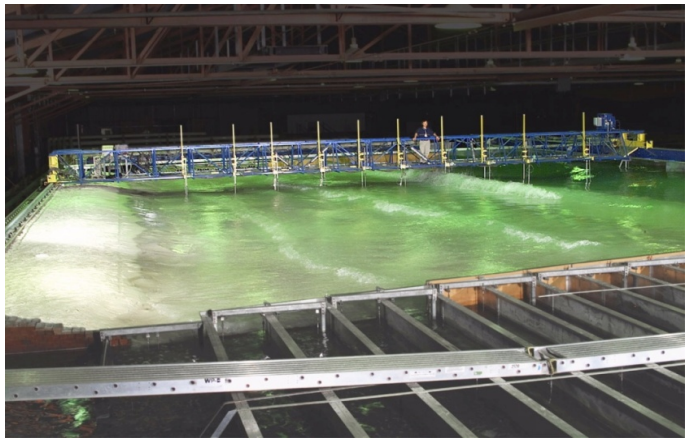

Fig. 6. Instrument bridge and downstream sediment traps (from CHL official website)

In this study, the data sets from the Base Case, Test 1, and Test 3 were employed to validate the predictive capability of the numerical model as follows:

- **Base Case:** Base Case 1 (BC1), Base Case 2 (BC2), and Base Case 4 (BC4)
- **Test 1:** Test 1 Case 1 (T1C1), Test 1 Case 4 (T1C4), and Test 1 Case 8 (T1C8)
- **Test 3:** Test 3 Case 1 (T3C1), Test 3 Case 4 (T3C4), and Test 3 Case 6 (T3C6)

In BC1, the currents were only generated by random waves, and the longshore flux of water was re-circulated from the downstream end to upstream end of the basin by the turbine pumps. In BC2, the currents were the combination of wave-induced current and external current. In this case, the external current was imposed across the model beach by re-circulating 2 times the wave-induced longshore flux of water. As for BC2, the external current was also imposed in BC4 by re-circulating 1.5 times the wave-induced longshore flux of water. In all runs of the Base Case, the data were measured at 11 cross-shore profiles from upstream to downstream. The numerical model was validated against the data sets from three Base Cases including the significant wave height, longshore current, wave setup, and longshore sediment flux (for detail see **Paper I**).

Test 1 encompassed eight experimental runs of approximately 190 min duration each. In all these runs, the current was only generated by random waves, and a rubble-mound detached breakwater was used that was 4 m long and located 4 m from the initial still-water shoreline. The data were measured at 13 cross-shore profiles from upstream to downstream for all runs of the Test 1. In T1C1, the initial beach topography was quite uniform in the alongshore direction, and the initial shoreline was straight and parallel to the detached breakwater (see Fig. 7a). In T1C4, the salient had the tip located approximately midway between the initial shoreline and the detached breakwater. The initial bathymetry of T1C8 had a salient close to equilibrium with its tip almost reaching to the detached breakwater. And after this run, the tombolo was fully developed (see Fig. 7b).

The validations of the numerical model concerning the hydrodynamics and beach morphology evolution were presented in the **Paper II** and **Paper IV**, respectively.

Test 3 included six experimental runs of approximately 180 min duration each on a natural beach with a T-head groin centrally located in the alongshore direction of the model beach. In all runs of Test 3, the current was generated by waves and the water was re-circulated by the pumping systems, and the data were also measured at 13 cross-shore profiles from upstream to downstream. As for T1C1, the initial beach topography of T3C1 was quite uniform in the alongshore direction, and the initial shoreline was parallel to the head section of the T-head groin. Fig. 8a illustrates the wave action in the vicinity of the T-head groin during experimental run T3C4. After this run, the salient updrift of the T-head groin stem reached to the head section of this structure (Fig. 8b). The beach was likely to reach equilibrium after the run T3C6. The validations of the numerical model regarding the hydrodynamics and morphological changes based on these data sets were presented in detail in **Paper IV**.

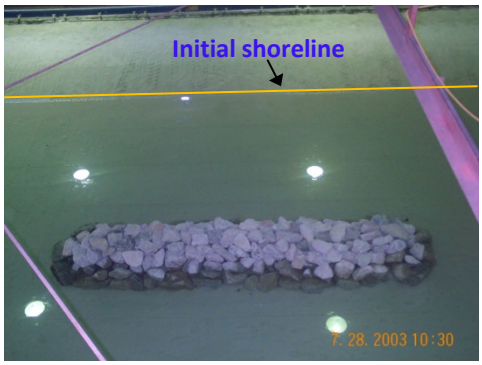

Fig. 7a. Before experimental run T1C1

(from Gravens and Wang, 2003)

Fig. 7b. Tombolo developed after T1C8

(from Gravens and Wang, 2003)

Fig. 8a. During experimental run T3C4

(from Gravens and Wang, 2004)

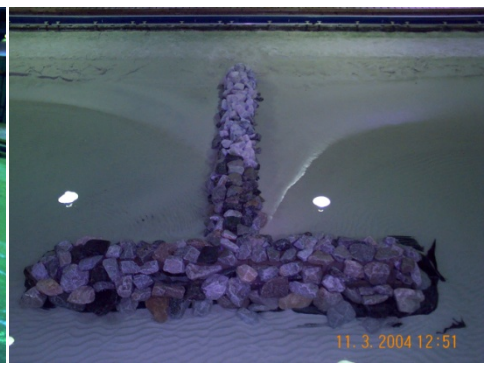

Fig. 8b. Salient developed after T3C4

(from Gravens and Wang, 2004)

5 Selected Results and Discussions

5.1 Nearshore Wave Conditions

The calculation of the nearshore wave field was compared against the measurements obtained from the series of experiments in the LSTF basin. The simulations showed that the wave conditions predicted by Modified-EBED model significantly improved compared to those obtained by the original EBED model. **Paper I** presented the comparisons between measurements and calculations of significant wave height for three selected test cases without structure: BC1, BC2, and BC4. As can be seen in Fig. 9, the calculated significant wave height obtained by EBED model for BC1 overpredicted in the surf zone, whereas the one obtained by Modified-EBED model agreed well with measurements.

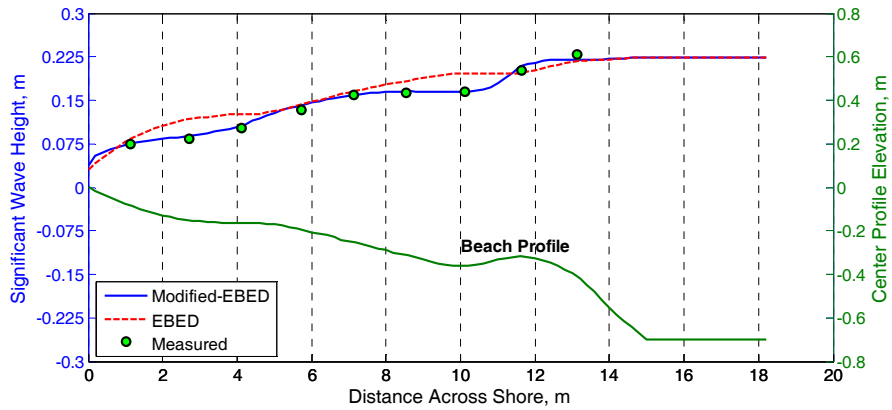

Fig. 9. Calculated and measured significant wave height for Case BC1

Papers II and IV presented the detailed comparisons between calculated and measured significant wave height in the vicinity of the breakwater and T-head groin. Fig. 10 illustrates the comparison of calculated significant wave height and measurement around the detached breakwater for T1C4. The model validation for T3C4 concerning the significant wave height around the T-head groin is shown in Fig. 11. As for BC1, the calculations of significant wave height obtained by Modified-EBED model were also better than those from the original EBED model. The Modified-EBED model reproduced well the wave conditions in the surf zone as well as in the lee of the detached breakwater and T-head groin.

Quantitative assessment of the EBED and Modified-EBED models using root-mean-square (rms) error clearly showed the modified model produced better agreement with measurements. For example, the rms error in significant wave height by Modified-EBED model for BC1 was only 3.64 %, where as it was 12.96 % by the original EBED model (**Paper I**). For T1C4, the rms errors in significant wave height were 8.39% and 11.75 % for the Modified-EBED and original EBED models, respectively (**Paper II**).

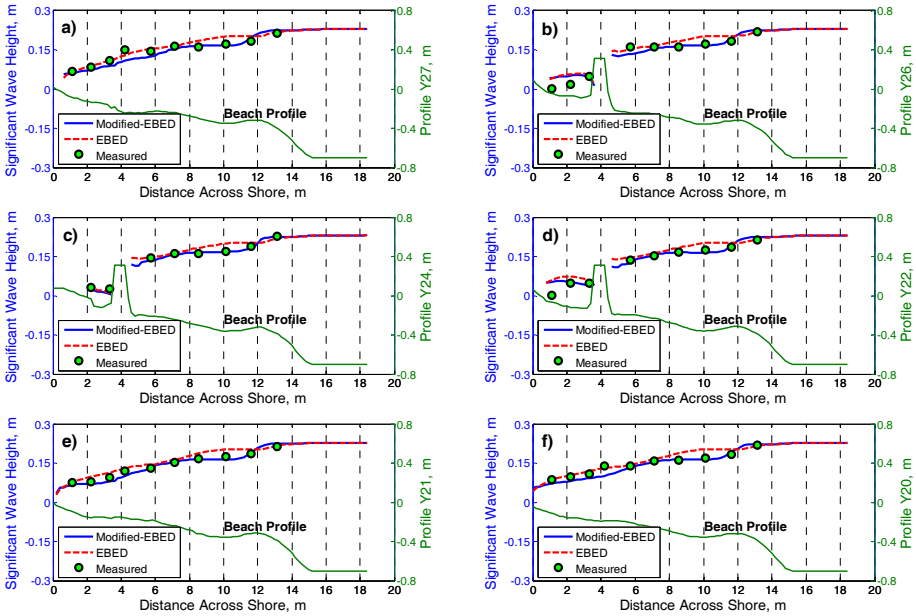

Fig. 10. Calculated and measured significant wave height for Case T1C4

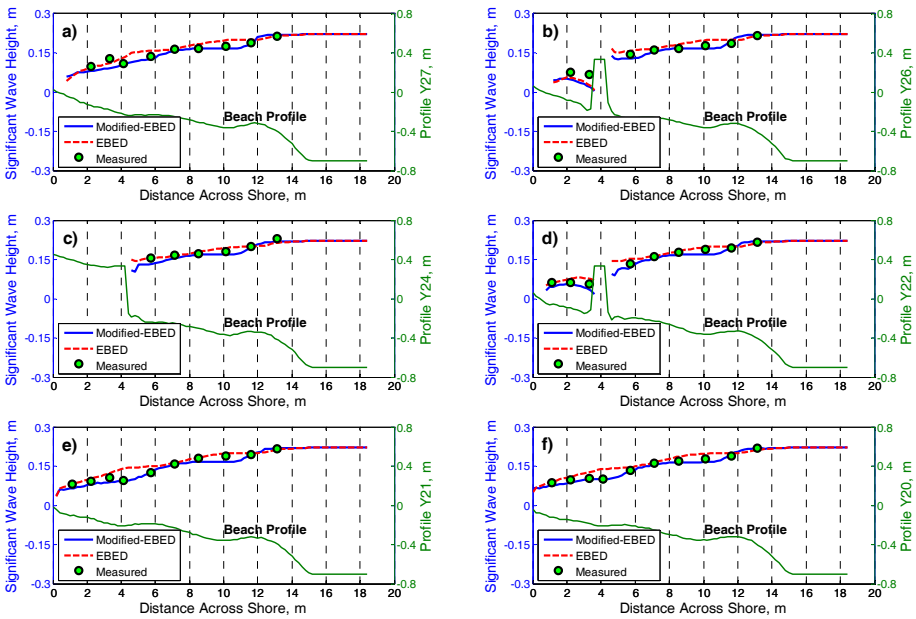

Fig. 11. Calculated and measured significant wave height for Case T3C4

As discussed in **Papers I, II, and IV**, the wave field simulation is the crucial first step in modeling beach morphological evolution. The accuracy of the current and sediment transport fields is strongly dependent on the output from the wave model. The diffraction term was included in the wave model so it can describe the diffraction effects in the lee of detached breakwater and T-head groin. The simulations showed that the calculated significant wave height in the lee of these structures agreed well with measurements, implying that the diffraction effects were well modeled in the random wave transformation model. In addition, the energy dissipation due to wave breaking plays a key role in calculating the wave conditions in the surf zone. In this study, the modification of the energy dissipation was based on Dally *et al.* (1985) model in which the decay and stable parameters were determined by Eq. (5), producing a significant improvement in calculating the wave conditions in the surf zone. Therefore, the Modified-EBED model can provide more accurate results to be used for calculating nearshore wave-induced currents and sediment transport rates.

The random wave transformation model was also applied to calculate the wave conditions at Hai Hau beach, Vietnam (**Paper V**). The output of model was used for determining the shoreline evolution at this area. The simulations showed the calculated shoreline changes were in good agreement with measurements, implying the wave model produced satisfactory wave conditions in this area.

5.2 Nearshore Currents and Wave Setup

The calculations of nearshore wave-induced currents and wave setup were compared against the measurements from the LSTF. **Paper I** presented the comparison between calculated longshore current and wave setup and observations for BC1, BC2, and BC4. The current was only generated by waves in test case BC1, whereas an external current was also given in BC2 and BC4. As can be seen in Fig. 12, including the roller effects, the peak of the calculated longshore current for BC1 was shifted toward the shoreline and the magnitude of the current also increased in the surf zone, producing better agreement with measurements. The calculated wave setup for BC1 and the corresponding measurements are shown in Fig. 13. In general, both calculations of wave setup with and without roller were in good agreement with observations.

Paper II validated the model against three data sets of LSTF regarding the wave and current fields around a detached breakwater. A detailed comparison between the calculated longshore current, cross-shore current, and wave setup, and the measurements along 12 cross-shore profile lines were carried out. Figs. 14 and 15 show the comparisons of calculated and measured longshore current and cross-shore current for T1C4, respectively. In general, the longshore current was in good agreement with the measurements, whereas the cross-shore current somewhat underestimated the measurements. The eddy simulated downstream the breakwater caused a significant difference between calculated and measured cross-shore current at profile Y21 and Y20 (see Fig. 15e and f). In this study, the undertow was not included in the model, which is probably the main reason for these discrepancies. However, the agreement between the calculations and observations was

quite good in the lee of detached breakwater. Although the calculated wave setup was overpredicted compared to the measurements, the absolute errors between calculations and measurements were relatively small (for detail see **Paper II**).

Paper IV also validated the wave-induced currents for three test cases with a T-head groin. As for the test cases with detached breakwater, the obtained results on the longshore current agreed well with measurements, and the cross-shore current was also underestimated compared to the measurements.

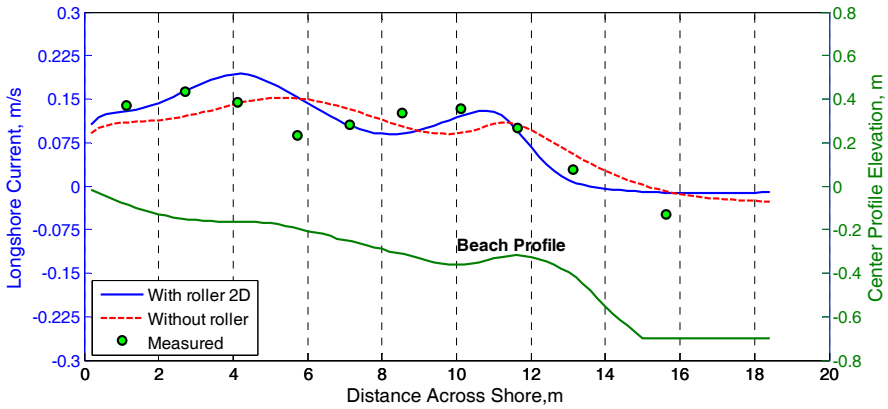

Fig. 12. Calculated and measured longshore current for Case BC1

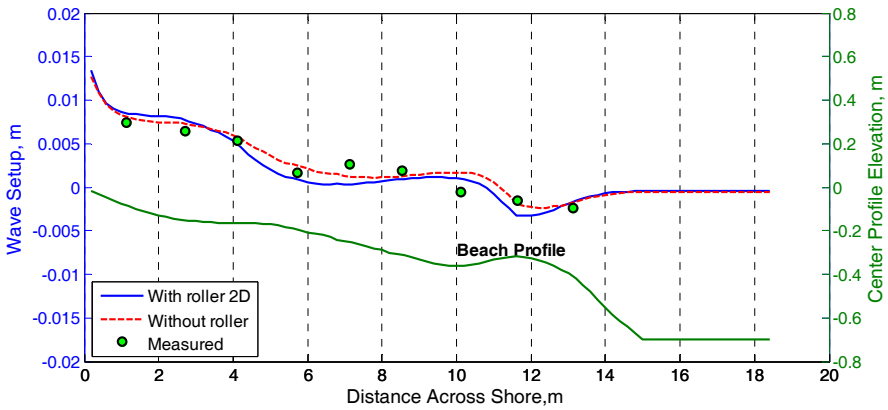

Fig. 13. Calculated and measured wave setup for Case BC1

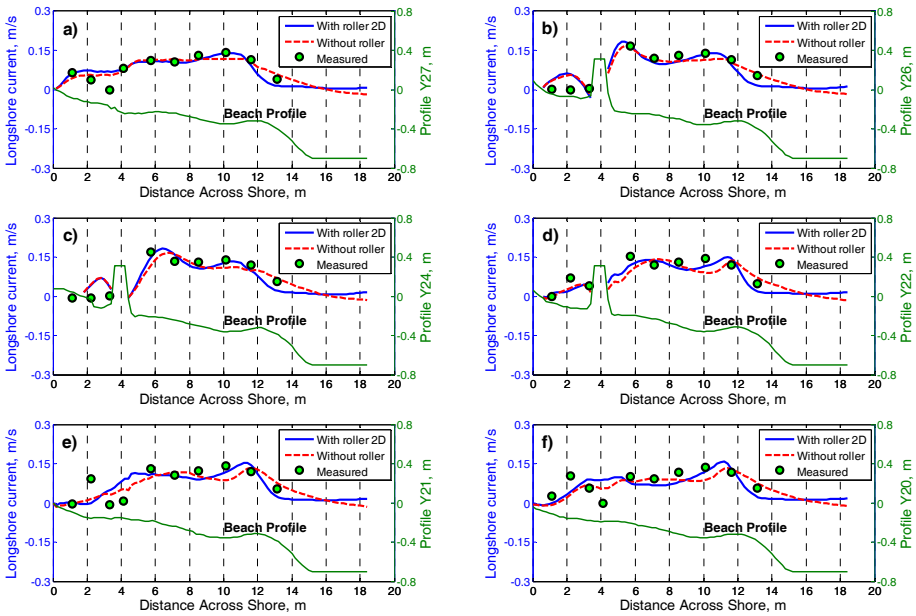

Fig. 14. Calculated and measured longshore current for Case T1C4

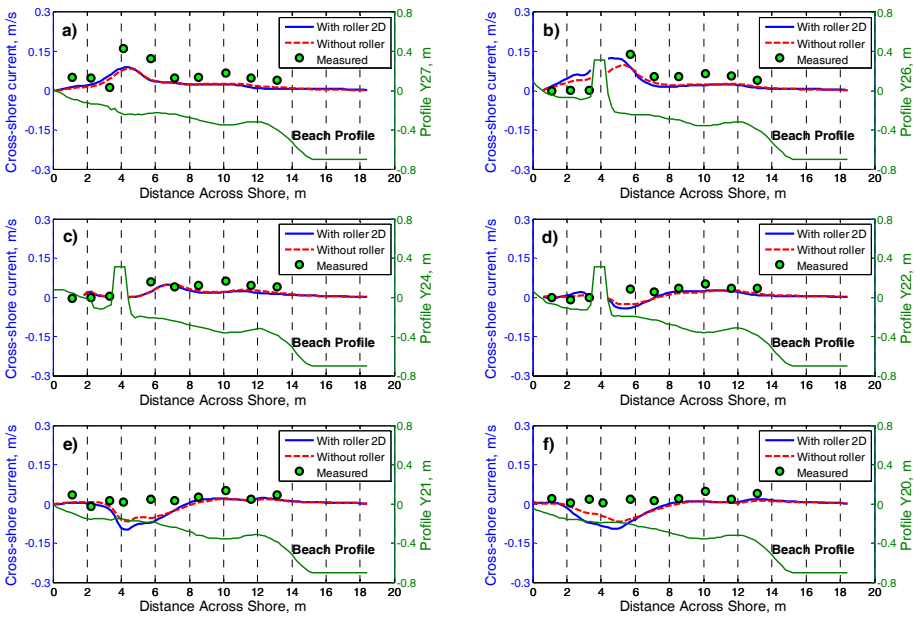

Fig. 15. Calculated and measured cross-shore current for Case T1C4

5.3 Sediment Transport

Papers I and **III** describe the comparison of calculated longshore sediment flux and corresponding measurements. Figs. 16 and 17 show the comparison between the calculated and measured longshore sediment flux for BC1 and BC4, respectively. As can be seen, the calculations obtained based on the Lund-CIRP formula agreed fairly well with measurements at offshore and outer surf zone. However, the discrepancies between the calculations and measurements near the shoreline were significant. Using the AD-Lund-CIRP formula with the modifications of the pick-up and deposition rates, the obtained results were in good with measurements from the swash zone to the offshore.

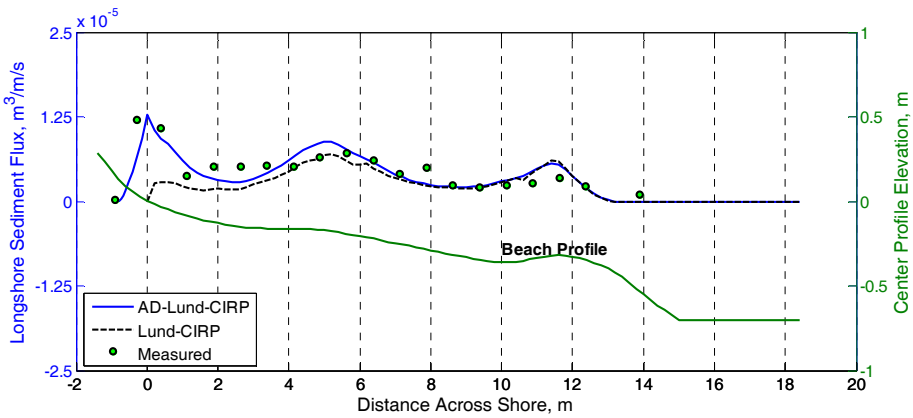

Fig. 16. Calculated and measured longshore sediment flux for Case BC1

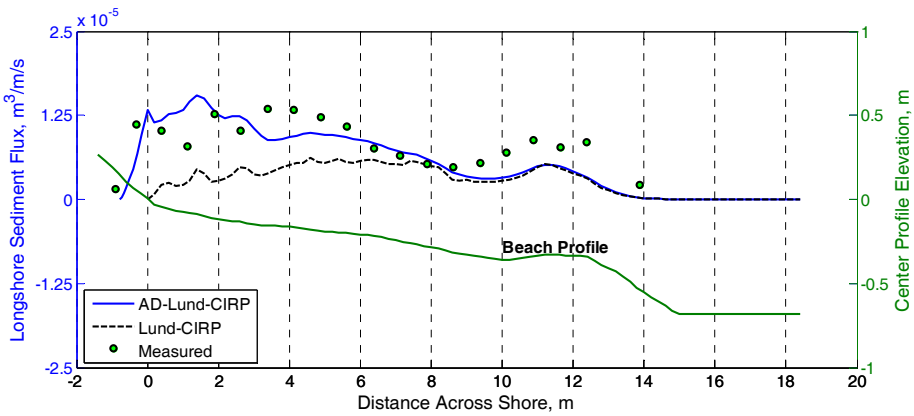

Fig. 17. Calculated and measured longshore sediment flux for Case BC4

Modifications of the pick-up and deposition rates are nessessary to accurately simulate the sediment transport rates in both the swash and inner surf zones. Without these

modifications, the results from the AD-Lund-CIRP formula decrease too quickly seaward from the still-water shoreline and similar results to Lund-CIRP formula is obtained in the inner surf zone and offshore zone. Thus, the introduced modifications make the simulated sediment transport rates more reasonable and improve the agreement with the observations from LSTF basin.

The bottom roughness is one of the parameters in calculations of sediment transport rate that the model is most sensitive to. Using total roughness, including grain-related roughness, form-drag roughness, and sediment-related roughness will produce shear stresses that may be used to calculate the sediment transport rate with some confidence. However, the formula for sediment-related roughness, given by Wilson (1966, 1989), is of implicit type and therefore an iterative method needs to be employed for solving the non-linear equation of sediment-related roughness. In this study, the Newton-Raphson method was used for solving this equation, yielding rapid convergence.

5.4 Morphological Evolution

The model validation of morphological evolution in the vicinity of detached breakwater and T-head groin based on the LSTF data sets are presented in **Paper IV**. Fig. 18 illustrates a comparison between the calculated and measured bed levels after 190 min for T1C4. The solid line represents the calculated bed level, whereas the dotted line shows the measurements. As can be seen, the simulated beach morphological evolution in the vicinity of the detached breakwater agreed rather well with the measurements, especially regarding the salient development in the lee of the breakwater.

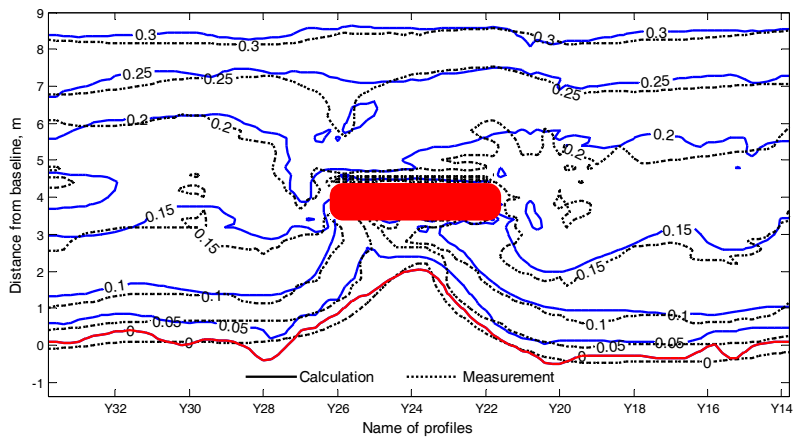

Fig. 18. Calculated and measured bed level after 190 min for Case T1C4

Fig. 19 shows the comparison between the calculated bed levels after 180 min and the measurements for T3C4. The computations showed that the beach evolution was fairly

well predicted; especially the shoreline change was in good agreement with the observations. However, the calculated sand accumulation downdrift the T-head groin exceeded what was observed in the data.

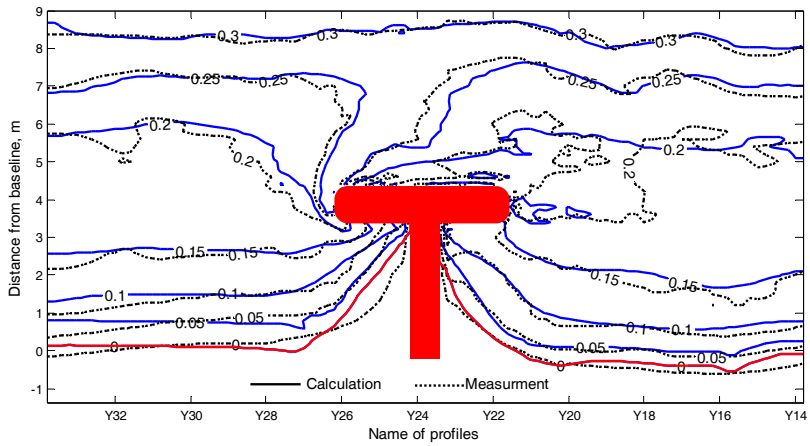

Fig. 19. Calculated and measured bed level after 180 min for Case T3C4

The prediction of beach morphological change strongly depends on not only the output of the models for waves, nearshore currents, and sediment transport, but also on the numerical method for solving the sediment volume conservation equation. Eq. (68) is a highly non-linear equation, and it is not easy to obtain a highly accurate solution. For example, many numerical models have employed the Lax-Wendroff scheme for solving this equation. However, this scheme suffers from the generation of nonphysical numerical oscillations (Hudson *et al.*, 2005; Long *et al.*, 2008). When this scheme is implemented, the bed celerity or bed form phase speed (Johnson and Zyserman, 2002; Long *et al.*, 2008) need to be determined, which may cause large errors in the calculations if the gradient of the bed form is relatively small. Johnson and Zyserman (2002) recommended smoothing and filtering techniques to overcome the dispersion problem associated with the Lax-Wendroff scheme. Recently, several high-order schemes were introduced by Callaghan *et al*. (2006) and Long *et al*. (2008) that can be applied to solve the continuity equation without resorting to smoothing or filtering techniques and that enable high accuracy in the solution. However, when calculating the value of the bed level at one cell, a number of values on the bed levels in nearby cells need to be included. Therefore, ghost cells must be employed at open and solid boundaries (Long *et al.*, 2008), which can cause significant errors if the coastal area is complex and coastal structures are present.

In this study, the first-order upwind scheme FTBS (forward in time, backward in space) was employed to solve the sediment conservation equation. Although the FTBS scheme has lower accuracy than high-order schemes, FTBS is stable and the obtained bed level changes were reasonable and in good agreement compared with the LSTF data. Furthermore, it is quite straightforward to implement and the model can be applied to

complex coastal areas including structures. However, smoothing is required in the present study. In future studies, more advanced numerical schemes will be investigated and applied in order to obtain accurate solutions to bed level change, at the same time as smoothing is avoided.

6 Conclusions

The main conclusions of this study can be summarized in the following points:

- A unified numerical model of beach morphological evolution due to waves and currents was developed. It includes five sub-models, including nearshore random wave transformation, surface roller, wave-induced current, sediment transport, and morphological change models. Each sub-model has been validated carefully against the high-quality data sets obtained from the LSTF basin. The model can be applied to simulate the beach evolution in the vicinity of coastal structures under wave and current action. Tidal water level variations were not included in the present study, but the model is prepared to handle this situation as well.

- The predictions of wave conditions in the surf zone were significantly improved after the energy dissipation term due to wave breaking was modified, providing reasonable and accurate wave conditions for the nearshore wave-induced current and sediment transport models.

- The importance of roller effects in calculation of wave-induced current was also investigated. The roller not only causes a shift in the peak of the longshore current towards the shoreline but it also increases the magnitude of the longshore current in the surf zone. By using a 2D surface roller model, energy conservation was expressed more accurately than for the 1D model.

- The predictions of longshore current were in good agreement with observations. However, the calculated cross-shore current was often underestimated compared to the measurements. The undertow current was not included in the model, which is probably the main cause of the discrepancy between calculations and measurements of the cross-shore current. The simulated wave setup somewhat overestimates the measured data, however, the absolute differences between calculations and measurements were relatively small.

- The computation of sediment transport rate in the swash zone needs to be included in models of beach morphological evolution. The sediment exchange between land and sea directly affects both the sub-aerial and sub-aqueous evolution of the beach. In the swash zone, the frequent uprush and backwash result in high transport rates in both the cross-shore and alongshore directions. Therefore, it is necessary to compute the transport rates in the swash zone, and couple those to the transport in the inner surf zone in order to realistically simulate the beach topography evolution. Prior to this work, studies on the swash zone transport were often undertaken separately from the inner surf zone, or not included at all in the modeling beach morphological evolution.

- Understanding the impacts of coastal structures on beach morphological evolution plays a key role in engineering projects for constructing harbors or preventing the

beach erosion. Thus, accurate predictions of hydrodynamics and morphological evolution in the vicinity of coastal structures are necessary and important. In this study, the developed model reproduced the beach evolution in the vicinity of the detached breakwater and the T-head groin rather well compared with the measurements from the LSTF data. In the future, the numerical model will be further validated against observed data from laboratories and the field, in order to improve and ensure the predictive capability of model. Finally, it is expected that the model can be applied in coastal engineering projects for predicting the beach evolution due to waves and currents in the vicinity of coastal structures.

7 References

Andersen, O.H., Hedegaard, I.B., Deigaard, R., de Girolamo, P., Madsen, P., 1988. Model for morphological changes under waves and current. In: *Proc. IAHR Symposium on Mathematical Modelling of Sediment Transport in the Coastal Zone*, Copenhagen. DHI, Horsholm, pp. 310-319.

Battjes, J.A., 1972. Setup due to irregular wave. *Proceedings 13th International Conference on Coastal Engineering*, ASCE, Vancouver, pp. 1993– 2004.

Battjes, J.A., 1975. Modeling of turbulence in the surf zone. *Proceedings 2nd Symposium on Modeling and Techniques*, ASCE, San Francisco, pp. 1050-1061.

Bayram, A., Larson, M., Miller, H.C., Kraus, N.C., 2001. Cross-shore distribution of longshore sediment transport: comparison between predictive formulas and field measurements. *Coastal Engineering* 44, 79-99.

Booij, N., Holthuijsen, L.H., Ris, R.C., 1996. The 'SWAN' wave model for shallow water. *Proceedings 25th International Conference on Coastal Engineering*, ASCE, Orlando, pp. 668–676.

Booij, N., Holthuijsen, L.H, Doorn, N., Kieftenburg, A. T. M. M., 1997. Diffraction in a spectral wave model. *Proc. 3rd Int. Symposium Ocean Wave Measurement and Analysis Wave '97*, ASCE, New York, pp. 243-255.

Bouws, E., Günther, H., Rosenthal, W., Vincent, C. L., 1985. Similarity of the wind wave spectrum in finite depth water 1. Spectral Form. *J. Geophys. Res.*, 90(C1), 975–986, doi:10.1029/JC090iC01p00975.

Bowen, A.J., 1969. The generation of longshore currents on a plane beach. *Journal of Marine Research* 27 (2), 206-215.

Brøker, I., Zyserman, J., Madsen, E. Ø., Mangor, K., Jensen, J., 2007. Morphological modelling: a tool for optimisation of coastal structures. *Journal of Coastal Research* 23(5), 1148-1158.

Callaghan, D.P., Saint-Cast, F., Nielsen, P., Baldock, T.E., 2006. Numerical solutions of the sediment conservation law; a review and improved formulation for coastal morphological modelling. *Coastal Engineering* 53, 557-571.

Camenen, B., Larroude, P., 2003. Comparison of sediment transport formulae for the coastal environment. *Coastal Engineering* 48, 111-132.

Camenen, B., Larson, M., 2005. A general formula for non-cohesive bed load sediment transport. *Estuarine, Coastal and Shelf Science* 63, 249-260.

Camenen, B., Larson, M., 2007. A unified sediment transport formulation for coastal inlet application. *Technical report ERDC/CHL CR-07-1*, US Army Engineer Research and Development Center, Vicksburg, MS.

Camenen, B., Larson, M., 2008. A general formula for noncohesive suspended sediment transport. *Journal of Coastal Research* 24(3), 615-627.

CHL official website. http://chl.erdc.usace.army.mil/lstf (28 October, 2010).

Dally, W. R., Brown, C. A., 1995. A modeling investigation of the breaking wave roller with application to cross-shore currents. *Journal of Geophysical Research* 100(C12), 24873-24883.

Dally, W. R., Dean, R. G., Dalrymple, R. A., 1985. Wave height variation across beaches of arbitrary profile. *Journal of Geophysical Research* 90(C6), 11917-11927.

Dally, W. R., Osiecki, D. A., 1994. The role of rollers in surf zone currents. *Proceedings 24th International Conference on Coastal Engineering*, ASCE, Kobe, pp. 1895-1905.

De Vriend, H.J. , Bakker, W.T., Bilse, D.P., 1994. A morphological behaviour model for the outer delta of mixed-energy tidal inlets. *Coastal Engineering* 23, 305-327.

De Vriend, H.J., Zyserman, J., Nicholson, J., Roelving, J.A., Péchon, P., Southgate, H.N., 1993. Medium-term 2DH coastal area modeling. *Coastal Engineering* 21, 193-224.

Deigaard, R., Justesen, P., Fredsoe, J., 1991. Modeling of undertow by one-equation turbulence model. *Coastal Engineering* 15, 431-458.

Denot, T., Aelbrecht, D., 1999. Numerical modelling of seabed evolution in the vicinity of a groin system. *Proc. Coastal Structures'99*, A.A. Balkema, Vol. 2, pp. 849-855.

Ding, Y., Wang, S.S.Y., Jia, Y., 2006. Development and validation of a quasi-three-dimensional coastal area morphological model. *Journal of Waterway, Port, Coastal and Ocean Engineering* 132(6), 462-476.

Ding, Y., Wang, S.S.Y., 2008. Development and application of coastal and estuarine morphological process modeling system. *Journal of Coastal Research*, *Special Issue* 52, 127-140.

Drønen, N., Deigaard, R., 2007. Quasi-three-dimensional modelling of the morphology of longshore bars. *Coastal Engineering* 54, 197-215.

Duncan, J.H., 1981. An experimental investigation of breaking waves produced by a towed hydrofoil. In: *Proc. R. Soc. London*, A377, pp. 331-348.

Elder, J.W., 1959. The dispersion of marked fluid in turbulent shear flow. *Journal of Fluid Mechanics* 5, 544-560.

Elfrink, B., Baldock, T., 2002. Hydraudynamics and sediment transport in the swash zone: a review and perspectives. *Coastal Engineering* 45, 149-167.

Falconer, R. A., 1980. Modelling of planform influence on circulation in harbors. *Proceedings 17th International Conference on Coastal Engineering*, ASCE, Sydney, pp. 2726-2744.

Gelfenbaum, G., Roelvink, J.A., Meijs, M., Buijsman, M., Ruggiero, P., 2003. Process-based morphological modeling of Gray Harbor inlet at decadal timescales. *Proceedings of Coastal Sediments'03*.

Gobbi, M.F., Kirby, J.T., Wei, G., 2000. A fully nonlinear Boussinesq model for surface waves. Part 2. Extension to $O(kh)^4$. *J. Fluid Mech.* 405, 181-210.

Goda, Y., 2000. *Random sees and design of maritime structures*. World Scientific Press, Singapore, 464 pp.

Goda, Y., 2006. Examination of the influence of several factors on longshore current computation with random waves. *Coastal Engineering* 53, 157-170.

Gravens, M.B., 1996. Approach to modeling inlet and beach evolution. *Proceedings 25th International Conference on Coastal Engineering*. ASCE, Orlando, pp. 4477–4490.

Gravens, M.B., Wang, P., 2007. Data report: Laboratory testing of longshore sand transport by waves and currents; morphology change behind headland structures. *Technical Report, ERDC/CHL TR-07-8*, Coastal and Hydraulics Laboratory, US Army Engineer Research and Development Center, Vicksburg, MS.

Gravens, M.B., Wang, P., Kraus, N.C., Hanson, H., 2006. Physical model investigation of morphology development at headland structures. *Proceedings 30th International Conference on Coastal Engineering*, World Scientific Press, pp. 3617–3629.

Hamilton, D.G., Ebersole, B.A., 2001. Establishing uniform longshore currents in large-scale sediment transport facility. *Coastal Engineering* 42 (3), 199-218.

Hanson, H., Aarninkhof, S, Capobianco, M., Jimenez, J.A., Larson, M., Nicholls, R.J., Plant, N.G., Southgate, H.N., Steetzel, H.J., Stive, M.J.F., de Vriend, H.J., 2003. Modelling of Coastal Evolution on Yearly to Decadal Time Scales. *Journal of Coastal Research* 19(4), 790-811.

Hanson, H., Kraus, N. C., 1989. GENESIS: Generalized model for simulating shoreline change, Report 1: Technical Reference. *Technical Report CERC-89-19*, U.S. Army Engineer Waterways Experiment Station, Coastal Engineering Research Center, Vicksburg, MS.

Hanson, H., Larson, M. 1992. Overview of beach change numerical modeling. In: *W. James and J. Niemczynowicz, Eds., Water, Development, and Environment*, Lewis Publishers, Ann Arbor, pp 322-347.

Hasselmann, K., Bamett, T.P., Bouws, E., Carlson, H., Cartwright, D.E., Enke, K., Ewing, J.A., Gienapp, H., Hassetmann, D.E., Kruseman, P., Meerburg, A., Mfiller, P., Olbers, K.J., Richter, K., Sell, W., Walden, W.H., 1973. Measurements of wind-wave growth and swell decay during the Joint North Sea Wave Project (JONSWAP). *Deutsche Hydrograph, Zeit., Erganzung-se&Reihe A* 8(12).

Hedges, T.S., Mase, H., 2004. Modified Hunt's equation incorporating wave setup. *Journal of Waterway, Port, Coastal and Ocean Engineering* 130 (3), 109-113.

Holman, R.A., 1986. Extreme value statistics for wave run-up on a natural beach. *Coastal Engineering* 9, 527–544.

Holthuijsen, L.H., Herman, A., Booij, N., 2003. Phase-decoupled refraction-diffraction for spectral wave models. *Coastal Engineering* 49, 291-305.

Hoffman, J.D., 2001. *Numerical methods for engineers and scientists* (2nd edition). Marcel Dekker, Inc., USA, 823 pp.

Houston, J.R., 2003. The coastal structure debate – public & policy aspects. In: *Mohan, K., Magoon, O., Pirrello (Ed), Advances in Coastal Structure Design*, ASCE, pp. 1-17.

Hudson, J., Damgaard, J., Dodd, N., Chesher, T., Cooper, A., 2005. Numerical approaches for 1D morphodynamic modeling. *Coastal Engineering* 52, 691– 707.

Hunt, I.A., 1959. Design of seawalls and breakwaters. *Journal of Waterways and Harbors Division* 85, 123-152.

Johnson, H.K., 1994. A General 2DH Coastal Morphology Modelling System - M21MORF. *DHI Water and Environment*, Denmark, Hørsholm. 64 pp.

Johnson, H.K., 2004. Coastal area morphological modelling in the vicinity of groins. *Proceedings 29th International Conf. on Coastal Engineering*, ASCE, pp. 2646-2658.

Johnson, H. K., Brøker, I. and Zyserman, J. A. 1994. Identification of some relevant processes in coastal morphological modeling. *Proceedings 24th International Conference on Coastal Engineering*, ASCE, Kobe, Japan, pp. 2871-2885.

Jonhson, H.K., Zyserman, J.A., 2002. Controlling spatial oscillations in bed level update schemes. *Coastal Engineering* 46, 109-126.

Johnson, H.K., Zyserman, J.A., Brøker, I., Mocke, G., Smit, F., Finch, D., 2005. Validation of a coastal area morphological model along the Dubai coast. *Proceedings of Arabian Coast 2005*, Dubai.

Kana, T.W., Hayter, E.J., Work, P.A., 1999. Mesoscale sediment transport at southeastern US tidal inlets: conceptual model applicable to mixed energy settings. *Journal of Coastal Research* 15 (2), 303–313.

Kobayashi, N., 2003. Numerical modeling as a design tool for coastal structures. In: *Mohan, K., Magoon, O., Pirrello (Ed), Advances in Coastal Structure Design*, ASCE, pp. 80-96.

Koutitas, C.G., 1988. *Mathematical models in coastal engineering*. Pentech Press, London, England, 156 pp.

Kraus, N.C., 2000. Reservoir model of ebb-tidal shoal evolution and sand bypassing. *Journal of Waterway, Port, Coastal, and Ocean Engineering* 126 (6), 305–313.

Kraus, N. C., Larson, M., 1991. NMLONG: Numerical model for simulating the longshore current; Report 1: Model development and tests. *Technical Report DRP-91-1*, U.S. Army Engineer Waterways Experiment Station, Vicksburg, MS.

Larson, M., Kraus, N.C., 1989. SBEACH: Numerical Model for Simulating Storm-Induced Beach Change; Report 1 - Empirical Foundation and Model Development. *Technical Report CERC-TR-89-9-RPT-1,* U.S. Army Engineer Waterways Experiment Station, Coastal Engineering Research Center, Vicksburg, MS.

Larson, M., Kraus, N.C., 2002. NMLONG: Numerical model for simulating longshore current; Report 2: Wave-current interaction, roller modeling, and validation of model enhancements. *Technical Report ERDC/CHL TR-02-22*, US Army Engineer Research and Development Center, Vicksburg, MS.

Larson, M., Kraus, N.C., Byrnes, M.R., 1989. SBEACH: Numerical Model for Simulating Storm-Induced Beach Change; Report 2 - Numerical Formulation and Model Tests. *Technical Report CERC-TR-89-9-RPT-2*, Army Engineer Waterways Experiment Station, Coastal Engineering Research Center, Vicksburg, MS.

Larson, M., Kubota, S., Erikson, L., 2004. Swash-zone sediment transport and foreshore evolution: field experiments and mathematical modeling. *Marine Geology* 212, 61-79.

Larson, M., Wamsley, T.V., 2007. A formula for longshore sediment transport in the swash. *Proceedings Coastal Sediments '07*, ASCE, New Orleans, pp. 1924-1937.

Latteux, B., 1980. Harbour design including sedimentological problems using mainly numerical techniques. *Proceedings 17th International Conference on Coastal Engineering*, ASCE, Sydney, pp. 2213-2229.

Leont'yev, I.O., 1999. Modelling of morphological changes due to coastal structures. *Coastal Engineering* 38, 143-166.

Lesser, G.R., Roelvink, J.A, van Kester, J.A.T.M., Stelling, G.S., 2004. Development and validation of a three-dimensional morphological model. *Coastal Engineering* 51, 883-915.

Lin, L., Demirbilek, Z., Mase, H., Zheng, J., Yamada, F., 2008. CMS-Wave: A Nearshore Spectral Wave Processes Model for Coastal Inlets and Navigation Projects. *Technical Report ERDC/CHL TR-08-13*, US Army Engineer Research and Development Center, Vicksburg, MS.

Lippmann, T.C., Brookins, A.H., Thornton, E.B., 1996. Wave energy transformation on natural profiles. *Coastal Engineering* 27, 1-20.

Long, W., Kirby, J.T., Shao, Z., 2008. A numerical scheme for morphological bed level calculations. *Coastal Engineering* 55, 167-180.

Longuet-Higgins, M.S., 1970. Longshore current generated by obliquely incident sea waves. *Journal of Geophysical Research* 75 (33), 6779–6801.

Longuet-Higgins, M.S., Stewart, R.W., 1964. Radiation stresses in water waves; a physical discussion with applications. *Deep Sea Research* 11, 529-562.

Maruyama, K., Takagi, T., 1988. A simulation system of near-shore sediment transport for the coupling of the sea-bottom topography, waves and currents. In: *Proc. IAHR Symposium on Mathematical Modelling of Sediment Transport in the Coastal Zone*, Copenhagen, pp. 300-309.

Madsen, P.A., Murray, R. Sorensen, O.R., 1991. A new form of the Boussinesq equations with improved linear dispersion characteristics. *Coastal Engineering* 15, 371-388.

Madsen, P.A., Sorensen, O.R., Schäffer, H.A., 1997. Surf zone dynamics simulated by a Boussinesq type model. Part II: surf beat and swash oscillations for wave groups and irregular waves. *Coastal Engineering* 32, 289-319.

Madsen, P.A., Warren, I.R., 1984. Performance of a numerical short-wave model. *Coastal Engineering* 8, 73-93.

Mase, H., 1988. Spectral characteristics of random wave run-up, *Coastal Engineering* 12, 175-189.

Mase, H., 2001. Multi-directional random wave transformation model based on energy balance equation. *Coastal Engineering Journal* 43(4), 317-337.

Mase, H., Oki, K., Hedges, T.S., Li, H. J., 2005. Extended energy-balance-equation wave model for multidirectional random wave transformation. *Ocean Engineering* 32, 961–985.

Mayer, R.H., Kribel, D.L., 1994. Wave runup on composite-slope and concave beaches. *Proceedings 24th International Conference of Coastal Engineering*, ASCE, 2325-2339.

Militello, A., Reed, C.W., Zundel, A.K., Kraus, N.C., 2004. Two-dimensional depth-averaged circulation model M2D: version 2.0, Report 1, Technical document and User's Guide. *Technical Report ERDC/CHL TR-04-2*, Coastal and Hydraulics Laboratory, US Army Engineer Research and Development Center, Vicksburg, MS.

Militello, A., Reed, C.W., Kraus, N.C., Ono, N., Larson, M., Camenen, B., Hanson, H., Wamsley, T., Zundel, A.K., 2006. Two-dimensional depth-averaged circulation Model CMS-M2D: Version 3.0, Report 2,Sediment Transport and Morphology Change. *Technical Report ERDC/CHL TR-06-9*, Coastal and Hydraulics Laboratory, US Army Engineer Research and Development Center, Vicksburg, MS.

Nairn, R.B., Roelvink, J.A., Southgate, H.N., 1990. Transition zone width and implications for modeling surfzone hydrodynamics. *Proceedings 22nd International Conference on Coastal Engineering*, ASCE, Delft, pp. 68– 81.

Nairn, R.B., Southgate, H.N., 1993. Deterministic profile modelling of nearshore processes. Part 2. Sediment transport and beach profiledevelopment. *Coastal Engineering* 19(1–2), 57–96.

Nam, P.T., Larson, M., Hanson, H., Hoan, L.X., 2009. A numerical model of nearshore waves, currents, and sediment transport. *Coastal Engineering* 56, 1084-1096.

Nam, P.T., Larson, M., 2009. A model of wave and current fields around coastal structures. *Proc. Coastal Dynamics 2009*, World Scientific Press, ISBN-13-978-981-4282-46-8 (with CD-ROM)

Nam, P.T., Larson, M., 2010. Model of nearshore waves and wave-induced currents around a detached breakwater. *Journal of Waterway, Port, Coastal and Ocean Engineering* 136 (3), 156-176.

Nicholson, J., Broker, I., Roelvink, J.A., Price, D., Tanguy, J.M., Moreno, L., 1997. Intercomparison of coastal area morphodynamic models. *Coastal Engineering* 31, 97-123.

Nishimura, H., 1988. Computation of nearshore current. In: *Horikawa, K. (Ed), Nearshore dynamics and coastal processes*. University of Tokyo Press, Tokyo, Japan, pp. 271-291.

Nwogu, O., 1993. Alternative form of Boussinesq equations for nearshore wave propagation. *Journal of Waterway, Port, Coastal, and Ocean Engineering* 119 (6), 618-638.

Pelnard-Considere, R., 1956. Essai de Theorie de l'Evolution des Forms de Rivages en Plage de Sable et de Galets. *Fourth Journees de l'Hydralique*, *les energies de la Mer*, Question III, Rapport No. 1., pp. 289–298.

Radder, A.C., 1979. On the parabolic equation method for water wave propagation. *J. Fluid Mech.* 95 (1), 159–176.

Reid, R.O., Bodine, B.R., 1968. Numerical model for storm surges in Galveston Bay. *Journal of Waterways and Harbors Division* 94 (WWI), 33-57.

Reniers, A.J.H.M., Battjes, J.A., 1997. A laboratory study of longshore currents over barred and non-barred beach. *Coastal Engineering* 30, 1-22.

Rivero, F.J., Arcilla, A.S, Carci, E., 1997. Analysis of diffraction in spectral wave models. *Proc. 3rd Int. Symposium Ocean Wave Measurement and Analysis Wave '97*, ASCE, New York, pp. 431-445.

Roelvink, J.A., Banning, G.K.F.M.v., 1994. Design and development of DELFT3D and application to coastal morphodynamics. In: *Verwey, Minns, Babovic, Maksimovic (Eds.), Proceeding of Hydroinformatics '94 Conference*. Balkema, Rotterdam, pp. 451–455.

Roelvink, D., Reniers, A., van Dongeren, A., van Thiel de Vries, J., McCall, R., Lescinski, J., 2010. Modelling storm impacts on beaches, dunes and barrier islands. *Coastal Engineering* 56, 1133-1152.

Roelvink, J.A., Uittenbogaard, R.E., Liek, G.J., 1999. Morphological modelling of the impact of coastal structures. *Proc. Coastal Structures'99*, A.A. Balkema, Vol. 2, pp.865-871.

Ruessink, B.G., Miles, J.R, Feddersen, F., Guza, R.T., Elgar, S., 2001. Modeling the alongshore current on barred beaches. *Journal of Geophysical Reseach* 106 (C10), 22451-22463.

Ruessink, B.G., Terwindt, J.H.J., 2000. The behaviour of nearshore bars on the time scale of years: a conceptual model. *Marine Geology* 163, 289–302.

Saied, U.M., Tsanis, I.K., 2005. ICEM: Integrated Coastal Engineering Model. *Journal of Coastal Research* 21(6), 1275-1268.

Soulsby, D. H., 1997. *Dynamics of marine sands: A manual for practical applications*. Thomas Telford Publications, London, England, 249 pp.

Soulsby, R.L., Whitehouse, R.J.S.W., 1997. Threshold of sediment motion in coastal environments. *Proceedings of Pacific Coasts and Ports '97 Conference*, Christchurch, Vol. 1, pp. 149-154.

Steetzel, H.J., de Vroeg, H., van Rijn, L.C., Stam, J.-M., 2000. Long-term modelling of the Holland coast using a multi-layer model. *Proceedings 27th International Conference on Coastal Engineering*. ASCE, Sydney, Australia, pp. 2942–2955.

Steijn, R., Roelvink, D., Rakhorst, D., Ribberink, J., Overeem, J.V., 1998. North-Coast of Texel: A comparison between reality and prediction. *Proceedings 26th International Conference on Coastal Engineering*, ASCE, pp. 2281-2293.

Stive, M.J.F., De Vriend, H.J., 1994. Shear stresses and mean flow in shoaling and breaking waves. *Proceedings 24th International Conference on Coastal Engineering*, ASCE, Kobe, pp. 594-608.

Stockdon, H.F., Holman, R.B., Howd, P.A., Sallenger Jr., A.H., 2006. Empirical parameterization of setup, swash, and runup. *Coastal Engineering* 53, 573-588.

Svendsen, I.A., 1984a. Wave heights and set-up in a surf zone. *Coastal Engineering* 8, 303-329.

Svendsen, I.A., 1984b. Mass flux and undertow in a surf zone. *Coastal Engineering* 8, 347-365.

Swart, D. H., 1974. Offshore sediment transport and equilibrium beachprofiles. *Delft Hydraulics Laboratory Publications* 131, Delft, The Netherlands, 302 pp.

Takayama, T., Ikeda, N., Hiraishi, T., 1991. Wave transformation calculation considering wave breaking and reflection. *Rept. Port Harbor Res. Inst.* 30 (1), 21–67.

Tajima, Y., Madsen, O.S., 2006. Modeling near-shore waves, surface rollers, and undertow velocity profiles. *J. Waterway, Port, Coastal, and Ocean Eng.* 132 (6), 429 – 438.

Thornton, E.B., 1970. Variation of longshore current across the surf zone. *Proceedings 12th International Conference on Coastal Engineering*, ASCE, Washington D.C., pp. 291-308.

Thornton, E.B., Guza, R.T., 1983. Transformation of wave height distribution. *Journal of Geophysical Research* 88 (C10), 5925– 5938.

Thornton, E.B., Guza, R.T., 1986. Surf zone longshore currents and random waves: field data and models. *Journal of Physical Oceanography* 16, 1165– 1178.

Van Dongeren, A., Reniers, A., Battjes, J., 2003. Numerical modeling of infragravity wave response during DELIAH. *Journal of Geophysical Research* 108 (C9), 3288, doi: 10.1029/2002JC001332.

Van Dongeren, A., Sancho, F.E., Svendsen, I.A., Putrevu, U., 1994. SHORECIRC: a quasi 3-D nearshore model. *Proceedings 24th International Conference on Coastal Engineering*, ASCE, Kobe, pp. 2741-2754.

Van Dongeren, A., Svendsen, I.A., 2000. Nonlinear and 3D effects in leaky infragravity waves. *Coastal Engineering* 41, 467-496.

Van Rijn, L., 1993. *Principles of sediment transport in rivers, estuaries, andcoastal seas*. Aqua Publications, Amsterdam, The Netherlands, 673 pp.

WAMDI group, 1988. The WAM model-a third generation ocean wave prediction model. *Journal of Physical Oceanography* 18, 1775–1810.

Wang, P., Ebersole, B.A., Smith, E.R., Johnson, B.D., 2002a. Temporal and spatial variations of surf-zone currents and suspended sediment concentration. *Coastal Engineering* 46, 175-211.

Wang, P., Smith, E.R., Ebersole, B.A., 2002b. Large-scale laboratory measurements of longshore sediment transport under spilling and plunging breakers. *Journal of Coastal Research* 18(1), 118-135.

Watanabe, A., 1987. 3-Dimensional Numerical Model of Beach Evolution. *Proceeding of the Conference on Coastal Sediments'87*, ASCE, pp. 802-817.

Watanabe, A., 1988. Numerical model of beach topography change. In: *Horikawa, K. (Ed), Nearshore dynamics and coastal processes*. University of Tokyo Press, Tokyo, Japan, pp. 241-243.

Watanabe, A., Maruyama, K., Shimizu, T., Sakakiyama, T, 1986. Numerical prediction model of three-dimensional beach deformation around a structure. *Coastal Engineering Journal* 29, 179-194.

Wei, G., Kirby, J.T., Grilli, S.T., Subramanya, R., 1995. A fully nonlinear Boussinesq model for surface waves. Part 1: Highly nonlinear unsteady waves. *J. Fluid Mech.* 294, 71–92.

Wilson, K., 1966. Bed-load transport at high shear stress. *Journal of the Hydraulics Division* 92(11), 49-59.

Wilson, K.C., 1989. Friction of wave-induced sheet flow. *Coastal Engineering* 12, 371–379.

Zanuttigh, B., 2007. Numerical modelling of the morphological response induced by low-crested structures in Lido di Dante, Italy. *Coastal Engineering* 54, 31-47.

Zyserman, J.A., Johnson, H.K., 2002. Modelling morphological processes in the vicinity of shore-parallel breakwaters. *Coastal Engineering* 45, 261-284.

Zyserman, J.A., Johnson, H.K., Zanuttigh, B., Martinelli, L., 2005. Analysis of far-field erosion induced by low-crested rubble-mound structures. *Coastal Engineering* 52, 977-994.

Paper I

A numerical model of nearshore waves, currents, and sediment transport

Nam, P.T., Larson, M., Hanson, H., Hoan, L.X., 2009.

In: *Coastal Engineering*, Vol. 56, 1084-1096.

Coastal Engineering 56 (2009) 1084–1096

Contents lists available at ScienceDirect

Coastal Engineering

journal homepage: www.elsevier.com/locate/coastaleng

A numerical model of nearshore waves, currents, and sediment transport

Pham Thanh Nam [a,b,*], Magnus Larson [a], Hans Hanson [a], Le Xuan Hoan [a,b]

[a] Department of Water Resources Engineering, Lund University, Box 118, S-22100, Lund, Sweden
[b] Center for Marine Environment, Research and Consultation, Institute of Mechanics, Vietnamese Academy of Science and Technology, 264 Doi Can, Hanoi, Vietnam

ARTICLE INFO

Article history:
Received 29 August 2008
Received in revised form 9 April 2009
Accepted 15 June 2009
Available online 27 August 2009

Keywords:
Mathematical modeling
Random wave
Nearshore current
Swash zone
Sediment transport
Surface roller

ABSTRACT

A two-dimensional numerical model of nearshore waves, currents, and sediment transport was developed. The multi-directional random wave transformation model formulated by Mase [Mase, H., 2001. Multi-directional random wave transformation model based on energy balance equation. Coastal Engineering Journal 43(4), 317-337.] based on an energy balance equation was employed with an improved description of the energy dissipation due to breaking. In order to describe surface roller effects on the momentum transport, an energy balance equation for the roller was included following Dally and Brown [Dally, W.R., Brown, C.A., 1995. A modeling investigation of the breaking wave roller with application to cross-shore currents. Journal of Geophysical Research 100(C12), 24873-24883.]. Nearshore currents and mean water elevation were modeled using the continuity equation together with the depth-averaged momentum equations. Sediment transport rates in the offshore and surf zone were computed using the sediment transport formulation proposed by Camenen and Larson [Camenen, B., Larson, M., 2005. A general formula for non-cohesive bed load sediment transport. Estuarine, Coastal and Shelf Science 63, 249-260.; Camenen, B., Larson, M., 2007. A unified sediment transport formulation for coastal inlet application. Technical report ERDC/CHL CR-07-1, US Army Engineer Research and Development Center, Vicksburg, MS.; Camenen, B., Larson, M., 2008. A general formula for non-cohesive suspended sediment transport. Journal of Coastal Research 24(3), 615-627.] together with the advection–diffusion equation, whereas the swash zone transport rate was obtained from the formulas derived by Larson and Wamsley [Larson, M., Wamsley, T.V., 2007. A formula for longshore sediment transport in the swash. Proceedings Coastal Sediments '07, ASCE, New Orleans, pp. 1924–1937.]. Three high-quality data sets from the LSTF experimental facility at the Coastal and Hydraulics Laboratory in Vicksburg, USA, were used to evaluate the predictive capability of the model. Good agreement between computations and measurements was obtained with regard to the cross-shore variation in waves, currents, mean water elevation, and sediment transport in the nearshore and swash zone. The present model will form the basis for predicting morphological evolution in the nearshore due to waves and currents with special focus on coastal structures.

1. Introduction

Accurate predictions of waves, nearshore currents, and sediment transport play a key role in solving coastal engineering problems, especially those related to beach morphological evolution. Waves and currents mobilize and transport sediment, and gradients in the transport cause deposition or erosion of sediment, affecting the local topography. Gradients in transport rate may occur naturally or be induced by man-made structures and activities such as groins, seawalls, detached breakwaters, dredging, and beach nourishment. In order to predict the beach morphological evolution for the purpose of engineering analysis and design, a robust model of nearshore waves, currents, and sediment transport is required.

There have been a number of studies on numerical modeling of nearshore waves, currents, and sediment transport (a brief review of relevant previous work is described in the next section). However, hydrodynamic and sediment transport processes are highly complex in the nearshore and swash zone, and presently there is no general model that yields robust and reliable predictions to be used in engineering studies for a wide range of conditions. Furthermore, the lack of high-quality and synchronized experimental data makes model validation difficult.

The overall objective of this study was to develop a robust and reliable numerical model of nearshore waves, currents, and sediment transport which can be applied in coastal engineering projects. First, the present paper discusses modifications of a multi-directional random wave transformation model (EBED), which was originally developed by Mase (2001), to improve the predictive capability of wave properties in the surf zone. Then, a model for nearshore currents due to random waves in the nearshore zone is developed. In order to make this model applicable for a

* Corresponding author. Department of Water Resources Engineering, Lund University, Box 118, S-22100, Lund, Sweden.
E-mail address: Thanh_Nam.Pham@tvrl.lth.se (P.T. Nam).

0378-3839/$ – see front matter © 2009 Elsevier B.V. All rights reserved.
doi:10.1016/j.coastaleng.2009.06.007

variety of conditions including complex alongshore bathymetry, a general depth-averaged two-dimensional model of the nearshore currents due to breaking waves and tides was formulated, although in this paper the focus is on the wave-induced currents. The two-dimensional creation and evolution of the surface roller in connection with wave breaking is modeled based on a period-averaged energy balance, as proposed by Dally and Osiecki (1994), Dally and Brown (1995), and Larson and Kraus (2002). Finally, a model to calculate the sediment transport in the nearshore zone, including the surf and swash zones, is developed based on the transport formulation by Camenen and Larson (2005, 2007, 2008), Larson and Wamsley (2007), and the advection–diffusion equation. The present model will subsequently form the basis for calculating beach topography change due to waves and currents.

The paper is structured as follows: Section 2 provides a brief review of previous work relevant to the present model development. In Section 3 the model description is given, including the four sub-models: (1) the wave model; (2) the surface roller model; (3) the nearshore wave-induced current model; and (4) the sediment transport model. Section 4 briefly describes the data sets employed from the Large-Scale Sediment Transport Facility (LSTF) basin of the Coastal and Hydraulics Laboratory (CHL), U.S. Army Engineer Research and Development Center (ERDC), in Vicksburg, United States. Section 5 summarizes the results of detailed model comparison with these data sets. Section 6 encompasses a discussion on various modeling results pertaining to the wave energy dissipation, surface roller and lateral mixing effects, bottom roughness height, suspended transport obtained by advection–diffusion equation, and sediment transport in swash zone. Finally, the conclusions are given in Section 7.

2. Review of relevant previous work

Waves in coastal areas display random characteristics; thus, random wave models are needed to properly assess the wave environment. Random wave transformation models can be classified into (i) phase-resolving models, and (ii) phase-averaging models. The first type of model, for example the ones based on the Boussinesq equations, is expressed through the conservation equations of mass and momentum (Madsen and Warren, 1984, Madsen et al., 1991, 1997; Nwogu, 1993). These models describe the main physical processes in the coastal area (e.g., shoaling, diffraction, refraction, and dissipation) at the intra-wave scale. Thus, they require fine resolution in space and time and, therefore, their applications are often only suitable for small coastal areas and short-term simulations. On the other hand, phase-averaging models, commonly based on the energy balance equation, describe slowly varying wave quantities (for example, wave amplitude and wave energy) on the scale of a wavelength. Thus, they can be applied for the prediction of multi-directional random wave transformation over large coastal areas. Originally, the non-stationary wave models WAM (WAMDI group, 1988) and SWAN (Booij et al., 1996) were based on phase-averaged equations including source terms. However, diffraction was not included in these models. Then, several attempts have been made in order to include diffraction effects in the phase-averaging wave model. For example, diffraction effects were included into the characteristic velocities through the wave number containing the second derivative of wave amplitude with respect to the spatial coordinates (Booij et al., 1997; Rivero et al., 1997; Holthuijsen et al., 2003). Although these models can be applied in the coastal zone containing structures, the numerical schemes seem to be unstable, especially for the discontinuities and singularities occurring (see Holthuijsen et al., 2003).

Mase (2001) developed a random wave transformation model called EBED in which diffraction effect was included. The diffraction term was derived from a parabolic approximation of the wave equation. The numerical scheme is stable and the model can be applied for complex coastal areas with structures. In the present study, the EBED model was employed to calculate wave transformation after modifications to more accurately predict the wave conditions in the surf zone. Although, structures were not included in the investigated data of this study, the long-term objective is to model the hydrodynamics and morphological evolution in the vicinity of structures. Therefore, it is necessary to employ a wave model that includes diffraction.

There have been a number of numerical models for wave-driven currents after the concept of radiation stress was introduced by Longuet-Higgins and Stewart (1964). Early simulations of longshore current induced by regular waves, for a simple plan form beach, were carried out by Bowen (1969), Longuet-Higgins (1970), and Thornton (1970). The disadvantage of these semi-analytic models is the occurrence of an abrupt change in longshore current at the break point. By introducing an eddy viscosity term (i.e., lateral mixing) in the momentum equation for the longshore current, the physically unrealistic current distribution at the breaker-line was eliminated. Since the early models, significant progress has been made concerning nearshore currents generated by random waves. The pioneering work of Battjes (1972) illustrated that the longshore current generated by random waves is smooth in the surf zone, even though the lateral mixing term is not included. Thornton and Guza (1986) presented a model for the longshore current based on their random wave breaking model (Thornton and Guza, 1983). Van Dongeren et al. (1994, 2003), and Van Dongeren and Svendsen (2000) developed a quasi-3D nearshore hydrodynamic model named SHORECIRC, which is capable of describing several phenomena such as the edge waves, surf beats, infragravity waves, and longshore current. Kraus and Larson (1991), Larson and Kraus (2002) developed the NMLong model for computing the longshore current focusing on barred beaches. Militello et al. (2004) developed the M2D model for simulating the nearshore current due to tide, waves, wind, and rivers. Recently, Goda (2006) examined the influence of several factors on the longshore current under random waves. He demonstrated that significant differences in wave height and longshore velocity resulted depending on the employed random wave breaking model. Thus, selecting a wave model that can accurately simulate surf-zone conditions is important when computing wave-induced nearshore currents.

Much research has demonstrated that the surface roller plays an important role in generating nearshore currents. The roller was initially investigated in the laboratory by Duncan (1981) and first applied theoretically by Svendsen (1984a,b) to improve the modeling of wave setup and undertow in the surf zone. Then, the roller model, including the roller energy gradients in the energy flux balance based on the roller theory of Svendsen (1984a,b), was employed in many studies related to wave-induced currents (e.g. Nairn et al., 1990; Deigaard et al., 1991; Stive and De Vriend, 1994; Lippmann et al., 1996; Reniers and Battjes, 1997; Ruessink et al., 2001). Van Dongeren et al. (2003) extended the roller energy flux balance equation derived by Nairn et al. (1990), and they obtained calculations of longshore current that were in good agreement with the data from the DELILAH field experiment. Based on the depth-integrated and period-averaged energy balance equation, Dally and Osiecki (1994), and Dally and Brown (1995) developed a roller model for the evolution of the roller itself. Larson and Kraus (2002) applied this model in NMLong to improve longshore current simulations. In the energy balance equation, the energy dissipation per unit area after Dally et al. (1985) was used instead of the gradient in the depth-integrated time-averaged wave-induced energy flux in the x-direction. In general, the roller energy flux is only considered in the cross-shore direction in the balance equation. In the present study, the approaches by Dally and Brown (1995) and Larson and Kraus (2002) were followed, and the energy flux term in alongshore direction was included in the energy balance equation for the evolution of the roller itself.

Calculating sediment transport in the nearshore zone is a challenge because of the complexity of the hydrodynamics and the variety of governing phenomena. There are a number of nearshore sediment transport formulas that have been developed through the years for different types of applications in coastal engineering. For example, several formulas were examined and evaluated by Bayram et al. (2001), and Camenen and Larroude (2003). However, these formulas

have typically described a specific set of physical processes and been validated with limited data. Recently, Camenen and Larson (2005, 2007, 2008) developed a unified sediment transport formulation, which has been validated for a large set data on longshore and cross-shore sediment transport from the laboratory and field. Performance of the new sediment transport formulation was compared to several popular existing formulas, and the new formulation yielded the overall best predictions among investigated formulations, and therefore, it was employed in this study.

The mechanics of sediment transport in the swash zone have received less attention than the surf zone. However, the swash zone is important for the sediment exchange between land and sea, which in turn affects both the sub-aerial and sub-aqueous evolution of the beach. The limited number of studies, as well as lack of measurement data on net transport in the swash, has made it difficult to formulate mathematical models based on a detailed understanding of the governing physics. In spite of these difficulties, significant progress has been made in the last decade concerning the hydrodynamics and sediment transport conditions in the swash zone (see Elfrink and Baldock, 2002; Larson et al., 2004; Larson and Wamsley, 2007). In this study, the formulas of hydrodynamics and sediment transport rates in swash zone of Larson and Wamsley (2007) were employed. The obtained sediment transport rate at the still-water shoreline was used as boundary condition for computing the suspended load in the inner surf zone, which was derived from the advection–diffusion equation.

3. Model description

3.1. Wave model

3.1.1. The random wave model EBED

Mase (2001) developed a multi-directional random wave transformation model based on the energy balance equation with energy dissipation and diffraction terms (EBED). The governing equation, for steady state, is expressed as follows,

$$\frac{\partial(v_x S)}{\partial x}+\frac{\partial(v_y S)}{\partial y}+\frac{\partial(v_\theta S)}{\partial \theta}=\frac{\kappa}{2\omega}\left\{(CC_g\cos^2\theta S_y)_y-\frac{1}{2}CC_g\cos^2\theta S_{yy}\right\}-\varepsilon_b S \tag{1}$$

where S is the angular-frequency spectrum density, (x, y) are the horizontal coordinates, θ is the angle measured counterclockwise from the x axis, ω is the frequency, C is the phase speed, and C_g the group speed, (v_x, v_y, v_θ) are the propagation velocities given by,

$$(v_x, v_y, v_\theta)=\left(C_g\cos\theta, C_g\sin\theta, \frac{C_g}{C}\left(\sin\theta\frac{\partial C}{\partial x}-\cos\theta\frac{\partial C}{\partial y}\right)\right) \tag{2}$$

The first term on the right-hand side is added in the balance equation in order to represent the diffraction effects, and κ is a free parameter that can be optimized to change the influence of the diffraction effects. The second term represents the wave energy dissipation due to wave breaking, and ε_b is the energy dissipation coefficient. The output from the wave transformation model includes three main wave parameters: significant wave height H_s, significant wave period T_s, and mean wave direction $\bar{\theta}$.

3.1.2. The modified-EBED model

The original EBED model is stable and can be applied to the complex beach topography of coastal zones containing structures. However, the obtained output from the model often overestimates the wave parameters in the surf zone compared to measurements. The overestimation is due mainly to the algorithm describing wave energy dissipation caused by wave breaking. In the EBED model, the energy dissipation coefficient was determined by the Takayama et al. (1991) model. The calculation of this coefficient is rather complex and the coefficient does not easily lend itself to calibration.

In this study, a new approach for calculating the energy dissipation term, which was based on the Dally et al. (1985) model, was employed for improving the predictive capability of the wave model. The model is referred to as the Modified-EBED model in this paper hereafter. Thus, a modified energy balance equation is proposed as follows,

$$\frac{\partial(v_x S)}{\partial x}+\frac{\partial(v_y S)}{\partial y}+\frac{\partial(v_\theta S)}{\partial \theta}=\frac{\kappa}{2\omega}\left\{(CC_g\cos^2\theta S_y)_y-\frac{1}{2}CC_g\cos^2\theta S_{yy}\right\}-\frac{K}{h}C_g(S-S_{stab}) \tag{3}$$

where h is the still-water depth, K is dimensionless decay coefficient, S_{stab} is the stable wave spectrum density, which is determined based upon the stable wave height H_{stab} ($=\Gamma h$), with Γ being a dimensionless empirical coefficient.

Assuming that the spectrum density S and the stable spectrum density S_{stab} are functions of H_s^2 and H_{stab}^2, respectively, the dissipation term in Eq. (3) can be rewritten as,

$$D_{diss}=\frac{K}{h}C_g S\left[1-\left(\frac{\Gamma h}{H_s}\right)^2\right]. \tag{4}$$

In the Dally et al. (1985) model, the recommended values for Γ and K were 0.4 and 0.15, respectively. Goda (2006) used his formula in 1975 for determining the decay coefficient, $K=3(0.3+2.4\,s)/8$, where s is the bottom slope. In the Modified-EBED model, in order to obtain a good description of wave conditions in the surf zone for the LSTF data, the coefficients were modified according to:

$$\begin{cases}\Gamma=0.45, K=\dfrac{3}{8}(0.3-19.2s) & : s<0\\ \Gamma=0.45+1.5s, K=\dfrac{3}{8}(0.3-0.5s) & : s\geq 0\end{cases}. \tag{5}$$

The wave radiation-driven stresses were determined by the output from the wave model,

$$S_{xx}=\frac{E}{2}[2n(1+\cos^2\bar{\theta})-1] \tag{6}$$

$$S_{yy}=\frac{E}{2}[2n(1+\sin^2\bar{\theta})-1] \tag{7}$$

$$S_{xy}=S_{yx}=\frac{E}{2}n\sin 2\bar{\theta} \tag{8}$$

where $E=\rho g H_{rms}^2/8$ is the wave energy per unit area, and $n=C_g/C$ is the wave index.

3.2. Surface roller model

The wave energy balance equation for the surface roller in two dimensions is expressed as (Dally and Brown, 1995; Larson and Kraus, 2002),

$$P_D+\frac{\partial}{\partial x}\left(\frac{1}{2}MC_r^2\cos^2\bar{\theta}\right)+\frac{\partial}{\partial y}\left(\frac{1}{2}MC_r^2\sin^2\bar{\theta}\right)=g\beta_D M \tag{9}$$

where P_D is the wave energy dissipation ($=KC_g\rho g(H_{rms}^2-(\Gamma h))^2)/(8h)$), M is the wave-period-averaged mass flux, C_r is the roller speed ($\approx$C), and β_D is the roller dissipation coefficient.

The stresses due to the rollers are determined as follows:

$$R_{xx}=MC_r\cos^2\bar{\theta} \tag{10}$$

$$R_{yy} = MC_r \sin^2 \bar{\theta} \tag{11}$$

$$R_{xy} = R_{yx} = MC_r \sin 2\bar{\theta}. \tag{12}$$

3.3. Nearshore current model

The governing equations for the nearshore currents are written as (Militello et al., 2004),

$$\frac{\partial(h+\eta)}{\partial t} + \frac{\partial q_x}{\partial x} + \frac{\partial q_y}{\partial y} = 0 \tag{13}$$

$$\frac{\partial q_x}{\partial t} + \frac{\partial u q_x}{\partial x} + \frac{\partial v q_x}{\partial y} + g(h+\eta)\frac{\partial \eta}{\partial x} = \frac{\partial}{\partial x} D_x \frac{\partial q_x}{\partial x} + \frac{\partial}{\partial y} D_y \frac{\partial q_x}{\partial y} + f q_y - \tau_{bx} + \tau_{Sx} \tag{14}$$

$$\frac{\partial q_y}{\partial t} + \frac{\partial u q_y}{\partial x} + \frac{\partial v q_y}{\partial y} + g(h+\eta)\frac{\partial \eta}{\partial y} = \frac{\partial}{\partial x} D_x \frac{\partial q_y}{\partial x} + \frac{\partial}{\partial y} D_y \frac{\partial q_y}{\partial y} - f q_x - \tau_{by} + \tau_{Sy} \tag{15}$$

where η is the water elevation, q_x,q_y is the flow per unit width parallel to the x and y axis, respectively, u,v is the depth-averaged velocity in x and y direction, respectively, g is the acceleration due to gravity, D_x,D_y are the eddy viscosity coefficients, f is the Coriolis parameter, τ_{bx},τ_{by} are the bottom stresses, and τ_{Sx},τ_{Sy} are the wave stresses (the latter variables are all in the x and y directions, respectively).

The depth-averaged horizontal eddy viscosity coefficient can be calculated as a function of the total water depth, current speed, and bottom roughness according to Falconer (1980),

$$D_0 = 1.154 g(h+\eta)\frac{|U|}{C_z^2} \tag{16}$$

where C_z is the Chezy roughness coefficient.

In the surf zone, the eddy viscosity is simulated as a function of the wave properties,

$$D_1 = \varepsilon_L \tag{17}$$

where ε_L represent the lateral mixing below the trough level. Kraus and Larson (1991) expressed this term as,

$$\varepsilon_L = \Lambda u_m H_{rms} \tag{18}$$

in which H_{rms} is the root-mean-square wave height, Λ is an empirical coefficient, and u_m is the wave orbital velocity at the bottom.

In the transition zone, the eddy viscosity is calculated as,

$$D_2 = (1-\alpha)D_0 + \alpha D_1 \tag{19}$$

where α is weighting parameter $(=(H_{rms}/(h+\eta))^3$, see Militello et al., 2004).

The bottom stresses under combined current and waves are determined from Nishimura (1988),

$$\tau_{bx} = C_b\left[\left(U_{wc} + \frac{\omega_b^2}{U_{wc}}\cos^2\bar{\theta}\right)u + \left(\frac{\omega_b^2}{U_{wc}}\cos\bar{\theta}\sin\bar{\theta}\right)v\right] \tag{20}$$

$$\tau_{by} = C_b\left[\left(U_{wc} + \frac{\omega_b^2}{U_{wc}}\sin^2\bar{\theta}\right)v + \left(\frac{\omega_b^2}{U_{wc}}\cos\bar{\theta}\sin\bar{\theta}\right)u\right] \tag{21}$$

in which C_b is the bottom friction coefficient, U_{wc}, and ω_b are given by,

$$U_{wc} = \frac{1}{2}\left\{\sqrt{|u^2+v^2+\omega_b^2+2(u\cos\bar{\theta}+v\sin\bar{\theta})\omega_b|} + \sqrt{|u^2+v^2+\omega_b^2-2(u\cos\bar{\theta}+v\sin\bar{\theta})\omega_b|}\right\} \tag{22}$$

$$\omega_b = \frac{\sigma H_{rms}}{\pi \sinh[k(h+\eta)]} \tag{23}$$

where σ is the wave frequency, and k the wave number.

The wave stresses are derived from the wave transformation model and the surface roller model. They are expressed by the following formulas:

$$\tau_{Sx} = -\frac{1}{\rho_w}\left[\frac{\partial}{\partial x}(S_{xx}+R_{xx}) + \frac{\partial}{\partial y}(S_{xy}+R_{xy})\right] \tag{24}$$

$$\tau_{Sy} = -\frac{1}{\rho_w}\left[\frac{\partial}{\partial x}(S_{xy}+R_{xy}) + \frac{\partial}{\partial y}(S_{yy}+R_{yy})\right]. \tag{25}$$

3.4. Sediment transport

3.4.1. Swash zone

Larson and Wamsley (2007) developed the formula for the net transport rates in the cross-shore and longshore direction, respectively, as,

$$q_{bc,net} = K_c \frac{\tan\phi_m}{\tan^2\phi_m - (dh/dx)^2}\frac{u_0^3}{g}\left(\frac{dh}{dx} - \tan\beta_e\right)\frac{t_0}{T} \tag{26}$$

$$q_{bl,net} = K_l \frac{\tan\phi_m}{\tan^2\phi_m - (dh/dx)^2}\frac{u_0^2 v_0}{g}\frac{t_0}{T} \tag{27}$$

where $q_{bc,net}$, $q_{bl,net}$ are the net transport in the cross-shore and longshore direction, respectively, K_c and K_l are empirical coefficients, ϕ_m the friction angle for a moving grain ($\approx$30°), β_e the foreshore equilibrium slope, u_0,v_0 and t_0 the scaling velocities and time, respectively, and T the swash duration (assumed that T is equal to the incident wave period). The swash zone hydrodynamics without friction, which were derived based on the ballistic theory, were employed in the model (for details see Larson and Wamsley, 2007).

3.4.2. Nearshore zone (offshore and surf zone)

Camenen and Larson (2005, 2007, 2008) developed a general transport formulation for bed load and suspended load under combined waves and current. It is referred as the Lund-CIRP formula in this paper hereafter. It can be used for both sinusoidal and asymmetric waves. To simplify calculations, the waves are assumed to be sinusoidal, having no asymmetry. Thus, the contribution to the transporting velocity from waves is negligible, implying that only the current moves the material. In such case, the bed load transport can be expressed as,

$$\frac{q_{bc}}{\sqrt{(s-1)g d_{50}^3}} = a_c\sqrt{\theta_c}\theta_{cw,m}\exp\left(-b_c\frac{\theta_{cr}}{\theta_{cw}}\right) \tag{28}$$

where the transport q_{bc} is obtained in the direction of the current, the transport normal to the current is zero, s is the relative density between sediment and water, d_{50} is the median grain size, a_c and b_c are empirical coefficients, $\theta_{cw,m}$ and θ_{cw} are the mean and maximum Shields parameters due to wave and current interaction, respectively, θ_{cr} is the critical Shields parameter, and θ_c is the Shields parameter due to current.

The suspended load is calculated based on the assumption of an exponential concentration profile and a constant velocity over the water column,

$$q_s = U_c c_R \frac{\varepsilon}{w_s}\left[1-\exp\left(-\frac{w_s d}{\varepsilon}\right)\right] \tag{29}$$

where U_c is current velocity, c_R is the reference concentration at the bottom, w_s is the sediment fall speed, ε is the sediment diffusivity, and d is the total depth $(=h+\eta)$.

The bed reference concentration is obtained from,

$$c_R = A_{cR}\theta_{cw,m}\exp\left(-4.5\frac{\theta_{cr}}{\theta_{cw}}\right) \tag{30}$$

where the coefficient A_{cR} is written as,

$$A_{cR} = 3.5\,10^{-3}\exp(-0.3d_*) \tag{31}$$

with $d_* = \sqrt[3]{(s-1)g/\upsilon^2}\,d_{50}$ being the dimensionless grain size and υ is the kinematic viscosity of water.

The sediment fall speed is determined from Soulsby (1997) as:

$$w_s = \frac{\upsilon}{d_{50}}\left[\left(10.36^2 + 1.049d_*^3\right)^{1/2} - 10.36\right]. \tag{32}$$

The sediment diffusivity is related to the energy dissipation as (Battjes, 1975; Camenen and Larson, 2008),

$$\varepsilon = \left(\frac{k_b^3 D_b + k_c^3 D_c + k_w^3 D_w}{\rho}\right)^{1/3} d \tag{33}$$

where the energy dissipation from wave breaking (D_b) and from bottom friction due to current (D_c) and waves (D_w) were simply added, and k_b, k_c and k_w are coefficients (see Camenen and Larson, 2008).

Alternatively, the suspended load can be obtained by solving the advection–diffusion equation. The advection–diffusion equation is obtained from the continuity of depth-averaged suspended sediment transport as,

$$\frac{\partial(\overline{C}d)}{\partial t} + \frac{\partial(\overline{C}q_x)}{\partial x} + \frac{\partial(\overline{C}q_y)}{\partial y} = \frac{\partial}{\partial x}\left(K_x d\frac{\partial\overline{C}}{\partial x}\right) + \frac{\partial}{\partial x}\left(K_y d\frac{\partial\overline{C}}{\partial y}\right) + P - D \tag{34}$$

where $\overline{C}$ is the depth-averaged sediment concentration, K_x and K_y are the sediment diffusion coefficient in x and y direction, respectively, P is the sediment pick-up rate, and D is the sediment deposition rate.

The sediment diffusion coefficient can be calculated by Elder (1959) as,

$$K_x = K_y = 5.93u_{*c}d \tag{35}$$

where u_{*c} is shear velocity from the current only.

The sediment pick-up and deposition rates, respectively, are obtained as,

$$P = c_R w_s \tag{36}$$

$$D = \frac{\overline{C}}{\beta_d} w_s \tag{37}$$

where β_d is a coefficient calculated based on Camenen and Larson (2008); see also Militello et al., 2006),

$$\beta_d = \frac{\varepsilon}{w_s d}\left[1-\exp\left(-\frac{w_s d}{\varepsilon}\right)\right]. \tag{38}$$

The suspended transport rates in the x and y directions can be calculated from Eq. (34) as:

$$q_{sx} = \overline{C}q_x - K_x d\frac{\partial\overline{C}}{\partial x} \tag{39}$$

$$q_{sy} = \overline{C}q_y - K_y d\frac{\partial\overline{C}}{\partial y}. \tag{40}$$

The sediment transport rate is often large near the shoreline because of swash uprush and backwash processes. For example, the measurements from LSTF showed a peak in the sediment transport rate close to the shoreline that was larger than in the inner surf zone. The computed sediment transport rates obtained from currently available formulas often tend to decrease too rapidly from the swash zone towards the offshore. Thus, the interaction between the swash zone and the inner part of the surf zone is not well described. Therefore, the calculations of sediment transport may not agree with measurements in this region, unless some modifications are introduced.

In the present study, we use the sediment transport at the still-water shoreline obtained from swash zone computations as the boundary value for computing suspended load in the surf zone using the advection–diffusion equation. Furthermore, the pick-up and deposition rates described in the Eqs. (36) and (37), respectively, were also modified as follows,

$$\tilde{P} = P\left[1 + \vartheta\frac{\overline{V}}{v_0}\exp\left(-\mu\frac{d}{R}\right)\right] \tag{41}$$

$$\tilde{D} = \frac{D}{\left[1 + \vartheta\frac{\overline{V}}{v_0}\exp\left(-\mu\frac{d}{R}\right)\right]} \tag{42}$$

where ϑ and μ are free non-negative coefficients, $\overline{V}$ is the mean velocity across the profile, R is the runup height. The velocity $\overline{V}$ is determined as the average longshore current across the surf zone, v_0 is obtained from swash zone computation, and R is calculated by the Hunt (1959) formula.

The total load, given by the bed load from the Lund-CIRP formula and the suspended load calculated by the advection–diffusion equation with the above modifications, is referred to as AD-Lund-CIRP hereafter. The above modifications increase the suspended sediment load near the shoreline. The empirical parameter values introduced are related to the magnitude of longshore current, scaling velocity, water depth, and runup height. Although the modifications are somewhat ad hoc, the model produces more reasonable computed sediment fluxes in agreement with the investigated measured data.

4. Large-Scale Sediment Transport Facility (LSTF) data

Five series of movable bed physical model experiments were carried out in the LSTF basin (see Hamilton and Ebersole, 2001; Wang et al., 2002) at the Coastal and Hydraulics Laboratory of the U.S. Army Engineer Research and Development Center in Vicksburg, Mississippi by Gravens and Wang (2007), and Gravens et al. (2006). The first series of experiments, referred to as "Base Cases", including four runs of approximately 160 min each on a natural beach (without structure), were aimed at generating high-quality data sets for testing and validation of sand transport formulas due to waves and currents. The

Table 1.
Measurement locations for LSTF Base Cases.

Measured locations	ADV1	ADV2	ADV3	ADV4	ADV5	ADV6	ADV7	ADV8	ADV9	ADV10
Distance to shoreline (m)	1.125	2.725	4.125	5.73	7.125	8.525	10.125	11.625	13.125	15.625

four remaining series of experiments were designed to generate data sets for testing and validation of the development of tombolos in the lee of nearshore detached breakwaters and T-head groins. Spilling breaking waves were generated by four wave generators. The beach consisted of very well-sorted fine quartz sand with a median grain size of 0.15 mm. The longshore current generated by the obliquely incident waves was circulated with twenty turbine pumps through twenty flow channels at the updrift and downdrift ends of the basin.

In this study, the Base Cases were used for validation of the model. In Base Case 1 (BC-1) the longshore current was induced by random waves and circulated by the turbine pumps. Base Case 2 (BC-2) encompassed the wave-induced current and an external longshore current which was generated by recirculating two times the wave-generated longshore flux of water. In Base Case 3 (BC-3) the wave generators were not operated so it was not used for testing the numerical model. Similar to BC-2, the external longshore current was also imposed across the model beach in Base Case 4 (BC-4) by recirculating 1.5 times the wave-generated longshore flux of water. The wave height, wave period, and wave setup were measured by thirteen capacitance gauges. However, the wave sensor at ADV10 did not work so the measured data on wave conditions at this location was not available. The data on nearshore current were collected and measured by ten Acoustic Doppler Velocimeters (ADVs). Ten wave and current sensors were collocated at ten cross-shore locations and synchronized in time for each of the eleven cross-shore sections. These locations are presented in Table 1. The remaining wave sensors, Gauge#11, Gauge#12 and Gauge#13, were located at three alongshore positions, 18.43 m seaward from the still-water shoreline, to measure wave conditions outside the toe of the movable beach (see Fig. 1). Twenty-one gravity-feed sediment traps located at the downdrift end of the movable bed model beach, in which two traps were located in the swash zone, were used to measure the magnitude and cross-shore distribution of sand transport. Beach profiles at the interval between 0.25 and 4 m were measured by rod and acoustic survey techniques after each model run.

5. Model simulation results

The computational grid for the LSTF beach was generated based on interpolation of measured beach profile data from profile Y34 to profile Y14 (see Fig. 1). The grid size was 0.2×0.2 m, and the measurements at Gauge#11, Gauge#12, and Gauge#13 were used as offshore wave conditions. The detailed information of the wave conditions at these points for cases BC-1, BC-2, and BC-4 are presented in Table 2. A TMA spectrum was assumed at the offshore boundary with the parameter values $\gamma = 3.3$, $\sigma_a = 0.07$, $\sigma_b = 0.09$, and $S_{max} = 25$. Values for the decay and stable coefficients were determined from Eq. (5). Because the beach topography of the Base Cases is fairly uniform in the alongshore direction, the variation in alongshore significant wave height and longshore current was relative small. Therefore, the comparisons between calculation and measurement in this paper were only made at the profile Y24 (center profile).

Fig. 2 shows the comparison between calculated and measured significant wave height for case BC-1. The dashed line is the calculated significant wave height obtained by the original EBED model, which overestimated the wave height in the surf zone compared to the measured data. By employing the new method for calculating wave energy dissipation due to breaking, the Modified-EBED model produced improved results. The calculated significant wave height agreed well with the measured data at all measurement locations. The root-mean-square (rms) error of the significant wave height obtained by Modified-EBED model was only 3.6%, whereas it was 13.0% for the EBED model.

The output from the Modified-EBED model, such as significant wave height, wave direction, and wave period, as well as wave-driven stresses, were employed to calculate the nearshore currents. The

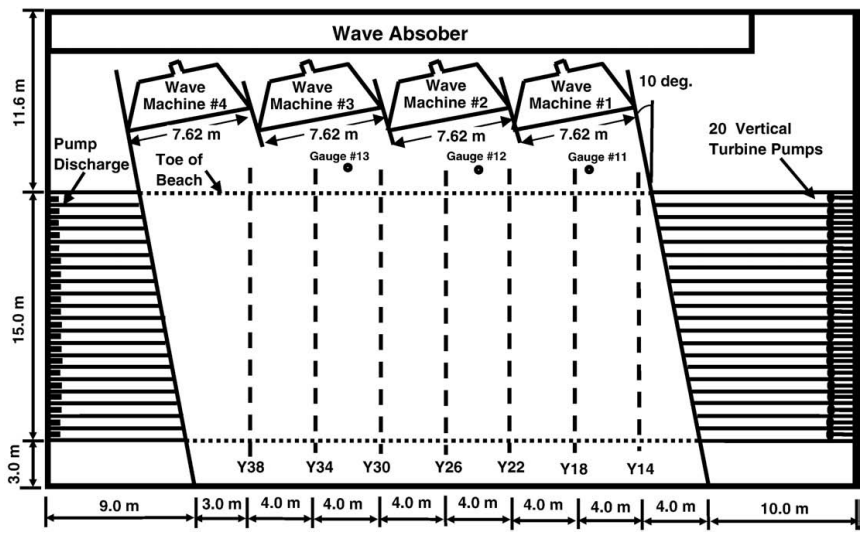

Fig. 1. Configuration of LSTF basin (Gravens and Wang, 2007).

Table 2
Offshore wave conditions for LSTF Base Cases.

Data sets	Gauges	H_{mo} (m)	T_p (s)	Θ (°)
BC-1	#11	0.220	1.444	6.5
	#12	0.225	1.468	6.5
	#13	0.228	1.465	6.5
BC-2	#11	0.213	1.439	6.5
	#12	0.226	1.469	6.5
	#13	0.228	1.460	6.5
BC-4	#11	0.216	1.447	6.5
	#12	0.221	1.472	6.5
	#13	0.222	1.460	6.5

Chezy coefficient was specified to be 40, the coefficient for lateral mixing $\Lambda = 0.5$, the roller dissipation coefficient $\beta_D = 0.1$, and the time step 0.02 s. The water fluxes on the upstream boundary were given based on measured data on longshore current at profile Y34. The downstream boundary was treated as an open boundary.

Fig. 3 illustrates the measurement data and computations of the wave-induced longshore current with and without roller. The roller effects did not only cause a shift in the longshore current towards the shoreline but also increased the maximum current in the surf zone. Although there were differences between measured and calculated longshore current with the roller at ADV3 and ADV4, the tendency after including the roller is to improve the agreement with measured data in the surf zone. The rms errors of the calculated longshore current with and without roller were 27.2% and 29.8%, respectively.

The comparison of calculated and measured wave setup is presented in Fig. 4. Both calculations of wave setup with and without roller agree well with the measurements. The setup without roller yielded slightly better agreement with the measurements compared to the setup with roller. Although the rms error of wave setup with roller (32.5%) was higher than without roller (24.3%), the difference between the computations was relatively small.

In order to calculate the scaling velocities, the runup height and wave angle prior to runup are needed. The runup height was determined by the Hunt (1959) formula. The wave angle prior to runup was given by the wave angle at the cell next to the shoreline from the Modified-EBED model output. The foreshore equilibrium slope was determined based on the observed topographical data. The values of K_c and K_I were both set to 0.0008, following Larson and Wamsley (2007).

The computed longshore sediment flux in the swash zone is presented by the dashed line in Fig. 5. There were only two measurement points in the swash zone, but the calculated longshore sediment flux is in good agreement with the measured data.

The output from the Modified-EBED model and the nearshore wave-induced currents with roller were used to determine the Shields parameters due to waves and currents. The kinematic viscosity of water υ was set to 1.36×10^{-6} m^2/s, and the density of water and sediment was given as 1000 kg/m^3 and 2650 kg/m^3, respectively. The critical Shields parameter was determined by the Soulsby and Whitehouse formula (see Soulsby, 1997). The coefficient values in the bedload transport formula a_c and b_c were given as 12 and 4.5, respectively (see Camenen and Larson, 2005). In the suspended load formula, a value of $k_b = 0.017$ was employed and k_c and k_w were calculated based on the Schmidt number (see Camenen and Larson, 2008). The coefficient values $\vartheta = 9.3$ and $\mu = 2.4$ were employed for calculating the pick-up and deposition rates. In addition, the total load formula of Watanabe (1987) with a transport coefficient equal to 1.0 was employed to compare with the Lund-CIRP and AD-Lund-CIRP.

The computations of the longshore sediment flux in the nearshore are presented in Fig. 5. There was only a slight difference in the longshore sediment flux between the Lund-CIRP and Watanabe formulas, and these calculations agree fairly well with the measured data in the offshore and outer surf zone. However, there is a significant difference between measurements and computations near the shoreline for these two formulas. Using AD-Lund-CIRP overcomes this discrepancy. Based on the calculations of longshore sediment flux in the swash zone and the modifications of pick-up and deposition rates in the advection–diffusion equation, the computed longshore sediment flux in the inner part of the surf zone also agrees with the measurements. The rms error of longshore sediment flux obtained by AD-Lund-CIRP for both swash zone and nearshore zone was 33.2%, better than those by Lund-CIRP (49.1%) and by Watanabe (49.6%).

The computations of waves, nearshore current, and sediment transport for BC-2 and BC-4 were carried out in the same manner as for BC-1. The coefficient values used for BC-1 were kept the same in the simulations for BC-2 and BC-4.

The significant wave height, longshore current, wave setup, and longshore sediment flux for BC-2 were presented in Figs. 6–9, respectively. As for BC-1, the wave predictions by the Modified-EBED model were better than those by the EBED model agreeing well with the measured data. The longshore current and wave setup were also well predicted (including roller effects). Although the overall shape of cross-shore distribution of the longshore current was in good agreement with the data, the magnitude of the current at ADV3 and ADV4 was overestimated. Sediment transport rate in the swash zone agreed well with the measured data. The difference between longshore sediment flux obtained by Lund-CIRP and Watanabe was more pronounced in the surf zone than for BC-1, especially between 0.2 m and 5.6 m seaward of the still-water shoreline. However, computations

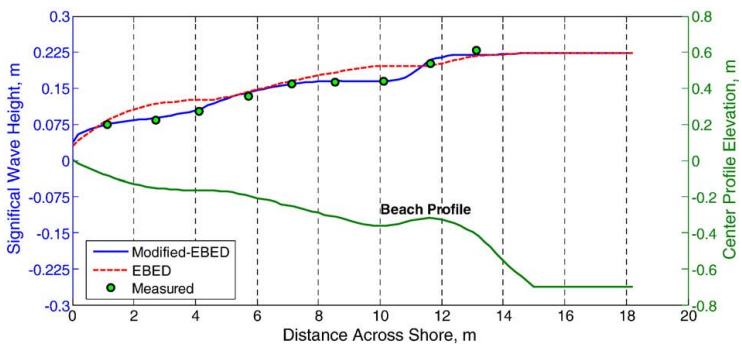

Fig. 2. Computed and measured significant wave height for LSTF BC-1.

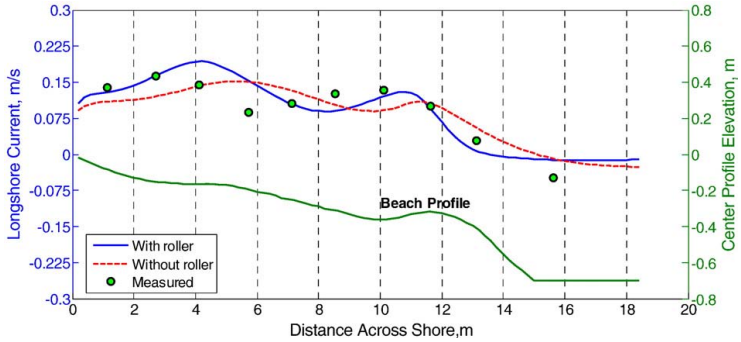

Fig. 3. Computed and measured longshore current for LSTF BC-1.

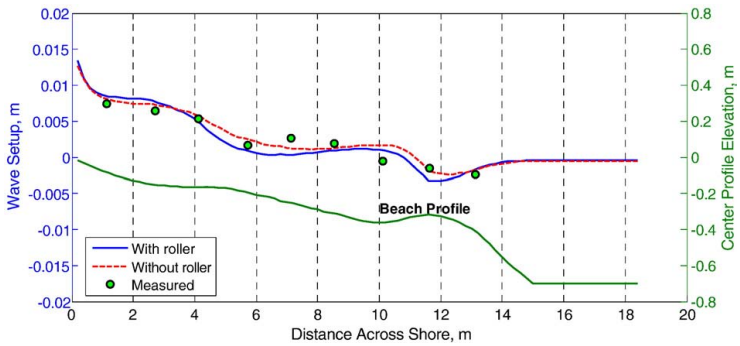

Fig. 4. Computed and measured wave setup for LSTF BC-1.

with both Lund-CIRP and Watanabe showed the same tendency of decreasing sediment flux towards the shoreline as for BC-1. Calculation with AD-Lund-CIRP, including the swash zone computation, produced reasonable sediment fluxes from the swash zone to the offshore.

Computational results and comparison with measurements for BC-4 regarding significant wave height, longshore current, wave setup, and longshore sediment flux were presented in Figs. 10–13, respectively. The significant wave height obtained by Modified-EBED agreed well with the measured data, except at ADV3 and ADV4, and the nearshore current model produced satisfactory predictions of the longshore current. However, in this run, the measured wave setup at ADV1, ADV2, ADV3, and ADV4 were too small compared to the calculated results, especially at ADV3 and ADV4 where wave setdown was observed. The mean water elevation should normally increase in the surf zone for a monotonically increasing profile, similar to what was observed in BC-1 and BC-2, so the data may contain some errors at these gauges. From ADV5 to ADV10, the calculated wave setup agrees well with the measured data. The computed longshore sediment fluxes were not as good as for BC-1 and BC-2. It was difficult to obtain good agreement between calculated and measured sediment flux in the inner surf zone near the shoreline, but AD-Lund-CIRP gave the best predictions of the longshore sediment flux compared to the Lund-CIRP and Watanabe formulas.

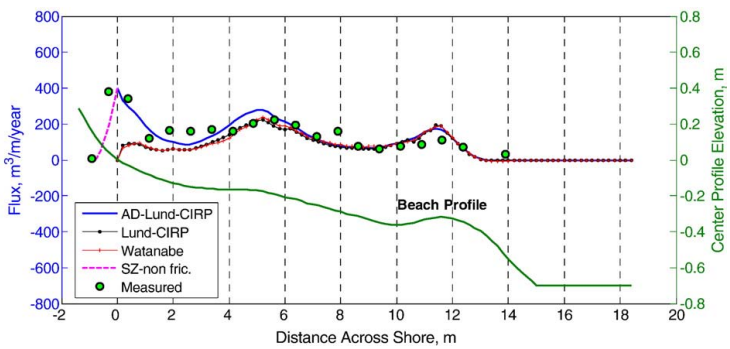

Fig. 5. Computed and measured longshore sediment flux for LSTF BC-1.

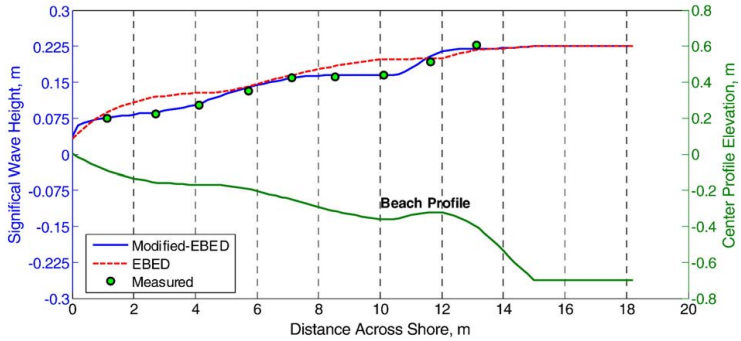

Fig. 6. Computed and measured significant wave height for LSTF BC-2.

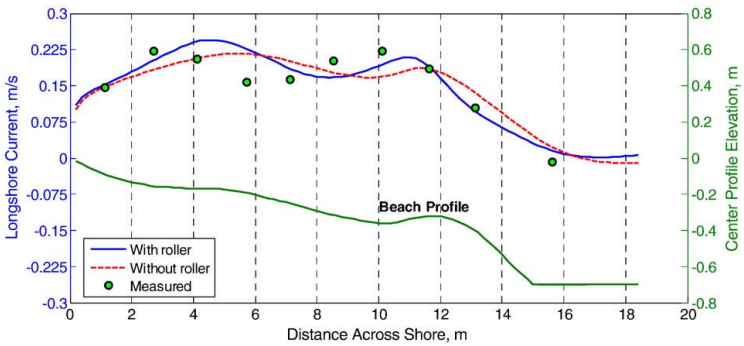

Fig. 7. Computed and measured longshore current for LSTF BC-2.

A quantitative assessment of the predictive capacity of the model was performed based on the rms error. Table 3 summarizes in detail the rms errors between computations and measurements for significant wave height obtained by the Modified-EBED and EBED model, and for the longshore current and wave setup with and without roller. Table 4 presents the quantitative assessment of the longshore sediment transport calculations in both the nearshore and the swash zone. The assessment showed that the developed model can produce reasonable computational results for the investigated data sets.

6. Discussion

In the neashore zone, energy dissipation due to wave breaking is an important process to describe in the wave model. The Takayama approach used in the original EBED model often caused an over-estimation of the wave heights in the surf zone. Thus, the modification of the energy dissipation calculations in the EBED model following Dally et al. (1985) implied a significant improvement in computing waves in the surf zone. However, appropriate values on the decay and stable coefficients should be given. The coefficient values determined

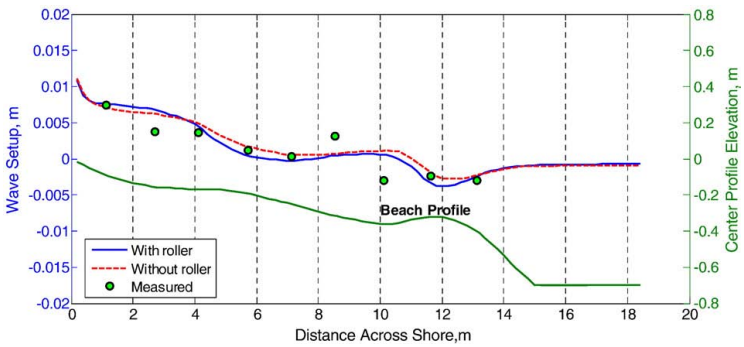

Fig. 8. Computed and measured wave setup for LSTF BC-2.

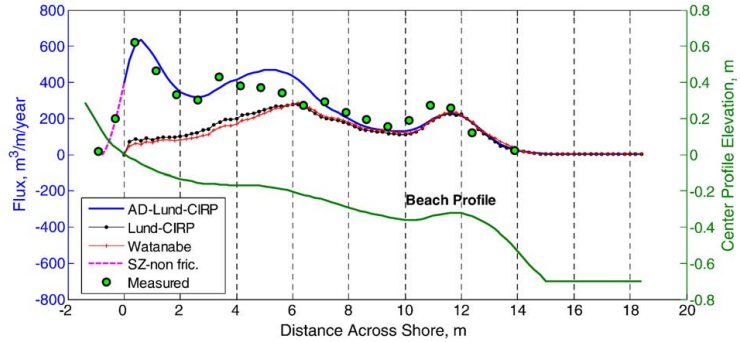

Fig. 9. Computed and measured longshore sediment flux for LSTF BC-2.

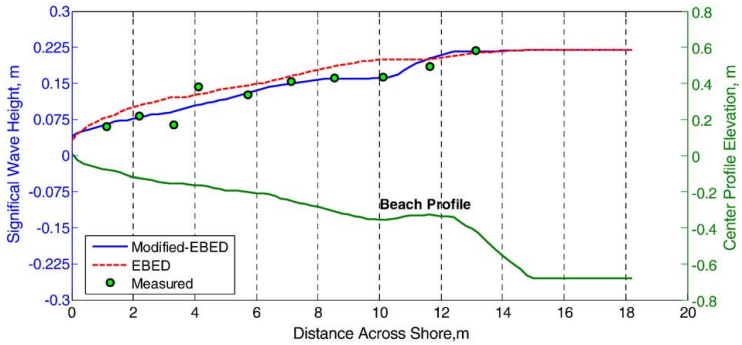

Fig. 10. Computed and measured significant wave height for LSTF BC-4.

from Eq. (5) produced good results for the Base Cases, but this equation needs to be validated with other laboratory and field data to ensure its general applicability.

Surface roller effects are necessary to include when calculating nearshore currents generated by waves. It is not only the peak of the longshore current that shifts towards the shoreline, but also the magnitude of the longshore current in the surf zone increases. The roller effects on the nearshore currents were in agreement with previously published works. By using the 2D surface roller model, energy conservation was expressed in a better manner than with the 1D model. Because the bathymetry of the LSTF basin for the Base Cases was fairly uniform, the roller energy flux alongshore in Eq. (9) was very small and could be neglected. However, this term should be included in calculations for the areas with complex bathymetry in order to obtain more accurate wave-induce currents.

Lateral mixing makes the cross-shore variation in the wave-induced longshore current smoother, and for monochromatic waves this phenomenon is needed to avoid a discontinuity at the break point. However, in the case of random waves the lateral mixing is less needed since gradual wave breaking across the profile occurs, producing a smooth forcing. Reniers and Battjes (1997) found that lateral mixing was needed to model the case of random waves breaking over a barred profile. For such a profile shape, a major portion of the waves may break on the bar and reform in the trough. In

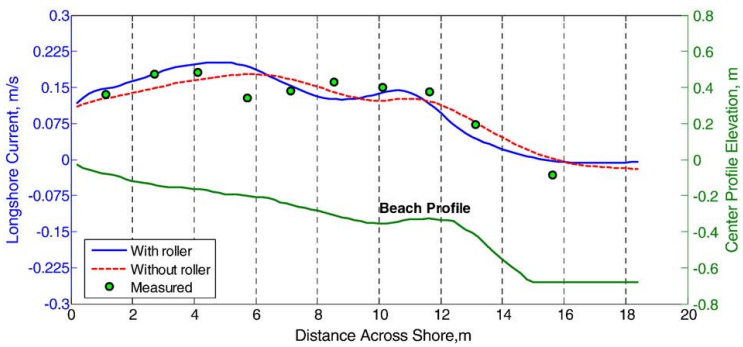

Fig. 11. Computed and measured longshore current for LSTF BC-4.

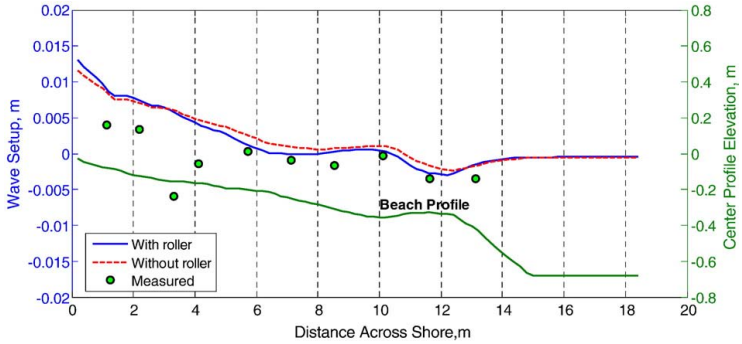

Fig. 12. Computed and measured wave setup for LSTF BC-4.

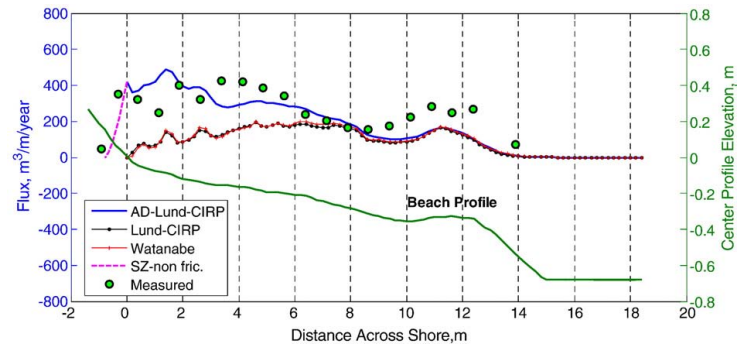

Fig. 13. Computed and measured longshore sediment flux for LSTF BC-4.

model simulations, this behavior implies little forcing in the trough and small currents here. By applying lateral mixing, this reduction in the current velocity may be counteracted. Sensitivity tests on the importance of the lateral mixing coefficient in the present study showed small effects, probably because of the profile shape changing rather gradually in the area of breaking waves.

The sediment transport typically displays great sensitivity to the roughness. Using the total roughness, including the grain-related roughness, form-drag roughness, and sediment-related roughness will produce shear stresses that may be used to calculate the sediment transport rates with some confidence. However, the formula of sediment-related roughness, which is given by Wilson (1989), is of the implicit type (for details, see Militello et al., 2006, pp. 18–20). Therefore, an iterative approach is required for solving the non-linear equation describing this roughness. In the present calculations, the Newton–Rhapson method was used for solving this equation yielding rapid convergence.

Calculating the suspended load using the advection–diffusion equation produces a smoother sediment transport rate distribution than the Lund-CIRP formula. Moreover, it can be applied to situations where suspended sediment concentration changes in time and space at a high rate, for example, at river mouths, tidal inlets, and in the vicinity of structures. Another advantage of the advection–diffusion equation is that the model uses the sediment transport rate at shoreline from the swash-zone calculations as the boundary condition for computing the suspended sediment transport in the inner surf zone.

The swash uprush and backwash occur rapidly and frequently in the swash zone, which may induce increased transport rates in the inner surf zone. If the pick-up and deposition rates were not modified ($\vartheta = 0$), the distribution of the longshore sediment transport rate would drop at a high rate seaward of the still-water shoreline, and then be similar to the calculation with the Lund-CIRP formula. Thus, it would not agree well with the investigated measured data near the shoreline. The calibration of the coefficients ϑ and μ was made for BC-1 using a range of values. The sensitivity to these coefficients is shown in Fig. 14. Based on the calibrated values for ϑ and μ, we calculated the longshore sediment flux for BC-2 and BC-4. The calibration showed that $\vartheta = 9.3$ and $\mu = 2.4$ were the most suitable values. Nevertheless, the modification of the formulas introduced and the optimal coefficient values should be validated with further data to improve the accuracy calculation of sediment transport not only for laboratory but also for field conditions.

Table 3
Root-mean-square error (%) for significant wave height, longshore current, and wave setup.

Data sets	H_s Modified-EBED	H_s EBED	v With roller	v Without roller	η With roller	η Without roller
BC-1	3.64	12.96	27.20	29.81	32.50	24.32
BC-2	3.92	14.12	17.61	19.57	51.42	52.04
BC-4	11.47	18.53	20.76	18.47	151.31	158.29

Table 4
Root-mean-square error (%) for longshore sediment transport flux.

Data sets	AD-Lund-CIRP	Lund-CIRP	Watanabe
BC-1	33.21	49.12	49.64
BC-2	18.34	59.23	62.72
BC-4	34.73	59.08	58.83

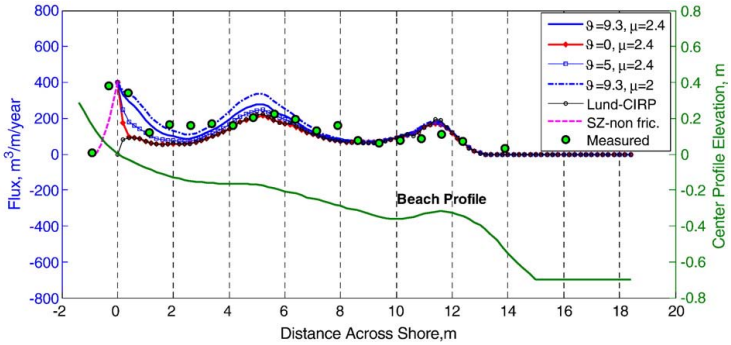

Fig. 14. Sensitive of coefficients ϑ and μ to sediment transport rate for LSTF BC-1.

7. Conclusions

A unified numerical model of nearshore waves, wave-induced currents, and sediment transport was developed. The energy dissipation due to wave breaking in the spectral wave transformation model EBED (Mase, 2001) was modified based upon the Dally et al. (1985) model, producing better predictions of the wave parameters in the surf zone. The evolution of the surface roller associated with the wave breaking after Dally and Brown (1995) was employed and enhanced, which improves the description of wave radiation stresses inside the surf zone. Including the roller shifts the nearshore current towards the shore, yielding better agreement between calculations and measurements. Newly developed formulations for the sediment transport in both swash zone and nearshore zone were applied. The modifications of pick-up and deposition rates were effective for simulating the sediment transport in the near shoreline.

The capability of model to predict the nearshore waves, wave-induced current, and sediment transport, was evaluated by comparison with three high-quality data sets from the LSTF at the Coastal and Hydraulics Laboratory. These simulations showed that the model yields reasonable predictions for the conditions studied. Thus, the model is expected to provide reliable input for calculating the morphological evolution due to waves and currents.

Acknowledgments

This work was partly funded by Sida/SAREC in the framework of the Project VS/RDE/03 "The evolution and sustainable management in the coastal areas of Vietnam" (PTN and LXH), and partly by the Inlet Modeling System Work Unit of the Coastal Inlets Research Program, U.S. Army Corps of Engineers (ML and HH). Dr. Hajime Mase at Kyoto University kindly supplied the source code for the EBED model. Dr. Ping Wang at University of South Florida and Mr. Mark Gravens at CHL provided the experimental data from their tests, which is greatly appreciated. The authors would also like to thank Dr. Nicholas C. Kraus at the U.S Army Corps of Engineers Coastal Inlet Research Program (CIRP) for the experimental data. The authors would also like to thank Dr. Nguyen Manh Hung, and the late Prof. Pham Van Ninh for their great contributions to the Project VS/RDE/03 and comments on early drafts of this paper. Finally, the authors would also like to thank the anonymous reviewers for their valuable comments.

References

Battjes, J.A., 1972. Setup due to irregular wave. Proceedings 13th International Conference on Coastal Engineering, ASCE, Vancouver, pp. 1993–2004.
Battjes, J.A., 1975. Modeling of turbulence in the surf zone. Proceedings 2nd Symposium on Modeling and Techniques, ASCE, San Francisco, pp. 1050–1061.
Bayram, A., Larson, M., Miller, H.C., Kraus, N.C., 2001. Cross-shore distribution of longshore sediment transport: comparison between predictive formulas and field measurements. Coastal Engineering 44, 79–99.
Booij, N., Holthuijsen, L.H., Ris, R.C., 1996. The 'SWAN' wave model for shallow water. Proceedings 25th International Conference on Coastal Engineering, ASCE, Orlando, pp. 668–676.
Booij, N., Holthuijsen, L.H, Doorn, N., Kieftenburg, A.T.M.M., 1997. Diffraction in a spectral wave model. Proc. 3rd Int. Symposium Ocean Wave Measurement and Analysis Wave '97, ASCE, New York, pp. 243–255.
Bowen, A.J., 1969. The generation of longshore currents on a plane beach. Journal of Marine Research 27 (2), 206–215.
Camenen, B., Larroude, P., 2003. Comparison of sediment transport formulae for the coastal environment. Coastal Engineering 48, 111–132.
Camenen, B., Larson, M., 2005. A general formula for non-cohesive bed load sediment transport. Estuarine, Coastal and Shelf Science 63, 249–260.
Camenen, B., Larson, M., 2007. A unified sediment transport formulation for coastal inlet application. Technical report ERDC/CHL CR-07-1, US Army Engineer Research and Development Center, Vicksburg, MS.
Camenen, B., Larson, M., 2008. A general formula for noncohesive suspended sediment transport. Journal of Coastal Research 24 (3), 615–627.
Dally, W.R., Osiecki, D.A., 1994. The role of rollers in surf zone currents. Proceedings 24th International Conference on Coastal Engineering. ASCE, Kobe, pp. 1895–1905.
Dally, W.R., Brown, C.A., 1995. A modeling investigation of the breaking wave roller with application to cross-shore currents. Journal of Geophysical Research 100 (C12), 24873–24883.
Dally, W.R., Dean, R.G., Dalrymple, R.A., 1985. Wave height variation across beaches of arbitrary profile. Journal of Geophysical Research 90 (C6), 11917–11927.
Deigaard, R., Justesen, P., Fredsoe, J., 1991. Modeling of undertow by one-equation turbulence model. Coastal Engineering 15, 431–458.
Duncan, J.H., 1981. An experimental investigation of breaking waves produced by a towed hydrofoil. Proc. R. Soc. London vol. A377, 331–348.
Elder, J.W., 1959. The dispersion of marked fluid in turbulent shear flow. Journal of Fluid Mechanics 5, 544–560.
Elfrink, B., Baldock, T., 2002. Hydraudynamics and sediment transport in the swash zone: a review and perspectives. Coastal Engineering 45, 149–167.
Falconer, R.A., 1980. Modelling of planform influence on circulation in harbors. Proceedings 17th International Conference on Coastal Engineering. ASCE, Sydney, pp. 2726–2744.
Goda, Y., 2006. Examination of the influence of several factors on longshore current computation with random waves. Coastal Engineering 53, 157–170.
Gravens, M.B., Wang, P., 2007. Data report: laboratory testing of longshore sand transport by waves and currents; morphology change behind headland structures. Technical Report, ERDC/CHL TR-07-8, Coastal and Hydraulics Laboratory, US Army Engineer Research and Development Center, Vicksburg, MS.
Gravens, M.B., Wang, P., Kraus, N.C., Hanson, H., 2006. Physical model investigation of morphology development at headland structures. Proceedings 30th International Conference on Coastal Engineering. World Scientific Press, San Diego, pp. 3617–3629.
Hamilton, D.G., Ebersole, B.A., 2001. Establishing uniform longshore currents in large-scale sediment transport facility. Coastal Engineering 42 (3), 199–218.
Holthuijsen, L.H., Herman, A., Booij, N., 2003. Phase-decoupled refraction–diffraction for spectral wave models. Coastal Engineering 49, 291–305.
Hunt, I.A., 1959. Design of seawalls and breakwaters. Journal of Waterways and Harbors Division 85, 123–152.
Kraus, N.C., Larson, M., 1991. NMLONG: Numerical model for simulating the longshore current; report 1: model development and tests. Technical Report DRP-91-1, U.S. Army Engineer Waterways Experiment Station, Vicksburg, MS.
Larson, M., Kraus, N.C., 2002. NMLONG: numerical model for simulating longshore current; report 2: wave–current interaction, roller modeling, and validation of model enhancements. Technical Report ERDC/CHL TR-02-22, US Army Engineer Research and Development Center, Vicksburg, MS.
Larson, M., Wamsley, T.V., 2007. A formula for longshore sediment transport in the swash. Proceedings Coastal Sediments '07. InASCE, New Orleans, pp. 1924–1937.

Larson, M., Kubota, S., Erikson, L., 2004. Swash-zone sediment transport and foreshore evolution: field experiments and mathematical modeling. Marine Geology 212, 61–79.
Lippmann, T.C., Brookins, A.H., Thornton, E.B., 1996. Wave energy transformation on natural profiles. Coastal Engineering 27, 1–20.
Longuet-Higgins, M.S., 1970. Longshore current generated by obliquely incident sea waves. Journal of Geophysical Research 75 (33), 6779–6801.
Longuet-Higgins, M.S., Stewart, R.W., 1964. Radiation stresses in water waves; a physical discussion with applications. Deep Sea Research 11, 529–562.
Madsen, P.A., Warren, I.R., 1984. Performance of a numerical short-wave model. Coastal Engineering 8, 73–93.
Madsen, P.A., Murray, R., Sorensen, O.R., 1991. A new form of the Boussinesq equations with improved linear dispersion characteristics. Coastal Engineering 15, 371–388.
Madsen, P.A., Sorensen, O.R., Schäffer, H.A., 1997. Surf zone dynamics simulated by a Boussinesq type model. Part II: surf beat and swash oscillations for wave groups and irregular waves. Coastal Engineering 32, 289–319.
Mase, H., 2001. Multi-directional random wave transformation model based on energy balance equation. Coastal Engineering Journal 43 (4), 317–337.
Militello, A., Reed, C.W., Zundel, A.K., Kraus, N.C., 2004. Two-dimensional depth-averaged circulation model M2D: version 2.0, report 1, technical document and user's guide. Technical Report ERDC/CHL TR-04-2, Coastal and Hydraulics Laboratory, US Army Engineer Research and Development Center, Vicksburg, MS.
Militello, A., Reed, C.W., Kraus, N.C., Ono, N., Larson, M., Camenen, B., Hanson, H., Wamsley, T., Zundel, A.K., 2006. Two-dimensional depth-averaged circulation model CMS-M2D: version 3.0, report 2,sediment transport and morphology change. Technical Report ERDC/CHL TR-06-9, Coastal and Hydraulics Laboratory, US Army Engineer Research and Development Center, Vicksburg, MS.
Nairn, R.B., Roelvink, J.A., Southgate, H.N., 1990. Transition zone width and implications for modeling surfzone hydrodynamics. Proceedings 22nd International Conference on Coastal Engineering. ASCE, Delft, pp. 68–81.
Nishimura, H., 1988. Computation of nearshore current. In: Horikawa, K. (Ed.), Nearshore Dynamics and Coastal Processes. InUniversity of Tokyo Press, Tokyo, Japan, pp. 271–291.
Nwogu, O., 1993. Alternative form of Boussinesq equations for nearshore wave propagation. Journal of Waterway, Port, Coastal, and Ocean Engineering 119 (6), 618–638.
Reniers, A.J.H.M., Battjes, J.A., 1997. A laboratory study of longshore currents over barred and non-barred beach. Coastal Engineering 30, 1–22.
Rivero, F.J., Arcilla, A.S, Carci, E., 1997. Analysis of diffraction in spectral wave models. Proc. 3rd Int. Symposium Ocean Wave Measurement and Analysis Wave '97. ASCE, New York, pp. 431–445.
Ruessink, B.G., Miles, J.R., Feddersen, F., Guza, R.T., Elgar, S., 2001. Modeling the alongshore current on barred beaches. Journal of Geophysical Research 106 (C10), 22451–22463.
Soulsby, R.L., 1997. Dynamics of marine sands. Thomas Telford, HR Wallingford, London.
Stive, M.J.F., De Vriend, H.J., 1994. Shear stresses and mean flow in shoaling and breaking waves. Proceedings 24th International Conference on Coastal Engineering. ASCE, Kobe, pp. 594–608.
Svendsen, I.A., 1984a. Wave heights and set-up in a surf zone. Coastal Engineering 8, 303–329.
Svendsen, I.A., 1984b. Mass flux and undertow in a surf zone. Coastal Engineering 8, 347–365.
Takayama, T., Ikeda, N., Hiraishi, T., 1991. Wave transformation calculation considering wave breaking and reflection. Rept. Port Harbor Res. Inst. 30 (1), 21–67.
Thornton, E.B., 1970. Variation of longshore current across the surf zone. Proceedings 12th International Conference on Coastal Engineering. ASCE, Washington D.C., pp. 291–308.
Thornton, E.B., Guza, R.T., 1983. Transformation of wave height distribution. Journal of Geophysical Research 88 (C10), 5925–5938.
Thornton, E.B., Guza, R.T., 1986. Surf zone longshore currents and random waves: field data and models. Journal of Physical Oceanography 16, 1165–1178.
Van Dongeren, A., Sancho, F.E., Svendsen, I.A., Putrevu, U., 1994. SHORECIRC: a quasi 3-D nearshore model. Proceedings 24th International Conference on Coastal Engineering. ASCE, Kobe, pp. 2741–2754.
Van Dongeren, A., Svendsen, I.A., 2000. Nonlinear and 3D effects in leaky infragravity waves. Coastal Engineering 41, 467–496.
Van Dongeren, A., Reniers, A., Battjes, J., 2003. Numerical modeling of infragravity wave response during DELIAH. Journal of Geophysical Research 108 (C9), 3288. doi:10.1029/2002JC001332.
WAMDI group, 1988. The WAM model-a third generation ocean wave prediction model. Journal of Physical Oceanography 18, 1775–1810.
Wang, P., Ebersole, B.A., Smith, E.R., Johnson, B.D., 2002. Temporal and spatial variations of surf-zone currents and suspended sediment concentration. Coastal Engineering 46, 175–211.
Watanabe, A., 1987. 3-dimensional numerical model of beach evolution. Proceedings Coastal Sediments '87. ASCE, pp. 802–817.
Wilson, K.C., 1989. Friction of wave-induced sheet flow. Coastal Engineering 12, 371–379.

Paper II

Model of nearshore waves and wave-induced currents around a detached breakwater

Nam, P.T., Larson, M., 2010.

In: *Journal of Waterway, Port, Coastal, and Ocean Engineering*, Vol. 136, No. 3, 156-176.

Model of Nearshore Waves and Wave-Induced Currents around a Detached Breakwater

Pham Thanh Nam[1] and Magnus Larson[2]

Abstract: A numerical model that combines a random wave transformation and a wave-induced current model was developed in order to predict the wave and current fields around a detached breakwater. The wave field was determined using the EBED model, as reported by Mase in 2001, with a modified energy dissipation term. The surface roller associated with wave breaking was modeled based on a modification of the equations in works by Dally and Brown, and Larson and Kraus, in which the term for the roller energy flux in the alongshore direction was added to the energy balance equation. The nearshore currents and water elevation were determined from the continuity equation together with the depth-averaged momentum equations. The model was validated by three unique high-quality data sets obtained during experiments on detached breakwaters in the large-scale sediment transport facility basin at the Coastal and Hydraulics Laboratory in Vicksburg, Miss. The calculated significant wave height and longshore current were in good agreement with these measurements, whereas the cross-shore current was underestimated because undertow processes were not included in the modeling (depth-averaged equations employed). The calculated wave setup was somewhat overestimated; however, the absolute differences between the calculations and measurements were overall relatively small.

DOI: 10.1061/(ASCE)WW.1943-5460.0000038

CE Database subject headings: Breaking waves; Surf zones; Hydrodynamics; Nearshore; Water circulation; Breakwaters.

Author keywords: Breaking waves; Surf zone; Hydrodynamics; Nearshore circulation; Breakwaters.

Introduction

Detached breakwaters are frequently used to create favorable wave and current conditions in coastal areas. Thus, these structures are often employed for shore protection purposes since they reduce the longshore sediment transport generated by obliquely incident breaking waves preventing erosion along specific coastal stretches. A quantitative understanding of nearshore waves and currents in the vicinity of detached breakwaters is essential for the design and analysis of such structures with focus on the morphological evolution. Waves and currents mobilize, suspend, and transport sediment and gradients in the transport rate cause deposition or erosion of sediment, affecting the local bathymetry. A reliable and robust model of nearshore waves and currents is required to effectively predict sediment transport and the associated beach morphological evolution.

The wave energy balance equation is commonly applied for the prediction of multidirectional random wave transformation over large coastal areas. Originally, the nonstationary wave models WAM (WAMDI group 1988), and SWAN (Booij et al. 1996) were based on the energy balance equation with source terms. However, diffraction was not included in these models, which made it difficult to apply them to coastal areas containing engineering structures. Mase (2001) introduced the diffraction term into the wave energy balance equation using a parabolic approximation. The wave transformation model thus derived, referred to here as the EBED model, is stable and can be applied to complex coastal areas containing structures. However, the experience of the writers, during this and previous modeling studies, is that predictions by the EBED model often overestimate wave heights in the surf zone. Thus, the EBED model was modified in the present study before applying it to calculate the nearshore wave conditions.

Much research has demonstrated that the surface roller plays an important role in the generation of nearshore currents and changes in the mean water level. The roller was first applied theoretically by Svendsen (1984a, b) to improve the modeling of wave setup and undertow in the surf zone. Dally and Brown (1995) further developed the roller model based on a depth-integrated and period-averaged energy balance equation. The model was validated with a number of laboratory data sets, which showed good agreement between computations and measurements. Larson and Kraus (2002) also applied this roller model in the NMLong numerical model, which was developed to simulate the longshore current across a single profile line. The wave energy dissipation per unit area after Dally et al. (1985) was substituted for the gradient of energy flux (per unit length of crest) in the x direction of the energy balance for the roller. In almost all previous studies, the energy balance for the rollers was only taken in the cross-shore direction. Recently, Tajima and Madsen (2006) enhanced the energy balance equation in two dimensions. However, despite this improvement, it is still difficult to estimate how much broken wave energy dissipation is transferred into the sur-

[1]Doctoral Student, Dept. of Water Resources Engineering, Lund Univ., Box 118, SE-22100 Lund, Sweden; and, Researcher, Center for Marine Environment, Research and Consultation, Institute of Mechanics, Vietnamese Academy of Science and Technology, 264 Doi Can, Hanoi, Vietnam (corresponding author). E-mail: thanh_nam.pham@tvrl.lth.se

[2]Professor, Dept. of Water Resources Engineering, Lund Univ., Box 118, SE-22100 Lund, Sweden. E-mail: magnus.larson@tvrl.lth.se

Note. This manuscript was submitted on February 5, 2009; approved on September 30, 2009; published online on April 15, 2010. Discussion period open until October 1, 2010; separate discussions must be submitted for individual papers. This paper is part of the ***Journal of Waterway, Port, Coastal, and Ocean Engineering***, Vol. 136, No. 3, May 1, 2010. ©ASCE, ISSN 0733-950X/2010/3-156–176/$25.00.

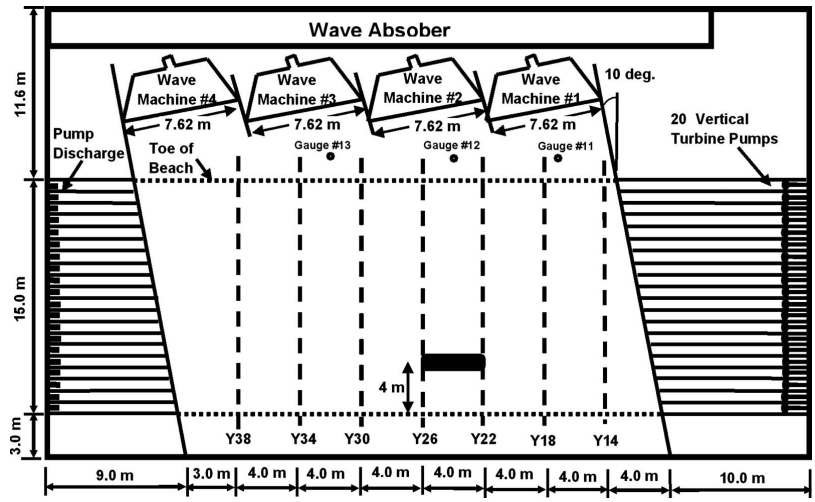

Fig. 1. Detached breakwater layout within LSTF for Tests 1 and 2 (Gravens and Wang 2007)

face roller, which decreases the accuracy in the calculation of the roller energy flux. In the present study, the approaches by Dally and Brown (1995) and Larson and Kraus (2002) were followed, and the energy flux term in the alongshore direction was included in the energy balance equation for the rollers.

There have been a number of studies on numerical models simulating the hydrodynamics in the vicinity of detached breakwaters. For example, Watanabe et al. (1986) simulated nearshore waves and currents around a detached breakwater and a groin, comparing the calculations with laboratory data. Péchon et al. (1997) employed seven numerical models for simulating the waves and currents in the vicinity of detached breakwaters, and intercompared them based on the laboratory data of Mory and Hamm (1997). However, these studies only dealt with regular waves and normal incidence. Sørensen et al. (1998) simulated the wave-induced horizontal nearshore circulation based on a time-domain Boussinesq-type model, and validated it with laboratory data. The computed wave height and wave setup were in good agreement with measurements for a limited number of profile lines. However, the comparison of calculated wave-induced currents with measurements was not detailed, especially for the test case on random waves. Zyserman and Johnson (2002) used a quasi three-dimensional model, dealing with random waves, to simulate flow, sediment transport, and morphological evolution.

Table 1. Offshore Wave Conditions

Data sets	Gauges	H_{mo} (m)	T_p (s)	θ (degrees)
T1C1	#11	0.219	1.442	6.5
	#12	0.236	1.470	6.5
	#13	0.226	1.459	6.5
T1C4	#11	0.222	1.452	6.5
	#12	0.232	1.472	6.5
	#13	0.225	1.464	6.5
T1C8	#11	0.219	1.457	6.5
	#12	0.236	1.468	6.5
	#13	0.224	1.461	6.5

Although the model produced reasonable-looking results of wave, current, and sediment transport, no validation was made due to lack of measurement data.

The objective of the present study was to develop a robust and reliable numerical model of nearshore waves and wave-induced currents, with the emphasis on coastal areas containing detached breakwaters. In order to do this, the wave energy dissipation due to wave breaking was modified in the energy balance equation of the EBED model. The modification resulted in better agreement between calculated and measured wave parameters for the data sets investigated. The two-dimensional creation and evolution of the surface roller associated with breaking waves was modeled based on an energy balance equation, which improved the prediction of radiation stresses due to rollers. These improvements then allowed for the development of a model of nearshore currents generated by random waves. In order to extend the model capability to a variety of conditions, including complex alongshore bathymetry, a general depth-averaged two-dimensional model of nearshore currents due to breaking waves, wind, and tides was developed. However, in the present paper the focus is on the wave-induced currents. The validation of the model developed was based on high-quality and synchronized data from experiments on detached breakwaters carried out in the large-scale sediment transport facility (LSTF) basin of the Coastal and Hydraulics Laboratory (CHL), U.S. Army Engineer Research and Development Center, in Vicksburg, Mississippi, United States.

Wave Model

Random Wave Model EBED

EBED is a multidirectional random wave transformation model, developed by Mase (2001) and based on the energy balance equation including energy dissipation and diffraction terms. The governing equation for steady state is expressed as follows:

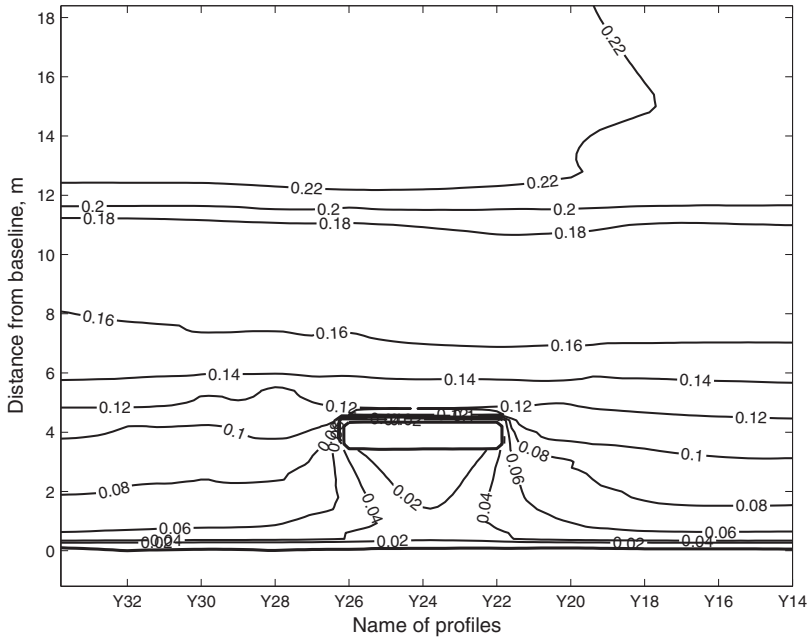

Fig. 2. Distribution of calculated significant wave height for LSTF Case T1C1

$$\frac{\partial(v_x S)}{\partial x} + \frac{\partial(v_y S)}{\partial y} + \frac{\partial(v_\theta S)}{\partial \theta} = \frac{\kappa}{2\omega}\left\{(CC_g \cos^2\theta S_y)_y - \frac{1}{2}CC_g \cos^2\theta S_{yy}\right\} - \varepsilon_b S \quad (1)$$

where S=angular-frequency spectrum density; (x,y)=horizontal coordinates; θ=angle measured counterclockwise from the x axis; v_x, v_y, and v_θ=propagation velocities in their respective coordinate direction; ω=frequency; C=phase speed; and C_g=group speed. The first term on the right-hand side is added in the balance equation in order to represent the diffraction effects, and κ is a free parameter that can be optimized to change the influence of the diffraction effects. The second term represents the wave energy dissipation due to breaking waves, and ε_b is the energy dissipation coefficient. The output from the wave transformation model includes three main wave parameters: significant wave height H_s, significant wave period T_s, and mean wave direction $\bar{\theta}$ [for details see Mase (2001)].

Modified-EBED Model

The EBED model is stable and can be applied to complex beach topographies in coastal zones containing structures. However, it often overpredicts the wave heights in the surf zone compared to measurements. The overestimation is due mainly to the algorithm describing wave energy dissipation caused by wave breaking. In the EBED model, the energy dissipation coefficient is determined by the Takayama et al. (1991) model. The calculation of this coefficient is rather complex and the coefficient does not easily lend itself to calibration.

In this study, we modified the energy dissipation term based on the Dally et al. (1985) model in order to improve the predictive capability of the wave model in the surf zone. The modified energy balance equation proposed is as follows:

$$\frac{\partial(v_x S)}{\partial x} + \frac{\partial(v_y S)}{\partial y} + \frac{\partial(v_\theta S)}{\partial \theta} = \frac{\kappa}{2\omega}\left\{(CC_g \cos^2\theta S_y)_y - \frac{1}{2}CC_g \cos^2\theta S_{yy}\right\} - \frac{K}{h}C_g(S - S_{\text{stab}}) \quad (2)$$

where h=still-water depth; K=dimensionless decay coefficient; and S_{stab}=stable wave spectrum density, which is a function of the stable wave height H_{stab} ($=\Gamma h$), with Γ being a dimensionless empirical coefficient. The model is referred to as the Modified-EBED model hereafter.

Several previous studies have dealt with the empirical coefficients Γ and K. The value of these coefficients can be given by constants, e.g., $\Gamma=0.4$ and $K=0.15$ (Dally et al. 1985), or empirical expressions containing the bottom slope [see Goda (2006) and Tajima and Madsen (2006)]. In the Modified-EBED model, a good description was obtained of the wave conditions in the surf zone for the LSTF data by modifying the expressions for the coefficients proposed by Goda (2006) as follows:

$$\begin{cases} \Gamma = 0.45, & K = \dfrac{3}{8}(0.3 - 19.2s): \quad s < 0 \\ \Gamma = 0.45 + 1.5s, & K = \dfrac{3}{8}(0.3 - 0.5s): \quad 0 \le s \le 0.6 \end{cases} \quad (3)$$

where s=bottom slope.

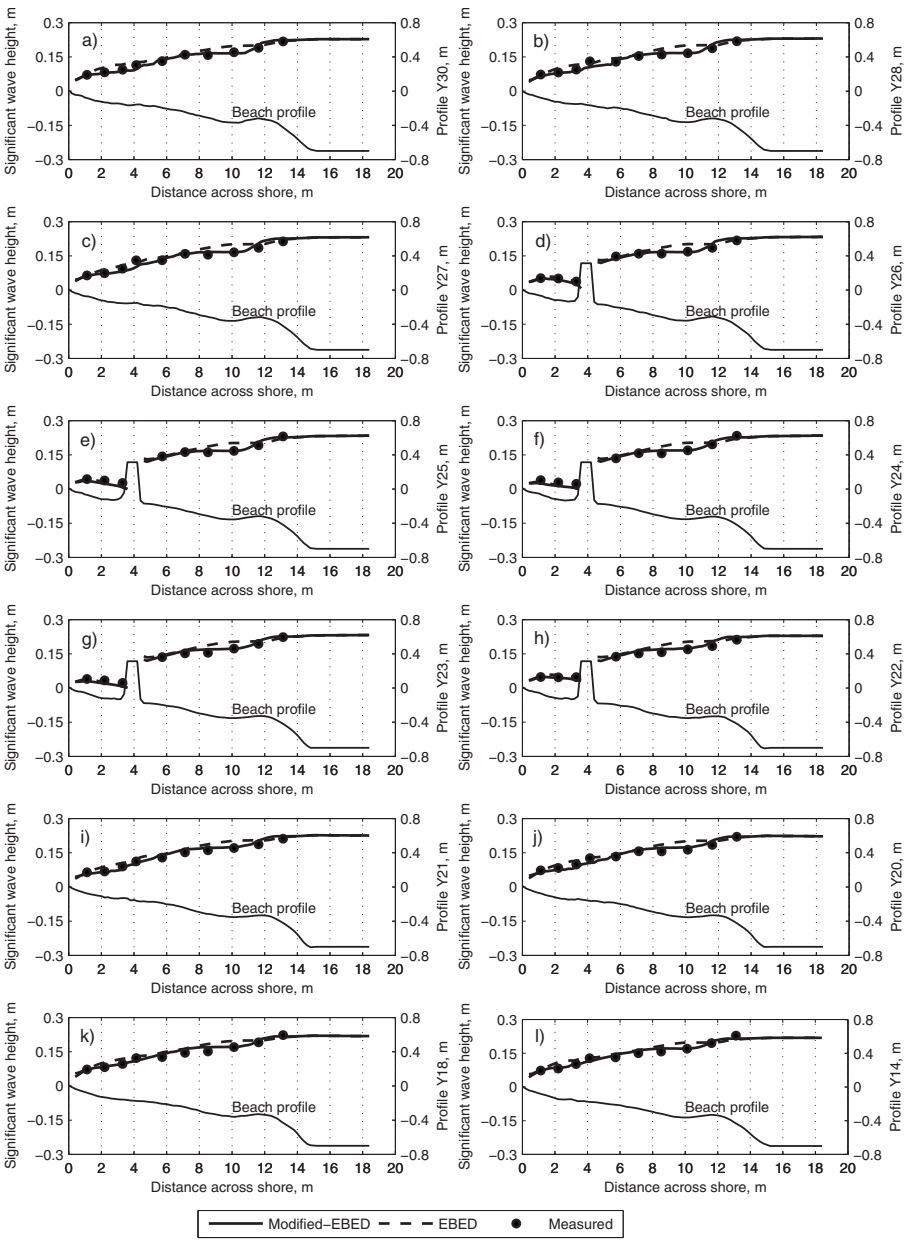

Fig. 3. Comparison of calculated and measured significant wave heights for LSTF Case T1C1

Surface Roller Model

The wave energy balance equation for surface rollers in two dimensions is expressed as (Dally and Brown 1995; Larson and Kraus 2002):

$$P_D + \frac{\partial}{\partial x}\left(\frac{1}{2}MC_r^2\cos^2\bar{\theta}\right) + \frac{\partial}{\partial y}\left(\frac{1}{2}MC_r^2\sin^2\bar{\theta}\right) = g\beta_D M \quad (4)$$

where P_D=wave energy dissipation [$=KC_g\rho g(H_{\text{rms}}^2 - (\Gamma h)^2)/(8h)$]; M=period-averaged mass flux; C_r=roller speed ($\approx C$); and β_D=roller dissipation coefficient.

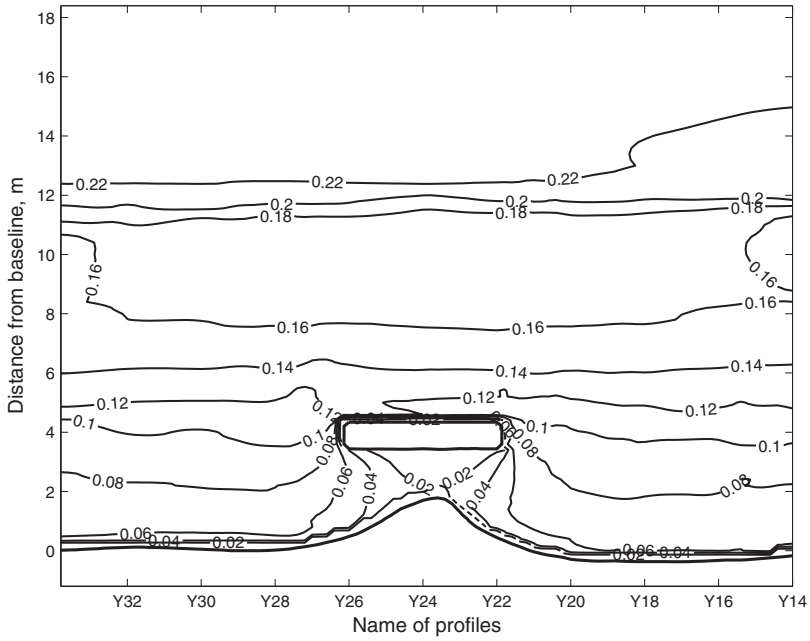

Fig. 4. Distribution of calculated significant wave height for LSTF Case T1C4

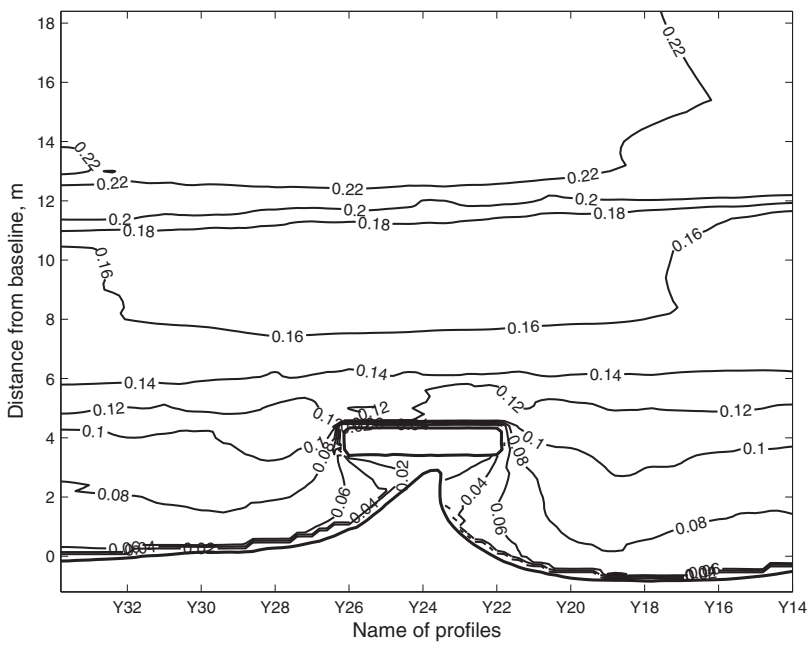

Fig. 5. Distribution of calculated significant wave height for LSTF Case T1C8

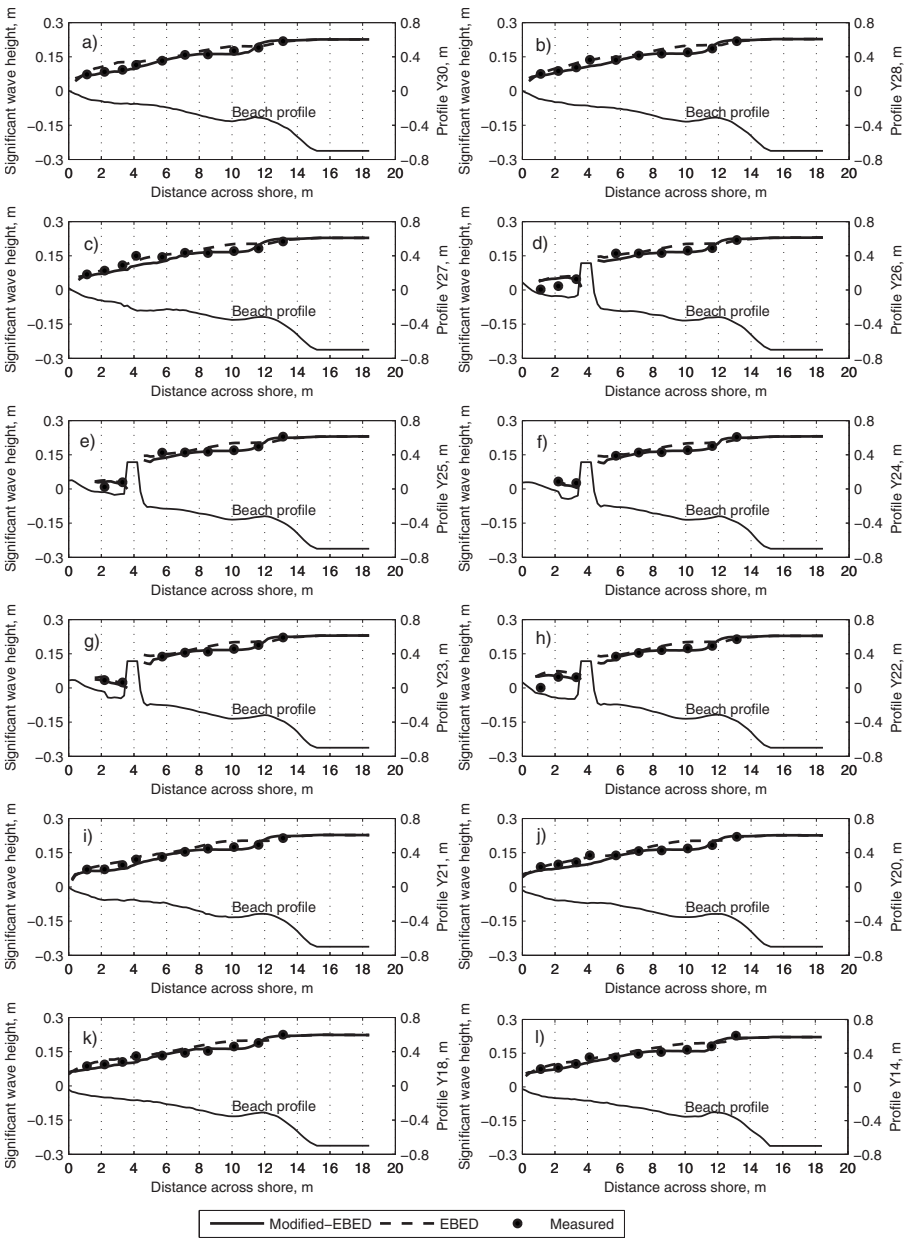

Fig. 6. Comparison of calculated and measured significant wave heights for LSTF Case T1C4

Nearshore Current Model

The governing equations for nearshore currents are written as (Militello et al. 2004)

$$\frac{\partial(h+\eta)}{\partial t}+\frac{\partial q_x}{\partial x}+\frac{\partial q_y}{\partial y}=0 \tag{5}$$

$$\frac{\partial q_x}{\partial t}+\frac{\partial u q_x}{\partial x}+\frac{\partial v q_x}{\partial y}+g(h+\eta)\frac{\partial \eta}{\partial x}$$
$$=\frac{\partial}{\partial x}D_x\frac{\partial q_x}{\partial x}+\frac{\partial}{\partial y}D_y\frac{\partial q_x}{\partial y}+fq_y-\tau_{bx}+\tau_{Sx} \tag{6}$$

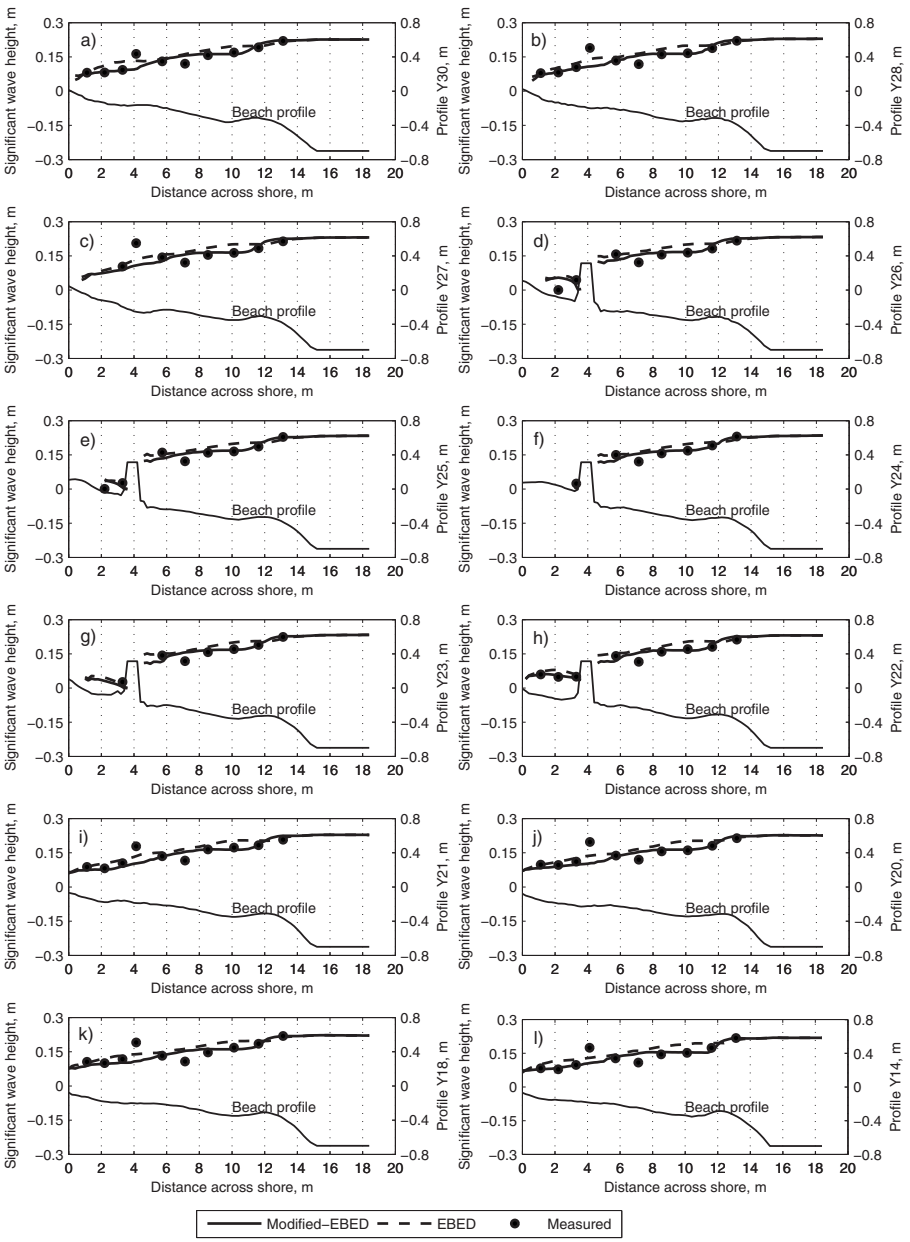

Fig. 7. Comparison of calculated and measured significant wave heights for LSTF Case T1C8

$$\frac{\partial q_y}{\partial t} + \frac{\partial u q_y}{\partial x} + \frac{\partial v q_y}{\partial y} + g(h+\eta)\frac{\partial \eta}{\partial y} = \frac{\partial}{\partial x} D_x \frac{\partial q_y}{\partial x} + \frac{\partial}{\partial y} D_y \frac{\partial q_y}{\partial y} - f q_x - \tau_{by} + \tau_{Sy} \quad (7)$$

where η=water elevation; q_x and q_y=flow per unit width parallel to the x and y axes, respectively; u and v=depth-averaged velocity components in the x and y directions, respectively; g=acceleration due to gravity; D_x and D_y=eddy viscosity coefficients; f=Coriolis parameter; τ_{bx} and τ_{by}=bottom stresses; and τ_{Sx} and τ_{Sy}=wave stresses (the latter variables are all in the x- and y-directions, respectively).

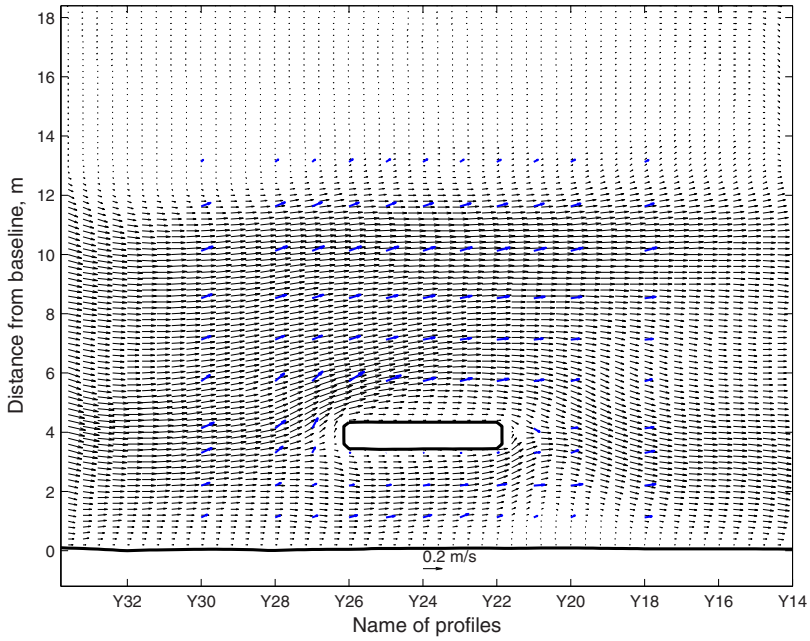

Fig. 8. Distribution of calculated and measured nearshore currents for LSTF Case T1C1

Outside the surf zone, the depth-averaged horizontal eddy viscosity coefficient can be calculated as a function of the total water depth, current speed, and bottom roughness according to Falconer (1980). In the surf zone, the eddy viscosity was taken to be a function of the wave properties following Kraus and Larson (1991). The bottom stresses under combined current and waves were determined from Nishimura (1988).

The wave stresses are derived from the wave transformation model and the surface roller model. They are given by the following equations:

$$\tau_{Sx} = -\frac{1}{\rho_w}\left[\frac{\partial}{\partial x}(S_{xx}+R_{xx})+\frac{\partial}{\partial y}(S_{xy}+R_{xy})\right] \tag{8}$$

$$\tau_{Sy} = -\frac{1}{\rho_w}\left[\frac{\partial}{\partial x}(S_{xy}+R_{xy})+\frac{\partial}{\partial y}(S_{yy}+R_{yy})\right] \tag{9}$$

where ρ_w=water density; S_{xx}, S_{xy}, and S_{yy}=wave-driven radiation stresses; and R_{xx}, R_{xy}, and R_{yy}=radiation stresses due to the roller. These stresses are determined from

$$S_{xx} = \frac{E}{2}[2n(1+\cos^2\bar{\theta})-1]; \quad S_{yy} = \frac{E}{2}[2n(1+\sin^2\bar{\theta})-1];$$

$$S_{xy} = S_{yx} = \frac{E}{2}n\sin 2\bar{\theta} \tag{10}$$

$$R_{xx} = MC_r\cos^2\bar{\theta}; \quad R_{yy} = MC_r\sin^2\bar{\theta}; \quad R_{xy} = R_{yx} = MC_r\sin 2\bar{\theta} \tag{11}$$

where $E=\rho_w g H_{\text{rms}}^2/8$ is the wave energy per unit area and $n=C_g/C$=wave index.

LSTF Data

Five series of movable bed physical model experiments were conducted in the LSTF basin by Gravens et al. (2006) and Gravens and Wang (2007). A main objective of these experiments was to generate high-quality data sets for validating models to simulate the development of tombolos in the lee of nearshore detached breakwaters and T-head groins. The initial beach was constructed

Table 2. RMS Error (%) of Significant Wave Height, Longshore Current, Cross-Shore Current, and Wave Setup

Data sets	H_s modified-EBED	H_s EBED	v with roller	v without roller	u with roller	u without roller	η with roller	η without roller
T1C1	6.96	12.36	22.67	19.55	88.71	86.25	77.48	84.80
T1C4	8.39	11.75	35.73	34.24	92.66	82.97	83.65	94.13
T1C8	19.26	20.33	36.65	38.02	107.49	99.45	100.50	110.34

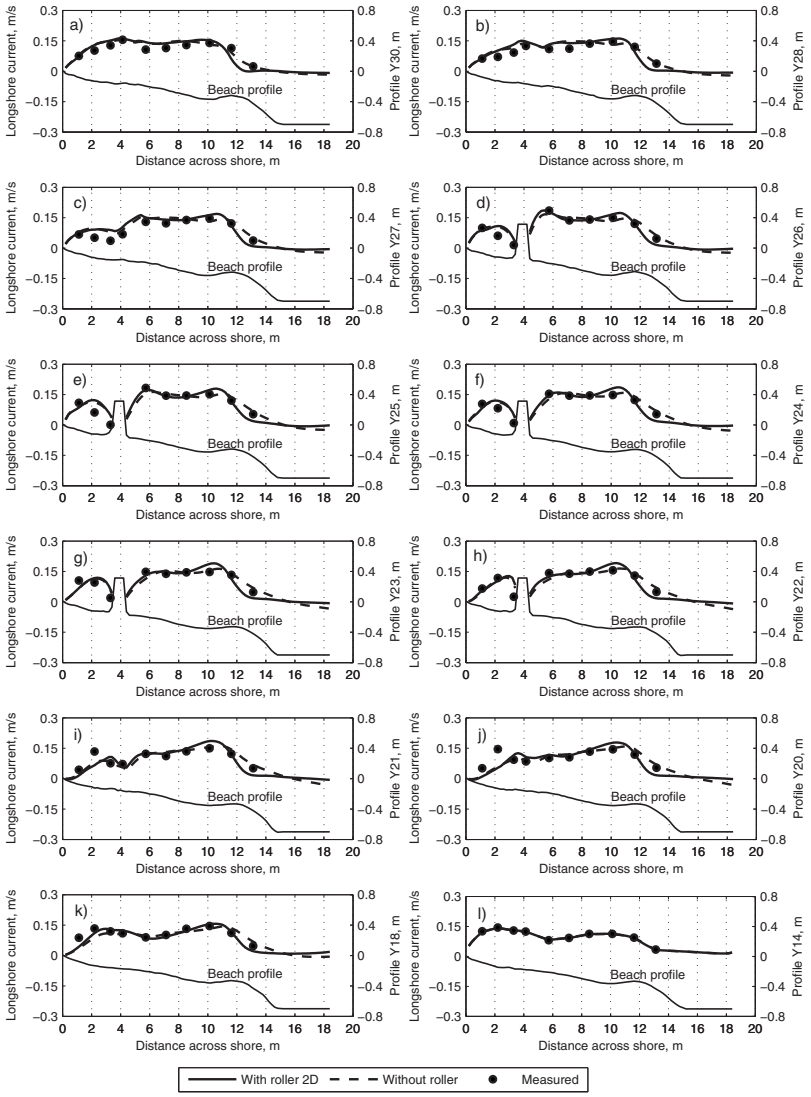

Fig. 9. Comparison of calculated and measured longshore currents for LSTF Case T1C1

with shore-parallel bottom contours and consisted of very well-sorted fine quartz sand with a median grain size of 0.15 mm. Four wave generators were programmed to produce spilling breaking waves in all experiments. The LSTF external pump system was used to maintain longshore current with a given cross-shore distribution.

Test 1 (T1), from which data were employed in this study, encompassed eight experimental runs of approximately 190 min each. In all these runs, a rubble-mound detached breakwater was used that was 4 m long and located 4 m from the initial still-water shoreline. The detached breakwater was constructed parallel to the initial shoreline (see Fig. 1). Three runs—T1C1, T1C4, and T1C8—were selected in order to evaluate the predictive capability of the model regarding nearshore waves and currents corresponding to three morphological developments of the salient: (1) initial conditions with no salient; (2) distinct salient with the tip located approximately midway between the initial shoreline and the detached breakwater; and (3) salient close to equilibrium with its tip almost reaching to the detached breakwater (close to a tombolo).

The wave height, wave period, and wave setup were measured using 13 capacitance gauges, whereas the data on nearshore current were collected and measured by 10 acoustic-Doppler velocimeters (ADVs). Ten wave and current sensors were colocated in a cross-shore array on the instrumentation bridge. The ten locations were 1.125 m (ADV1), 2.725 m (ADV2), 3.3 (ADV3), 4.125 m

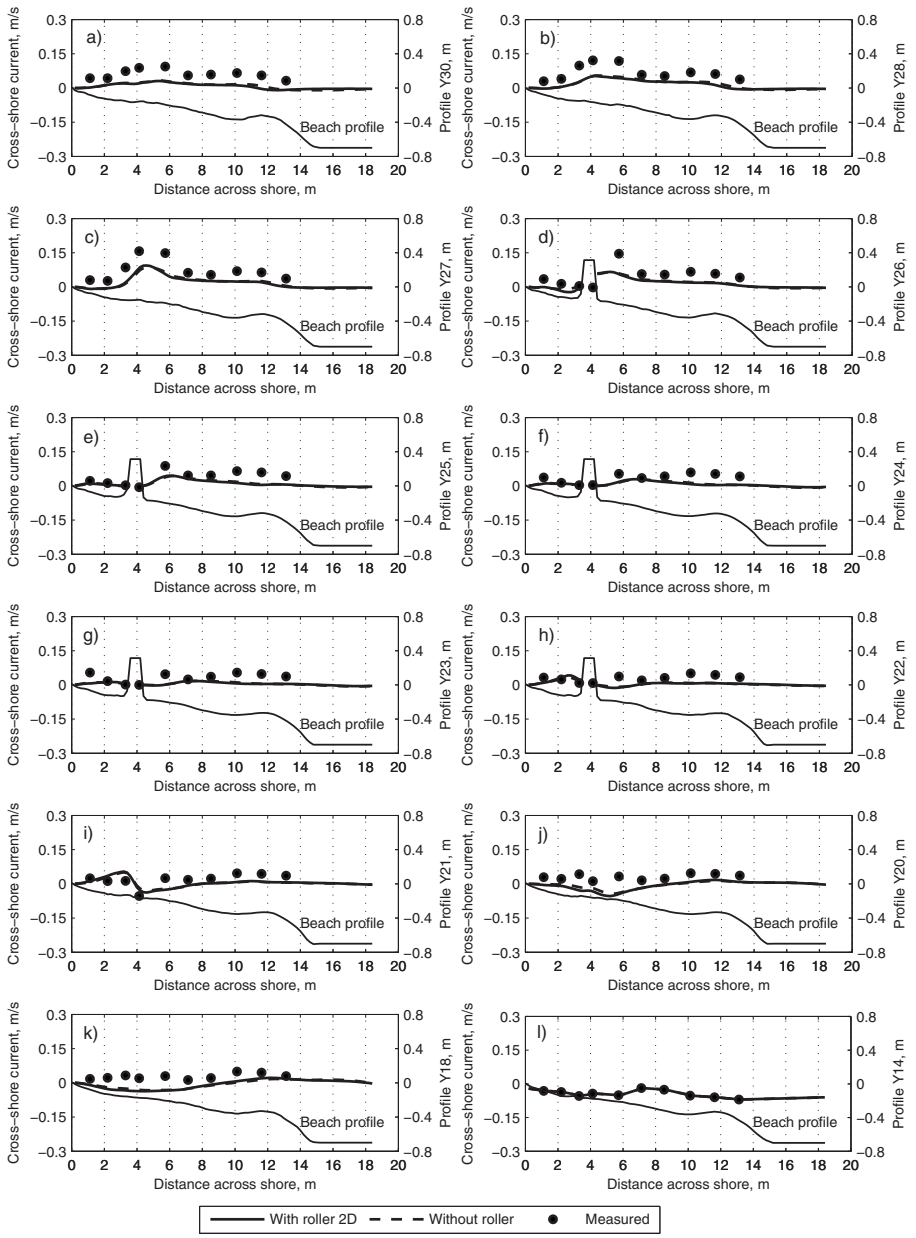

Fig. 10. Comparison of calculated and measured cross-shore currents for LSTF Case T1C1

(ADV4), 5.73 m (ADV5), 7.125 m (ADV6), 8.525 m (ADV7), 10.125 m (ADV8), 11.625 m (ADV9), and 13.125 m (ADV10) seaward from the initial still-water shoreline. To measure wave conditions seaward of the toe of the movable beach, the three remaining wave sensors—Gauge#11, Gauge#12, and Gauge#13—were located at three alongshore positions, a distance 18.43 m seaward from the initial still-water shoreline (see Fig. 1).

The LSTF data employed to validate the model were collected

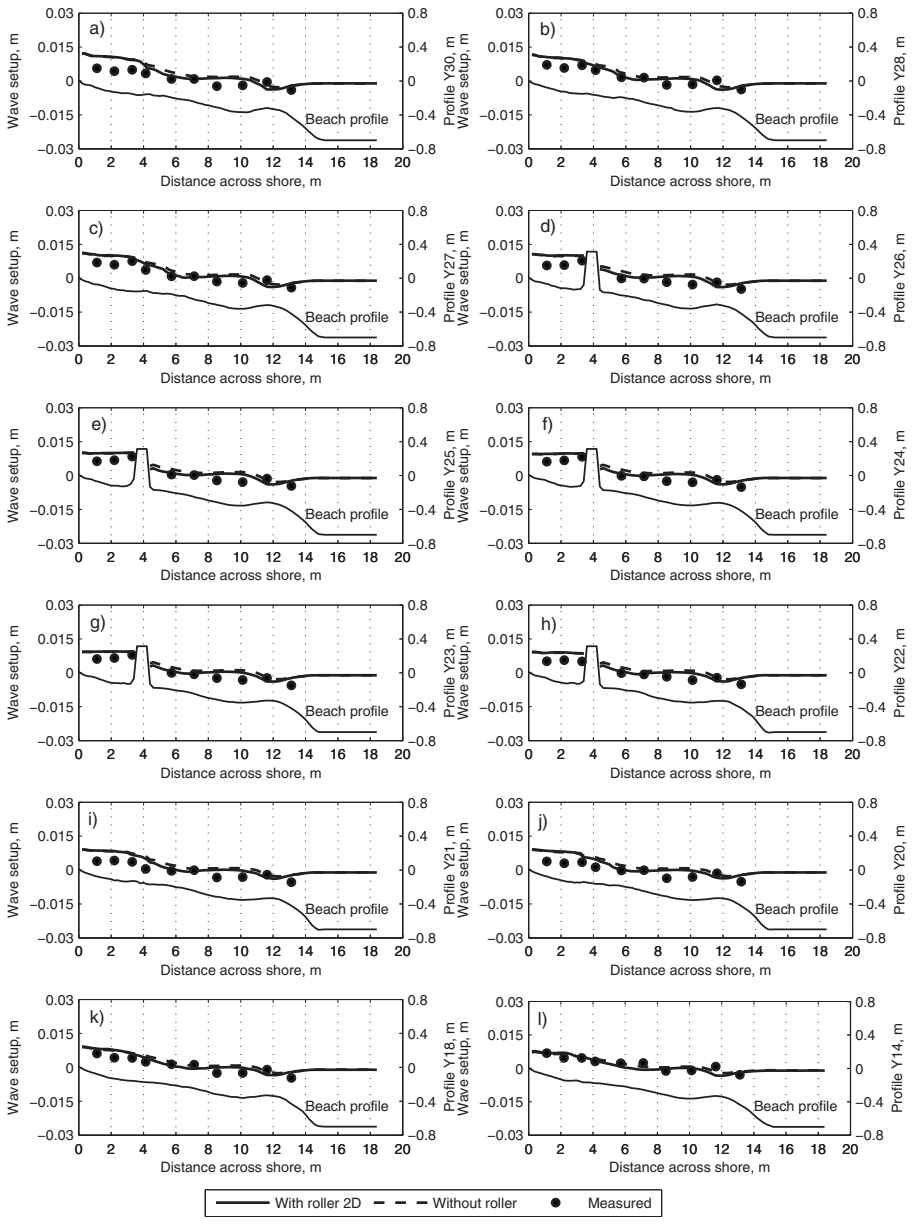

Fig. 11. Comparison of calculated and measured wave setups for LSTF Case T1C1

and analyzed by M. B. Gravens and P. Wang, personal communication, 2009. A Matlab routine using the semistandard power spectral density (PSD) and cross spectral density (CSD) (Welch 1967) functions were employed for spectral analyses of water level, current, and sediment concentration. Wave setup is the average water level over the 10-min sampling. The depth-averaged velocity is obtained by a simple averaging of the measured velocities at 3 to 8 levels through the water column. For more detailed information, see Wang et al. (2002a,b, 2003) and Wang (2006).

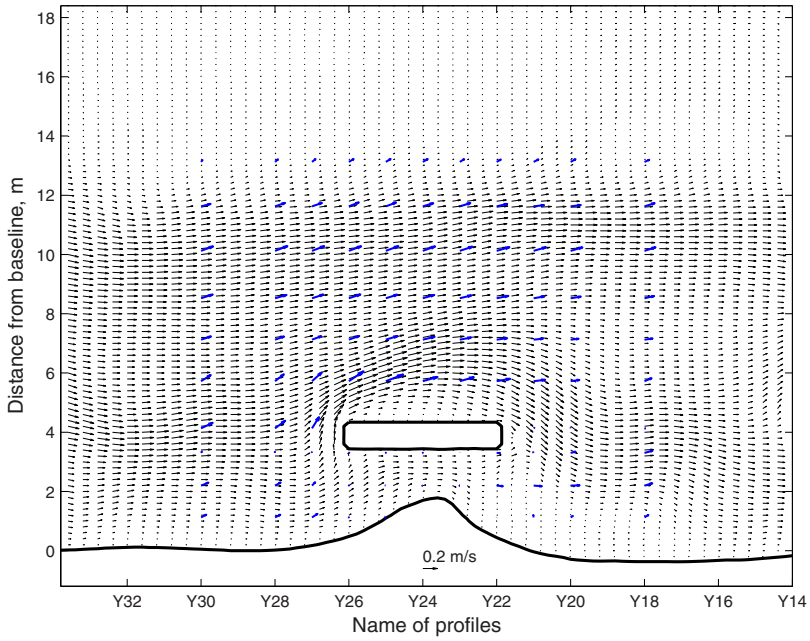

Fig. 12. Distribution of calculated and measured nearshore currents for LSTF Case T1C4

Comparison with LSTF Data

Comparison of Significant Wave Height

The computational grid for T1C1 was generated based on the beach profile data, from profile Y34 to profile Y14, through interpolation with a cell size 0.2×0.2 m. The wave measurements at Gauge#11, Gauge#12, and Gauge#13 were used as offshore wave conditions (model input). Detailed information of the offshore wave conditions at these points is presented in Table 1. A Texel, Marsen, and Arsloe (TMA) shallo-water spectrum was assumed at the offshore boundary with the parameter values $\gamma=3.3$, $\sigma_a=0.07$, $\sigma_b=0.09$, and the angular spreading of the waves $S_{\max}=25$. The decay and stable coefficients in the wave model were determined from Eq. (3).

Fig. 2 shows the spatial distribution of significant wave height obtained from the Modified-EBED model for T1C1. The wave diffraction effects are clearly seen behind the detached breakwater. Fig. 3 describes in detail the comparison between the computed results for the significant wave height and the corresponding measurements at 12 profile lines, from profile Y30 to profile Y14. The dashed line is the calculated significant wave height obtained with the original EBED model, which overestimated the wave height in the surf zone compared to the measured data, especially at ADV7 and ADV8 for all profile lines.

As can be seen, the Modified-EBED model based on a new approach for calculating wave energy dissipation produced improved results. The calculated significant wave height agreed well with the measured data at all measurement locations along the profile lines.

The computations of nearshore waves for T1C4 and T1C8 were carried out in the same manner as for T1C1. Figs. 4 and 5 show the contour lines of calculated significant wave height for T1C4 and T1C8, respectively. These figures clearly illustrate the impact of the salient development on the wave diffraction behind the detached breakwater. The simulations also demonstrated that the model remains stable in spite of the complex topography that develops behind the breakwater and that it produces robust and reliable results.

The detailed comparisons between the measured and calculated significant wave height along the 12 profile lines for T1C4 and T1C8 are presented in Figs. 6 and 7, respectively. As for T1C1, the wave predictions obtained with the Modified-EBED model were better than those by the original EBED model. As can be seen in the figures, the EBED model often overpredicts the wave heights at ADV7, ADV8, and ADV9. Although the significant wave height at some measurement locations near the shoreline was slightly underestimated by the Modified-EBED model, it successfully reproduced the significant wave height for both T1C4 and T1C8.

Quantitative assessment of the EBED and Modified-EBED models using the RMS error clearly shows that the modified model produced better agreement with the measured data. For example, the RMS error in the significant wave height obtained by the Modified-EBED model for T1C1 was only 6.96%, whereas it was 12.36% for the EBED model. For T1C8, the measurement of the significant wave height at ADV4 for several profile lines might not be correct [see Figs. 7(a–c and i–l)], thus it caused the RMS errors to become higher than that of T1C1 and T1C4. How-

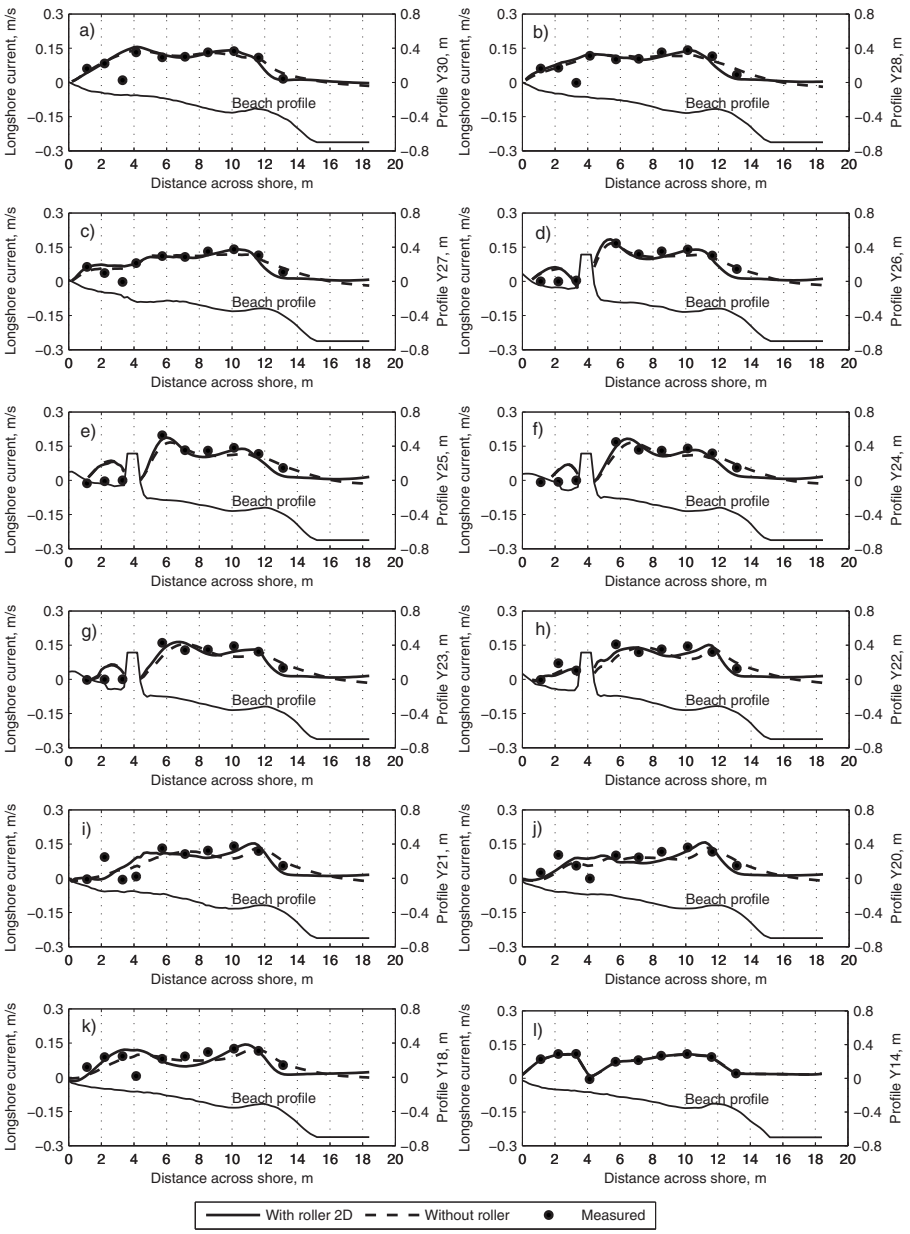

Fig. 13. Comparison of calculated and measured longshore currents for LSTF Case T1C4

ever, the RMS error for the significant wave height obtained using the Modified-EBED model (19.26%) was also better than that by the EBED model (20.33%). Table 2 summarizes in detail the RMS errors between computations and measurements for the significant wave height obtained by the EBED and the Modified-EBED model.

Mass Flux Obtained by 2D and 1D Surface Roller Model

The wave energy dissipation per unit area, P_D, was determined based on the RMS wave height, which can be derived from the wave calculations with the Modified-EBED model. The roller dis-

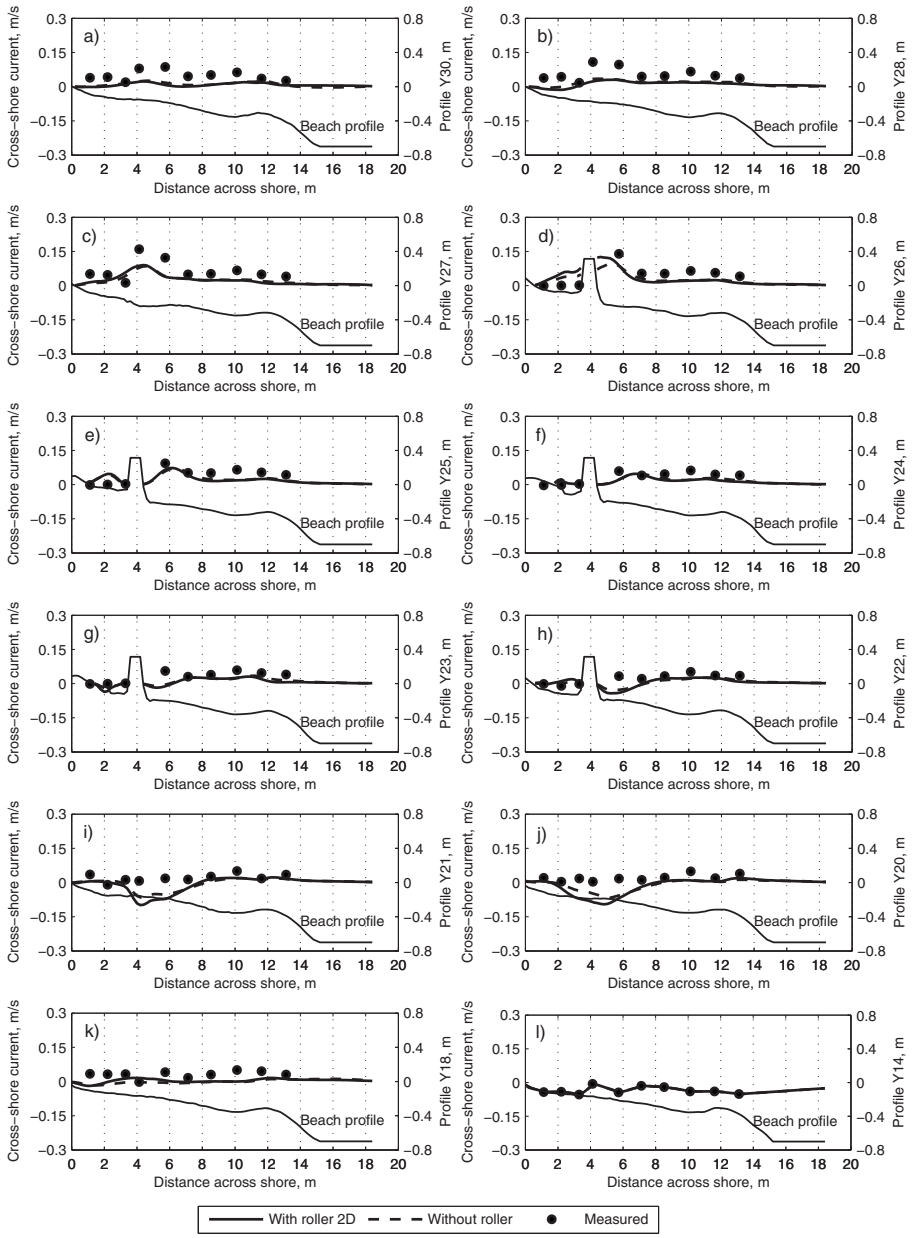

Fig. 14. Comparison of calculated and measured cross-shore currents for LSTF Case T1C4

sipation coefficient was set to 0.1 (Dally and Brown 1995). The maximum roller mass fluxes, M, obtained by Eq. (4) for T1C1, T1C4, and T1C8 were 9.33, 9.74, and 14.78 kg/m/s, respectively. If the energy flux term in the alongshore direction was neglected in Eq. (4), giving rise to a 1D surface roller model, these maximum values of mass flux would change to 9.28, 8.35, and 13.58 kg/m/s, respectively.

The relative difference in roller mass flux obtained with the 2D

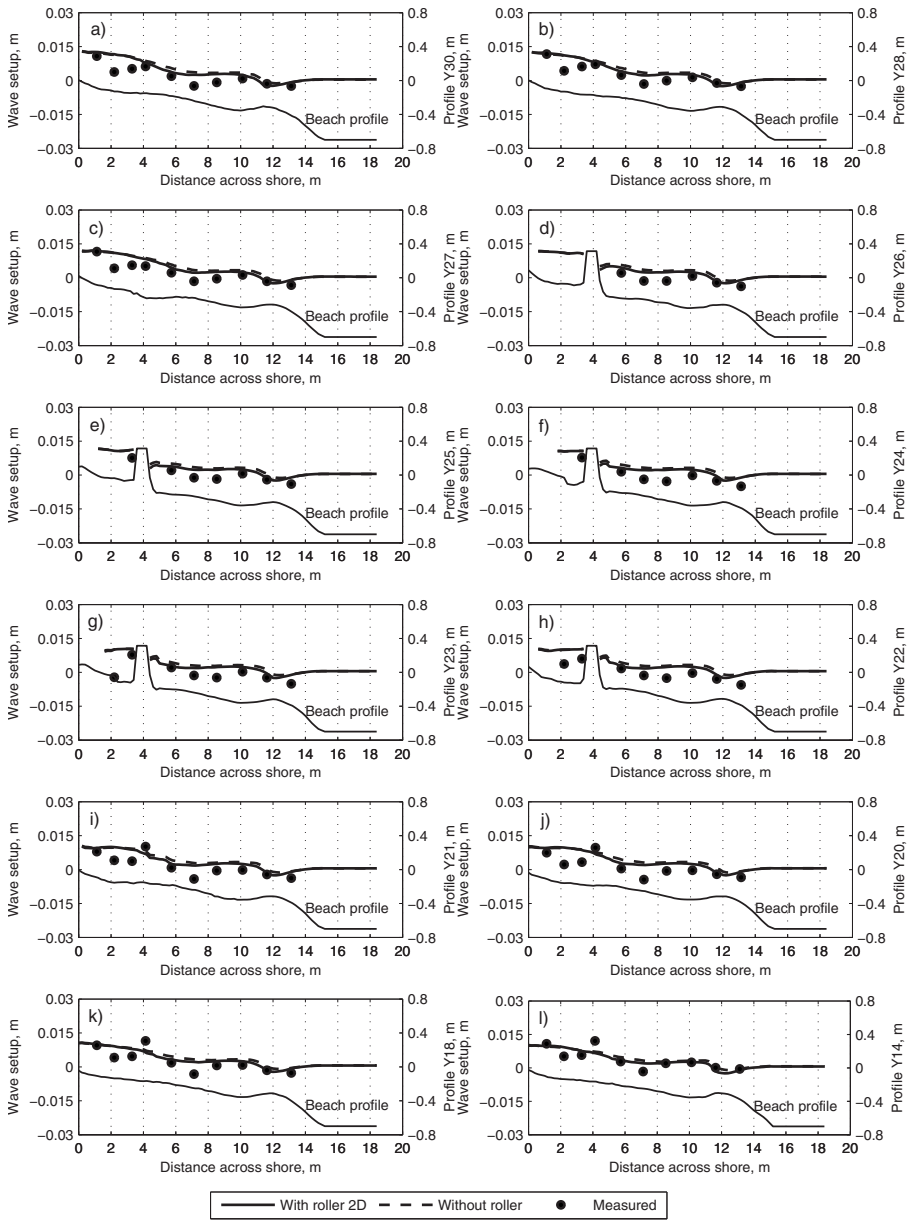

Fig. 15. Comparison of calculated and measured wave setups for LSTF Case T1C4

and 1D surface roller models for the test cases investigated was rather small. The maximum of the relative difference can be about 10% at some locations where the waves were broken. However, the absolute difference in mass flux was very small, implying that the difference between the wave stresses due to the roller obtained by the 2D and 1D surface roller model for the investigated cases was not significant. Thus, for similar conditions it may be possible to employ a 1D instead of a 2D model to save time in the model execution, although this is something that has to be examined for the particular application.

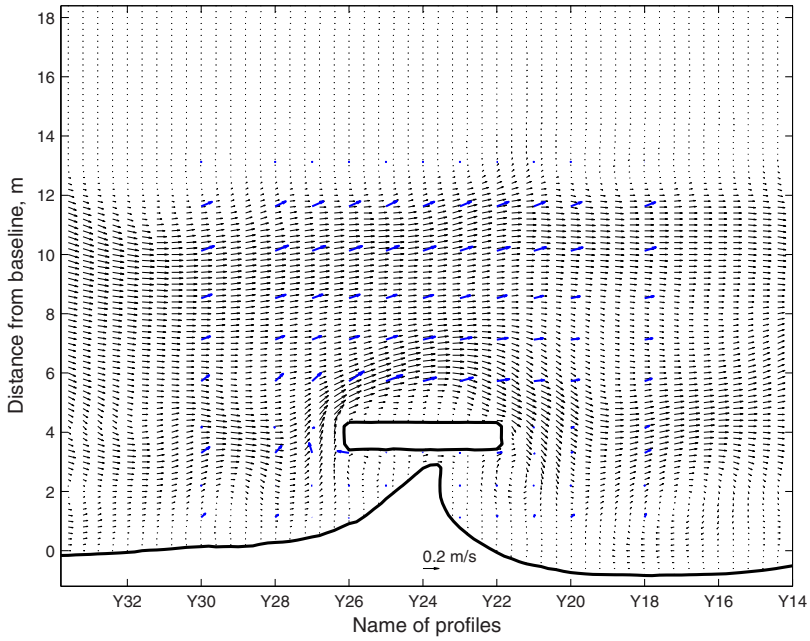

Fig. 16. Distribution of calculated and measured nearshore currents for LSTF Case T1C8

Comparison of Longshore Current, Cross-Shore Current, and Wave Setup

The output from the Modified-EBED model, including the significant wave height, wave direction, and wave period, was employed to calculate the nearshore current. The wave-driven stresses and the stresses due to the roller were derived from the Modified-EBED model and the surface roller model, respectively. The Manning coefficient was given as 0.025 to determine the bottom friction stresses. At both the upstream and downstream boundary, the water fluxes were given based on the measurement data of nearshore current on profiles Y34 and Y14. At the offshore boundary, the radiation boundary condition was employed (Reid and Bodine 1968).

Fig. 8 shows the spatial distribution of calculated and measured nearshore currents for T1C1. Note that the calculated vectors were plotted at 0.4-m interval in the alongshore direction, and measured vectors were presented by using the bold vectors. The calculation shows a small eddy was created on the right of the detached breakwater. Normally, two symmetric eddies are created in the lee of a detached breakwater, if the incident wave direction is perpendicular to the shoreline, the bathymetry is uniform in the alongshore direction, and the water fluxes are free to be transmitted through the lateral boundaries. However, in the T1C1 run, the incident waves were oblique to the shoreline, and the influx and outflux of water were specified at the upstream and downstream boundaries based on the measured velocities. Therefore, in the T1C1 run, only one eddy was created and it was shifted to the right in the lee of the detached breakwater.

Figs. 9 and 10 show the detailed comparison between the calculated and measured longshore current and cross-shore current with and without roller at the 12 profile lines for T1C1. Note that the longshore current is the velocity component parallel to the y axis (with positive value when the flow is from left to right) and cross-shore current is the component perpendicular to this axis (with positive value in the offshore direction). The computational results show that the surface roller not only shifted the peak of the longshore current toward the shoreline but also increased the maximum current in the surf zone. As can be seen, the longshore current with and without roller agreed well with the measurements. The calculated cross-shore current with roller was quite similar to the one without roller, and the current agreed fairly well with measurements in the lee of the detached breakwater, although it underestimated the measurements at some profiles near the upstream and downstream boundaries. The main reason for the underestimation is probably that the undertow current was not accounted for in the model.

Fig. 11 compares the measured and computed wave setup for the 12 profile lines of T1C1. The calculated wave setup with roller was slightly different from that without roller. The model reproduced the wave setup well, although the setup tends to be overestimated compared to the measured data at ADV1, ADV2, and ADV3.

Fig. 12 illustrates the spatial distribution of the calculated and measured nearshore currents for T1C4. The calculated eddy to the right of the detached breakwater was larger and stronger than for T1C1 due to the salient. Fig. 13 shows the detailed comparison between the calculated and measured longshore current. As for T1C1, the model also produced good agreement with the measurement, especially for the locations seaward of the detached breakwater. However, the measured longshore current was small at ADV1, ADV2, and ADV3 from profile lines Y23 to Y26. The calculated longshore current overestimated measurements at these locations [see Figs. 13(d–g)].

The detailed comparison between the calculated and measured

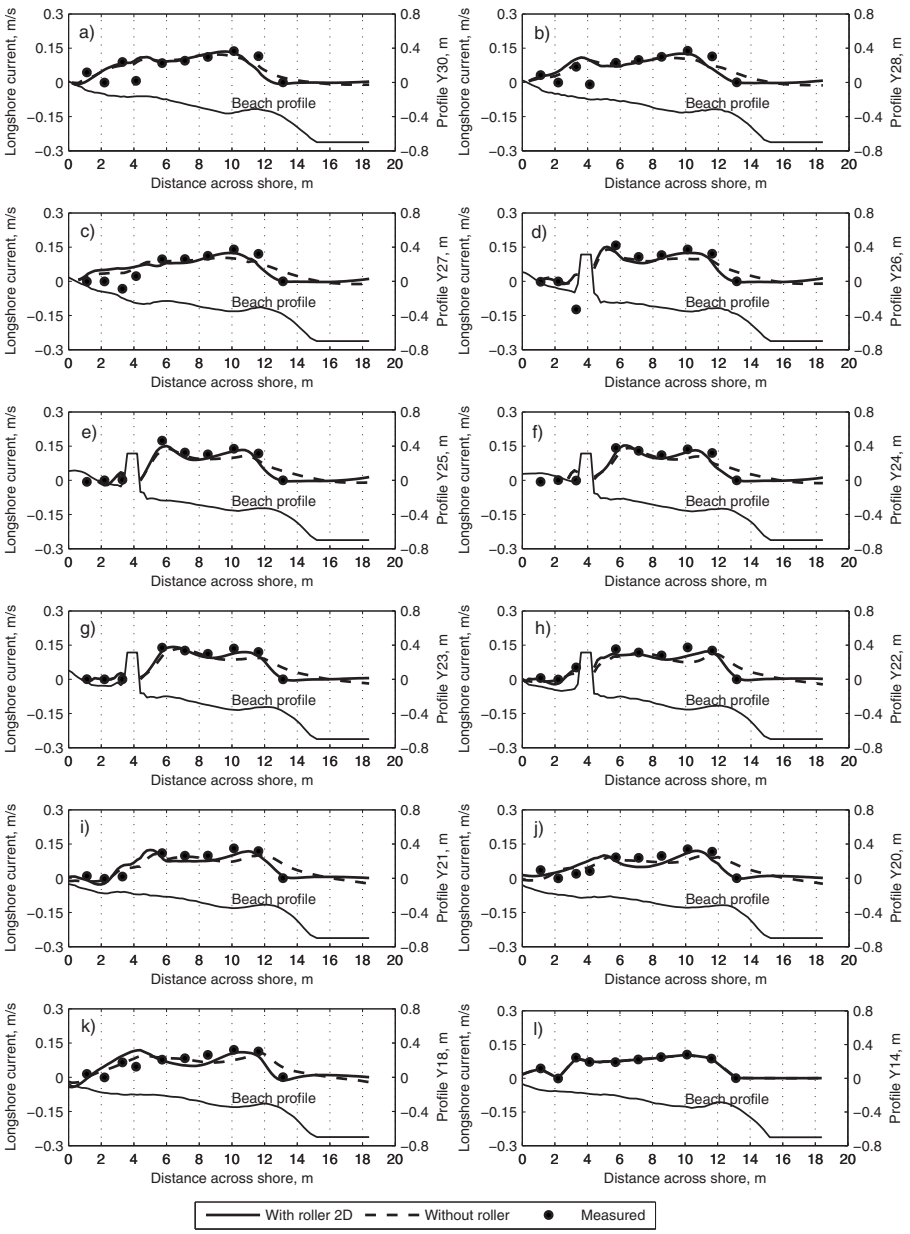

Fig. 17. Comparison of calculated and measured longshore currents for LSTF Case T1C8

cross-shore current for T1C4 is presented in Fig. 14. As for T1C1, the cross-shore current agreed fairly well with measurement in the lee of detached breakwater. The direction of the calculated cross-shore current was shoreward at ADV4, ADV5, and ADV6 of the profiles Y21 and Y20 [see Figs. 14(i and j)], where the measured current distribution was quite flat and close to zero. Again, the likely explanation for this discrepancy is not including the undertow in the modeling, which would add a seaward contribution to the current under wave trough level.

Fig. 15 shows the comparison between calculated and measured wave setup for T1C4. In general, the calculated wave setup agreed fairly well with the measurements from ADV4 to ADV10,

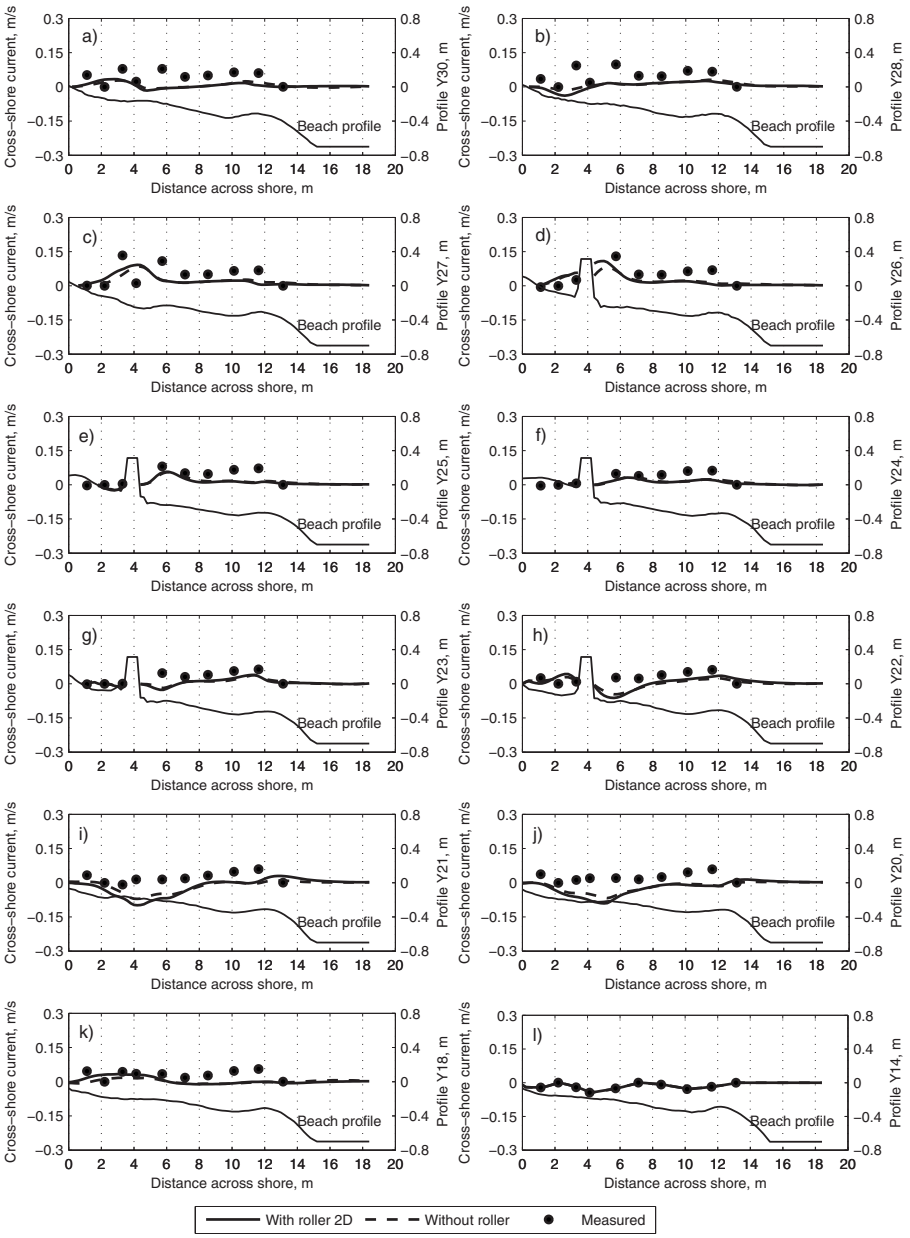

Fig. 18. Comparison of calculated and measured cross-shore currents for LSTF Case T1C8

but some overestimation occurred at ADV2 and ADV3. The wave setup was not observed at some locations in very shallow water behind the detached breakwater.

Fig. 16 shows the spatial distribution of the calculated and measured nearshore current for T1C8. Because the tip of the salient was close to the detached breakwater, the calculated eddy was even stronger than for T1C4. Fig. 17 presents the detailed comparison between calculated and measured longshore current at the 12 profile lines. In general, the model reproduced rather well the longshore current observed in the measurement along all profile lines. The cross-shore computation was also in good agreement with measurement in the lee of detached break-

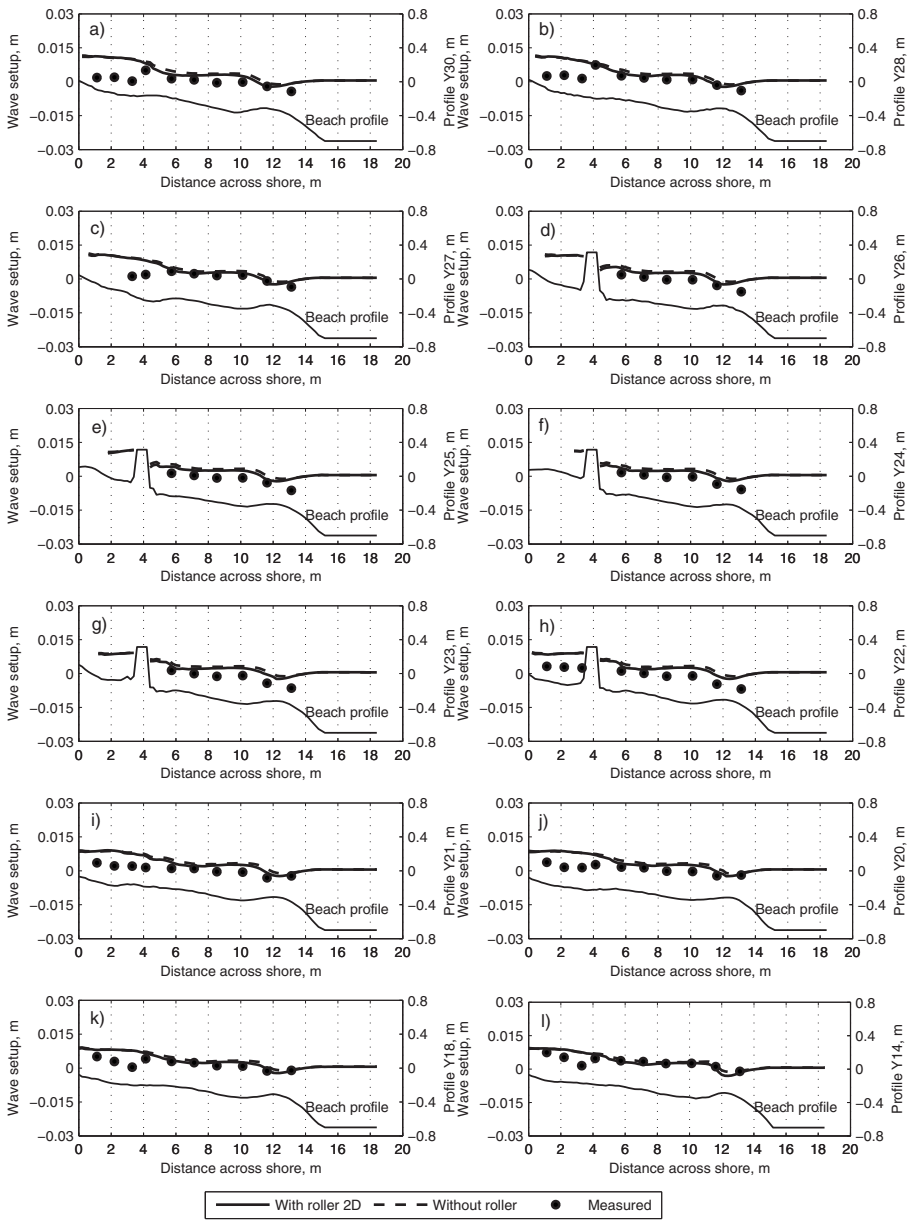

Fig. 19. Comparison of calculated and measured wave setups for LSTF Case T1C8

water [see Figs. 18(d–h)]. However, as for T1C4, the cross-shore current was underestimated compared to the measurements and had a shoreward direction at profiles Y21 and Y20 [Figs. 18(i and j)].

Fig. 19 illustrates the comparison between measured and calculated wave setup for T1C8. Similar to T1C4, the calculated wave setup was in quite good agreement with the measurements from ADV4 to ADV10. In the very shallow water (ADV1, ADV2, and ADV3), the calculated wave setup overestimated the measurements. The gauges were probably recording in very shallow water, affecting the accuracy of the collected water levels.

A quantitative assessment of the agreement between measured and calculated longshore current, cross-shore current, and wave setup was also performed based on the RMS error between cal-

Table 3. Absolute Error (m) of Wave Setup

Data sets	η With roller	η Without roller
T1C1	0.0019	0.0025
T1C4	0.0024	0.0031
T1C8	0.0032	0.0035

culations and measurements (see Table 2). For T1C1 and T1C4, the RMS errors of longshore current without roller were slightly better than those with roller. The calculated cross-shore current agreed fairly well with the measurements in the lee of the detached breakwater, but underestimated the current at the remaining measurement locations, causing larger RMS errors.

In addition, the absolute error was also used to compare the wave setup calculations with the measurements. Table 3 summarizes in detail the absolute error in the wave setup for the three investigated test cases. Although the relative RMS error of wave setup was quite large, the absolute error was relatively small. For example, in test case T1C1, the RMS errors of wave setup with and without roller were 77.48% and 84.80%, respectively. However, the corresponding absolute errors were only 0.0019 and 0.0025 m.

Discussion

This study involved a modification of the energy dissipation calculation due to breaking used in the EBED model developed by Mase (2001). The modification was based on Dally et al. (1985), producing a significant improvement in calculating the wave conditions in the surf zone. As a result, the Modified-EBED is able to provide more accurate input for the numerical model used to simulate the nearshore currents, as well as for models employed to determine the sediment transport and morphological evolution.

The importance of the roller in calculating wave-induced currents was also investigated. Roller effects not only shifts the peak of the longshore current toward the shoreline, but they also increase the magnitude of the longshore current in the surf zone. By using a 2D surface roller model, energy conservation was expressed more accurately than with the 1D model. For the three test cases from the LSTF data investigated, the difference in roller mass fluxes obtained by 2D and 1D surface model was small. However, the 2D surface roller model should be employed for areas with complex bathymetry and high wave energy in order to obtain more accurate wave-induced currents.

The absolute error in wave setup was small, although a large relative error was obtained. For the LSTF data, the instrument errors were quite small, typically less than 2% (M. B. Gravens and P. Wang, personal communication, April 28, 2009), and all the instruments were checked before the measurements. However, the measurements at some locations near the shoreline were difficult to carry out due to very shallow water and the wave and current sensors could be over the water surface. Furthermore, the air bubbles from breaking waves penetrated into the water column potentially affecting the observed values (Hamilton and Ebersole 2001). Therefore, the RMS errors in the wave setup were quite large at certain measurement locations for the three investigated test cases.

The numerical models for nearshore waves and wave-induced currents employed several empirical coefficients that could be specified with confidence and that have potential for general applicability. The decay and stable coefficients, which were determined by Eq. (3), produced good results regarding the wave field for the LSTF data. However, these equations should be validated with other laboratory and field data to ensure their general applicability. The roller dissipation and the bottom friction coefficients directly affect the speed and the cross-shore distribution of longshore currents. In the present study, the value of the roller dissipation coefficient was set to 0.1 following the recommendation of Dally and Brown (1995), and the Manning coefficient was given as 0.025 to determine the bottom friction based on calibration. These values provided good agreement between the computations and the measurements. The eddy viscosity coefficients, which were determined by Falconer (1980) and Kraus and Larson (1991), make the cross-shore variation in wave-induced current smoother, but their effects on the current magnitude is relatively small.

Conclusions

The present study represents one of the first attempts to validate, in a comprehensive manner, a numerical model developed for predicting the wave and current field around a detached breakwater. Such a model is a necessary component in any system to simulate the bathymetric evolution in response to nearshore structures in the coastal zone.

A general, robust, and reliable numerical model was developed to predict nearshore waves and currents in coastal areas with structures present that induce complex topographic conditions. The energy dissipation algorithm for wave breaking in the multidirectional random wave transformation model EBED (Mase 2001) was modified after Dally et al. (1985), producing more accurate wave fields in the surf zone. The creation and evolution of surface roller was employed and enhanced based on the model of Dally and Brown (1995) and Larson and Kraus (2002) in order to improve the wave radiation stresses in the surf zone. The nearshore currents and water elevation were determined from the continuity equation together with the depth-averaged momentum equations.

The developed model was validated by employing high-quality data sets from three experimental test cases in the LSTF basin involving a detached breakwater (Gravens et al. 2006; Gravens and Wang 2007). These simulations showed that the model well reproduced the significant wave height and longshore current at all measured locations. The calculated cross-shore current underestimated the measurements along several profile lines, probably because the undertow was not included in the model. Although the calculated wave setup often overestimated the measurements, the absolute error was relatively small. Therefore, the model is expected to provide reliable input for calculating the sediment transport and morphological evolution in the vicinity of coastal structures due to waves and currents.

Acknowledgments

This work was partly funded by Sida/SAREC in the framework of the Project VS/RDE/03 "The evolution and sustainable management in the coastal areas of Vietnam," partly by Lars Erik Lundbergs Scholarship Foundation, and partly by the Inlet Modeling System Work Unit of the Coastal Inlets Research Program, U.S. Army Corps of Engineers. Dr. Hajime Mase at Kyoto University kindly supplied the source code for the EBED model. Dr. Ping

Wang at University of South Florida and Mr. Mark Gravens at CHL provided the experimental data from their tests, which is greatly appreciated. The writers thank Mrs. Margaret Newman-Nowicka at Lund University for her useful language comments. The writers thank Dr. Nguyen Manh Hung, and the late Prof. Pham Van Ninh for their great contributions to the Project VS/RDE/03 and comments on early drafts of this paper. Finally, the writers thank the anonymous reviewers for their valuable comments.

References

Booij, N., Holthuijsen, L. H., and Ris, R. C. (1996). "The 'SWAN' wave model for shallow water." *Proc., 25th Int. Conf. on Coastal Engineering*, ASCE, New York, 668–676.

Dally, W. R., and Brown, C. A. (1995). "A modeling investigation of the breaking wave roller with application to cross-shore currents." *J. Geophys. Res.*, 100(C12), 24873–24883.

Dally, W. R., Dean, R. G., and Dalrymple, R. A. (1985). "Wave height variation across beaches of arbitrary profile." *J. Geophys. Res.*, 90(C6), 11917–11927.

Falconer, R. A. (1980). "Modelling of planform influence on circulation in harbors." *Proc., 17th Int. Conf. on Coastal Engineering*, ASCE, New York, 2726–2744.

Goda, Y. (2006). "Examination of the influence of several factors on longshore current computation with random waves." *Coastal Eng.*, 53, 157–170.

Gravens, M. B., and Wang, P. (2007). "Data report: Laboratory testing of longshore sand transport by waves and currents; morphology change behind headland structures." *Technical Rep. No. ERDC/CHL TR-07-8*, Coastal and Hydraulics Laboratory, U.S. Army Engineer Research and Development Center, Vicksburg, Miss.

Gravens, M. B., Wang, P., Kraus, N. C., and Hanson, H. (2006). "Physical model investigation of morphology development at headland structures." *Proc., 30th Int. Conf. on Coastal Engineering*, World Scientific, Singapore, 3617–3629.

Hamilton, D. G., and Ebersole, B. A. (2001). "Establishing uniform longshore currents in large-scale sediment transport facility." *Coastal Eng.*, 42(3), 199–218.

Kraus, N. C., and Larson, M. (1991). "NMLONG: Numerical model for simulating the longshore current; report 1: Model development and tests." *Technical Rep. No. DRP-91-1*, U.S. Army Engineer Waterways Experiment Station, Vicksburg, Miss.

Larson, M., and Kraus, N. C. (2002). "NMLONG: Numerical model for simulating longshore current; report 2: Wave-current interaction, roller modeling, and validation of model enhancements." *Technical Rep. No. ERDC/CHL TR-02-22*, U.S. Army Engineer Research and Development Center, Vicksburg, Miss.

Mase, H. (2001). "Multi-directional random wave transformation model based on energy balance equation." *Coast. Eng. Japan*, 43(4), 317–337.

Militello, A., Reed, C. W., Zundel, A. K., and Kraus, N. C. (2004). "Two-dimensional depth-averaged circulation model M2D: Version 2.0, report 1, technical document and user's guide." *Technical Rep. No. ERDC/CHL TR-04-2*, U.S. Army Engineer Research and Development Center, Vicksburg, Miss.

Mory, M., and Hamm, L. (1997). "Wave height, setup, and currents around a detached breakwater submitted to regular or random wave forcing." *Coastal Eng.*, 31, 77–96.

Nishimura, H. (1988). "Computation of neasrshore current." *Nearshore dynamics and coastal processes*, K. Horikawa, ed., University of Tokyo Press, Tokyo, 271–291.

Péchon, P., et al. (1997). "Intercomparision of wave-driven current models." *Coastal Eng.*, 31, 199–215.

Reid, R. O., and Bodine, B. R. (1968). "Numerical model for storm surges in Galveston Bay." *J. Wtrwy. and Harb. Div.*, 94(WWI), 33–57.

Sørensen, O. R., Schäffer, H. A., and Madsen, P. A. (1998). "Surf zone dynamics simulated by a Boussinesq type model. III. Wave-induced horizontal nearshore circulations." *Coastal Eng.*, 33, 155–176.

Svendsen, I. A. (1984a). "Mass flux and undertow in a surf zone." *Coastal Eng.*, 8, 347–365.

Svendsen, I. A. (1984b). "Wave heights and set-up in a surf zone." *Coastal Eng.*, 8, 303–329.

Tajima, Y., and Madsen, O. S. (2006). "Modeling near-shore waves, surface rollers, and undertow velocity profiles." *J. Waterway, Port, Coastal, Ocean Eng.*, 132(6), 429–438.

Takayama, T., Ikeda, N., and Hiraishi, T. (1991). "Wave transformation calculation considering wave breaking and reflection." *Rept. Port Harbor Res. Inst.*, 30(1), 21–67.

WAMDI Group. (1988). "The WAM model-a third generation ocean wave prediction model." *J. Phys. Oceanogr.*, 18, 1775–1810.

Wang, P. (2006). "Measuring longshore sediment transport in a large-scale 3-dimensional laboratory facility." *J. Coastal Res.*, 39, 816–821.

Wang, P., Ebersole, B. A., and Smith, E. R. (2003). "Beach-profile evolution under spilling and plunging breakers." *J. Waterway, Port, Coastal, Ocean Eng.*, 129(1), 41–46.

Wang, P., Ebersole, B. A., Smith, E. R., and Johnson, B. D. (2002a). "Temporal and spatial variations of surf-zone currents and suspended sediment concentration." *Coastal Eng.*, 46, 175–211.

Wang, P., Smith, E. R., and Ebersole, B. A. (2002b). "Large-scale laboratory measurements of longshore sediment transport under spilling and plunging breakers." *J. Coastal Res.*, 18(1), 118–135.

Watanabe, A., Maruyama, K., Shimizu, T., and Sakakiyama, T. (1986). "Numerical prediction model of three-dimensional beach deformation around a structure." *Coast. Eng. Japan*, 29, 179–194.

Welch, P. D. (1967). "The use of fast Fourier transformation for the estimation of power spectra: A method based on time averaging over short, modified periodograms." *IEEE Trans. Audio Electroacoust.*, 15, 70–73.

Zyserman, J. A., and Johnson, H. K. (2002). "Modelling morphological processes in the vicinity of shore-parallel breakwaters." *Coastal Eng.*, 45, 261–284.

Paper III

A unified sediment transport model for inlet application

Larson, M., Camenen, B., Nam, P.T., 2010.

Submitted to: *Journal of Coastal Research* (in press).

A Unified Sediment Transport Model for Inlet Application

Magnus Larson[a], Benoît Camenen[b], and Pham Thanh Nam[a]

[a]Department of Water Resources Engineering
Lund University
Box 118
S-22100 Lund
SWEDEN

[b]Cemagref
HHLY, 3 bis quai Chauveau
CP 220 F-69336
Lyon cedex 09
FRANCE

ABSTRACT

Robust and reliable formulas for predicting bed load and suspended load were developed for application in the nearshore zone where waves and currents may transport sediment separately or in combination. Also, a routine was included to determine the sediment transport in the swash zone, both in the longshore and cross-shore directions. An important objective of the development was to arrive at general sediment transport formulas suitable for a wide range of hydrodynamic, sedimentologic, and morphologic conditions that prevail around coastal inlets. Thus, the formulas yield transport rates under waves and currents, including the effects of breaking waves, wave asymmetry, and phase lag between fluid and sediment velocity for varying bed conditions. Different components of the formulas were previously validated with a large data set on transport under waves and currents, and in the present paper additional comparisons are provided for the complete formulas using data on longshore and cross-shore sediment transport from the laboratory and the field, encompassing the offshore, surf, and swash zones. The predictive capability of the new formulas is the overall highest among a number of existing formulas that were investigated. The complete set of formulas presented in the paper is collectively denoted the Lund-CIRP model.

Keywords: Bed load, suspended load, swash zone, waves, current, coastal inlets, mathematical model, transport formulas

INTRODUCTION

Many sediment transport formulas have been developed through the years for application in the coastal areas (Bayram *et al.*, 2001; Camenen and Larroude, 2003). However, these formulas have typically focused on describing a limited set of physical processes, which restrict their applicability in a situation where many processes act simultaneously to transport the sediment, for example, around a coastal inlet. Also, many of the formulas have not been sufficiently validated towards data, but they have typically been calibrated and validated against limited data sets. Thus, there is a lack of general sediment transport formulas valid under a wide range of hydrodynamic, sedimentologic, and morphologic conditions that yield reliable and robust predictions. In this paper such formulas are presented and validated against high-quality laboratory and field data on longshore and cross-shore sediment transport.

The coastal environment around an inlet encompasses hydrodynamic forcing of many different types, where waves, tides, wind, and river runoff are the most important agents for initiating water flows and associated sediment transport. Besides the oscillatory motion, waves induce mean currents in the surf zone (longshore currents, rip currents etc), stir up and maintain sediment in suspension through the breaking process, and cause swash motion and transport on the foreshore. The wind and tide generate mean circulation patterns that move sediment, especially in combination with waves. Also, on the bay side and in the vicinity of the inlet throat, river discharge to the bay might generate currents that significantly contribute to the net transport. Figure 1 illustrates some of the hydrodynamic forcing around an inlet that is important for mobilizing and transporting sediment.

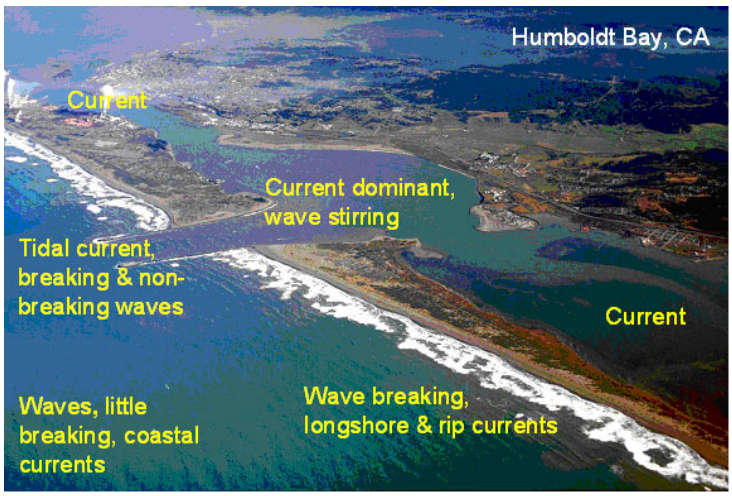

Figure 1. Hydrodynamic processes controlling the sediment transport in an inlet environment (from Camenen and Larson, 2007).

Predicting sediment transport and morphological evolution around an inlet is crucial for the analysis and design of different engineering activities that ensure proper functioning of the inlet for navigation (see Figure 2). Optimizing dredging operations due to channel infilling or minimizing local scour, which may threaten structural integrity, are examples of such activities. Furthermore, bypassing of sediment through the inlet shoals and bars are vital for the supply of material to downdrift beaches and any reduction in this transport may cause severe erosion and shoreline retreat. After an inlet opening, as the shoals and bars grow with little bypassing transport, downdrift erosion is common and varying engineering measures such as beach nourishment and structures might be needed. On the updrift side accumulation normally occurs, especially if the inlet has been stabilized with jetties, with shoreline advance and increased infilling in the channel.

Considering the inlet environment, a general sediment transport model should yield predictions of the transport rate taking into account the following mechanisms:

- Bed load and suspended load

- Waves and currents
- Breaking and non-breaking waves
- Slope effects
- Initiation of motion
- Asymmetric wave velocity
- Arbitrary angle between waves and current
- Phase-lag effects between water and sediment motion
- Realistic bed roughness estimates (*e.g.*, bed features)
- Swash-zone sediment transport

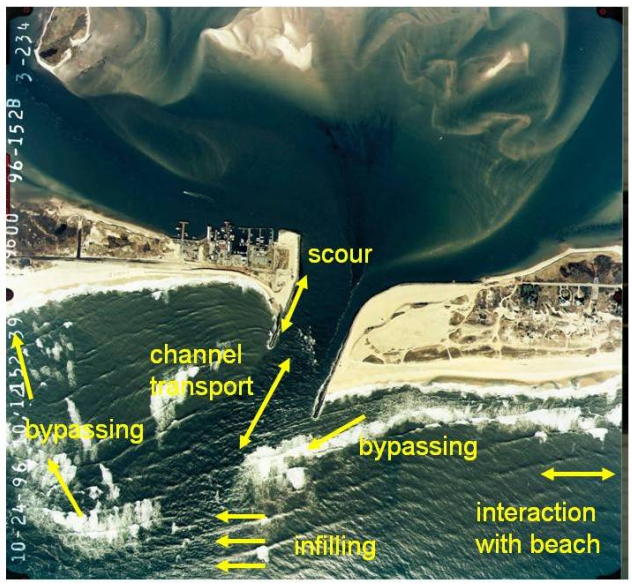

Figure 2. Engineering activities around an inlet for which predictions of sediment transport and morphological evolution are of importance (from Camenen and Larson, 2007).

In this paper, general formulas are presented to compute the sediment transport rate in an inlet environment that includes all of the above mechanisms. These formulas are mainly based on previous work by the authors (see Camenen and Larson, 2005; 2006; 2008), where different components of the formulas were developed, calibrated, and validated against extensive data sets. In the following the complete set of formulas is collectively denoted as the Lund-CIRP model. The primary objective of this study was to develop robust and reliable sediment transport formulas applicable under a wide range of conditions encountered at a coastal inlet, and to validate these formulas towards high-quality sediment transport rate measurements obtained in the laboratory or in the field.

This paper is organized as follows. The formulas developed to compute sediment transport are first described. Validation of the bed load and suspended load formulas, as well as five other existing formulas, was carried out based on laboratory and field measurements of the longshore and cross-shore sediment transport in the surf and offshore zone. Then, the transport in the swash zone was validated using laboratory data on the longshore transport rate. Finally, the conclusions are presented.

SEDIMENT TRANSPORT MODEL

Bed Load Transport

Camenen and Larson (2005) developed a formula for bed load transport based on the Meyer-Peter and Müller (1948) formula. The bed load transport (q_{sb}) may be expressed as follows,

$$\begin{aligned}\frac{q_{sbw}}{\sqrt{(s-1)gd_{50}^3}} &= a_w\sqrt{\theta_{net}}\,\theta_{cw,m}\exp\left(-b\frac{\theta_{cr}}{\theta_{cw}}\right)\\ \frac{q_{sbn}}{\sqrt{(s-1)gd_{50}^3}} &= a_n\sqrt{\theta_{cn}}\,\theta_{cw,m}\exp\left(-b\frac{\theta_{cr}}{\theta_{cw}}\right)\end{aligned} \tag{1}$$

where the subscripts w and n correspond, respectively, to the wave direction and the direction normal to the waves, s $(=\rho_s/\rho)$ is the specific gravity of the sediment, in which ρ_s is the density of the sediment and ρ of the water, g the acceleration due to gravity, d_{50} the median grain size, a_w, a_n, and b are empirical coefficients (to be discussed later), θ_{cr} the critical Shields number for initiation of motion (obtained from Soulsby, 1997), $\theta_{cw,m}$ the mean Shields number and θ_{cw} the maximum Shields number due to wave-current interaction, and $\theta_{cn}=f_c\left(U_c\sin\varphi\right)^2/\left((s-1)gd_{50}\right)/2$ (where f_c is the current-related friction factor, U_c the steady current velocity, and φ the angle between the wave and the current direction). In order to simplify the calculations, the mean and maximum Shields numbers due to wave-current interaction are obtained by vector addition: $\theta_{cw,m}=\left(\theta_c^2+\theta_{w,m}^2+2\theta_{w,m}\theta_c\cos\varphi\right)^{1/2}$ and $\theta_{cw}=\left(\theta_c^2+\theta_w^2+2\theta_w\theta_c\cos\varphi\right)^{1/2}$, where θ_c, θ_{wm}, and θ_w are the current, mean wave, and maximum wave Shields number, and $\theta_{w,m}=\theta_w/2$ for a sinusoidal wave profile.

The net sediment transporting Shields number θ_{net} in Eq. (1) is given by,

$$\theta_{net}=(1-\alpha_{pl,b})\theta_{cw,on}+(1+\alpha_{pl,b})\theta_{cw,off} \tag{2}$$

where $\theta_{cw,on}$ and $\theta_{cw,off}$ are the mean values of the instantaneous shear stress over the two half periods T_{wc} and T_{wt} (T_w=T_{wc}-T_{wt}, in which T_w is the wave period), and $\alpha_{pl,b}$ a

coefficient for the phase-lag effects (Camenen and Larson, 2006). In the same way as for the Dibajnia and Watanabe (1992) formula, the mean values of the instantaneous shear stress over a half period are defined as follows (see Figure 3),

$$\theta_{cw,on} = \frac{1}{T_{wc}} \int_0^{T_{wc}} \frac{f_{cw}(U_c \cos\varphi + u_w(t))^2}{2(s-1)gd_{50}} dt$$
$$\theta_{cw,off} = \frac{1}{T_{wt}} \int_{T_{wc}}^{T_w} \frac{f_{cw}(U_c \cos\varphi + u_w(t))^2}{2(s-1)gd_{50}} dt \quad (3)$$

where $u_w(t)$ is the instantaneous wave orbital velocity, t time, and f_{cw} the friction coefficient due to wave-current interaction introduced by Madsen and Grant (1976),

$$f_{cw} = X_v f_c + (1 - X_v) f_w \quad (4)$$

with $X_v = U_c / (U_c + U_w)$, where f_w is the wave-related friction factor, U_c the mean current velocity, and U_w the average of the peak velocities during the wave cycle (the root-mean-square (rms) value is used for random waves).

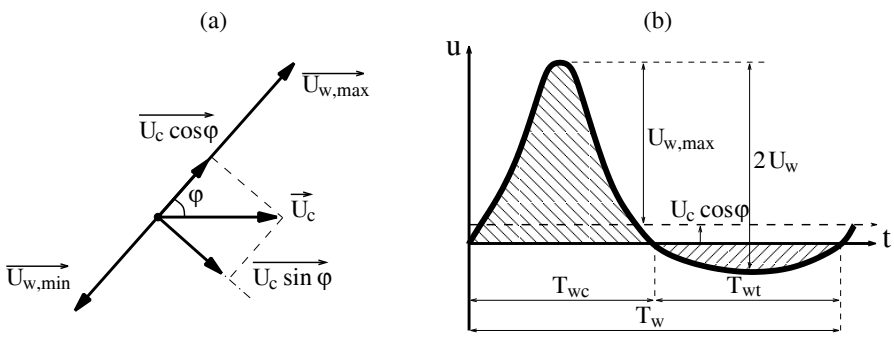

Figure 3. Definition sketch for current and wave direction and for bottom velocity profile in the direction of wave propagation (from Camenen and Larson, 2007).

Based on comparison with an extensive data set (Camenen and Larson, 2005), the following relationship is proposed for the transport coefficient a_w,

$$a_w = 6 + 6X_t \quad (5)$$

in which $X_t = \theta_c / (\theta_c + \theta_w)$. The coefficient for transport perpendicular to the waves, where only the current moves sediment, is set to a_n=12, and the coefficient in the term describing initiation of motion is b=4.5. The phase-lag effects are introduced through the coefficient $\alpha_{pl,b} = \alpha_{on} - \alpha_{off}$ following Camenen and Larson (2006; detailed coefficient expressions not given here).

Suspended Load Transport

In determining the suspended load q_{ss}, following the simplified approach by Madsen (1993) and Madsen *et al.* (2003), the vertical variation in the horizontal velocity was neglected and an exponential-law profile assumed for the sediment concentration. Camenen and Larson (2007) made a comparison between representing the velocity variation over the vertical in the sediment transport calculations and using the average velocity, finding a small difference in the obtained total suspended load. Thus, the suspended sediment load may be obtained from (Camenen and Larson, 2008),

$$\begin{aligned} q_{ssw} &= U_{c,net}\, c_R \frac{\varepsilon}{W_s} \left[1-\exp\left(-\frac{W_s h}{\varepsilon}\right)\right] \\ q_{ssn} &= U_c \sin\varphi\, c_R \frac{\varepsilon}{W_s} \left[1-\exp\left(-\frac{W_s h}{\varepsilon}\right)\right] \end{aligned} \tag{6}$$

where h is the water depth, $U_{c,net}$ the net mean current after a wave period, c_R the reference concentration at the bottom, W_s the sediment fall speed, and ε the sediment diffusivity. The ratio $W_s h/\varepsilon$ may often be assumed large, implying that the exponential term is close to zero. However, such an assumption may not be valid when strong mixing due to wave breaking is present. The bed reference concentration is obtained from,

$$c_R = A_{cR}\theta_{cw,m} \exp\left(-4.5\frac{\theta_{cr}}{\theta_{cw}}\right) \tag{7}$$

in which the coefficient A_{cR} is given by,

$$A_{cR} = 3.5\cdot 10^{-3} \exp(-0.3 d_*) \tag{8}$$

where $d_* = \sqrt[3]{(s-1)g/\nu^2}\, d_{50}$ is the dimensionless grain size and ν the kinematic viscosity.

The sediment diffusivity is related to the energy dissipation (Battjes and Janssen 1978),

$$\varepsilon = \left(\frac{D}{\rho}\right)^{1/3} h \tag{9}$$

in which D is the total effective dissipation expressed as,

$$D = k_b^3 D_b + k_c^3 D_c + k_w^3 D_w \tag{10}$$

where the energy dissipation from wave breaking (D_b) and from bottom friction due to current (D_c) and waves (D_w) were simply added, and k_b, k_c, and k_w are coefficients. The coefficient k_b corresponds to an efficiency coefficient related to wave breaking, whereas k_c and k_w are related to the Schmidt number (Camenen and Larson, 2007). The mean value for the vertical sediment diffusivity employed in the exponential concentration profile may be determined by integrating the vertical variation in the diffusivity (Camenen and Larson, 2007). Assuming a parabolic profile for this variation (Dally and Dean, 1984), the mean value over the depth (for a steady current or waves, respectively) may be written as follows,

$$\varepsilon_j = \left(\frac{D_j}{\rho} \right)^{1/3} h = k_j u_{*j} h \tag{11}$$

where k_j is a function of a non-dimensional number σ_j expressing the ratio between the vertical eddy diffusivity of particles and the vertical eddy viscosity of water (inverse of the common definition of the Schmidt number), and u_{*j} is the shear velocity due to current or waves only with subscript j taking on the values c (current) or w (waves), respectively. In case of a steady current, $k_c = \sigma_c \kappa / 6$ ($\kappa = 0.41$ is von Karman's constant), whereas for waves $k_w = \sigma_w \kappa / 3\pi$. The following expression was developed,

$$\begin{aligned} \sigma_j &= A_{j1} + A_{j2} \sin^2 \left(\frac{\pi}{2} \frac{W_s}{u_{*j}} \right) && \frac{W_s}{u_{*j}} \le 1 \\ \sigma_j &= 1 + \left(A_{j1} + A_{j2} - 1 \right) \sin^2 \left(\frac{\pi}{2} \frac{W_s}{u_{*j}} \right) && \frac{W_s}{u_{*j}} > 1 \end{aligned} \tag{12}$$

where j is a subscript equal to c or w, and A_{c1}=0.4 and A_{c2}=3.5 or A_{w1}=0.15 and A_{w2}=1.5. For wave-current interaction, a weighted value is employed:

$$\sigma_{cw} = X_t \sigma_c + \left(1 - X_t \right) \sigma_w \tag{13}$$

The net mean current is defined in a similar way to the net Shields number for the bed load in order to take into account a possible sediment transport due to wave asymmetry, as well as possible phase-lag effects on the suspended concentration,

$$U_{c,net} = \left(1 - \alpha_{pl,s} \right) U_{cw,on} + \left(1 + \alpha_{pl,s} \right) U_{cw,off} \tag{14}$$

where $\alpha_{pl,s}$ is the coefficient describing phase-lag effects on the suspended load (Camenen and Larson, 2006; detailed coefficient expressions not given here), and $U_{cw,j}$ is the rms value of the velocity (wave + current) over the half period T_{wj}, where the subscript j should be replaced either by *on* (onshore) or *off* (offshore) (see also Figure 3) according to:

$$U_{cw,on} = \sqrt{\frac{1}{T_{wc}}\int_0^{T_{wc}} (U_c \cos\varphi + u_w(t))^2 dt}$$
$$U_{cw,off} = \sqrt{\frac{1}{T_{wt}}\int_{T_{wc}}^{T_w} (U_c \cos\varphi + u_w(t))^2 dt} \quad (15)$$

In case of a steady current $U_{c,net} = U_c$.

The bottom slope may influence the sediment transport, especially if it is close to the critical value given by the wet internal friction angle of the sediment. In order to take into account the local slope, the transport rate may be multiplied with a function containing the local slope and a coefficient,

$$q_s^* = q_s\left(1 - \beta\frac{\partial z_b}{\partial s}\right) \quad (16)$$

where β is a coefficient for the slope effects (0.5<β<2) and $\partial z_b/\partial s$ is the local slope. Bailard (1981) presented values on the coefficient β that depends on the sediment transport regime.

Swash Zone Transport

Larson *et al.* (2004) and Larson and Wamsley (2007) developed formulas for the net transport rate in the swash zone,

$$q_{bc,net} = K_c \frac{\tan\phi_m}{\tan^2\phi_m - (dh/dx)^2}\frac{u_0^3}{g}\left(\frac{dh}{dx} - \tan\beta_e\right)\frac{t_0}{T}$$
$$q_{bl,net} = K_l \frac{\tan\phi_m}{\tan^2\phi_m - (dh/dx)^2}\frac{u_0^2 v_0}{g}\frac{t_0}{T} \quad (17)$$

where $q_{bc,net}$ and $q_{bl,net}$ are the net transport rates over a swash cycle in the cross-shore and longshore directions, respectively, K_c and K_l are empirical coefficients, ϕ_m the friction angle for a moving grain, β_e the foreshore equilibrium slope, u_0, v_0 the scaling velocities (cross-shore and longshore directions, respectively) and t_0 the scaling time, and T the swash duration (taken to be similar to the incident wave period). Ballistics theory, neglecting friction, may be employed to compute swash zone hydrodynamics including the scaling parameters and their variation across the foreshore (see Larson and Wamsley, 2007).

The interaction between uprush and backwash processes in the vicinity of the shoreline induces considerable sediment stirring and movement, which is of importance to describe when the sediment exchange between the swash zone and the inner surf zone is modeled.

Since horizontal advection and diffusion of sediment is particularly significant in this region, it may be necessary to include those processes in a model instead of calculating local transport rates under the assumption that horizontal sediment exchange is negligible. By solving the advection-diffusion (AD) equation for the sediment concentration (suspended load), a more realistic description of the horizontal mixing is obtained in the inner surf zone.

The two-dimensional time- and depth-averaged AD equation is expressed for steady-state conditions as,

$$\frac{\partial\left(\overline{C}q_x\right)}{\partial x}+\frac{\partial\left(\overline{C}q_y\right)}{\partial y}=\frac{\partial}{\partial x}\left(K_x h\frac{\partial\overline{C}}{\partial x}\right)+\frac{\partial}{\partial x}\left(K_y h\frac{\partial\overline{C}}{\partial y}\right)+P-S \tag{18}$$

where $\overline{C}$ is the depth-averaged sediment concentration, q_x and q_y are the flow per unit width parallel to the x and y axes, respectively, K_x and K_y are the sediment diffusion coefficients in x and y direction, respectively, P is the sediment pick-up rate, and S is the sediment deposition rate. From Elder (1959), the sediment diffusion coefficient is estimated as,

$$K_x = K_y = 5.93u_{*c}h \tag{19}$$

where u_{*c} is the shear velocity from the current only. This equation was used by Buttolph *et al.* (2006) to describe sediment diffusion in Eq. 18, although Elder (1959) derived his expression based on studies on longitudinal dispersion in a channel. However, qualitatively good results have been achieved with this formulation for a number of test cases. Buttolph *et al.* (2006) also included additional mixing due to waves in the sediment diffusion coefficient, but this was not done here.

The sediment pick-up and deposition rates, respectively, are given by,

$$P = c_R W_s \tag{20}$$

$$S = \frac{\overline{C}}{\beta_d}W_s \tag{21}$$

where β_d is a coefficient calculated based on Camenen and Larson (2008; see also Buttolph *et al.*, 2006):

$$\beta_d = \frac{\varepsilon}{w_s h}\left[1-\exp\left(-\frac{W_s h}{\varepsilon}\right)\right] \tag{22}$$

Simplified Transport Formulas

The Lund-CIRP model was developed to describe a wide range of different processes occurring around a coastal inlet. Thus, to apply the complete formulas might be time-consuming or require extensive background data not always available. In many cases satisfactory results can be achieved with simplified versions of the formulas where certain processes or phenomena are not included. For example, wave asymmetry is often important immediately seaward of the surf zone, but in a regional perspective the asymmetry may be neglected with little loss in simulation results. By not including wave asymmetry gains are made in calculation speed, since the integration over the wave cycle may be greatly simplified. Also, the difficulties in estimating the asymmetry over large spatial areas are avoided. Most regional wave models used in simulating the morphological evolution rely on linear wave theory and do not yield any information on the wave asymmetry. Another phenomenon that is often neglected is the phase lag between water flow and sediment movement, which may have effects on the net sediment transport rate over a wave cycle. The importance of the phase lag depends on the hydrodynamic and sediment characteristics. Thus, a simplified version of the transport formulas would employ Eqs. 1 and 6 with only the current contributing to the net sediment transporting velocity.

APPLICATION OF SEDIMENT TRANSPORT FORMULAS

Background and Data Employed

Various components of the Lund-CIRP model presented in the previous section were validated in earlier studies against extensive data sets on sediment transport, and empirical expressions were derived for the most important coefficient values. These data sets consisted mainly of laboratory experiments, although field data were also included to some extent. Camenen and Larson (2005, 2006, 2008) presented the results of the comparison for current, waves, and wave-current interaction. Both sinusoidal and asymmetric waves were included, as well as non-breaking and breaking waves. Selected existing formulas, commonly used in engineering studies, were also employed to compute the transport rates and comparison with the Lund-CIRP model showed that overall this model displayed the best agreement with data. The swash zone transport formula was validated by Larson *et al*. (2004) and Larson and Wamsley (2006) with regard to the cross-shore and longshore components, respectively.

In the following, the complete formulas are compared to data from the laboratory and the field where measurements were simultaneously collected at several locations along a profile under realistic wave and current conditions. Data on the longshore sediment transport rate from the Large-scale Sediment Transport Facility (LSTF) at the Coastal and Hydraulics Laboratory (CHL) in Vicksburg, Mississippi, and from several field experiments at the Field Research Facility (FRF) of CHL in Duck, North Carolina, were employed. Also, data on the cross-shore sediment transport rate were used from the Duck field experiments. Previously the various components of the Lund-CIRP model were validated mainly with point values, often under a limited set of hydrodynamic forcing and

under conditions that are not completely analogous to a natural beach (*e.g.*, oscillatory water tunnels). Thus, the present testing constitutes a more general validation of the complete formulas.

A number of commonly utilized transport formulas were also employed to compute the transport rate, including the formulas of Bijker (1968), Bailard (1981), van Rijn (1989), Watanabe (1992), and Dibajnia and Watanabe (1992). These formulas were selected because they are often used in numerical models of the morphological evolution. It should be noted that similarly to the present formula the Bijker, Bailard, and van Rijn formulas estimate the bed load and suspended load separately, whereas the Watanabe and Dibajnia/Watanabe formulas directly estimate the total load. The Bailard, Dibajnia/Watanabe, and Lund-CIRP model take into account the effects of wave asymmetry on the total sediment transport (a large portion of the transport rates derived from the measurements do not include this effect). Furthermore, in the Dibajnia/Watanabe and the Lund-CIRP model the phase-lag effects are taken into account (again, this is not done in the transport rates derived from the measurements).

An important quantity for many of these formulas is the Shields parameter. The roughness height was estimated using the Soulsby (1997) method, which includes roughness contributions from sediment grains (*i.e.*, skin friction), bed forms, and sediment transport. The ripple characteristics were estimated using the Grasmeijer and Kleinhans (2004) equations, and roughness due to sediment transport was obtained from the formula by Wilson (1989). Uncertainties in the final results are to a large degree related to the calculation of the bottom shear stress, which in turn depends on the bed roughness. The roughness in the presence of ripples is especially difficult to estimate and there are several formulas available to do this (Camenen, 2009). Often a particular sediment transport formula has been developed using a specific method to calculate the roughness and shear stress. However, in this study the same method was used for all formulas, which may have produced less good agreement with the data for some of the formulas.

Validation of Longshore Sediment Transport

The Lund-CIRP model was validated with measured longshore sediment transport rates from two data sets, namely a laboratory experiment carried out in the LSTF (Wang *et al*., 2002) and field experiments (SandyDuck) performed at the FRF (for a summary of the field experiments, see Miller, 1998; 1999). For these experiments, the sediment transport rate was estimated based on the measured time-averaged sediment concentration and velocities. Thus, the transport rates mainly reflect the current-related suspended load, and most of the bed load together with the effects from the waves on the transporting velocity are not included (in the concentration measurements close to the bottom, some portion of the bed load might have been captured since the gages were close to the bed). Because the wave asymmetry, defined as $r_w = U_{w,\max} / U_w - 1$ (for notation, see Figure 3), was not recorded, r_w was estimated using the method proposed by Dibajnia *et al*. (2001) (examples of calculated results are shown in Figures 4a, 5a, and 7a). For the LSTF data set, the cross-shore current (undertow) was not measured, and in order to compute the total shear stress the undertow was estimated using the model developed by Svendsen (1984) (Figure 4a).

These calculations are a source of error in the computation of the suspended load. For the LSTF experiments, measurements of the total load were also carried out using a trap system at the downdrift end of the basin. A comparison between the two measurement methods (Figure 4b) indicates the order of magnitude of the uncertainties in the experimental results. It also shows that suspended load is prevailing.

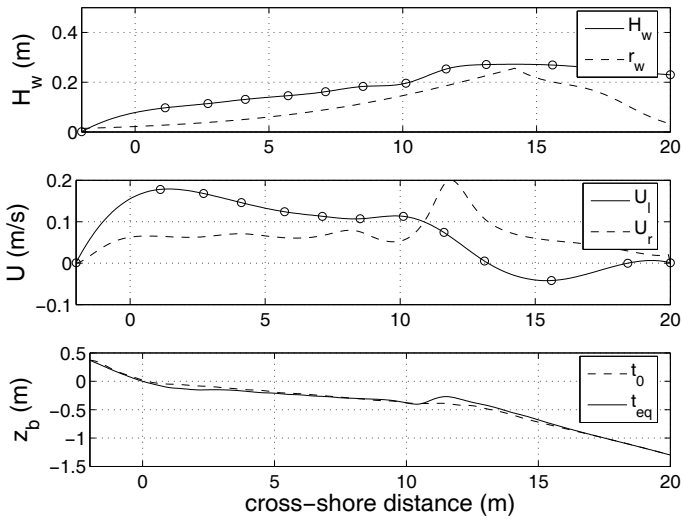

Figure 4 (a). Cross-shore distribution of hydrodynamic parameters together with beach profile shape.

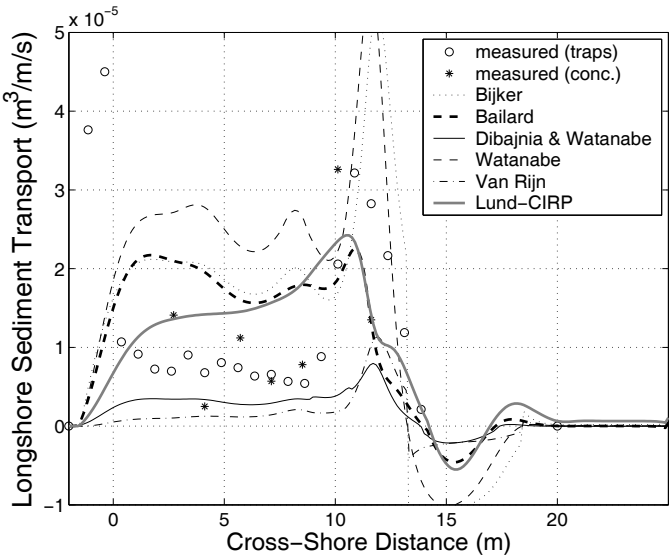

Figure 4 (b). Cross-shore distribution of the longshore sediment transport rate together with predictions from six studied formulas for an LSTF case (Test 3).

In Figure 4 are typical results presented for the LSTF experiment (case with spilling breaking waves). The Watanabe formula tends to overestimate the transport rates in the surf zone, whereas the van Rijn and Dibajnia/Watanabe formulas markedly underestimate the rates. The Lund-CIRP model yields results of the correct magnitude, even if the peak in the transport rate in the outer surf zone is broader and less pronounced compared to the measured peak. This partly results from the computation of the ripple characteristics which are found to be smaller on the bar and thus induce a smaller bottom shear stress. Close to the swash zone (still-water shoreline was located at x=0), all formulas largely underestimate the longshore sediment transport rate. The influence of the swash zone is significant near the shoreline, and since the formulas do not include longshore transport in the swash they fail to reproduce the measurements in this region. Thus, a special sediment transport formula for the swash zone should be included as will be discussed later in the paper. Also, the formulas yielded a small negative transport along a limited portion of the profile outside the surf zone, since the measured current was negative in this region (at one measurement point). The observed sediment transport did not display any negative values, implying that wave-induced sediment transport may prevail over the current-related transport in this area. Only the Bailard and Dibajnia/Watanabe formulas and the Lund-CIRP model could potentially describe this situation.

Figure 5 illustrates typical results obtained for the SandyDuck experiments with regard to the longshore sediment transport rate (case from February 4th 1998). The variation in the data and the scatter in the predictions are larger than for the LSTF data, partly because the measurements took place under less controlled conditions. In some cases wind was a significant factor in generating the current. Most of the formulas predict similar cross-shore variation, but the magnitude differs greatly. The Lund-CIRP model, as well as the Bijker formula, tends to overestimate the transport rate, whereas the Dibajnia/Watanabe and Bailard formula underestimate the rates (see Table 1 and Figure 5b). The Watanabe and Dibajnia/Watanabe formulas yield the total load, so overestimation is expected. Thus, the underestimation by the Dibajnia/Watanabe formula is somewhat surprising.

Table 1 presents statistical results for the comparison between all studied formulas and the experimental data from LSTF (4 experimental cases encompassing in total 92 data points) and SandyDuck (6 experimental cases encompassing in total 66 data points). The table presents the percentage of data correctly predicted within a factor 2 or 5, and the mean value and standard deviation of the function $f(q_{ss}) = \log\left|q_{ss,pred} / q_{ss,meas}\right|$, where $q_{ss,pred}$ and $q_{ss,meas}$ are the predicted and measured values, respectively. The Watanabe formula presents the best results for the SandyDuck data but yields poor agreement for the LSTF data. Similarly, the Bailard and Dibajnia/Watanabe formulas seem to be sensitive to the scale of the experiments. These two formulas yield overestimation for the laboratory experiment, whereas they underestimate the results for the field experiment (the Watanabe formula displays the opposite behavior). This behavior may be due to the formulas not being a function of the total shear stress (which varies with the scale of the experiment), but only of the velocity profile (Bailard and Dibajnia/Watanabe formula) or that they are too simple to include all the parameters for the bed load and suspended load (Watanabe formula). For the experimental cases studied on the longshore sediment transport rate the Bailard formula and the Lund-CIRP model yield the overall best results.

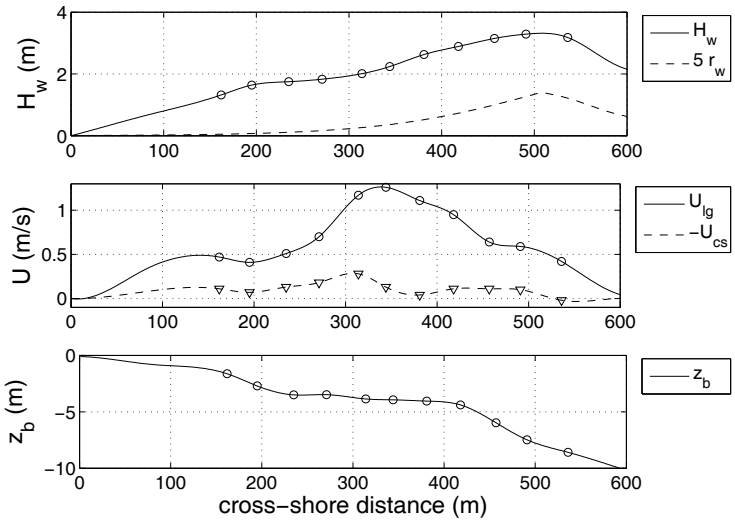

Figure 5 (a). Cross-shore distribution of hydrodynamic parameters together with beach profile shape

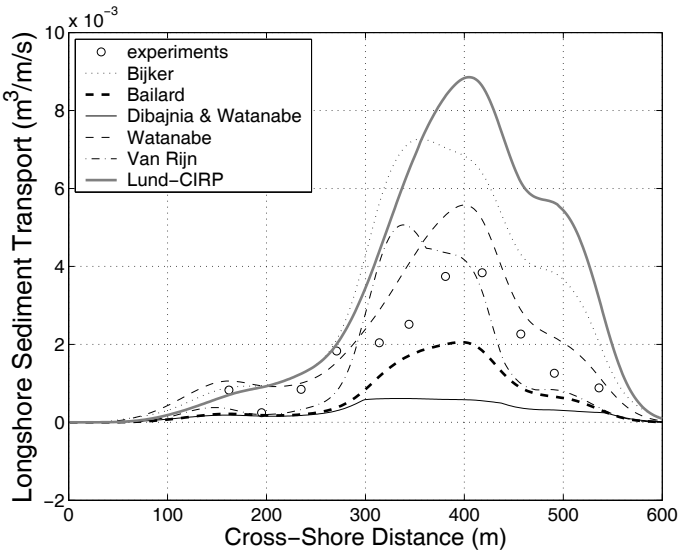

Figure 5 (b). Cross-shore distribution of the longshore sediment transport rate together with predictions from six studied formulas for a SandyDuck case (Feb. 4th 1998)

As a summary, Figure 6 shows the prediction of the longshore transport rate (*i.e.*, mainly suspended load) across the beach profile for all data points from the LSTF and SandyDuck experiments using the Lund-CIRP model, where the predicted rates were normalized with the measured rates. The plot in Figure 6a shows the underestimation near the swash zone, whereas in the zone of incipient breaking transport rates may be over- or underestimated.

Larger scatter is obtained in the comparison for the SandyDuck data (Figure 6b), together with the overestimation of the transport rates pointed out earlier.

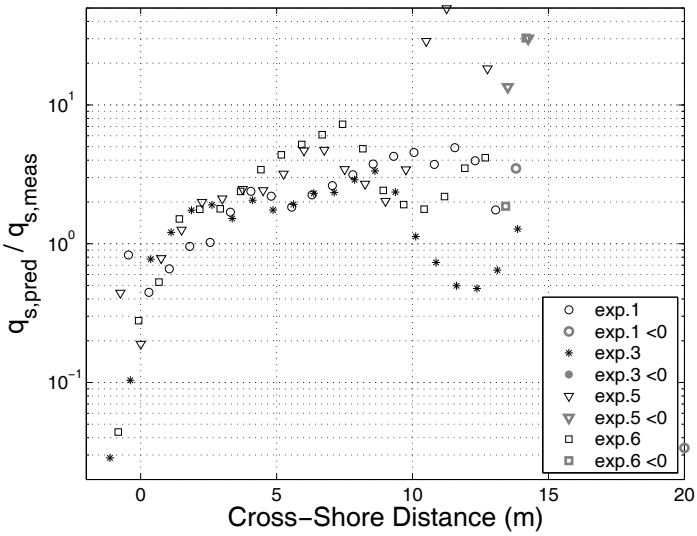

(a) the LSTF data

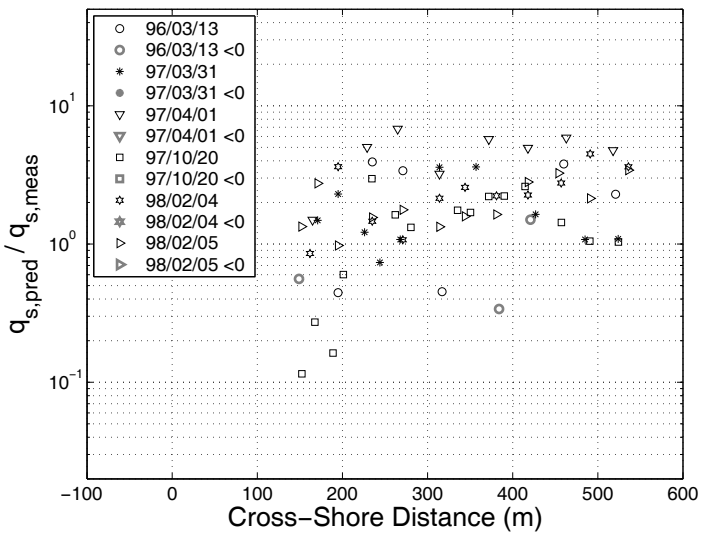

(b) the SandyDuck data

Figure 6. Prediction of the longshore transport rate across the profile using the Lund-CIRP model

Table 1. Prediction of longshore transport rate for the LSTF and SandyDuck experiments.

Author(s)	Pred. x2	Pred. x5	mean(f (qss))	std(f (qss))
LSTF data (4 cross-shore profiles, 92 experiments)				
Bijker (1968)	18%	71%	1.4	1.5
Bailard (1981)	20%	75%	1.1	1.4
Van Rijn (1989)	27%	59%	−0.8	1.9
Watanabe (1992)	11%	60%	1.4	1.3
Dibajnia & Watanabe (1992)	35%	75%	−0.4	1.5
Lund-CIRP	33%	79%	0.8	1.5
SandyDuck data (6 cross-shore profiles, 66 experiments)				
Bijker (1968)	35%	85%	0.8	0.5
Bailard (1981)	30%	68%	−1.3	0.8
Van Rijn (1989)	20%	48%	−1.5	1.2
Watanabe (1992)	61%	91%	0.1	0.9
Dibajnia & Watanabe (1992)	17%	63%	−1.4	0.6
Lund-CIRP	39%	85%	0.4	1.0

Validation of Cross-Shore Sediment Transport

The cross-shore transport (mainly suspended load) was also available from the SandyDuck experiments. Compared to the longshore transport, the predictions of the cross-shore transport with the formulas are often more uncertain because the input conditions are less well known due to the complex flow situation. Figure 7 presents some typical results obtained for the experimental case from March 12th 1996. The Bijker, van Rijn, and Watanabe formulas and the Lund-CIRP model induce a sediment transport which is in the same direction as the undertow, that is, in the offshore direction. On the contrary, the Bailard, Dibajnia/Watanabe formula (and the Lund-CIRP model if $U_{c,net}$ is used) allow for a sediment transport in the opposite direction to the mean current, if asymmetric waves are prevailing. Onshore sediment transport due to wave asymmetry often occurs seaward of the point of incipient breaking. Computations with these two latter formulas were performed with the asymmetry taken into account, although the transport rate obtained from the measurements would only include the transport associated with the mean current (*i.e.*, undertow). If $U_{c,net}$ is used, the Lund-CIRP appears to be quite sensitive to the balance between undertow and wave asymmetry, indicated by the rapid change in transport direction around the point of incipient breaking. Since the experimental data do not include the wave-induced sediment transport, the results differ quite a lot between the formulas outside the surf zone, where the wave asymmetry is strong.

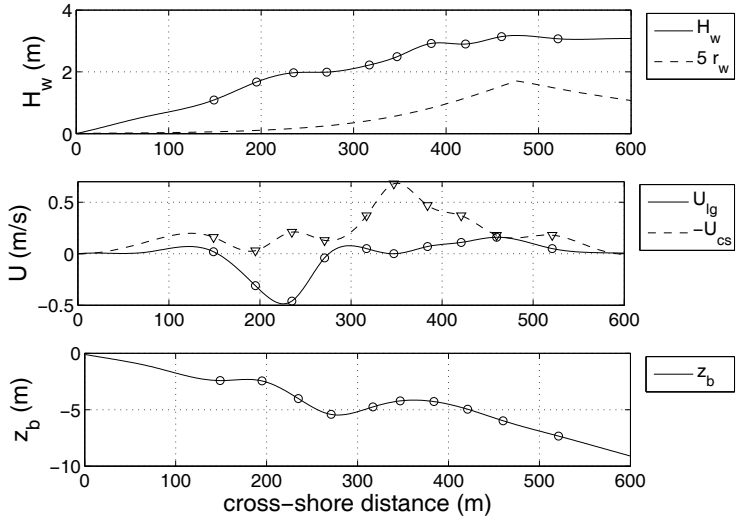

Figure 7 (a). Cross-shore distribution of hydrodynamic parameters together with beach profile shape

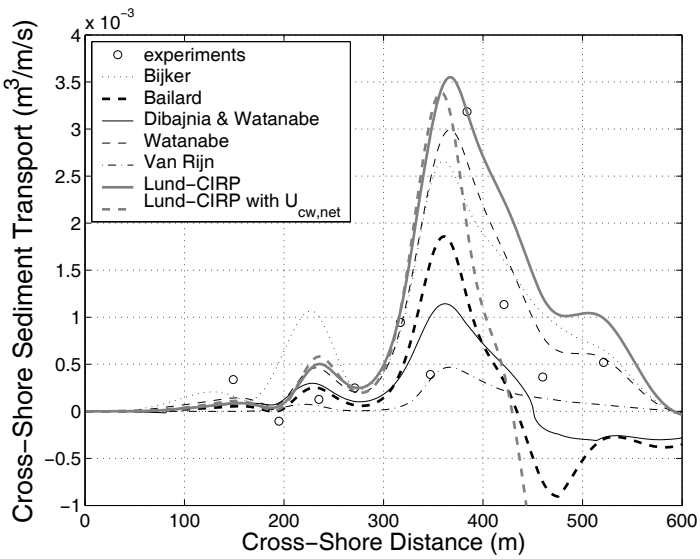

Figure 7 (b). Cross-shore distribution of the cross-shore sediment transport rate together with predictions from six studied formulas for a SandyDuck case. (March 12th 1996)

Table 2 presents the statistical results for all the formulas concerning the SandyDuck experiments. The agreement achieved for the cross-shore transport rate, as indicated by the table, seems to be poorer than for the longshore transport rate (Table 1). The Watanabe formula presents the best results, which is surprising since it was calibrated for longshore

transport. However, as discussed previously, the measured transport only includes the current-related transport, making the comparisons somewhat biased.

Table 2. Prediction of cross-shore transport rate for the SandyDuck experiments.

Author(s)	Pred. x2	Pred. x5	mean (f (qss))	std(f (qss))
SandyDuck data (6 cross-shore profiles, 66 experiments)				
Bijker (1968)	14%	41%	2.1	1.2
Bailard (1981)	24%	52%	0.1	1.5
Van Rijn (1989)	26%	55%	0.2	1.6
Watanabe (1992)	47%	68%	0.8	1.0
Dibajnia & Watanabe (1992)	35%	61%	0.0	1.2
Lund-CIRP	24%	67%	1.3	1.0

In Figure 8 are the predictions of the cross-shore transport with the Lund-CIRP model across the profile for all experimental cases from SandyDuck shown, where the predicted values were normalized with the measurements. The formula yields an overestimation of the transport in general and a significant scatter in the predicted values. This scatter is however the smallest among the studied formulas.

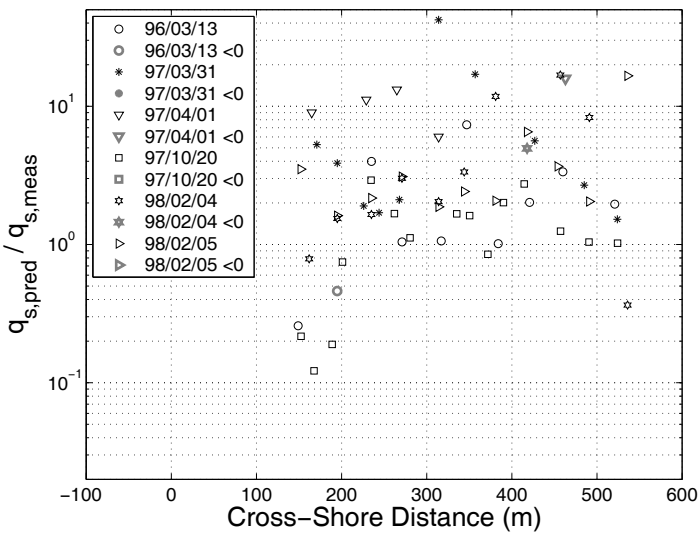

Figure 8. Predictions of the cross-shore transport rate across the beach profile for the SandyDuck data using the present formula, where the predicted values were normalized with the measured values.

An interesting data set was provided by Dohmen-Janssen and Hanes (2002). They measured both bed load and suspended load transport in a large wave flume under sheet-flow conditions (non-breaking waves). Results were obtained for four experimental cases, and the results of the comparisons with the formulas are presented in Table 3. Although a

small undertow occurred (opposite to the wave direction), the net sediment transport was directed onshore because of the prevailing asymmetric waves. The three formulas which assume that the direction of the current determines the direction of the sediment transport (Bijker, van Rijn, and Watanabe formulas) predict the wrong direction for the net total load. The Bailard, Dibajnia/Watanabe and the Lund-CIRP model yield the correct direction for the sediment transport, as well as good quantitative predictions. Dohmen-Janssen and Hanes (2002) observed that, in case of sheet flow, bed load was always prevailing and only 10% of the total load constituted suspended load for the hydrodynamic and sediment conditions studied. The Bailard formula (as well as the Bijker formula) predicts that suspended load dominated (q_{sb}/q_{ss}=0.02). The Dibajnia and Watanabe formula, since it was calibrated for sheet-flow conditions, yields results in good agreement with the observations. Finally, the Lund-CIRP model (as well as the Bailard formula) also yields good results, but it tends to overestimate the suspended load (q_{sb}/q_{ss}=0.2).

Table 3. Prediction of the cross-shore transport rate for the sheet-flow experiments by Dohmen-Janssen and Hanes (2002) (* denotes that transport in the opposite direction to the measurement is predicted).

Author(s)	Pred. x2	Pred. x5	mean(f (qss))	std(f (qss))	qsb/qss
Bijker (1968)	0%*	0%*	-1.1	0.4	0.02
Bailard (1981)	75%	100%	-0.4	0.7	0.20
Van Rijn (1989)	0%*	0%*	-0.3	0.2	1.4
Watanabe (1992)	0%*	0%*	-0.4	0.4	-
Dibajnia & Watanabe (1992)	100%	100%	-0.1	0.4	-
Lund-CIRP	100%	100%	0.3	0.6	0.16

Validation of Sediment Transport in the Swash Zone and Inner Surf Zone

The swash-zone transport formula was validated by comparing calculations with measurements from an experiment in the LSTF (Gravens and Wang, 2007). Since the cross-shore and longshore transport rates in the swash zone previously was validated against data (see Larson *et al*., 2004; Larson and Wamsley, 2006), the focus of the present study was on making comparisons across the entire profile where the effects of the coupling between the swash and inner surf zones was included. In order to model this coupling, the AD equation was employed to simulate horizontal sediment exchange (see Eq. 18).

When solving the AD equation for the surf and offshore zones, the sediment transport at the still-water shoreline obtained from swash zone computations was used as a boundary value for calculating suspended sediment concentration. Preliminary comparison with data indicated that the pick-up and deposition rate determined from Eqs. (20) and (21) yielded values that were to low. Thus, empirically based modifications to these rates were introduced as follows (Nam *et al*., 2009),

$$\overline{P} = P\left[1 + \vartheta \frac{\overline{V}}{v_0} \exp\left(-\mu \frac{d}{R}\right)\right] \tag{23}$$

$$\overline{S} = \frac{S}{\left[1 + \vartheta \frac{\overline{V}}{v_0} \exp\left(-\mu \frac{d}{R}\right)\right]} \tag{24}$$

where ϑ and μ are free non-negative coefficients, $\overline{V}$ is the mean velocity, and R is the runup height. The velocity $\overline{V}$ is determined as the average longshore current across the surf zone, v_0 is the longshore current in the swash zone, and R is calculated by the Hunt (1959) formula. Calibration showed tha $\vartheta = 9.3$ and $\mu = 2.4$ were the most suitable values for all experimental cases studied.

In order obtain all necessary quantities for calculating the sediment transport rate a wave transformation and a nearshore current model was employed to obtain the necessary hydrodynamic input (Nam *et al.*, 2009). Detailed comparison was made with the measured wave height and current at many locations across profile lines and the agreement between calculations and measurements were excellent. The measurements in the LSTF focused on the longshore sediment transport, where the transport rate was measured with the trap system at the downdrift end of the beach, and only comparisons with this transport component is shown here.

Figures 9 and 10 illustrate the calculated and measured longshore sediment transport rate for Cases BC-2 and BC-4, following the notation of Gravens and Wang (2007; for more details, see Nam *et al.*, 2009). Good agreement is obtained across the entire profile, although the transport rate is somewhat underestimated in the area of intense breaking, as observed previously for some cases. The transport rates in the swash zone and the inner part of the surf zone are well predicted, especially for Case BC-2. The marked improvement achieved by introducing the AD equation is illustrated through the reduction in the rms error. The rms error for BC-2 and BC-4 was about 18% and 35%, respectively, if the AD equation was used, whereas it was close to 60% for both cases without this equation.

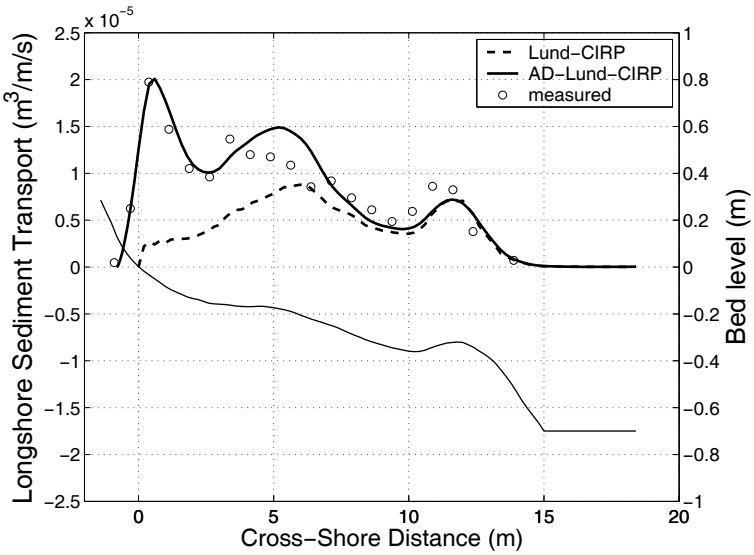

Figure 9. Computed and measured cross-shore distribution of longshore sediment transport rate for an LSTF case (BC-2)

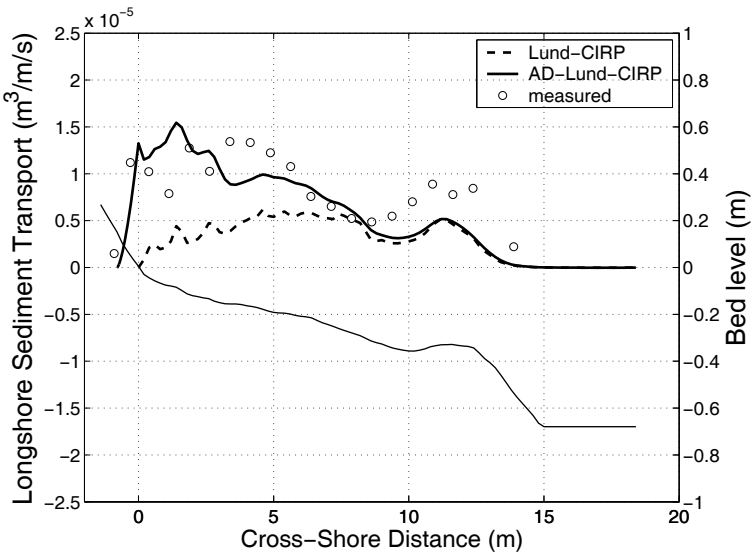

Figure 10. Computed and measured cross-shore distribution of longshore sediment transport rate for an LSTF case (BC-4)

SUMMARY AND CONCLUDING REMARKS

A new model for the total load sediment transport rate was presented based on previous work by Camenen and Larson (2005, 2006, 2008). This model, denoted as the Lund-CIRP model, describes the transport in terms of bed load and suspended load, and it is applicable for waves and current combined including the effects of wave asymmetry, phase lag, and wave breaking. Due to its generality, the model is especially well suited for application in an inlet environment where the hydrodynamic, sedimentologic, and topographic conditions vary greatly and many different processes should be taken into account simultaneously.

The various components of the Lund-CIRP model were previously calibrated and validated against a large amount of data from the laboratory and field, covering a wide range of conditions. In this study, further validation was performed considering the cross-shore distribution of longshore and cross-shore sediment transport using laboratory data from the LSTF and field data from the SandyDuck experiments. Also, some data from a large wave tank were employed to investigate cases when phase-lag effects prevail (*i.e.*, the net transport could be in the opposite direction to the mean current). Five existing sediment transport formulas were also utilized to calculate the transport rate for the studied experimental cases.

Overall the new formula produced the best agreement with the longshore transport data, although the Bijker (1968) formula also yielded acceptable results, except for the data that included phase-lag effects. The Watanabe formula overestimated the transport rates both for the laboratory and field data, whereas the Bailard and Dibajnia/Watanabe formulas consistently underestimated the rates for the field data and overestimated for the laboratory data. The van Rijn formula typically underestimated the transport rate for all cases. Concerning the cross-shore transport rates the comparison was less conclusive, partly because some of the background data had to be estimated using various calculation procedures. Also, the measurements only allow for the current-related transport to be estimated and any effects of wave asymmetry were not included (several of the formulas take into account asymmetry).

The sediment exchange between the swash and the surf zone was modeled by using the AD equation, where the swash transport rate at the shoreline constituted the shoreward boundary condition for the surf zone. Introducing the AD equation significantly improved the simulations in the inner part of the surf zone.

Acknowledgments

This work was conducted under the Inlet Modeling System Work Unit of the Coastal Inlets Research Program, U.S. Army Corps of Engineers (ML), and the Japanese Society for the Promotion of Science (BC). The work by PTN was partly funded by Sida/SAREC in the framework of the Project VS/RDE/03 and partly by the Lundberg Foundation. Comments by the anonymous reviewers are highly appreciated.

References

Bailard, J.A., 1981. An energetic total load sediment transport model for a plane sloping beach. *Journal of Geophysical Research*, 86(C11), 10938-10954.

Battjes, J. and Janssen, J.P.F.M., 1978. Energy loss and setup due to breaking of random waves. *Proceedings of the 16th International Coastal Engineering Conference*, ASCE, 569-587.

Bayram, A.; Larson, M.; Miller, H.C., and Kraus, N.C., 2001. Cross-shore distribution of longshore sediment transport: comparison between predictive formulas and field measurements. *Coastal Engineering*, 44(C5), 79-99.

Bijker, E., 1968. Littoral drift as function of waves and current. *Proceedings of the 11th International Coastal Engineering Conference*, ASCE, 415-435.

Buttolph, A.M.; Reed, C.W.; Kraus, N.C.; Ono, N.; Larson, M.; Camenen, B.; Hanson, H.; Wamsley, T., and Zundel, A.K., 2006. Two-dimensional depth-averaged circulation Model CMS-M2D: Version 3.0, Report 2, Sediment Transport and Morphology Change. Technical Report ERDC/CHL TR-06-9, Coastal and Hydraulics Laboratory, US Army Engineer Research and Development Center, Vicksburg, MS.

Camenen, B., 2009. Estimation of the wave-related ripple characteristics and induced bed shear stress. *Estuarine, Coastal and Shelf Science*, 84, 553-564.

Camenen, B. and Larroude, P., 2003. Comparison of sediment transport formulae for a coastal environment. *Coastal Engineering*, 48, 111-132.

Camenen, B. and Larson, M., 2005. A general formula for non-cohesive bed load sediment transport. *Estuarine, Coastal, and Shelf Science*, 63, 249-260.

Camenen, B. and Larson, M., 2006. Phase-lag effects in sheet flow transport. *Coastal Engineering*, 56, 531-542.

Camenen, B. and Larson, M., 2007. A unified sediment transport formulation for inlet application. Contract Report ERDC/CHL CR-07-1, Coastal and Hydraulics Laboratory, US Army Engineer Research and Development Center, Vicksburg, MS.

Camenen, B. and Larson, M., 2008. A suspended load sediment transport formula for the nearshore. *Journal of Coastal Research*, 24(3), 615-627.

Dally, W.R. and Dean, R.G., 1984. Suspended sediment transport and beach profile evolution. *Journal of Waterway, Port, Coastal and Ocean Engineering*, 110(1), 15-33.

Dibajnia, M. and Watanabe, A., 1992. Sheet flow under nonlinear waves and currents. *Proceedings of the 23rd International Coastal Engineering Conference,* ASCE, 2015-2029.

Dibajnia, M.; Moriya, T., and Watanabe, A., 2001. A representative wave model for estimation of nearshore local transport rate. *Coastal Engineering in Japan*, 43(1), 1-38.

Dohmen-Janssen, C. and Hanes, D., 2002. Sheet flow dynamics under monochromatic non-breaking waves. *Journal of Geophysical Research*, 107(C10), 13:1-13:21.

Elder, J.W., 1959. The dispersion of marked fluid in turbulent shear flow. *Journal of Fluid Mechanics*, 5, 544-560.

Grasmeijer, B. and Kleinhans, M.G., 2004. Observed and predicted bed forms and their effect on suspended sand concentration. *Coastal Engineering*, 51, 351-371.

Gravens, M.B. and Wang, P., 2007. Data report: Laboratory testing of longshore sand transport by waves and currents; morphology change behind headland structures. Technical Report ERDC/CHL TR-07-8, Coastal and Hydraulics Laboratory, US Army Engineer Research and Development Center, Vicksburg, MS.

Hunt, I.A., 1959. Design of seawalls and breakwaters. *Journal of Waterways and Harbors Division*, 85, 123-152.

Larson, M.; Kubota, S.; and Erikson, L., 2004. Swash-zone sediment transport and foreshore evolution: field experiments and mathematical modeling. *Marine Geology*, 212, 61-79.

Larson, M. and Wamsley, T.V., 2007. A formula for longshore sediment transport in the swash. *Proceedings Coastal Sediments '07*, New Orleans, ASCE, pp. 1924-1937.

Madsen, O.S., 1993. Sediment transport outside the surf zone. Unpublished technical report, Waterways Experiment Station, U.S. Army Corps of Engineer, Vicksburg, Mississippi, USA.

Madsen, O.S. and Grant, W.D., 1976. Sediment transport in the coastal environment. Technical Report 209, Massachusetts Institute of Technology, Cambridge, Massachusetts, USA.

Madsen, O.S.; Tajima, Y., and Ebersole, B.A., 2003. Longshore sediment transport: A realistic order-of-magnitude estimate. *Proceedings of Coastal Sediments '03*, ASCE (on CD).

Meyer-Peter, E. and Müller, R., 1948. Formulas for bed-load transport. Report, Second Meeting, *International Association of Hydraulic Structures Research*, Stockholm, Sweden, 39-64.

Miller, H.C., 1998. Comparison of storm longshore transport rates to predictions. *Proceedings of the 26th International Coastal Engineering Conference*, ASCE, 2954-2967.

Miller, H.C., 1999. Field measurements of longshore sediment transport during storm. *Coastal Engineering*, 36, 301-321.

Nam, P.T.; Larson, M.; Hanson, H., and Hoan, L.X., 2009. A numerical model of nearshore waves, currents, and sediment transport. *Coastal Engineering*, 56, 1084-1096.

Soulsby, R., 1997. Dynamics of marine sands. H.R. Wallingford, Ed. Thomas Telford.

Svendsen, I.A., 1984. Mass flux and undertow in the surf zone. *Coastal Engineering*, 8, 347-365.

van Rijn, L. 1989. Handbook sediment transport by currents and waves. Technical Report H461, Delft Hydraulics Laboratory, The Hague, The Netherlands.

Wang, P.; Ebersole, B.A., and Smith, E.R., 2002. Longshore sand transport – initial results from large-scale sediment transport facility. Technical Note CHETN-II-46, Coastal and Hydraulics Laboratory, U.S. Army Corps of Engineers, Vicksburg, Mississippi, USA.

Watanabe, A., 1992. Total rate and distribution of longshore sand transport. Proceedings of the 23rd International Coastal Engineering Conference, ASCE, 2528-2541.

Wilson, K.C., 1989. Friction of wave-induced sheet flow. *Coastal Engineering*, 12, 371-379.

Paper IV

A numerical model of beach morphological evolution due to waves and currents in the vicinity of coastal structures

Nam, P.T., Larson, M., Hanson, H., Hoan, L.X., 2010.

Submitted to: *Coastal Engineering* (under review).

A numerical model of beach morphological evolution due to waves and currents in the vicinity of coastal structures

Pham Thanh Nam[a,b], Magnus Larson[a], Hans Hanson[a], Le Xuan Hoan[a,b]

[a] *Water Resources Engineering, Lund University, Box 118, SE-22100 Lund, Sweden*

[b] *Institute of Mechanics, Vietnamese Academy of Science and Technology, 264 Doi Can, Hanoi, Vietnam*

Abstract

A numerical model was developed of beach morphological evolution in the vicinity of coastal structures. The model includes five sub-models for random wave transformation, surface roller development, nearshore wave-induced currents, sediment transport, and morphological evolution. The model was validated using high-quality data sets obtained during experiments with a T-head groin and a detached breakwater in the basin of the Large-scale Sediment Transport Facility at the Coastal and Hydraulics Laboratory in Vicksburg, Miss. The simulations showed that the model well reproduced the wave conditions, wave-induced currents, and beach morphological evolution in the vicinity of coastal structures. Both salient and tombolo formation behind a detached breakwater were simulated with good agreement compared to the measurements.

Keywords: *morphodynamics, random waves, wave-induced currents, surface roller, sediment transport, coastal structures.*

1. Introduction

1.1 Background and objectives

Numerical models of beach change are useful tools in engineering projects dealing with the morphological evolution of coastal areas. Thus, a number of numerical models have been developed through the years for application in beach erosion protection, harbor construction, and navy channel dredging. However, traditionally these models have focused on a limited set of processes characterized by certain time and space scales. For example, shoreline evolution models, which were the first type of models to be used in engineering studies, describe changes in the shoreline evolution due to gradients in the longshore transport. These models typically simulate shoreline evolution over decades with limited resolution of the response on the intra-annual scale. On the other hand, profile evolution models compute changes in the profile shape due to cross-shore transport only. Such models have traditionally been used to estimate the impact of storms, implying a characteristic scale for the processes on the order of days.

Coastal structures, such as groins and detached breakwaters, are frequently utilized in coastal engineering projects to prevent beach erosion. Thus, understanding the morphological evolution in the vicinity of coastal structure is necessary to achieve an optimal functional design. There have been many attempts to develop and apply numerical models for simulating beach topography change around structures (see brief review of

previous relevant studies in the following). However, the nearshore hydrodynamics and sediment transport processes are highly complex in the vicinity of coastal structures. Moreover, the validation of numerical models against high-quality data sets is still limited. Thus, the development of models that accurately predict the morphological evolution around structures remains a challenge.

The overall aim of this study is to develop a robust and reliable numerical model to simulate beach morphological evolution under waves and currents with the emphasis on the impact of coastal structures. Preferably, the model should describe the effects of both longshore and cross-shore sediment transport over time scales from individual storms to seasonal variations. In order to facilitate this, a number of sub-models were developed and improved, including (i) a random wave transformation model, (ii) a surface roller model, (iii) a nearshore wave-induced current model, (iv) a sediment transport model, and (v) a morphological evolution model. These sub-models were coupled together and validated with detailed, high-quality data from the Large-scale Sediment Transport Facility (LSTF) basin of the Coastal and Hydraulics Laboratory (CHL) in Vicksburg, Mississippi, United States.

The paper is structured as follow: Section 1.2 presents a brief review of previous relevant work. In Section 2, the sub-models are reviewed, and Section 3 introduces the LSTF data. Section 4 describes in detail the validation of the model with the LSTF data. A discussion of the simulation results is presented in Section 5. Finally, the conclusions are given in Section 6.

1.2 Brief review of previous relevant studies

Numerical models for simulating coastal morphological evolution have developed quickly during the recent decades. Development efforts have resulted in a wide range of models at different scales, including 1D, 2D, 3D, and quasi-3D models (*e.g.*, Hanson and Larson, 1992; de Vriend *et al.*, 1993; Zyserman and Johnson, 2002; Lesser *et al.,* 2004) and several of the models have been applied in coastal engineering projects. However, here we focus our review of numerical models that have been used for coastal morphological evolution in two dimensions with the emphasis on the response of the beach topography to coastal structures, such as breakwaters, jetties, and groins.

In their pioneering work, Watanabe *et al.* (1986) investigated the beach evolution in response to a detached breakwater. The wave, current, and sediment transport fields were computed from which the topographic evolution was determined. Calculations showed that the model could rather well reproduce small-scale laboratory measurements regarding the wave height and nearshore wave-induced current around a detached breakwater, but the agreement with the measured beach evolution was mainly qualitative.

Nicholson *et al.* (1997) investigated and inter-compared five numerical models for simulating the development of a salient and a tombolo in the lee of a detached breakwater. In general, the output from these models regarding the hydrodynamics and morphological evolution was in qualitative agreement between the models (no data were employed), but differences were observed. Seven factors were identified as causing the different outputs obtained from the five numerical models, including wave type, bed roughness, eddy viscosity, wave-current interaction, refraction, smoothing, and sediment transport formula.

Steijn *et al.* (1998) applied the Delft3D model to simulate the morphological change in the vicinity of a long dam constructed at the northern end of the Texel coast. The predictions by the model were in quantitative agreement with some of the observations. A scour hole that developed in front of the tip of the dam was rather well reproduced. Nevertheless, there were large differences between the observations and computations of the morphological evolution in other areas.

Denot and Aelbrecht (1999) modeled the seabed evolution around a groin system. Two hypothetical test cases with different groin spacing and incident waves were investigated. The calculated wave and current fields around the groins were in good qualitative agreement. However, the simulated seabed evolution for both cases did not show clear areas of accumulation and erosion in the vicinity of the two groins, as expected.

Roelvink *et al.* (1999) investigated the morphological response adjacent to harbor moles and groins by using a depth-averaged morphodynamic model. Different grid sizes were applied to evaluate differences in the scour hole development around the structures. However, the wave-induced current was not considered, so the longshore transport may not have been calculated accurately.

Leont'yev (1999) developed a numerical model to simulate morphological changes due to coastal structures. Several hypothetical test cases involving groins and detached breakwaters were simulated. The model was also validated based on small-scale laboratory data and the computed result of the bed level evolution was in good agreement with the measurements.

Zyserman and Johnson (2002) applied a quasi-three dimensional model of flow, sediment transport, and bed level evolution to simulate the beach morphological evolution in the vicinity of detached breakwaters. Selected results for three test cases with different locations and sizes of the breakwater showed that the model could produce reasonable results with respect to the wave, current, and sediment transport fields, although the calculations were not compared against measurements. However, when plotting their results, the resolution in the depth contours close to the shoreline was limited; for example, only contours deeper than -2 m was shown. Thus, the topographical change near the shoreline might not have been considered in detail.

Gelfenbaum *et al.* (2003) simulated long-term morphological evolution for Grays Harbor inlet by using the Delft3D model. Filtering techniques for wave and tidal inputs were employed to reduce the number of wave conditions and flow simulations. Both the cases with and without jetties were investigated, and the model results showed quantitative agreement with observations, which indicated erosion in the inlet channel and accretion on the flood and ebb deltas. However, the simulations were only carried out for one year, whereas the measured topographic change was determined for an interval of thirty years. Thus, the comparison between the calculated and measured bed changes was not synchronized. Furthermore, the model was not successful in simulating the accumulation observed at the North Jetty.

Johnson (2004) simulated the coastal morphological evolution in the vicinity of groins by using the DHI Coastal Area Morphological Modelling System (MIKE 21 CAMS). Several important aspects of the modeling system were investigated including the effects of the

sediment transport model, offshore wave height, offshore wave direction, tidal level variation, and groin spacing.

Saied and Tsanis (2005) developed a morphological model that was called the Integrated Coastal Engineering Model (ICEM). This model was tested with some hypothetical cases including detached breakwaters and groin systems. The computations for the hypothetical test cases produced results in good qualitative agreement with the expected response. Furthermore, a case study in Ras El-Bar in Egypt was employed to validate the model, and the computed shorelines were in quite good agreement with the measurements. However, detailed comparisons between calculations and measurements of the hydrodynamics and morphological evolution in the vicinity of the groins and detached breakwaters were not presented.

Johnson *et al.* (2005) validated the MIKE 21 CAMS model based on field data from the Dubai Coast. The wave transmission, overtopping, quasi-3D sediment transport, bed friction, and a global scale factor were manipulated to achieve reasonable calibration parameter values. The calculations of the bed evolution showed quite good agreement with the measurements.

Zyserman *et al.* (2005) and Zanuttigh (2007) modeled and analyzed the morphological response induced by low-crested structures on the adjacent seabed. These studies focused on the far-field erosion in the vicinity of roundheads and gaps between structures. The model was investigated by application at two field sites, Pellestrina and Lido di Dante, where groins and low-crested breakwaters were constructed to protect against beach erosion. The obtained simulation results were in good qualitative agreement with the measurements, especially the erosion near the roundheads of the breakwaters.

Ding *et al.* (2006), and Ding and Wang (2008), developed a quasi-3D morphological model that can be applied to coastal and estuarine morphological processes. The model was validated for a complex coastal area, which included detached breakwaters and a harbor. The calculated morphological change in the lee of the breakwaters was somewhat underestimated compared to the measurements. This was possibly because the sediment transport in the swash zone was not included in the model.

Brøker *et al.* (2007) also used MIKE 21 CAMS to optimize a new layout of the main breakwaters for the Thorsminde Harbor entrance. The recommended layout was constructed in 2004. However, the validation of the model was limited. The long-term beach evolution in the vicinity of new layout was not modeled, but only short simulations for selected storm conditions were carried out.

In summary, the development of numerical models of morphological evolution around coastal structures has encompassed significant improvements through the years. However, the morphodynamical processes are extremely complex and some are beyond our current state of knowledge. Furthermore, available high-quality data for validation are limited. Therefore, many of the previous modeling efforts neither included all relevant morphodynamical processes nor were validated against high-quality data from laboratories and field surveys.

2. Model description

The model that was developed includes sub-models to calculate the nearshore waves, currents, sediment transport, and the morphological change. The sub-models are briefly described in the following (for a more detailed discussion of the wave, current, and sediment transport sub-module, see Nam *et al.*, 2009; Nam and Larson, 2009 and 2010).

2.1 Modified-EBED model

Multi-directional and multi-frequency random wave transformation can be modeled based on the energy balance equation with diffraction and energy dissipation terms (Mase, 2001; Nam *et al.* 2009; Nam and Larson, 2009 and 2010) as,

$$\frac{\partial\left(v_x S\right)}{\partial x}+\frac{\partial\left(v_y S\right)}{\partial y}+\frac{\partial\left(v_\theta S\right)}{\partial \theta} = \frac{\kappa}{2\omega}\left\{\left(CC_g\cos^2\theta S_y\right)_y-\frac{1}{2}CC_g\cos^2\theta S_{yy}\right\}-\frac{K}{h}C_g\left(S-S_{stab}\right) \tag{1}$$

where S is the angular-frequency spectrum density, (x, y) the horizontal coordinates, θ the angle measured counterclockwise from the x axis, v_x, v_y, and v_θ the propagation velocities in their respective coordinate direction, ω the frequency, C the phase speed, and C_g the group speed, h the still water depth, κ a free parameter that can be optimized to change the influence of the diffraction effects, K a dimensionless decay coefficient, and S_{stab} the stable wave spectrum density, which is a function of the stable wave height H_{stab} $\left(=\Gamma h\right)$, with Γ being a dimensionless empirical coefficient. Based on Goda (2006), the coefficients K and Γ can be determined as,

$$\begin{cases}\Gamma=0.45,\ K=\dfrac{3}{8}(0.3-19.2m) & :\ m<0\\ \Gamma=0.45+1.5m,\ K=\dfrac{3}{8}(0.3-0.5m) & :0\le m\le 0.6\end{cases} \tag{2}$$

where m is the bottom slope.

The output from the model includes three main parameters: significant wave height, significant wave period, and mean wave direction. The wave-driven radiation stresses can be derived based on the output of the Modified-EBED model as,

$$S_{xx}=\frac{E}{2}\left[2n(1+\cos^2\bar{\theta})-1\right];\ S_{yy}=\frac{E}{2}\left[2n(1+\sin^2\bar{\theta})-1\right];\ S_{xy}=S_{yx}=\frac{E}{2}n\sin 2\bar{\theta} \tag{3}$$

where $E=\rho_w g H_{rms}^2/8$ is the wave energy per unit area, with ρ_w the water density, g the acceleration due to gravity, and $n=C_g/C$ the wave index.

2.2 Surface roller model

The surface roller was modeled based on the energy balance equation as (Dally and Brown, 1995; Larson and Kraus, 2002),

$$P_D + \frac{\partial}{\partial x}\left(\frac{1}{2}MC_r^2\cos^2\overline{\theta}\right) + \frac{\partial}{\partial y}\left(\frac{1}{2}MC_r^2\sin^2\overline{\theta}\right) = g\beta_D M \tag{4}$$

where P_D is the wave energy dissipation ($= KC_g\rho_w g(H_{rms}^2 - (\Gamma h)^2)/(8h)$), M the wave-period-averaged mass flux, C_r the roller speed ($\approx C$), and β_D the roller dissipation coefficient.

The stresses due to the roller were calculated as,

$$R_{xx} = MC_r\cos^2\overline{\theta};\ R_{yy} = MC_r\sin^2\overline{\theta};\ R_{xy} = R_{yx} = MC_r\sin 2\overline{\theta} \tag{5}$$

2.3 Nearshore currents model

The nearshore currents and water elevation can be determined based on the momentum equations and continuity equation as (Militello *et al.,* 2004),

$$\frac{\partial(h+\eta)}{\partial t} + \frac{\partial q_x}{\partial x} + \frac{\partial q_y}{\partial y} = 0 \tag{6}$$

$$\frac{\partial q_x}{\partial t} + \frac{\partial uq_x}{\partial x} + \frac{\partial vq_x}{\partial y} + g(h+\eta)\frac{\partial \eta}{\partial x} = \frac{\partial}{\partial x}D_x\frac{\partial q_x}{\partial x} + \frac{\partial}{\partial y}D_y\frac{\partial q_x}{\partial y} + fq_y - \tau_{bx} + \tau_{Sx} \tag{7}$$

$$\frac{\partial q_y}{\partial t} + \frac{\partial uq_y}{\partial x} + \frac{\partial vq_y}{\partial y} + g(h+\eta)\frac{\partial \eta}{\partial y} = \frac{\partial}{\partial x}D_x\frac{\partial q_y}{\partial x} + \frac{\partial}{\partial y}D_y\frac{\partial q_y}{\partial y} - fq_x - \tau_{by} + \tau_{Sy} \tag{8}$$

where η is the water elevation, q_x, q_y the flow per unit width parallel to the *x* and *y* axis, respectively, u, v the depth-averaged velocity in *x* and *y* direction, respectively, D_x, D_y the eddy viscosity coefficients, *f* the Coriolis parameter, τ_{bx}, τ_{by} the bottom stresses, and τ_{Sx}, τ_{Sy} the wave stresses (the latter variables are all in the *x*- and *y*-directions, respectively).

In this study, we only consider the wave-induced currents. The wave stresses were determined from the output of the Modified-EBED model, and from the surface roller model as,

$$\tau_{Sx} = -\frac{1}{\rho_w}\left[\frac{\partial}{\partial x}(S_{xx} + R_{xx}) + \frac{\partial}{\partial y}(S_{xy} + R_{xy})\right] \tag{9}$$

$$\tau_{Sy} = -\frac{1}{\rho_w}\left[\frac{\partial}{\partial x}(S_{xy} + R_{xy}) + \frac{\partial}{\partial y}(S_{yy} + R_{yy})\right] \tag{10}$$

The eddy viscosity in the offshore is determined based on the work by Falconer (1980), whereas the expression by Kraus and Larson (1991) is employed for the surf zone. The bottom stresses can be calculated from Nishimura (1998).

2.4 Sediment transport model

2.4.1 *Swash zone*

The net transport rates over several swash cycles in the cross-shore and longshore direction can be calculated based on the formula by Larson and Wamsley (2007) as,

$$q_{bc,net} = K_c \frac{\tan\phi_m}{\tan^2\phi_m - \left(dh/dx\right)^2} \frac{u_0^3}{g}\left(\frac{dh}{dx} - \tan\beta_e\right)\frac{t_0}{T} \tag{11}$$

$$q_{bl,net} = K_l \frac{\tan\phi_m}{\tan^2\phi_m - \left(dh/dx\right)^2} \frac{u_0^2 v_0}{g}\frac{t_0}{T} \tag{12}$$

where $q_{bc,net}$, $q_{bl,net}$ are the transport in the cross-shore and longshore direction, respectively, K_c and K_l empirical coefficients, ϕ_m the friction angle for a moving grain ($\approx 30\,\text{deg}$), β_e the foreshore equilibrium slope, u_0, v_0 and t_0 the scaling velocities and time, respectively, and T the swash duration (T is set equal to the incident wave period). The swash zone hydrodynamics without friction (yields u_0, v_0 and t_0), which were derived based on the ballistics theory, were employed in the model (for details see Larson and Wamsley, 2007).

2.4.2 *Nearshore zone (offshore and surf zone)*

The bed load transport is determined following the work by Camenen and Larson (2005, 2007),

$$\frac{q_{bc}}{\sqrt{(s-1)gd_{50}^3}} = a_c\sqrt{\theta_c}\,\theta_{cw,m}\exp\left(-b_c\frac{\theta_{cr}}{\theta_{cw}}\right) \tag{13}$$

where the transport q_{bc} is obtained in the direction of the current (the transport normal to the current is zero), s the relative density between sediment and water, d_{50} the median grain size, a_c and b_c empirical coefficients, $\theta_{cw,m}$ and θ_{cw} the mean and maximum Shields parameters due to wave and current interaction, respectively, θ_{cr} the critical Shields parameter, and θ_c the Shields parameter due to current.

The suspended load can be obtained by solving the advection-diffusion equation. The advection-diffusion equation is obtained from continuity in the depth-averaged suspended sediment transport as,

$$\frac{\partial\left(\overline{C}d\right)}{\partial t} + \frac{\partial\left(\overline{C}q_x\right)}{\partial x} + \frac{\partial\left(\overline{C}q_y\right)}{\partial y} = \frac{\partial}{\partial x}\left(K_x d\frac{\partial\overline{C}}{\partial x}\right) + \frac{\partial}{\partial x}\left(K_y d\frac{\partial\overline{C}}{\partial y}\right) + \overline{P} - \overline{D} \tag{14}$$

where $\overline{C}$ is the depth-averaged sediment concentration, K_x and K_y the sediment diffusion coefficient in x and y direction, respectively, $\overline{P}$ the sediment pick-up rate, and $\overline{D}$ the sediment deposition rate (for details see Nam *et al.*, 2009).

2.5 Morphological evolution model

The morphological evolution is based on the sediment volume conservation equation,

$$\frac{\partial h}{\partial t} = \frac{1}{1-n_p}\left(\frac{\partial q_{tot,x}}{\partial x} + \frac{\partial q_{tot,y}}{\partial y}\right) \tag{15}$$

where n_p is the porosity, and $q_{tot,x}$ and $q_{tot,y}$ the total load in x and y directions, respectively. In the offshore and surf zone, the total load is the sum of bed load and suspended load, which are calculated based on equations (13) and (14). In the swash zone, it is based on the transport rates obtained from (11) and (12).

3. LSTF data and selected test cases

Five series of physical model experiments were undertaken in the basin of the LSTF (Gravens *et al.*, 2006; Gravens and Wang, 2007; Hamilton and Ebersole, 2001; Wang *et al.*, 2002). The main aim of these experiments was to obtain high-quality data sets for validating formulas for sediment transport, as well as investigating the beach evolution in the vicinity of coastal structures. The first series of experiments consisted of four runs approximately 160 min each that were performed on a natural beach without structures. The second and third series of experiments, referred to as "Test 1" and "Test 2", were carried out with a detached breakwater in the basin that was located between profile Y22 and Y26, at four meter distance from the initial still water shoreline (see Fig. 1). The currents in Test 1 were generated by waves only, whereas in Test 2 the currents were a combination of wave-induced currents and external currents. Both Test 1 and Test 2 included eight runs approximately 190 min each. The fourth series, referred to as "Test 3", included six runs 180 min each, performed on the natural beach with a T-head groin (see Fig. 2). The last series of experiments, referred to as "Test 4", were conducted in the basin with a detached breakwater, but its length was shorter and its location was closer to the shoreline than those in Test 1 and Test 2.

In all experimental runs, spilling breaking waves were generated by four wave-makers and the water was re-circulated by the pumping systems located up- and downstream of the basin. Wave gages and acoustic doppler velocimeters were co-located at ten cross-shore positions on the instrument bridge: 1.125 m (ADV1), 2.2 m (ADV2), 3.3 m (ADV3), 4.125 m (ADV4), 5.73 m (ADV5), 7.125 m (ADV6), 8.525 m (ADV7), 10.125 m (ADV8), 11.625 m (ADV9), and 13.125 m (ADV10) seaward from the initial shoreline. This bridge moved in the alongshore direction, thus the wave conditions and currents could be observed at specific cross-shore profiles. Three wave gages (#11, #12, and #13) were located at three alongshore positions, 18.43 m seaward of the initial shoreline, to measure the wave conditions seaward of the toe of the movable beach. A rod and acoustic survey techniques were employed to measure the beach profiles after each experimental run. The beach in the basin consisted of well-sorted sand with a median grain size of 0.15 mm.

In this study, three runs from Test 3 (T3C1, T3C4, and T3C6), and three runs from Test 1 (T1C1, T1C4, and T1C8), were selected to evaluate the predictive capability of the model regarding nearshore waves, wave-induced currents, and morphological evolution for the T-head groin and detached breakwater experiment, respectively.

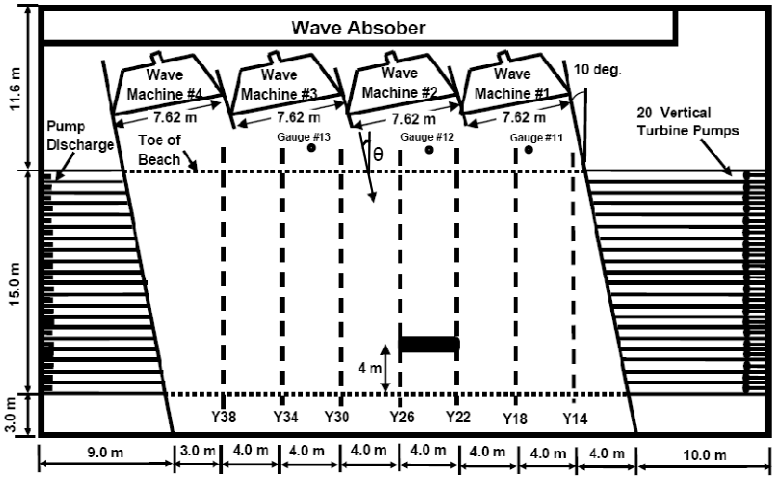

Fig. 1. Detached breakwater layout in the LSTF for Test 1 and 2 (Gravens and Wang, 2007)

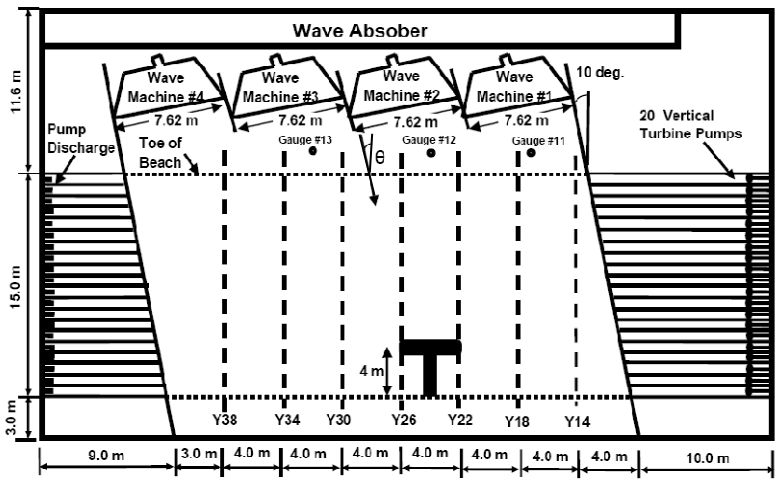

Fig. 2. T-head groin layout in the LSTF for Test 3 (Gravens and Wang, 2007)

4. Model validation against LSTF data

4.1 Model setup

The computational domain was covered by a rectangular grid with a cell size of 0.2 × 0.2 m, and interpolation was employed using the measured bathymetry data from profile Y34 to profile Y14.

The observed data at Gauges #11, #12, and #13 were used as the offshore wave conditions. Detailed information on the wave conditions at these gauges for the cases with a T-head groin and a detached breakwater is presented in Table 1. A Texel-Marsen-Arsloe (TMA)

spectrum was assumed at the offshore boundary with the parameter values $\gamma = 3.3,\ \sigma_a = 0.07,\ \sigma_b = 0.09$, and the angular spreading of the waves $S_{max} = 25$. The decay and stable coefficients were calculated from Eq. (2).

The roller dissipation coefficient was set to $\beta_D = 0.1$. A Manning coefficient of 0.025 was used to calculate the bottom friction. The measured velocities at profile Y34 and profile Y14 were employed to specify the influx and outflux of water at the lateral boundaries for the nearshore current model. At the offshore boundary, a radiation boundary condition was given following Reid and Bodine (1968).

The coefficient values of K_c and K_l were both specified as 0.0008 for determining the net transport rates in the swash zone in the cross-shore and longshore directions, respectively (Nam *et al.*, 2009), whereas the values of a_c and b_c in the bed load formula were selected as 12 and 4.5, respectively (Camenen and Larson, 2005). In Eq. (14), the value of the diffusion coefficients were set according to Elder (1959). The pick-up and deposition rates were calculated using the formulas of Nam *et al.* (2009), and the porosity in the mass conservation equation was set to 0.4. A time step of 60 s was selected for the morphological change model.

Table 1. Offshore wave conditions

Structure types	Data sets	Gauges	H_{mo} (m)	T_p (s)	θ (deg.)
T-head groin	T3C1	#11	0.218	1.447	6.5
		#12	0.231	1.477	6.5
		#13	0.223	1.450	6.5
	T3C4	#11	0.221	1.462	6.5
		#12	0.223	1.476	6.5
		#13	0.224	1.457	6.5
	T3C6	#11	0.220	1.459	6.5
		#12	0.222	1.470	6.5
		#13	0.225	1.458	6.5
Detached breakwater	T1C1	#11	0.219	1.442	6.5
		#12	0.236	1.470	6.5
		#13	0.226	1.459	6.5
	T1C4	#11	0.222	1.452	6.5
		#12	0.232	1.472	6.5
		#13	0.225	1.464	6.5
	T1C8	#11	0.219	1.457	6.5
		#12	0.236	1.468	6.5
		#13	0.224	1.461	6.5

Fig. 3 presents a flowchart for the calculation of beach topography evolution, including the feedback loops. Based on the input data (offshore wave conditions), the Modified-EBED model is employed to calculate the wave field in the nearshore zone. The mass flux due to the roller is determined through the roller model. Thus, the wave stresses is calculated based on the random wave transformation model and the roller model. After that, the

wave-induced current field at steady state is determined from the nearshore current model. The output from the wave and current models is used to compute the Shields parameters that are employed for determining the bed load in the offshore and surf zone. The coupling between the sediment transport in the swash and inner surf zone is included. When solving the advection-diffusion equation for the offshore and surf zone, the suspended sediment concentration at the still-water shoreline (boundary between swash and surf zone) is calculated based on the sediment transport rates obtained by the swash zone computations. The beach morphological change is determined from the volume conservation equation. In order to save time in the computations, the wave, current, and sediment transport fields are only re-calculated every n-th morphological time step (n=5 in the present study). The bed level is smoothed at an interval corresponding to 15 times the morphological time step, and the smoothing coefficient is 0.25 (Johnson and Zyserman, 2002).

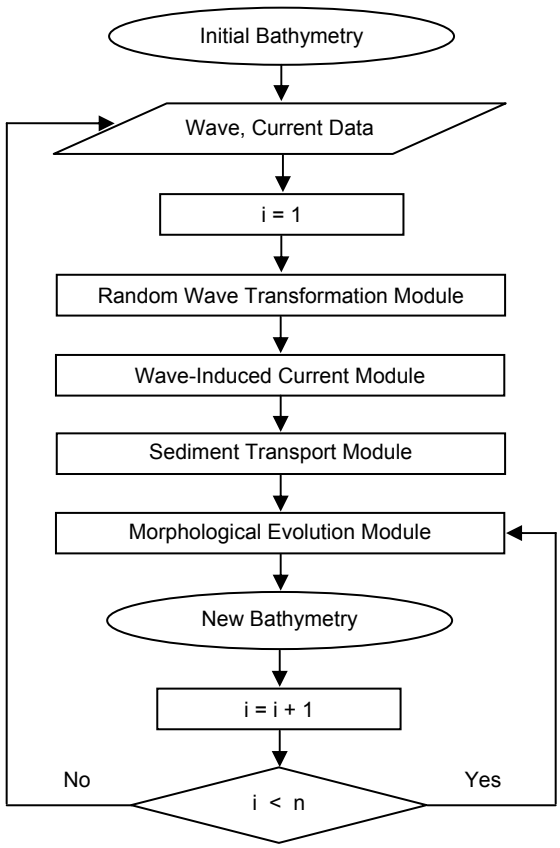

Fig. 3. Calculation procedure in the morphological evolution model

4.2 Model validation against data for T-head groin

The initial bathymetry for test case T3C1 consisted of the pre-run survey data of Test 3 in which the beach was designed to be quite uniform in the alongshore direction and the shoreline was straight. For test cases T3C4 and T3C6, the initial bathymetries were from the post-run survey data of the runs T3C3 and T3C5, respectively.

Fig. 4 shows a detailed comparison between calculations and measurements of the significant wave height along six selected profile lines in the vicinity of a T-head groin for T3C1 (see Fig. 2). The calculations obtained by the Modified-EBED model are described by the solid line, whereas the ones obtained by the original EBED model, are presented by the dashed line. As can be seen, the Modified-EBED model yielded improved predictions of significant wave height in the surf zone, resulting in more accurate wave stresses for calculating the wave-induced currents. Note that the measured data at ADV4 were not included, because the wave gage at this location did not work properly.

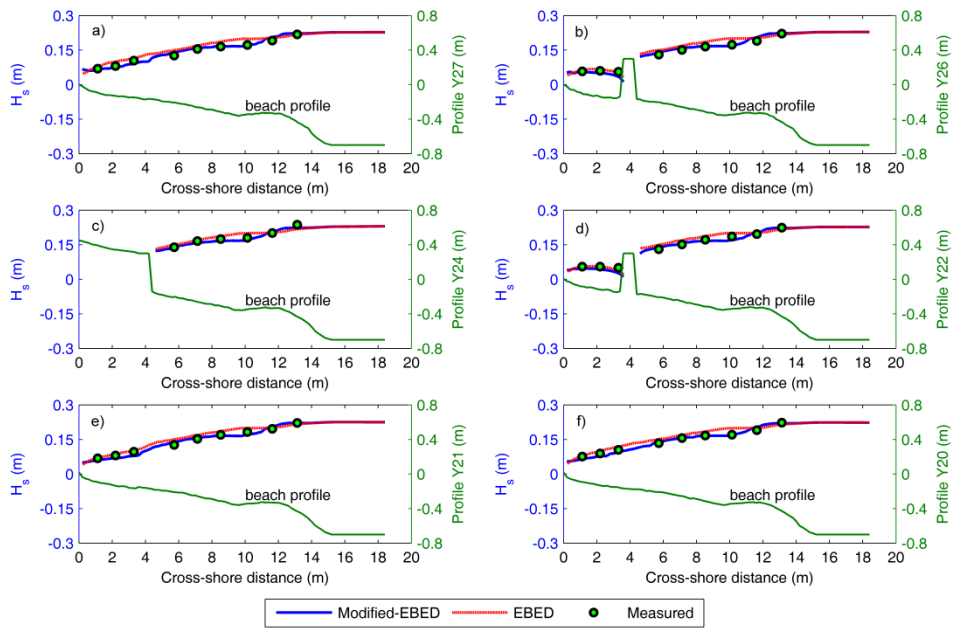

Fig. 4. Comparison of calculated significant wave height with measurements for Case T3C1

The wave-induced currents in the vicinity of the T-head groin were investigated and compared against the measurements for T3C1. Fig. 5 displays a detailed comparison between calculations and measurements of the longshore current for six selected profiles. In general, both calculated longshore currents with and without roller were in good agreement with the observations. The calculations with roller implied a current distribution that was slightly shifted towards the shoreline. The observations of longshore current at ADV9 and ADV10 were not correct (Gravens and Wang, 2009); thus, they were not employed in this comparison.

The comparison between calculated and measured cross-shore current for T3C1 is presented in Fig. 6. Calculated cross-shore currents somewhat underestimated the measurements, although they were in good agreement in the lee of the T-head groin. The calculated cross-shore currents with the roller were quite similar to those without roller. An eddy was calculated to occur around ADV3-ADV6 of profile Y20 and Y21; therefore, the cross-shore current had a shoreward direction here. Nevertheless, the measured data at these locations were relatively small and quite flat. Thus, the differences between measured and calculated cross-shore currents were significant at these locations (see Figs. 6e and f). In the present study, the undertow current was not included in the model, which is probably the main reason for these discrepancies.

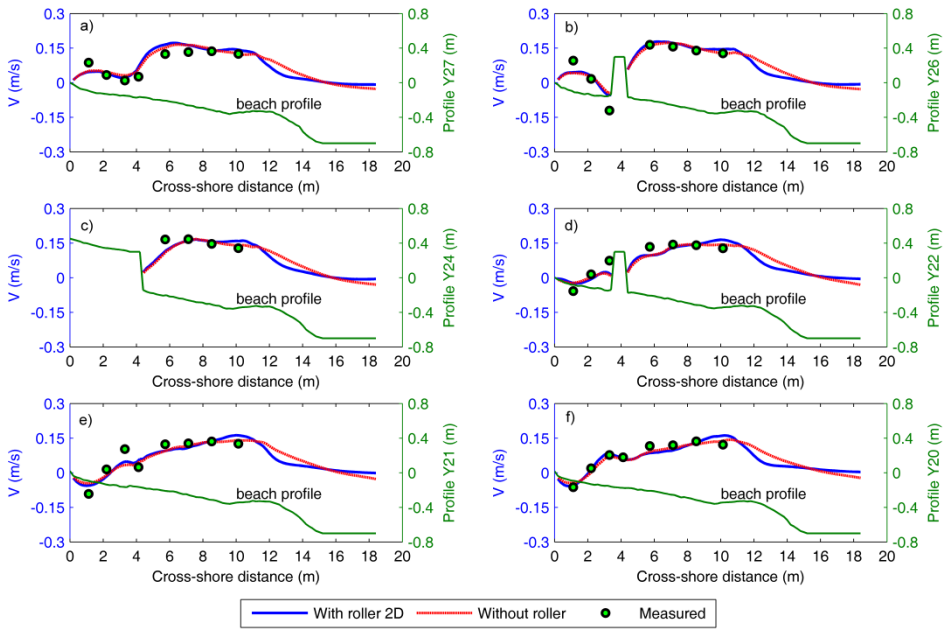

Fig. 5. Comparison of calculated longshore current with measurements for Case T3C1

The computed beach evolution after 180 min for Case T3C1 was compared with the measurements (see Fig. 7). The solid line represents the calculated bed level, whereas the dotted line shows the measurements. The calculated beach topography agreed rather well with the measurements, including the sand accumulation in the lee of T-head groin. However, there were some discrepancies between calculated and measured shoreline change up- and downdrift of the structure.

The computations of nearshore waves, wave-induced currents, and morphological evolution for T3C4 were carried out in the same manner as for T3C1. The wave conditions were also well predicted by the Modified-EBED model for this case. Although the calculations somewhat underestimated measurements, overall the Modified-EBED model reproduced well the significant wave height at all measurement locations (see Fig. 8).

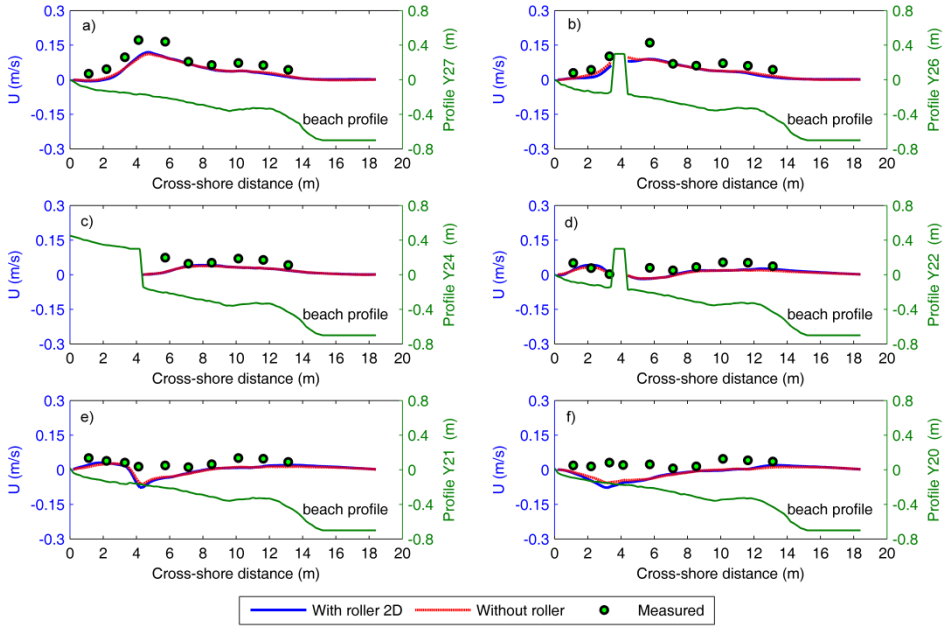

Fig. 6. Comparison of calculated cross-shore current with measurements for Case T3C1

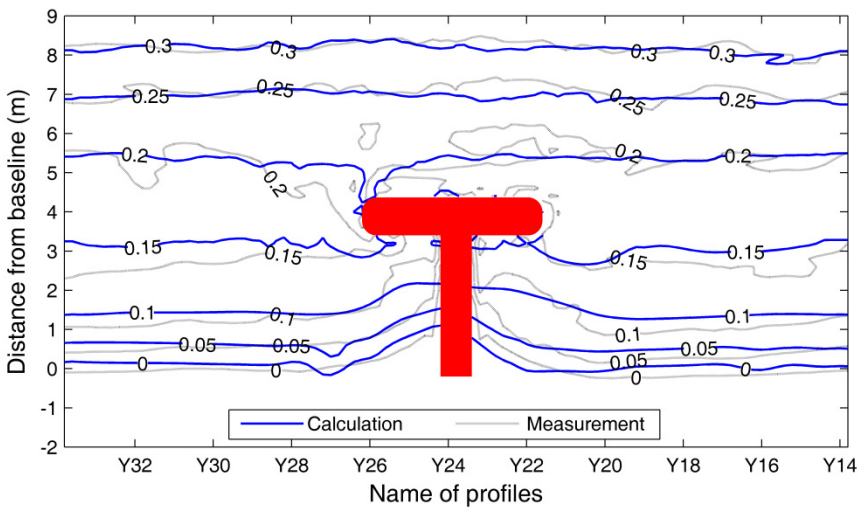

Fig. 7. Comparison of calculated bed level after 180 min with measurements for Case T3C1

Similarly to T3C1, the computed longshore current in the vicinity of the T-head groin for T3C4 was in good agreement with the measurements. As seen in Fig. 9, the computation of the longshore current with roller represented a slight improvement compared to the one without roller. The computed cross-shore current underestimated the measurements, but

the calculated eddy downstream the T-head groin was stronger than in T3C1, causing larger differences compared to the measurements in this area (see Figs. 10e and f). However, in general the calculations agreed well with the measurements in the lee of the T-head groin (Figs. 10b and d).

Fig. 11 shows the comparison between calculated bed levels after 180 min and measurements for T3C4. The computations showed that the beach evolution was fairly well predicted; especially, the shoreline changes were in good agreement with the observations. However, the calculated sand accumulation downdrift the T-head groin exceeded measured data.

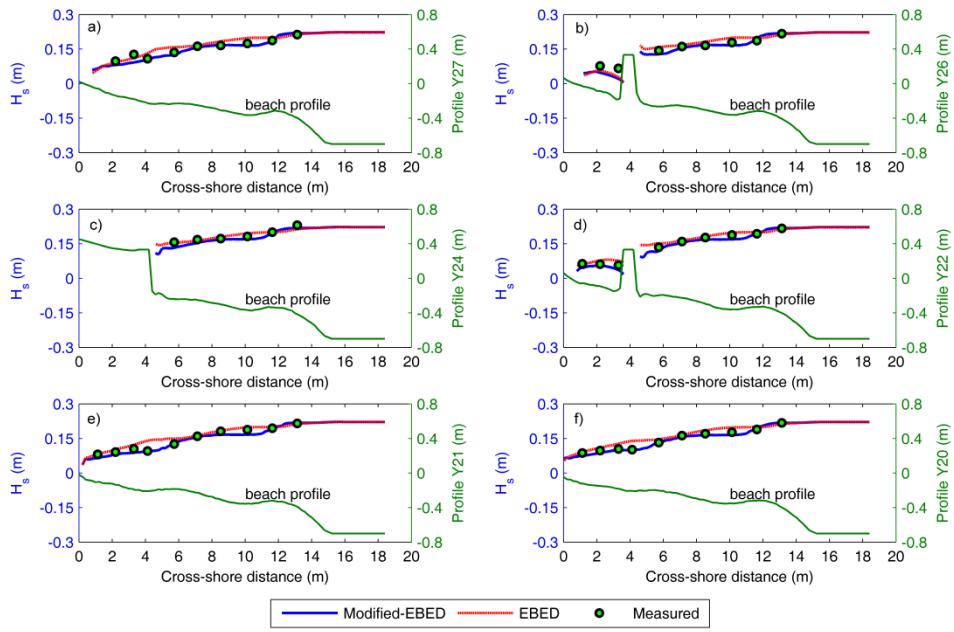

Fig. 8. Comparison of calculated significant wave height with measurements for Case T3C4

Fig. 12 shows the comparison of calculated significant wave height with the measurements for T3C6. As for T3C1 and T3C4, the wave predictions obtained by the Modified-EBED model were in good agreement with observations, and significant improvement was achieved at ADV7, ADV8, and ADV9 compared to the original EBED model.

Fig. 13 compares the measured and computed longshore current for six selected cross-shore profiles for T3C6. As can be seen, the calculations of the longshore current with roller agreed somewhat better with the measurements than the one without roller. In this case, the simulations of the longshore current were in good agreement with the observations not only in the surf zone, but also in the lee of the T-head groin.

A detailed comparison between the calculated and measured cross-shore current for T3C6 is presented in Fig. 14. As can be seen, the calculated cross-shore current with roller is quite similar to that without roller. As for the previous cases, the predicted cross-shore currents somewhat underestimated the observations. The eddy simulated downstream the T-head groin caused a significant difference between the calculated and observed cross-

shore currents at profile Y21 and Y20 (see Figs. 14e and f). However, as for T3C1 and T3C4, overall the agreement between measurements and calculations was quite good in the lee of T-head groin (see Figs. 14b and d).

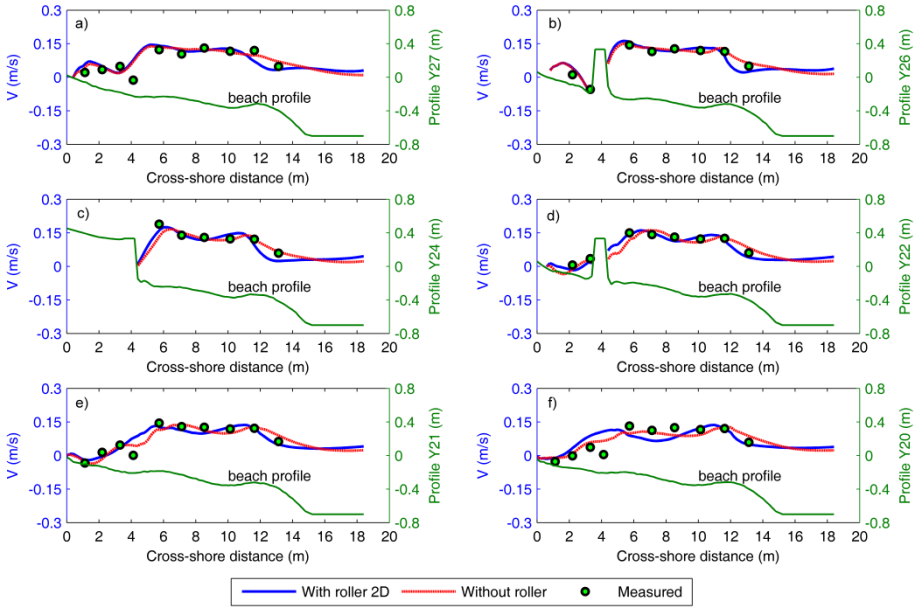

Fig. 9. Comparison of calculated longshore current with measurements for Case T3C4

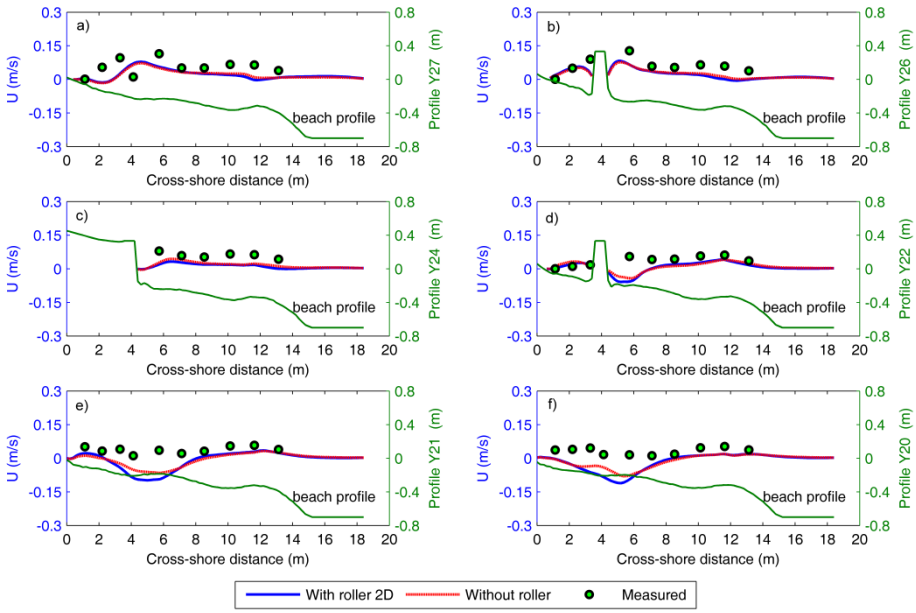

Fig. 10. Comparison of calculated cross-shore current with measurements for Case T3C4

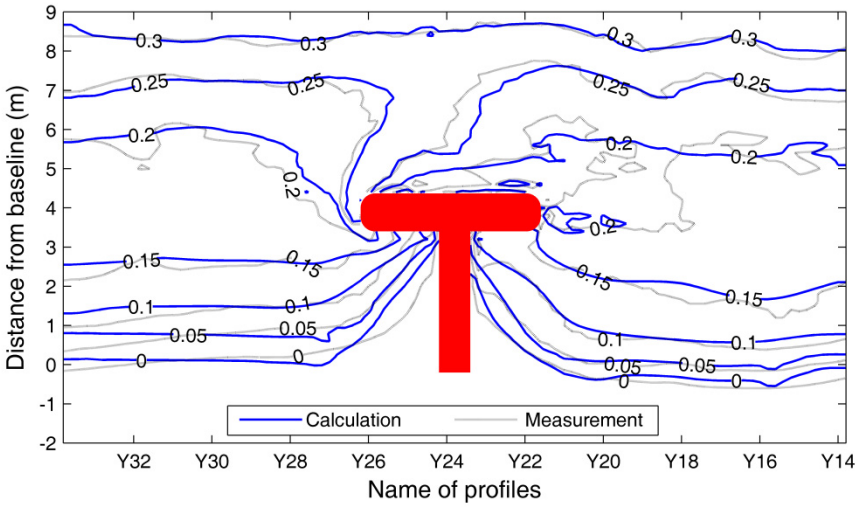

Fig. 11. Comparison of calculated bed level after 180 min with measurements for Case T3C4

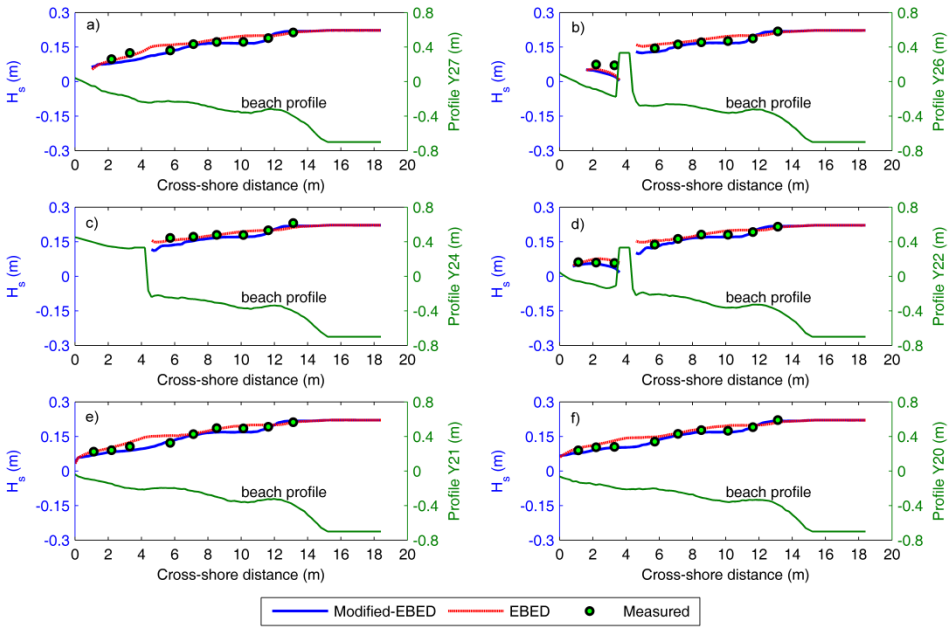

Fig. 12. Comparison of calculated significant wave height with measurements for Case T3C6

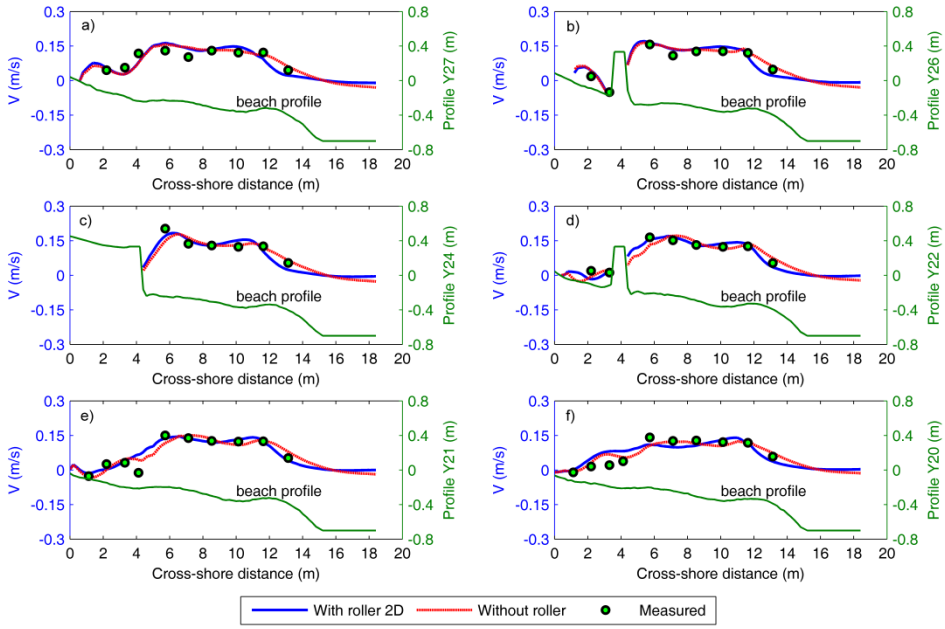

Fig. 13. Comparison of calculated longshore current with measurements for Case T3C6

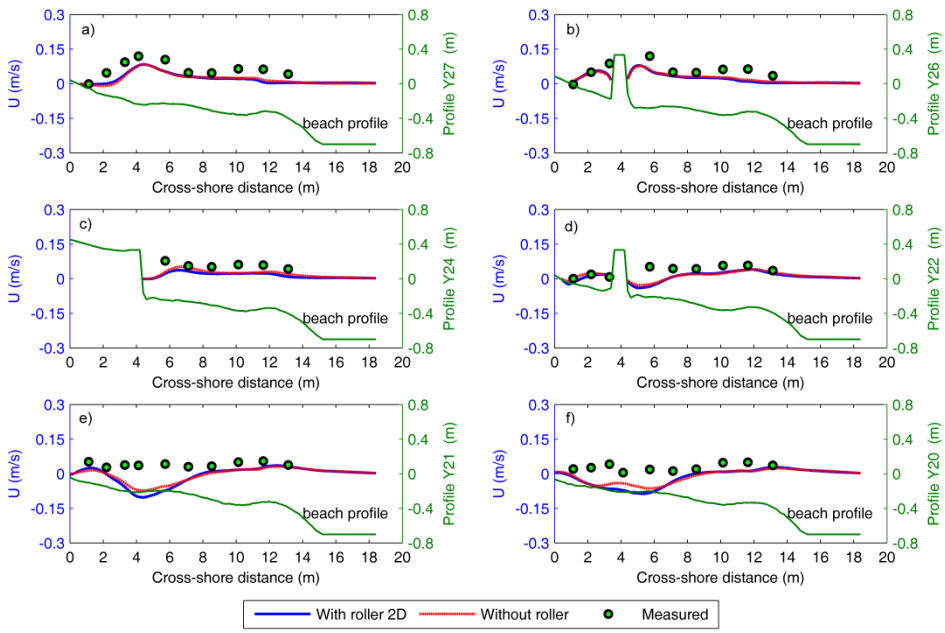

Fig. 14. Comparison of calculated cross-shore current with measurements for CaseT3C6

Fig. 15 shows the comparison between calculated and measured bed levels after 180 min for T3C6, and the simulated beach topography changes agreed well with the measurements. The salient was faithfully reproduced in the lee of T-head groin by the model. Although there were discrepancies at the updrift side, the calculated shoreline changes closely reproduced the measurements.

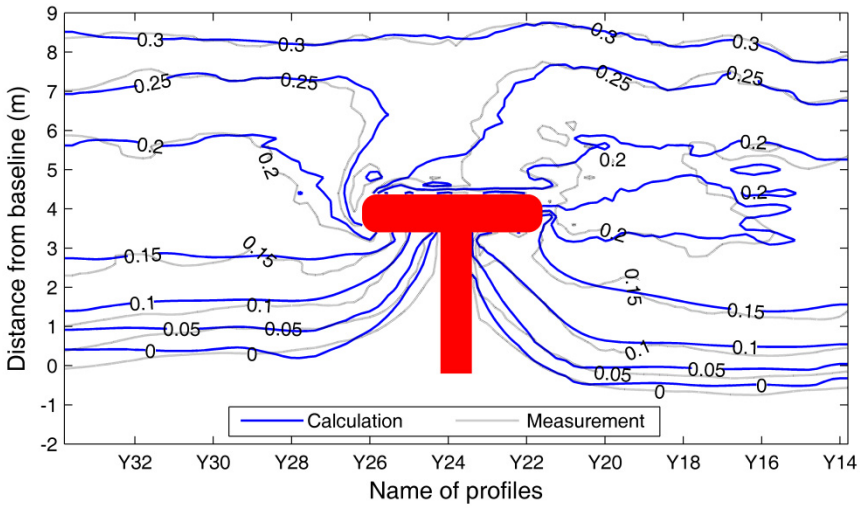

Fig. 15. Comparison of calculated bed level after 180 min with measurements for Case T3C6

4.3 Model validation against data for detached breakwater

As for T3C1, the initial bathymetry of test case T1C1 consisted of the pre-run survey data of Test 1; the beach was rather uniform in alongshore direction, and the shoreline was straight and parallel to the detached breakwater. The post-run survey data of the runs T1C3 and T1C7 were employed as initial bathymetries for the cases T1C4 and T1C8, respectively.

Model validation for Cases T1C1, T1C4, and T1C8 regarding the significant wave height, longshore current, cross-shore current, and wave setup were carried out and presented in Nam and Larson (2010). Therefore, only the validations for the beach morphological evolution are presented in the present study for these cases.

Fig. 16 shows a comparison of the calculated beach evolution after 185 min with the measurements for T1C1. The beach topography changed slightly seaward of detached breakwater. However, the salient developed significantly in the lee of the detached breakwater. The simulation showed that the calculation of the beach topographical change due to waves and currents were in good agreement with the measurements, especially concerning the salient development in the lee of detached breakwater. However, the difference between the calculated and measured downdrift shoreline was significant. The observations showed that the shoreline eroded downdrift; however, this response was not well reproduced by the model.

Fig. 17 illustrates a comparison between the calculated and measured bed levels after 190 min for T1C4. The simulated beach morphological evolution in the vicinity of detached breakwater agreed rather well with the measurements, especially regarding the salient development in the lee of the breakwater.

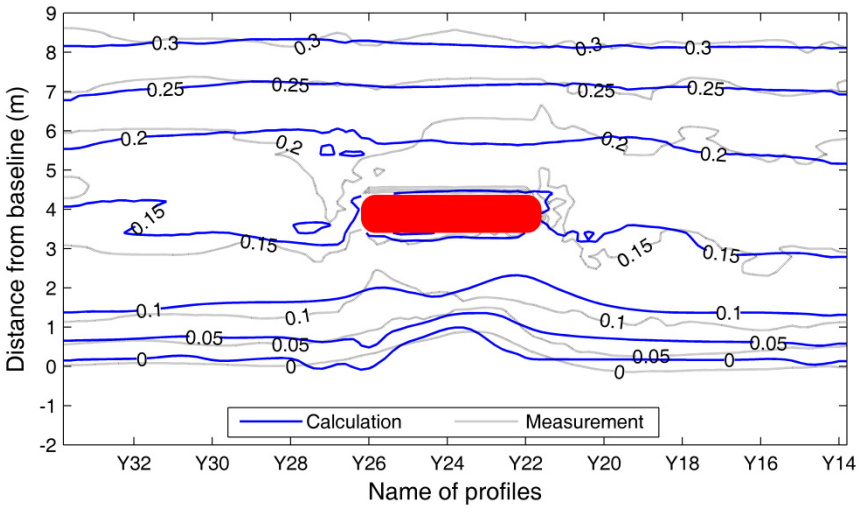

Fig. 16. Comparison of calculated bed level after 185 min against measurements for T1C1 case

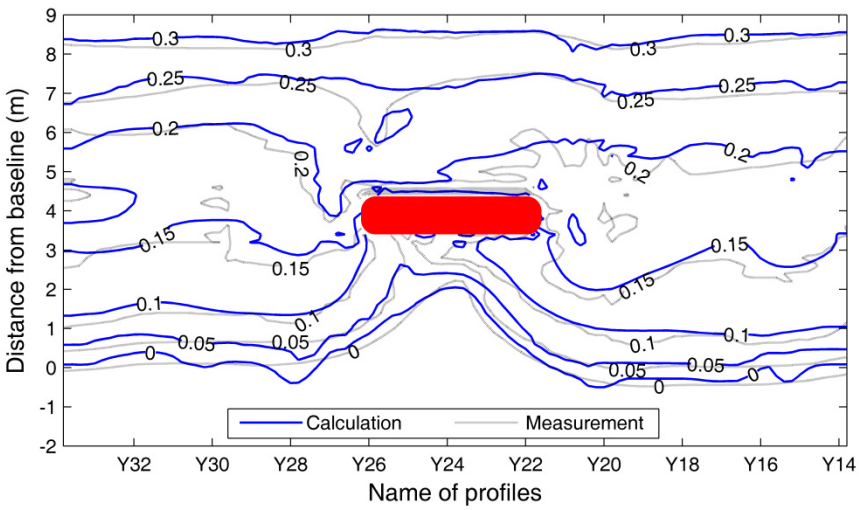

Fig. 17. Comparison of calculated bed level after 190 min with measurements for Case T1C4

The calculated bed levels after 185 min for T1C8, together with the corresponding measurements, are presented in Fig. 18. As can be seen, the beach topographical evolution was fairly well predicted by the model, and a tombolo was predicted to develop in the lee

of the detached breakwater in agreement with observations. However, the discrepancies between measurements and computations of bed level in the downdrift area were more significant than those for T1C1 and T1C4.

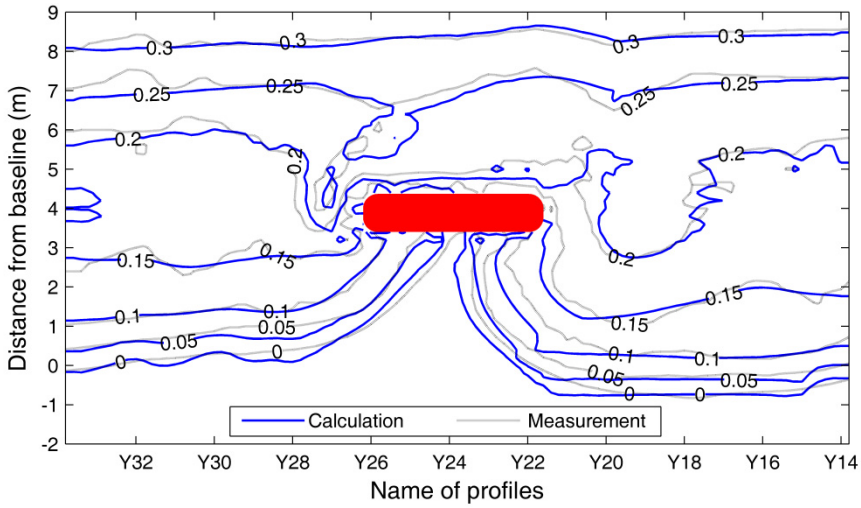

Fig. 18. Comparison of calculated bed level after 185 min with measurements for Case T1C8

5. Discussion

The wave field simulation is the crucial first step in modeling beach morphological evolution. The accuracy of the current and sediment transport fields is strongly dependent on the output from the wave model. In the present study, a diffraction term is included in the Modified-EBED model. Thus, this model can be applied to coastal areas that include structures, such as breakwaters and groins. The simulations showed that the calculations of significant wave height in the lee of detached breakwaters and T-head groins were in good agreement with the measurements, proving that the diffraction effects were well described by the model. As discussed in the previous studies of Nam *et al.* (2009) and Nam and Larson (2010), the energy dissipation due to wave breaking plays an important role in calculating the wave conditions in the surf zone. The energy dissipation is computed following the Dally *et al.* (1985) model, improving the predictions of the wave conditions in the surf zone. Thus, the Modified-EBED model can provide more accurate simulation results to be used for calculating nearshore wave-induced currents and sediment transport rates.

Calculation of wave-induced currents is also dependent on the roller effects. By including the roller, the peak of the longshore current is shifted shoreward and the magnitude of the longshore current is slightly increased in the surf zone compared to the case without roller. However, the surface roller has limited influence on the computational results for the cross-shore current. The calculated cross-shore currents with and without roller are quite similar. The numerical model can well reproduce the longshore current. However, the calculated cross-shore current is often underestimated compared to the measurements. The

undertow is not included in the model, most likely causing the differences between calculated and measured cross-shore currents.

Swash zone transport needs to be included in morphological evolution models. The sediment exchange between land and sea directly affects both the sub-aerial and sub-aquaeous evolution of the beach. In the swash zone, the frequent uprush and backwash result in high transport rates in both the cross-shore and alongshore directions. It is clearly shown in the experimental data sets obtained from the LSTF basin that the transport rate near the shoreline may be similar to the maximum values observed in the surf zone (Gravens and Wang, 2007; Nam *et al.*, 2009). Therefore, it is necessary to compute the transport rates in the swash zone, and couple those to the transport in the inner surf zone in order to realistically simulate the beach topography evolution.

The algorithm for solving the sediment volume conservation equation is an important subject. A number of numerical schemes have been introduced for solving this equation (see Callaghan *et al.*, 2006; and Long *et al.*, 2008). However, the equation is highly non-linear so it is not easy to obtain an accurate solution. For example, the Lax-Wendroff scheme was employed in many applications, but it requires that the bed celerity (Johnson and Zyserman, 2002) or bedform phase speed (Long *et al.* 2008) is determined, which may cause large errors in the calculations, if the gradient of bed forms is relatively small. Johnson and Zyserman (2002) recommended smoothing and filtering techniques to overcome the dispersion problem due to the Lax-Wendroff scheme. Recently, several high-order schemes were introduced by Callaghan *et al.* (2006) and Long *et al.* (2008) that can be applied to solve the continuity equation without resorting to smoothing or filtering techniques and that enables high accuracy solution. However, when calculating the value of the bed level at one cell, a number of values on the bed level in nearby cells need to be included. Therefore, ghost cells must be employed at open and solid boundaries (Long *et al.*, 2008), which can cause significant errors if the coastal area is complex and coastal structures are present. In this study, the first-order upwind scheme FTBS (forward in time, backward in space) was employed to solve the sediment conservation equation. Although the FTBS scheme has lower accuracy than high-order schemes, FTBS is stable and the obtained bed level changes were reasonable and in good agreement compared with the LSTF data. Furthermore, it is quite straightforward to implement and the model may be applied to complex coastal areas including structures. However, smoothing is required in the present study. In future studies, advanced numerical schemes will be continuously investigated and applied in order to obtain accurate solutions to bed level change, at the same time avoiding smoothing.

6. Conclusions

A unified numerical model of beach morphological evolution due to waves and currents was developed. It includes five sub-models, including nearshore random wave transformation, surface roller, wave-induced current, sediment transport, and morphological change models. The model was applied to simulate the beach evolution in the vicinity of coastal structures in a non-tidal environment under wave and current action.

The developed model was validated against six high-quality data sets from the experiments on the morphological impact of a T-head groin and a detached breakwater in the LSTF basin, at the Coastal and Hydraulics Laboratory, Vicksburg, Miss. The simulations showed

that the model could well produce the wave field compared to the measured data. Reasonably accurate wave-induced currents were also obtained with the model, although the cross-shore currents somewhat underestimated measurements because of neglecting the undertow. The calculated beach evolution in the vicinity of the breakwater and the T-head groin agreed rather well with the measurements. Thus, it is expected that the model can be applied in coastal engineering projects for predicting the beach evolution due to waves and currents in the vicinity of coastal structures.

Acknowledgments

This work was partly funded by Sida/SAREC in the framework of the Project VS/RDE/03 "*The evolution and sustainable management in the coastal areas of Vietnam*" (PTN and LXH), partly by Lars Erik Lundberg Scholarship Foundation (PTN), partly by J. Gust. Richert Foundation (PTN), partly by Vietnam's National Foundation for Science and Technology Development (NAFOSTED), code: 107.03-2010.04 (PTN and LXH), and partly by the Coastal Inlets Research Program of the U.S. Army Engineer Research and Development Center (ML and HH). Dr. Hajime Mase at Kyoto University kindly provided the source code for the EBED model. Dr. Ping Wang at Univeristy of South Florida and Mr. Mark Gravens at Coastal and Hydraulics Laboratory provided the experimental data from LSTF, which is greatly appreciated. The authors would also like to thank Dr. Nguyen Manh Hung and the late Prof. Pham Van Ninh for their great contributions to the Project VS/RDE/03. Permission was granted by Headquarters, U.S. Army Corps of Engineers, to publish this information.

References

Brøker, I., Zyserman, J., Madsen, E. Ø., Mangor, K., Jensen, J., 2007. Morphological modelling: a tool for optimisation of coastal structures. Journal of Coastal Research 23(5), 1148-1158.

Callaghan, D.P., Saint-Cast, F., Nielsen, P., Baldock, T.E., 2006. Numerical solutions of the sediment conservation law; a review and improved formulation for coastal morphological modelling. Coastal Engineering 53, 557-571.

Camenen, B., Larson, M., 2005. A general formula for non-cohesive bed load sediment transport. Estuarine, Coastal and Shelf Science 63, 249-260.

Camenen, B., Larson, M., 2007. A unified sediment transport formulation for coastal inlet application. Technical report ERDC/CHL CR-07-1, US Army Engineer Research and Development Center, Vicksburg, MS.

Dally, W. R., Brown, C. A., 1995. A modeling investigation of the breaking wave roller with application to cross-shore currents. J. Geophys. Res., 100(C12), 24873 – 24883.

Dally, W. R., Dean, R. G., Dalrymple, R. A., 1985. Wave height variation across beaches of arbitrary profile. J. Geophys. Res., 90(C6), 11917 – 11927.

De Vriend, H.J., Zyserman, J., Nicholson, J., Roelving, J.A., Péchon, P., Southgate, H.N., 1993. Medium-term 2DH coastal area modeling. Coastal Engineering 21, 193-224.

Denot, T., Aelbrecht, D., 1999. Numerical modelling of seabed evolution in the vicinity of a groin system. Proc. Coastal Structures'99, A.A. Balkema, Vol. 2, pp. 849-855.

Ding, Y., Wang, S.S.Y., Jia, Y., 2006. Development and validation of a quasi-three-dimensional coastal area morphological model. Journal of Waterway, Port, Coastal and Ocean Engineering 132(6), 462-476.

Ding, Y., Wang, S.S.Y., 2008. Development and application of coastal and estuarine morphological process modeling system. Journal of Coastal Research, Special Issue 52, 127-140.

Elder, J. W., 1959. The dispersion of marked fluid in turbulence shear flow. Journal of Fluid Mechanics 5, 544-560.

Falconer, R. A., 1980. Modelling of planform influence on circulation in Harbors. Proc., 17th Int. Conf. on Coastal Engineering, ASCE, Sydney, 2726 – 2744.

Goda, Y., 2006. Examination of the influence of several factors on longshore current computation with random waves. Coastal Engineering, 53, 157-170.

Gelfenbaum, G., Roelvink, J.A., Meijs, M., Buijsman, M., Ruggiero, P., 2003. Process-based morphological modeling of Gray Harbor inlet at decadal timescales. Proceedings of Coastal Sediments'03.

Gravens, M.B., Wang, P., 2009. Personal communication.

Gravens, M.B., Wang, P., 2007. Data report: Laboratory testing of longshore sand transport by waves and currents; morphology change behind headland structures. Technical Report, ERDC/CHL TR-07-8, Coastal and Hydraulics Laboratory, US Army Engineer Research and Development Center, Vicksburg, MS.

Gravens, M.B., Wang, P., Kraus, N.C., Hanson, H., 2006. Physical model investigation of morphology development at headland structures. Proceedings 30th International Conference on Coastal Engineering, World Scientific Press, pp. 3617–3629.

Hamilton, D.G., Ebersole, B.A., 2001. Establishing uniform longshore currents in large-scale sediment transport facility. Coastal Engineering 42 (3), 199-218.

Hanson, H., Larson, M. 1992. Overview of beach change numerical modeling. In: W. James and J. Niemczynowicz, Eds., Water, Development, and Environment, Lewis Publishers, Ann Arbor, pp 322-347.

Johnson, H.K., 2004. Coastal area morphological modelling in the vicinity of groins. Proc., 29th International Conf. on Coastal Engineering, ASCE, pp. 2646-2658.

Jonhson, H.K., Zyserman, J.A., 2002. Controlling spatial oscillations in bed level update schemes. Coastal Engineering 46, 109-126.

Johnson, H.K., Zyserman, J.A., Brøker, I., Mocke, G., Smit, F., Finch, D., 2005. Validation of a coastal area morphological model along the Dubai coast. Proceedings of Arabian Coast 2005, Dubai.

Kraus, N. C., Larson, M., 1991. NMLONG: Numerical model for simulating the longshore current; Report 1: Model development and tests. Technical Report DRP-91-1, U.S. Army Engineer Waterways Experiment Station, Vicksburg, MS.

Larson, M., Kraus, N.C., 2002. NMLONG: Numerical model for simulating longshore current; Report 2: Wave-current interaction, roller modeling, and validation of model enhancements. Technical Report ERDC/CHL TR-02-22, US Army Engineer Research and Development Center, Vicksburg, MS.

Larson, M., Wamsley, T.V., 2007. A formula for longshore sediment transport in the swash. Proc. Coastal Sediment'07, ASCE, pp. 1924-1937

Leont'yev, I.O., 1999. Modelling of morphological changes due to coastal structures. Coastal Engineering 38, 143-166.

Lesser, G.R., Roelvink, J.A, van Kester, J.A.T.M., Stelling, G.S., 2004. Development and validation of a three-dimensional morphological model. Coastal Engineering 51, 883-915.

Long, W., Kirby, J.T., Shao, Z., 2008. A numerical scheme for morphological bed level calculations. Coastal Engineering 55, 167-180.

Mase, H., 2001. Multi-directional random wave transformation model based on energy balance equation. Coastal Engineering Journal 43(4), 317-337.

Militello, A., Reed, C.W., Zundel, A.K., Kraus, N.C., 2004. Two-dimensional depth-averaged circulation model M2D: version 2.0, Report 1, Technical document and User's Guide. Technical Report ERDC/CHL TR-04-2, Coastal and Hydraulics Laboratory, US Army Engineer Research and Development Center, Vicksburg, MS.

Nam, P.T., Larson, M., Hanson, H., Hoan, L.X., 2009. A numerical model of nearshore waves, currents, and sediment transport. Coastal Engineering 56, 1084-1096.

Nam, P.T., Larson, M., 2009. A model of wave and current fields around coastal structures. Proc. Coastal Dynamics 2009, World Scientific Press, ISBN-13-978-981-4282-46-8 (with CD-ROM)

Nam, P.T., Larson, M., 2010. Model of nearshore waves and wave-induced currents around a detached breakwater. Journal of Waterway, Port, Coastal and Ocean Engineering 136 (3), 156-176.

Nicholson, J., Broker, I., Roelvink, J.A., Price, D., Tanguy, J.M., Moreno, L., 1997. Intercomparison of coastal area morphodynamic models. Coastal Engineering 31, 97-123.

Nishimura, H., 1988. Computation of neasrshore current. In: Horikawa, K. (Ed), Nearshore dynamics and coastal processes. University of Tokyo Press, Tokyo, Japan, pp. 271-291.

Reid, R.O., Bodine, B.R., 1968. Numerical model for storm surges in Galveston Bay. Journal of Waterways and Harbors Division 94 (WWI), 33-57.

Roelvink, J.A., Uittenbogaard, R.E., Liek, G.J., 1999. Morphological modelling of the impact of coastal structures. Proc. Coastal Structures'99, A.A. Balkema, Vol. 2, pp.865-871.

Saied, U.M., Tsanis, I.K., 2005. ICEM: Integrated Coastal Engineering Model. Journal of Coastal Research 21(6), 1275-1268.

Steijn, R., Roelvink, D., Rakhorst, D., Ribberink, J., Overeem, J.V., 1998. North-Coast of Texel: A comparison between reality and prediction. Proceedings 26th International Conference on Coastal Engineering, ASCE, pp. 2281-2293.

Wang, P., Ebersole, B.A., Smith, E.R., Johnson, B.D., 2002. Temporal and spatial variations of surf-zone currents and suspended sediment concentration. Coastal Engineering 46, 175-211.

Watanabe, A., Maruyama, K., Shimizu, T., Sakakiyama, T, 1986. Numerical prediction model of three-dimensional beach deformation around a structure. Coastal Engineering Journal 29, pp. 179-194.

Zanuttigh, B., 2007. Numerical modelling of the morphological response induced by low-crested structures in Lido di Dante, Italy. Coastal Engineering 54, 31-47.

Zyserman, J.A., Johnson, H.K., 2002. Modelling morphological processes in the vicinity of shore-parallel breakwaters. Coastal Engineering 45, 261-284.

Zyserman, J.A., Johnson, H.K., Zanuttigh, B., Martinelli, L., 2005. Analysis of far-field erosion induced by low-crested rubble-mound structures. Coastal Engineering 52, 977-994.

Paper V

Modeling shoreline evolution at Hai Hau Beach, Vietnam

Hoan, L.X., Hanson, H., Larson, M., Donnelly, C., Nam, P.T., 2010.

In: *Journal of Coastal Research*, Vol. 26, No. 1, 31-43.

Journal of Coastal Research	26	1	31–43	West Palm Beach, Florida	January 2010

Modeling Shoreline Evolution at Hai Hau Beach, Vietnam

Le Xuan Hoan[†‡], Hans Hanson[†], Magnus Larson[†], Chantal Donnelly[†], and Pham Thanh Nam[†‡]

[†]Lund University
Department of Water Resources Engineering
Box 118, SE-221 00 Lund
Sweden
Hoan.Le_Xuan@tvrl.lth.se

[‡]Vietnamese Academy of Science and Technology
Institute of Mechanics
264 Doi Can, Hanoi
Vietnam

ABSTRACT

HOAN, L.X.; HANSON, H.; LARSON, M.; DONNELLY, C., and NAM, P.T., 2010. Modeling shoreline evolution at Hai Hau Beach, Vietnam. *Journal of Coastal Research,* 26(1), 31–43. West Palm Beach (Florida), ISSN 0749-0208.

The coastline of Hai Hau District, located on the northeast coast of Vietnam with about 30 km of shoreline, is chronically eroding. Previous studies have tried to highlight the main causes of the erosion along this coastline, and several hypotheses exist. To examine the hypothesis that gradients in the longshore sediment transport rate and cross-shore fine sediment lost offshore are the main causes generating the serius erosion at Hai Hau Beach, a newly developed numerical model of shoreline change based on the one-line theory was applied and compared with data. Sea dike segments, reinforced by stones and mortar, were modeled using a seawall boundary condition, and the sediment continuity equation was modified to take into account the offshore transport of fine-grained sediment. The simulated shorelines agreed well with the measured shorelines, both for the calibration and validation periods. The calculated sediment budget shows that the net sediment transport is in the southward direction and that a large amount of fine-grained sediment is lost into deep water. These two sinks of sediment are believed to be the main causes of the serious erosion at Hai Hau Beach.

ADDITIONAL INDEX WORDS: *Hai Hau Beach, Ba Lat Mouth, shoreline evolution, sediment transport, fine sediment, shoreline modeling.*

INTRODUCTION

The Red River system laden with alluvia forms a flat fertile plain and 165 km of coastline, mainly belonging to the coastal Nam Dinh and Thai Binh Provinces in the northeast coast of Vietnam. The annual amount of sediment transported by the Red River system is about 100×10^6 tn (Ninh, Quynh, and Viet Lien, 2001; Pruszak *et al.,* 2002; Van Maren and Hoekstra, 2004), discharging into the Gulf of Tonkin through seven active mouths (from north to south): Van Uc, Thai Binh, Diem Dien, Tra Ly, Ba Lat, Lach Giang, and Day (Figure 1). These major river mouths represent very rapid accretion zones where the shoreline is expanding at a rate of about 15–100 m/y (Do *et al.,* 2007; Van Maren and Hoekstra, 2004).

The main portion of the coastline of Nam Dinh and Thai Binh Provinces, particularly at the seven active river mouths, is stable or accreting, while the coastline segment of Hai Hau District, the area of interest between Ha Lan and Lach Giang estuaries, is seriously eroding. According to several recent studies, the erosion rate averaged along the coastline is about 5–10 m/y (Donnelly *et al.,* 2004; Wijdeven, 2002), with a maximum rate reaching 19–35 m/y (Pruszak *et al.,* 2002).

Several studies have postulated hypotheses for the cause of the erosion at Hai Hau Beach. Saito (2001), Thanh *et al.* (2005), and Quynh Le *et al.* (2007) analyzed measured data of suspended sediment carried by the Red River system and showed that the total suspended load has significantly decreased (about 20–40%) after the construction of the Hoa Binh dam (built in 1983) and the Thac Ba dam (built in 1968) in the upstream part of the river. This implies that the total sediment supply to Hai Hau Beach has significantly diminished, which is suggested to be one of the main causes of the serious erosion there. Pruszak (1998) suggested that the construction of the Hoa Binh dam and/or the cutting off of the Ha Lan River (Figure 1) in 1955 caused a deficit in the sediment supply to the Hai Hau coast, resulting in serious erosion. Other proposed causes include deforestation (Pruszak, 1998), the reduction in sediment from river training, and sea level rise (Huan, 1996). However, satellite images and measured data on shoreline change show that the erosion at Hai Hau Beach started in the beginning of the 20th century, and it seems to have slowed down after 1966, well before these interferences with the natural river system (that is, the cutting off of the Ha Lan River and the building of the Hoa Binh and Thac Ba dams) occurred. Thus, these interferences cannot be the main reasons for the persistent erosion problems (Vinh *et al.,* 1996).

Do *et al.* (2007) analyzed the grain-size trends and transport vectors of the Red River Delta and showed that the dominant transport directions are perpendicular to the depth contours to a depth of about 25 m, and alongshore in the southward direction in coastal waters shallower than 5 m. Because the headland of the Ba Lat Estuary protrudes well from the mainland and the shoreline of Hai Hau runs in the NE-SW

DOI: 10.2112/08-1061.1 received 17 April 2008; accepted in revision 28 July 2008.

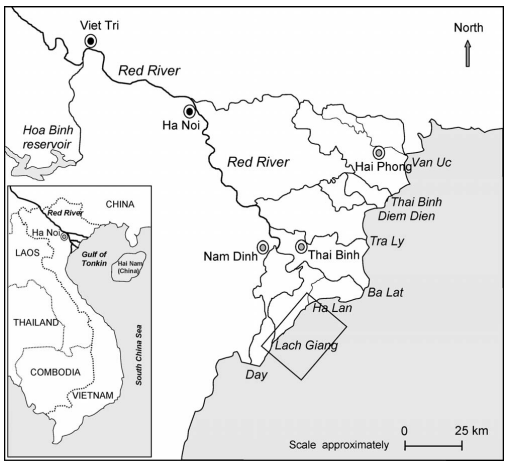

Figure 1. Study site and the distributaries of the Red River system.

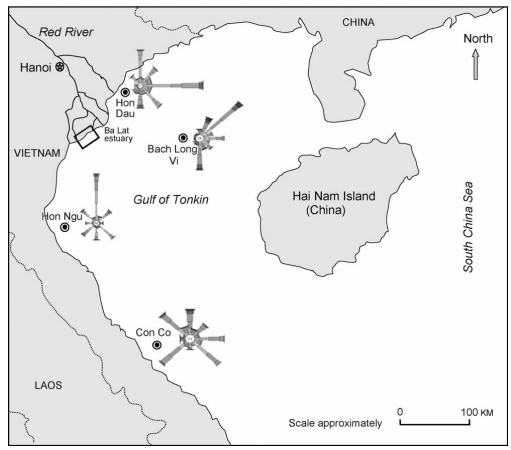

Figure 2. Wind roses at the stations around Hai Hau Beach, based on time series of 20 years (from 1976 to 1996) with four records a day and converted to 10 m above mean sea level.

direction (Figure 1), southward sediment transport from the Ba Lat falls into the deep water off Hai Hau Beach. Thus, this erosional beach is not supplied with sediment from the Ba Lat Mouth. Donnelly *et al.* (2004), Häglund and Svensson (2002), and Wijdeven (2002) suggested that coastal erosion at Hai Hau Beach is caused by net longshore sediment transport (LST) rates or, more specifically, gradients in the LST, and fine-grained-size sediment from the beach lost into deep water. This is believed to be the most likely cause for the retreat of Hai Hau Beach. However, none of the previous studies have been able to conclusively prove this.

The main objectives of the present study were to establish the cause of the erosion at Hai Hau Beach and to estimate the recession rate. A new numerical model based on the one-line theory of shoreline change was used to quantify the gradients in LST, to determine the cause of these gradients, and to model the shoreline response. In the future, the calibrated and validated model may assist in determining remediation measures to stabilize the shoreline. Measured shoreline positions in 1910, 1965, and 2000 were used to calibrate and validate the model.

ENVIRONMENTAL CONDITIONS AT THE SITE

Winds

The wind climate in the northern part of Vietnam is clearly distinguished by two main monsoons, the winter monsoon and the summer monsoon. The winter monsoon (November to March) is characterized by strong winds blowing from the north, lower temperature, and lower precipitation. The summer monsoon (May to September) is characterized by moderate winds blowing from the south, higher temperature, and higher precipitation. In addition, there is a transition period between the two main monsoons (April and October), characterized by light eastern trade winds with cool weather.

The wind roses at four stations around Hai Hau Beach (Figure 2) show that the wind field within the Gulf of Tonkin is markedly affected by the topography. Since the Bach Long Vi (BLV) station is located in the middle of the Gulf of Tonkin (on Bach Long Vi Island), away from the mainland, wind data recorded at this station are expected to be most representative for calculating offshore waves at Hai Hau Beach (Pruszak *et al.,* 2002; Wijdeven, 2002).

Nearshore Topography

The nearshore region of Hai Hau Beach has a very gentle slope, creating a relatively wide zone for wave transformation and energy dissipation (Pruszak *et al.,* 2002). A bathymetry map of the site extracted from a Vietnamese navy map with bathymetry corrections from 1980 shows that the depth contours at Hai Hau Beach are more or less parallel with the shoreline and that the offshore slope is rather constant (Figure 3). However, seaward of the Ba Lat Mouth, the slope is steeper and a more complex topography occurs, creating losses of alluvial sediment to offshore locations (Wijdeven, 2002). The mean beach slopes, based on cross-shore profiles measured in 2001, determined from the offshore distance to a depth of 7–8 m, are about 1.0–1.6%. Near the Ba Lat Mouth, the sea floor has a slope of 4.0% (Wijdeven, 2002). The results of a least-square fit with the equilibrium beach profile (EBP) shape introduced by Dean (1977) against four measured cross-shore profiles (profile numbers MC12, MC13, MC21, and MC22; see Figure 3) produced values of the scale parameter (A) in the range 0.063–0.081 $m^{1/3}$. This corresponds to a median grain size (D_{50}) of about 0.14–0.18 mm (see Figure 4 and Table 1).

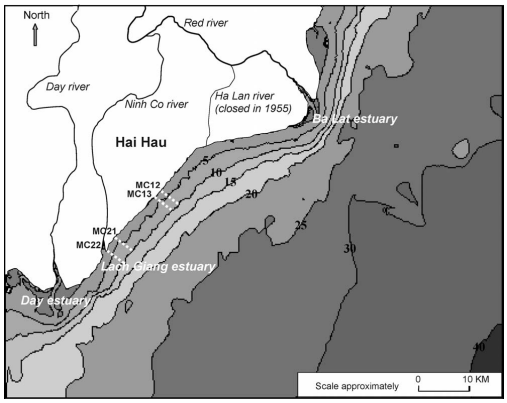

Figure 3. Bathymetry map of the site and locations of the measured cross-shore profiles.

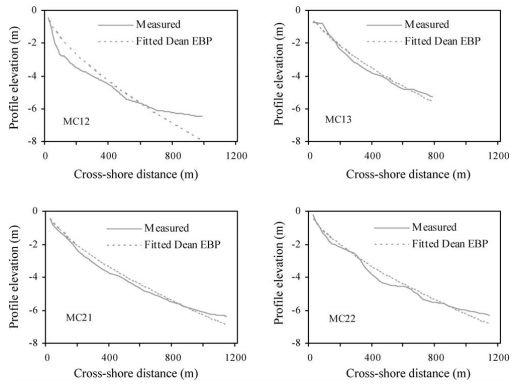

Figure 4. Comparison of measured profiles and fitted EBP at four cross-shore sections.

Wave Climate

Because of the prevailing wind climate, the deepwater wave regime in the Gulf of Tonkin has clear seasonal features. Based on the data from visual buoy observations at Hon Dau station, Pruszak *et al.* (2002) and Vinh *et al.* (1996) showed that in the winter the prevailing waves arrive from the northeast, whereas in the summer the waves come from the east and southeast (in deep water). Wind velocities during the winter monsoon are stronger than during the summer monsoon, generating higher waves in deep water relative to the summer monsoon. The estimated average wave height in deep water is in the range of 1.8–2.0 m for winter and 1.2–1.4 m for summer. However, the most pronounced seasonal difference is probably the frequency of occurrence of significant wave height, H_s: an H_s of 3 m is exceeded 10% of the time in the winter, whereas an H_s of 2 m is exceeded 10% of the time in the summer (Van Maren, 2004).

In the northern part of Vietnam, storms and typhoons mainly occur in July and August (during the summer period). On average two storm or typhoon events per year hit the coastline in the northern provinces of Vietnam. During storms or typhoons the deep water wave height can reach up to 8–10 m and the storm surge up to 2 m (Ninh, Quynh, and Viet Lien, 2001; Pruszak *et al.,* 2002; Sundstrom and Soderval, 2004; Vinh *et al.,* 1996).

For Vietnam in general and Hai Hau Beach in particular, long time series of wave measurements are not available. Within the framework of a program funded by the Swedish International Development Cooperation Agency (SIDA), four field campaigns were carried out at anchored stations off Hai Hau Beach in 2005 and 2006 (Hung *et al.,* 2006; Sjödahl and Kalantari, 2005). However, this field work was performed in moderate weather conditions and for short-term periods (around 10 d). The frequency of occurrence of significant wave heights, based on the measured data at the anchored station at a 20-m depth (Station S1; see Figure 5), show that in winter, measured wave heights were higher than in summer (Figure 6). In the winter, H_s exceeds 1.0 m during 10% of the measurement time, whereas in the summer H_s exceeds 0.6 m during 10% of measurement time.

Because the Gulf of Tonkin connects to the South China Sea through a large opening in the southeast direction (Figure 2), swell waves will occur in the Gulf of Tonkin when strong wave conditions exist in the South China Sea; for example, during strong monsoons, tropical storms, or typhoons. Recently, simultaneous measurements of wave and wind parameters at anchored stations around Hai Hau Beach indicate that swell wave height higher than 1.0 m occurred, even when wind conditions were calm (Hung *et al.,* 2006). Thus, tropical storms and typhoons occurring in the southern part of the South China Sea may damage the Hai Hau coast through the swell waves they generate.

Tides

Field observations show that astronomical tides are of a regular diurnal type. Tidal waves enter from the South China Sea and are partly reflected in the northern enclosure of the Gulf of Tonkin. With a length of approximately 500 km and a depth of 50 m, the resonance time of the basin is about 25 hours (Van Maren and Hoekstra, 2004), which is close to the period of the diurnal tides. Therefore, the diurnal components

Table 1. *Results of least-square fit to the measured profiles, with EBP shape introduced by Dean (1977).*

Profile Number	A ($m^{1/3}$)	D_{50} (mm)	E_{rms}[1]
MC12	0.081	0.18	0.72
MC13	0.063	0.14	0.23
MC21	0.063	0.14	0.25
MC22	0.064	0.14	0.33

[1] Root-mean-square deviation.

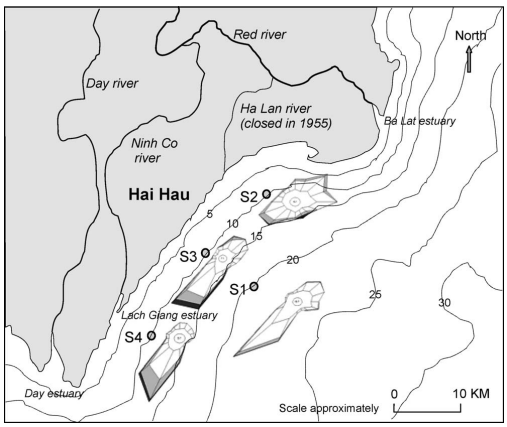

Figure 5. Current prisms based on short-term series of measured data in 2005 and 2006 at four anchored stations.

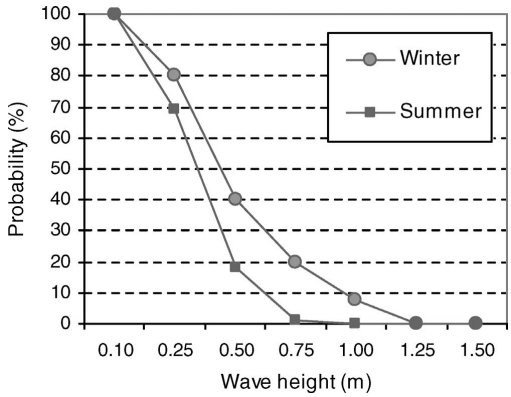

Figure 6. Frequency of occurrence of significant wave height, based on the short-term series of measured data in 2005 and 2006 at a depth of 20 m off Hai Hau Beach.

O1 and K1 are near resonance mode, and the amplitude of these components increases northward along the Vietnamese coastline (Guohong *et al.,* 1999). Tidal range in the study area varies from 0.5 m during neap tide to 3.2 m during spring tide.

Current Regime

The major current components in the nearshore zone include wave-induced currents, tidal currents, wind-driven currents, and river outflow (near the river mouths). These current components interact with the dynamic morphology and generate complicated nearshore current circulation patterns (Pruszak *et al.,* 2002).

Since the shoreline of Hai Hau Beach runs in the NE-SW direction, dominant wave directions in both winter and summer are largely oblique to the shoreline, resulting in strong wave-generated currents alongshore. At Hai Hau Beach, wave-induced currents are expected to be the dominant currents for generating sediment transport and morphological change.

The tidal currents play a primary role in the formation of tidal flats and tidal channels in the coastal low-lying wetland area. In the Gulf of Tonkin, tidal waves propagate from south to north, resulting in tidal currents that are northward during flood tide and southward during ebb tide. The average tidal flow in the nearshore zone, at a depth of about 5 m, has a velocity of 25–40 cm/s. The maximum tidal velocity may reach 60–80 cm/s (Pruszak *et al.,* 2002). Due to the asymmetry of tidal currents in the nearshore regions, the period of flood tide is shorter than that of ebb tide, 42% and 58% of the time, respectively, resulting in south-directed net tidal currents in the coastal zone (Van Maren and Hoekstra, 2004).

It is noteworthy that, based on measured data and numerical models, Ninh, Quynh, and Viet Lien (2001) and Van Maren and Hoekstra (2004) showed that the wind-driven current circulation is rotating counterclockwise, and its center is located in the middle of the Gulf of Tonkin during both the winter and summer monsoons. Therefore, in the nearshore zone of Hai Hau Beach, the residual current is consistently in the southward direction. However, as mentioned above, wind velocity during winter is stronger than that during summer, and the consistent wind current in winter is stronger than that in summer (Van Maren, 2004).

Long-term current measurements do not exist in Vietnam in general; field campaigns have mainly lasted from 2 to 7 days. Within the SIDA program, as mentioned above, four anchored stations of current measurements were set up off Hai Hau Beach (Figure 5). The field campaigns were carried out in 2005 and 2006, in January (typical winter month) and August (typical summer month), each campaign lasting about 10 days. The current prisms based on the integrated measurement data show that the residual currents are clearly in the southward direction in both winter and summer, except at station number 2 (S2) located at the northernmost point. Average current velocities occurring during the field campaign periods were about 30 cm/s, and maximum values were about 50–80 cm/s.

Riverine Budgets

The Red River brings a huge amount of sediment that is discharged into the Gulf of Tonkin through the seven active river mouths. The annual sediment load discharged to the sea has a clear seasonal variation. Rainfall in summer is much higher (about 80% of total annual rainfall) than in winter, resulting in most of the sediment load being discharged in summer (around 91–96% of the total of annual sediment load; see Van Maren and Hoekstra, 2004). The total sediment load discharged to the sea by the Red River is estimated in the range of 75–100 million tn per year. About 30% of the

total sediment load remains in the nearshore zone and develops sandy ridges and tidal flats (depths below 2 m); the remaining material passes the intertidal plain and goes offshore to deep water areas (depths of 2 m to 30 m; Do *et al.,* 2007; Pruszak *et al.,* 2002). Percent relative river discharge load per distributary of the Red River system are (from north to south in Figure 1): Van Uc, 19%; Thai Binh, 6%; Tra Ly, 9%; Ba Lat, 21%; Lach Giang, 6%; Day, 19%; and 20% for all smaller distributaries (Van Maren and Hoekstra, 2004).

Sea Dikes

In order to secure the coastal areas and to protect the inhabitants during storms or typhoons, sea dike defense systems have been constructed. At Hai Hau District the system comprises two parallel dikes with a distance of about 200–250 m in between. Their purpose is to withstand attacks by heavy storms or typhoons. During a storm or typhoon attack, if the first dike facing the sea fails, resulting in some dike sections being breached and the land between the two dikes inundated, then the second dike diminishes effects of flooding on the inhabitants and agricultural land behind this dike. When breaching at the first dike takes place, the land in between the two dikes is considered lost, and a new dike will be built behind the former second dike.

Overall, sea dike defense systems in Vietnam, including in the Hai Hau District, are made purely of soil or soil core covered by a revetment layer of stones. These sea dikes, therefore, often fail during heavy attacks such as storms or typhoons. Since the first dike in the Hai Hau District directly faces heavy attacks from the sea, it has been upgraded with stones and mortar. In a 5-year (1995–2000) project funded by the French government to upgrade the sea dike system of Nam Dinh Province, some dike sections at Hai Hau District were reinforced. However, these dike sections can only survive moderate weather conditions and may still fail during heavy attacks. This dike system is not capable of stopping the erosion, but it seems to decrease the erosion rate. The erosion of the sea dike system at Hai Hau does not depend only on the structure of the revetment; scours developing at the dike toe is another issue. The dike toe is gradually undermined even during moderate weather conditions, resulting in a series of cavelike features penetrating into the dike body. Thus, scours create favorable conditions for breaching and subsequent sea dike collapse when heavy attacks occur.

MODELING OF SHORELINE CHANGE

Offshore Wave Climate Estimation

In general, the main challenge in modeling of a coastal process is to estimate accurately the offshore wave climate. Long-term time series of offshore wave data are not available in Vietnam or at Hai Hau Beach. Therefore, offshore waves were hindcasted from wind data recorded at the wind stations around the study area. As mentioned previously, wind data at BLV station (see Figure 2) were preferred to estimate offshore waves (Pruszak *et al.,* 2002; Wijdeven, 2002). However, by comparing measured wave data with predictions from winds at Con Co (CC) station, Häglund and Svensson (2002) realized that the wind at CC station may significantly control the wave climate at Hai Hau Beach under certain circumstances. In order to derive a more representative wind climate for the waves, they suggested the approach of combining wind data at BLV and CC. In the present study, a long-term time series of waves (20 y from 1976 to 1996) was estimated by combining wind data at BLV and CC. The procedure for combining wind data postulated by Häglund and Svensson (2002) was applied. Wind data at BLV are mainly used to estimate the offshore waves, except when the wind comes from the angle band between SE and SW. In those cases, the offshore waves at Hai Hau Beach are approaching from the south, and thus they are partly controlled by the wind climate at CC station (see Figure 2). Therefore, within this angle band, wind data at CC was included in estimating the offshore waves by using the wind direction at CC and a weighted average value of the measured wind speeds at BLV and CC.

A commonly applied wave hindcasting method was used to calculate the offshore wave parameters. The Sverdrup-Munk-Bretschneider (SMB) method described in USACE (1984) was verified by comparing the wave climate hindcast with visually observed wave records at BLV station during 1 year, 1984 (Donnelly *et al.,* 2004; Häglund and Svensson, 2002). Thus, in this study the waves were calculated using the SMB method and used as input data to a nearshore wave transformation model.

In order to estimate the waves generated during extreme storms or typhoons, in the absence of measurements, a numerical model for storm- and typhoon-generated waves is most reliable. Here, for simplicity, the parametric wave model developed by Young in 1987, described in USACE (2002), based on results from simulations with a numerical spectral model, was used to estimate waves generated by extreme storms or typhoons.

Nearshore Wave Transformation

Some earlier studies (Häglund and Svensson, 2002; Pruszak *et al.,* 2002; Wijdeven, 2002) used one-dimensional wave transformation models to estimate the nearshore wave characteristics. However, the bathymetry offshore of Hai Hau Beach is complex, and in this case, a one-dimensional transformation is insufficient to account for the changes in wave angle that can have a significant effect on the sediment transport direction (Donnelly *et al.,* 2004). Donnelly *et al.* (2004), Hung, Hanson, and Dien (2006), and Sjödahl and Kalantari (2005) used the 2-D STeady State spectral WAVE (STWAVE) transformation model to calculate the inshore wave climate. STWAVE is a steady-state finite-difference model based on the wave-action balance equation (Smith, Sherlock, and Resio, 2001). Advantages of using STWAVE include the ability to model wave transformation over complicated bathymetry quickly and efficiently for many different wave spectra.

In the present study, another 2-D Energy Balance Equation with a Diffraction term (EBED) transformation model was applied to calculate the inshore wave climate. The EBED model was developed by Mase (2001) based on the energy-balance equation for multidirectional random waves, taking

into account wave shoaling, refraction, diffraction, and wave breaking. Advantages of using the EBED model include the ability to reproduce wave transformation over complicated bathymetry and the facilities for setting up the input and output for many different wave spectra. The 20-year-long hindcast time series of offshore waves was used as input data for the EBED model in order to reproduce the nearshore wave climate at Hai Hau Beach.

The shoreline of Hai Hau Beach runs in the NE-SW direction, whereas the shoreline around the Ba Lat Mouth primarily runs in the N-S direction (Figure 1). Thus offshore waves coming from N and NNE occur in deep water when wind blows from these directions, and a part of this wave energy is transported to the nearshore region of Hai Hau Beach via diffractive and refractive effects of the headland of the Ba Lat Estuary. Data from recent wave observations at Hai Hau Beach also indicate that inshore waves exist in the nearshore zone, while offshore waves as well as winds at BLV station are coming from the N or NNE direction. Offshore wave energy coming from both N and NNE constitutes a considerable amount, about 31%, of the total offshore wave energy. Therefore, it is necessary to take the waves coming from these directions into account. In principle, wave transformation models can reproduce waves with incoming angles of $-90°$ to $+90°$, referring to the offshore axis of the orthogonal coordinate system used. This implies that if the orthogonal coordinate system of the studied domain is rotated so that the x-axis is parallel with the shoreline (NE-SW direction), only incoming waves from NE to SW will be reproduced. Because a basic assumption is that waves are entering through the offshore boundary, it was decided that the wave grid should only be used for waves with incoming angles of $-45°$ to $+45°$. Thus, in order to represent all wave directions from N to SW, it was necessary to establish three orthogonal coordinate systems (Figure 7). On each coordinate system, incoming wave angles from $-45°$ to $+45°$ referring to the vertical axis (offshore-pointing y-axis) were simulated. The first system is rotated so that the y-axis is parallel to the NE direction (called System-NE), the second one is rotated so that the y-axis is parallel to the SE direction (called System-SE), and the third one is rotated so that the y-axis is parallel to the SW direction (called System-SW). Thus, the incoming wave angles from N to ENE, encompassing 75.7% of total offshore wave energy, are simulated on System-NE; the incoming wave angles from E to SSE, encompassing 13.8% of total offshore wave energy, are simulated on System-SE; and the incoming wave angles from S to SW, encompassing 8.1% of total offshore wave energy, are simulated on System-SW. Through this procedure, most of the offshore wave energy, up to 98%, was taken into account. The wave model domain was expanded in the northward direction over the Ba Lat Mouth (Figure 1) to examine the effects of the Ba Lat Estuary headland on the wave climate in the nearshore zone of Hai Hau Beach.

It is useful to investigate the difference in the simulated results of wave propagation between the respective coordinate systems. Two cases were examined, corresponding to the two borders between the coordinate systems (Figure 7). The first border, between System-NE and System-SE, is direction

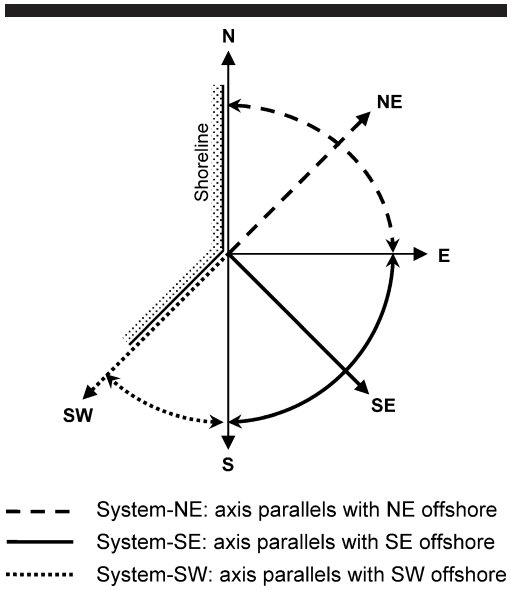

Figure 7. Sketch illustrating the rotation of the calculated coordinate system to simulate waves coming from N to SW.

E. The incoming wave angles from this direction correspond to $-45°$ in System-NE, whereas they correspond to $+45°$ in System-SE. The second border, between System-SE and System-SW, is direction S. The incoming wave angles from this direction correspond to $-45°$ and $+45°$ in System-SE and System-SW, respectively. Because only the nearshore wave climate is used as input data for the shoreline change model, wave parameters along the 7-m depth contour, outside the breaker line, were taken into consideration. Input offshore wave parameters for the wave propagation model used to test at the first border were as follows: significant wave height H_s = 2.3 m, and significant wave period T_p = 6.0 s. The average absolute differences along the 7-m depth contour with respect to wave height and wave angle are 0.06 m and 1.5°, respectively (Figures 8a and 8b). Consequently, the average relative difference in LST is 2.3% (Figure 8c). At the second border, input offshore wave parameters for the wave propagation model were H_s = 1.3 m and T_p = 5.0 s. The average absolute differences along the 7-m depth contour with respect to wave height and wave angle are 0.02 m and 1.9°, respectively (Figures 9a and 9b). Consequently, the average relative difference in LST is 2.6% (Figure 9c). These tests show that differences in simulated results for the wave climate in the nearshore zone between the different coordinate systems are not significant for the present application.

Shoreline Data

Shoreline data were obtained from maps and satellite images. Several difficulties were encountered when digitizing

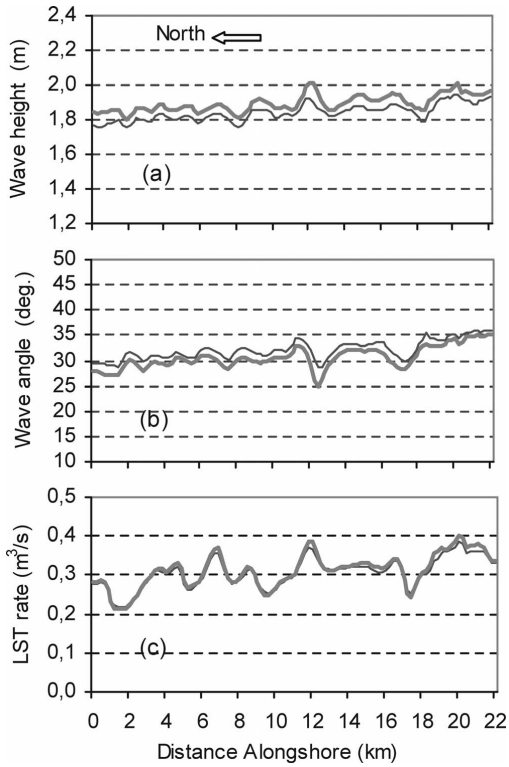

Figure 8. Comparison of simulated results of wave transformation and LST in the System-NE system (thin line) and the System-SE system (thick line) along the 7-m depth contour. (a) Wave height, (b) wave angle, (c) average relative difference in LST.

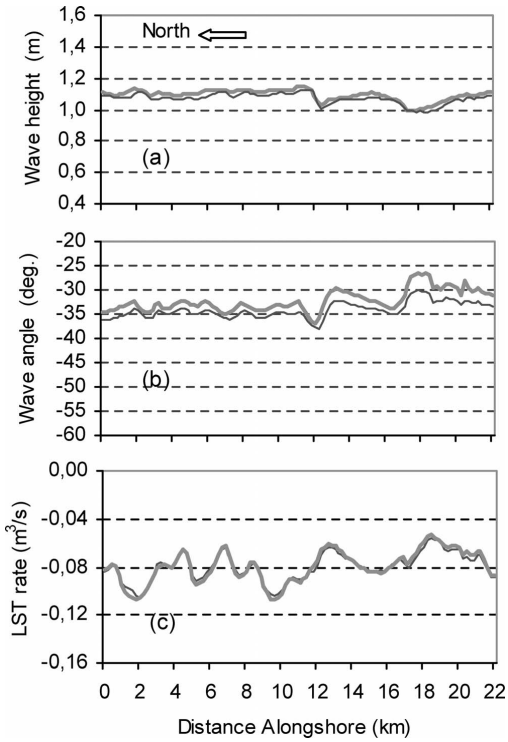

Figure 9. Comparison of simulated results of wave transformation and LST in the System-SW system (thin line) and the System-SE system (thick line) along the 7-m depth contour. (a) Wave height, (b) wave angle, (c) average relative difference in LST.

the map and satellite image data sets. Owing to the age of the maps and the different mapping authorities, the available maps employed different mapping projections based on different geographical ellipsoids and ellipsoidal data, and the shoreline was given at varying tidal data. It was therefore not possible to find full sets of coordinate transformation parameters to match the maps. The tidal data used for shoreline mapping was also unclear on the older maps. Donnelly *et al.* (2004) further investigated and determined that the accuracy of the shoreline digitization was in a range of ±8.5 to ±18.0 m, depending on the scale of the map.

Comparisons of historical shorelines from the past century showed an estimated coastline retreat of up to 14 m/y in some areas, with an alongshore average of 7 m/y. These figures, however, have reduced to a maximum of 8 m/y and an alongshore average of only about 1 m/y between 1992 and 2000. This is probably because by 1992, dikes were built to extend the full length of the shoreline, and 75% of these were upgraded between 1995 and 2000. Table 2 compares the shoreline erosion rates calculated in various earlier studies. As can be seen, the erosion rates calculated by Pruszak *et al.* (2002) differ substantially from those calculated by Wijdeven (2002) and Donnelly *et al.* (2004). This is probably because the data used for the shoreline comparisons of Pruszak *et al.* (2002) were not referenced geographically, nor was the tidal datum consistent. The larger erosion rates observed by Wijdeven (2002) for the period 1955–1965 can be explained because the 1955 French map was plotted using a different tidal datum to the other maps. The results of Wijdeven (2002) for the periods 1912–1955 and 1965–1995 are similar to the new rates from Donnelly *et al.* (2004).

Digitizing the shoreline required some simplifications to arrive at a shoreline suitable for one-line modeling. There are several minor estuaries and some sand spits along the Hai Hau coast. These were smoothed over in order to create a continuous, well-defined shoreline that could be modeled with one-line theory (Hanson, 1989). The estuaries, which were more significant in the first half of the century, were anticipated not to have significant influence on the overall

Table 2. *Calculated shoreline recession rates.*

Pruszak *et al.* (2002)		Wijdeven (2002)		Donnelly *et al.* (2004)	
Period (y)	Erosion Rate (m/y)	Period (y)	Erosion Rate[1] (m/y)	Period (y)	Erosion Rate[2] (m/y)
1905–1927	34.7	1912–1955	5.5–9.5	1910–1992	7.0 (14.0)
1927–1966	18.7	1955–1965	20.0–24.0	1992–2000[3]	1.0 (8.0)
1966–1992	3.6	1965–1995	6.0–9.0	—	—

[1] Erosion rates indicated are lower and upper boundary rates.
[2] Erosion rate averaged along the shoreline. Figure in parentheses is the maximum.
[3] This figure may not reflect mapping accuracy, but it indicates that erosion rates have decreased.

shoreline development because of their limited size. In the second half of the century, these estuaries were sealed off from the ocean by dikes and sluices, and hence they had an even lesser effect on the shoreline development. The longshore dike line in the latter part of the century was quite complicated, and spits could be seen building up across the recessed sections of the dike. The digitized shoreline was drawn across the seaward edge of such spits, so that the beach was assumed solid behind that stretch of shoreline.

In this study, the best available maps were from 1910 (Service Geographique de l'Indochine, the French colonial mapping service), 1965 (USACE Army Map Service), and 2000 (various Vietnamese mapping authorities). The shoreline of Hai Hau Beach was modeled between the Ha Lan Estuary in the north and the Lach Giang Estuary in the south (Figure 1). The shoreline appears to have been fairly stable at these locations. The section modeled varied therefore between 18 and 22 km in length (different stable shoreline points were identified as lateral boundaries for the calibration and validation periods of the modeling).

Sediment Transport and Shoreline Change Modeling

Some earlier investigations used varying methods to quantify the longshore sediment transport and shoreline change in the study area. The Coastal Engineering Research Center (CERC) formula (USACE, 1984) was used by Häglund and Svensson (2002) to calculate the longshore gradients in sediment transport. A one-dimensional wave transformation model was used to reproduce the inshore wave data with differing shoreline orientations to calculate a value for the sediment transport rate. Thus, this approach does not take into account gradients in breaking wave height along the shoreline. The BIJKER formula (Bijker, 1971) was used by Pruszak *et al.* (2002) and Wijdeven (2002) to calculate discrete values for sediment transport at various sites along the modeled coastline. The shoreline change model, GENESIS (Hanson, 1989), was used by Donnelly *et al.* (2004) and Hung, Hanson, and Dien (2006) to calculate sediment transport rates and shoreline evolution. In this approach, sediment transport rates at each cell are calculated based on a modified version of the CERC formula to take into account the longshore gradients in breaking wave height.

In this study, the shoreline change modeling is based on the theory of one-line model of shoreline change. The algorithms for the numerical modeling were developed by Hanson (1987). The general equation of shoreline change was derived from conservation of sediment volume. The continuity equation with respect to a local coordinate system, where the y-axis points offshore and the x-axis is oriented parallel to the trend of the shoreline, is expressed as

$$\frac{\partial y}{\partial t} + \frac{1}{(D_B + D_C)}\left(\frac{\partial Q}{\partial x} + q\right) = 0 \tag{1}$$

where x = longshore coordinate (m); y = cross-shore shoreline position (m); t = time (s); D_B = average berm elevation (m); D_C = depth of closure (m); Q = longshore sand transport rate (m^3/s); and q = source or sink of sand (m^3/s/m).

The empirical predictive formula for LST is expressed as (Hanson, 1987)

$$Q = (H^2 C_g)_b \left[a_1 \sin(2\theta_{bs}) - a_2 \cos\,\theta_{bs} \frac{\partial H}{\partial x}\right]_b \tag{2}$$

where H = wave height (m); C_g = wave group celerity given by linear wave theory (m/s); b = subscript denoting the breaking wave condition; θ_{bs} = angle of breaking waves to the local shoreline; and

$$a_1 = \frac{K_1}{16(\rho_s/\rho - 1)(1 - p)(1.416)^{(5/2)}} \tag{3}$$

$$a_2 = \frac{K_2}{8(\rho_s/\rho - 1)(1 - p)\tan\beta(1.416)^{(5/2)}} \tag{4}$$

where K_1 and K_2 = empirical coefficients, treated as calibration parameters; ρ_s = density of sand (kg/m^3); ρ = density of water (kg/m^3); p = porosity of sand on the bed; and tan β = average bottom slope from the shoreline to the depth of active longshore transport.

The hypotheses for the causes of erosion at Hai Hau Beach were introduced above. Under wave influence, eroded material is picked up from the seabed and transported in two directions: the longshore direction and the cross-shore direction. The former is expected to contain coarser sediment that is transported alongshore. This component is represented by the term $\partial Q/\partial x$ in Equation (1). The latter contains a larger amount of fine-grained sediment that is transported offshore and deposited further out in the Gulf of Tonkin. Such cross-shore sediment losses may be expressed in the one-line modeling through the term q (Equation [1]). Because classical one-line models of shoreline change do not include more complex relationships for q, it was necessary to develop such a relationship. In this study, the cross-shore loss of fine sediment depends on the rate of erosion, directly proportional to the gradient of LST rate through an offshore loss parameter α, which specifies the ratio of fine material in the eroded

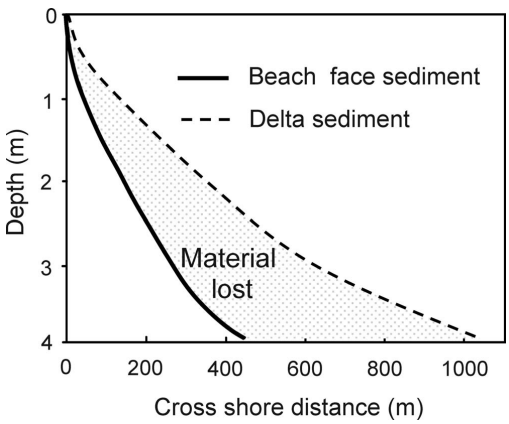

Figure 10. Comparison of equilibrium beach profiles behind the dikes and in the surf zone (Donnelly *et al.,* 2004).

sediment. The relationships employed are given by (Donnelly *et al.,* 2004)

$$q = \frac{\alpha}{1-\alpha}\frac{\partial Q}{\partial x}, \qquad \frac{\partial Q}{\partial x} > 0 \tag{5}$$

$$q = 0, \qquad \frac{\partial Q}{\partial x} \leq 0. \tag{6}$$

Equations (5) and (6) state that the loss of fine sediment only occurs during erosive conditions when the resident sediment is being mobilized. These equations were substituted into Equation (1) such that the sediment continuity equation is expressed in terms of α:

$$\frac{\partial y}{\partial t} + \frac{1}{(D_B + D_C)}\frac{1}{(1-\alpha)}\frac{\partial Q}{\partial x} = 0. \tag{7}$$

The value of the loss parameter was estimated by comparing equilibrium beach profiles for sediment samples taken behind the dikes and in the surf zone. Sediment behind the dikes consists of deltaic deposits laid down by the Red River distributaries. Sediment sampling shows the median grain size in this region, D_{50}, to be about 0.085 mm (Donnelly *et al.,* 2004). On the other hand, sediment in the surf zone, where finer sediments are put into suspension and carried offshore, is coarser, and samples gave D_{50} values of 0.15 to 0.20 mm (Donnelly *et al.,* 2004; Häglund and Svensson, 2002; compare with Table 1). If an equilibrium beach profile, as defined by Dean (1977), is constructed for each of these sediment samples (Figure 10), it may be assumed that α, the material loss, is the area difference in percent between the two profiles. This can then be expressed as (Donnelly *et al.,* 2004)

$$\alpha = 1 - \left(\frac{A_{delta}}{A_{surf}}\right)^{3/2} \tag{8}$$

where A_{delta} is the shape parameter in the equilibrium beach profile equation for deltaic sediments and A_{surf} is the shape parameter for the surf zone sediments. For the samples taken at Hai Hau Beach, α varied around 0.6–0.7. When calibrating the model, α was varied within this range.

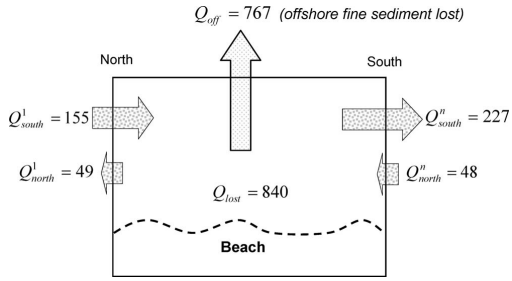

Figure 11. Sketch of calculated sediment budgets (values are multiplied by 10^3 m^3/y).

Sediment Budget Estimation

To obtain an overall view of the sediment entering and exiting the study area, a sediment budget was developed (see Figure 11). The sources and sinks in the sediment budget for the study area are defined as follows (particular values will be shown in the section "Modeled Sediment Budget"): At the north boundary (cell number 1), sediment enters through the southward longshore transport rate (Q^1_{south}) and exits through the northward transport (Q^1_{north}). Similarly, at the southern boundary (at cell number n), sediment enters through the northward transport (Q^n_{north}) and exits through the southward transport (Q^n_{south}). The fine sediment transported into deep water is denoted by Q_{off}.

Figure 12 illustrates how the offshore loss of sediment was computed. At each time step, the offshore loss is calculated as a function of the longshore transport gradient ($Q_{i+1} - Q_i$), as expressed by Equations (5) and (6). In Figure 12, erosion occurs in cells 1 and 2 because $Q_3 > Q_2 > Q_1$. Thus, these cells will experience offshore losses, q_1 and q_2. In cell 3 there is no erosion ($Q_4 < Q_3$) and, thus, no offshore losses. The total rate of offshore loss of fine sediment $q^{(t)}_{tot}$ at time step (t) was calculated as

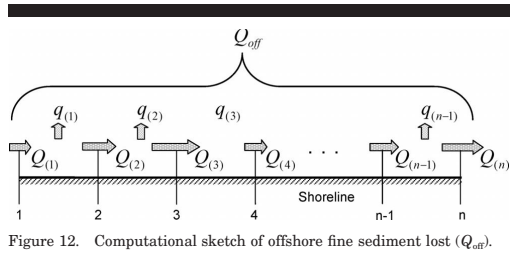

Figure 12. Computational sketch of offshore fine sediment lost (Q_{off}).

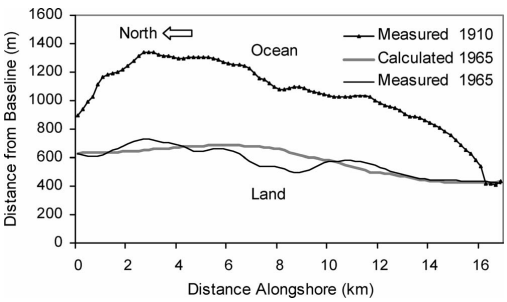

Figure 13. Measured and modeled shorelines from the period 1910 to 1965.

$$q_{\text{tot}}^{(t)} = \sum_{i=1}^{n-1} q_i. \tag{9}$$

The average loss of fine sediment over the simulation period was estimated from

$$Q_{\text{off}} = \frac{1}{T} \sum_{t=0}^{T} q_{\text{tot}}^{(t)} \Delta t \Delta x \tag{10}$$

where Δt is the time step and T is the total simulated time.

MODELING RESULTS

An implicit solution scheme was used to solve the coupled Equations (1) and (2) with space and time steps of 200 m and 1 hour, respectively. A stability parameter (R_s) of the calculation scheme is estimated on the basis of the Courant Criterion (Hanson and Kraus, 1989), where values of $R_s < 10$ are suggested. The model calculates values of R_s at each time step at each grid point alongshore and determines the maximum value. For both the calibration and validation period, the calculated maximum value of R_s is 4.8. In addition, depending on the interval of time series of input wave hindcast (DTW), the time step must be opted so that the model receives the input wave data at a specific time corresponding to DTW. To satisfy this requirement, the time step must be a proper fraction (*e.g.,* 1/2, 1/3) of DTW. Thus, with 6 hours of DTW and the maximum value of R_s mentioned above, the time step of 1 hour satisfies all critical conditions for the calculation scheme.

The model was calibrated and validated using the measured shorelines from 1910, 1965, and 2000 at Hai Hau Beach. Note that the Ha Lan Estuary, at the northern end of the beach (Figure 1), migrated during this period; hence a stable shoreline point at the northern end of Hai Hau Beach was not found. The northern boundary of the model was therefore simulated as a moving boundary. The average value of the shoreline movement at this boundary was estimated from the measured shoreline positions to be 4.4 m/y. This value is used for both the calibration and validation period.

To estimate how well the modeled shorelines agreed with the measured shorelines, two kinds of error were employed:

Table 3. *Summary of errors and erosion rates in calibration and validation.*

	Max Absolute Error (m)	% Average Relative Error	Max Erosion Rate (m/y)	Average Erosion Rate (m/y)
Calibration	133.7	9.0	12.1	8.7
Validation	123.4	9.1	12.7	6.8

maximum absolute error (in m) and average relative error (%). The maximum absolute error is defined as the maximum absolute difference between measured and modeled shorelines. The average relative error is estimated using the following formula:

$$\%\ \text{error} = \frac{\frac{1}{n}\sum_{i=1}^{n} \left| y_{\text{modeled}}^{(i)} - y_{\text{measured}}^{(i)} \right|}{\frac{1}{n}\sum_{i=1}^{n} \left| y_{\text{eroded}}^{(i)} \right|} \times 100 \tag{11}$$

where n = the number of cells alongshore; $y_{\text{modeled}}^{(i)}$ = the modeled shoreline position of cell i; $y_{\text{measured}}^{(i)}$ = the measured shoreline position of cell i; and $y_{\text{eroded}}^{(i)}$ = the distance between the measured initial and final shorelines, respectively, in cell i.

Model Calibration and Validation

The measured shorelines from 1910 and 1965 were used to calibrate the model. The parameter values during calibration were optimized based on error minimization (Figure 13). The calibration parameters obtained are $\alpha = 0.7$, $K_1 = 0.89$, and $K_2 = 0.50$. The maximum absolute error and average relative error for the calibration period are 133.7 m and 9.0%, respectively (Table 3).

Employing the above calibration parameters, the model was validated from 1965 to 2000 using the 1965 measured shoreline as the initial shoreline. For the period from 1995 to 2000, two sea dike segments reinforced by stones and mortar that were constructed in 1995 were represented using a seawall boundary condition (Figure 14). Maximum absolute error and average relative error for the validation period are 123.4 m and 9.1%, respectively (Table 3). The difference in the maximum rate of shoreline retreat between the calibration and validation periods is negligible, with values of 12.1 m/y and 12.7 m/y, respectively. However, the average rate of shoreline retreat shows a greater difference, with 8.7 m/y for the calibration period and 6.8 m/y for the validation period (Table 3).

Modeled Sediment Budget

The calculated values for the components in the sediment budget show that the total amount of sediment from sources is $Q_{\text{source}} = Q_{\text{south}}^{\text{l}} + Q_{\text{north}}^{n} = 203 \times 10^3$ m^3/y, and the total amount of sediment from sinks is $Q_{\text{sink}} = Q_{\text{north}}^{\text{l}} + Q_{\text{south}}^{n} + Q_{\text{off}} = 1043 \times 10^3$ m^3/y, where fine sediment lost offshore is 767×10^3 m^3/y (70% of total sink volume). Thus, the annual sediment volume lost from the area is $Q_{\text{lost}} = Q_{\text{sink}} - Q_{\text{source}} = 840 \times 10^3$ m^3/y.

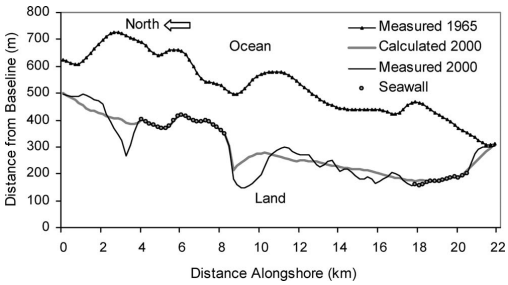

Figure 14. Measured and modeled shorelines from the period 1965 to 2000.

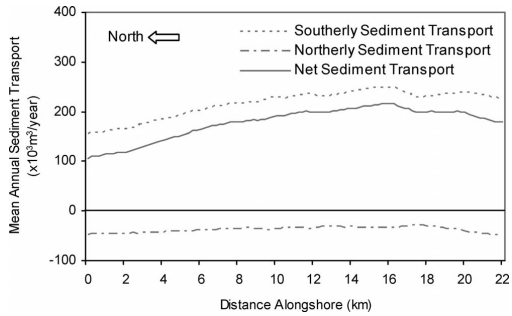

Figure 15. Spatial distribution of annual longshore sediment transport rates.

There is a large difference in the LST rates between the southward and northward directions. Overall, the southerly directed sediment transport rate is around 150×10^3 to 250×10^3 m^3/y, whereas the northerly sediment transport rate is only about 30×10^3 to 50×10^3 m^3/y, constituting about 15% of the gross sediment transport rate. The result is a significant net sediment transport rate in the southward direction with values in the range of 100×10^3 to 200×10^3 m^3/y (Figure 15). It should be stressed that the curves in Figure 15 and the block arrows in Figure 11 represent averages and that the net local transport gradients in space that determine the offshore sediment transport are not shown. As previously discussed, the offshore losses are proportional to the transport gradient during erosive conditions and without such gradients there will be no offshore losses.

DISCUSSION

This model does not simulate the fine details of the shoreline shape; however, the general trend and magnitude of shoreline change are well reproduced during both the calibration and the validation periods, including the influence of the seawalls through the boundary conditions (Figures 13 and 14). Average relative errors for the calibration and validation periods are 9.0% and 9.1%, respectively, and maximum absolute errors are 133.7 m and 123.4 m, respectively (Table 3). Annual shoreline retreat rates estimated from the measured shorelines decreased from 8.7 m during the calibration period to 6.8 m during the validation period. This shows that the average erosion rate at Hai Hau Beach has been slowing down during recent decades.

As mentioned above, the sea dike system in Hai Hau District was constructed purely of soil, and then, before 2000, only some segments were reinforced with stones and mortar. Even though these sea dike segments may fail during heavy storm or typhoon attacks, in the present model they were treated as seawalls because they survived during the simulating period. However, these seawalls were subsequently completely destroyed by heavy typhoon attacks in 2005. Based on a report on the state of the sea dikes in Hai Hau District (Lam *et al.,* 2005), there were two reinforced sea dike segments that were described with the seawall boundary condition during the validation period. The first one belongs to Hai Loc Commune in the northern part of the area and faces attacks from the sea resulting in higher erosion intensity at the two ends of the seawall. The second one belongs to Hai Hoa Commune in the southern part; it does not face the sea, and therefore no effects have been observed. Due to the net sediment transport in the southward direction, higher intensity of erosion takes place at the south end of the northern reinforced sea dike.

Because of the different wind energy supply between winter and summer, offshore wave energy in the winter (coming from the north) is much greater than that in the summer (coming from the south). Estimates of the offshore wave energy from the wave hindcast show that in winter (from November to March) about 52.2% of the total offshore wave energy is supplied, while in summer (from May to September) only 29.3% is supplied. On the other hand, since the shoreline of Hai Hau Beach runs in the NE-SW direction (about 40° with respect to the N direction), incoming wave angles from N to ESE, generating the LST in the southward direction, encompass about 81% of the total offshore wave energy. Incoming wave angles from SE to SW, generating the LST in the northward direction, encompass only about 17% of the total offshore wave energy (Table 4). Thus, the southward sediment transport, encompassing about 85% of the gross transport, is much higher than the northward sediment transport, making up only about 15% of the gross transport (Figure 15); this results in a large net sediment transport to the south. In addition, gradients in the LST rates to the south (in winter) are higher than in the transport to the north (in summer), and therefore there is a large amount of fine sediment being transported into deep water during the winter (Figure 11). This implies that the serious erosion at Hai Hau Beach mainly occurs during the winter period.

According to previous studies, river outflow and riverine sediment from the Red River seldom reach the Hai Hau coastline (Do *et al.,* 2007; Pruszak *et al.,* 2002; Van Maren, 2004). The sediment from the Red River is mainly deposited within a 10-km area around the river mouth (Van Maren, 2004), and the remaining finer sediment is transported to

Table 4. *Distribution of offshore wave energy estimated from the wave hindcast.*

Direction	N	NNE	NE	ENE	E	ESE	SE	SSE	S	SSW	SW	WSW	W	WNW	NW	NNW
% energy	4.5	26.7	42.1	2.4	3.6	1.3	3.1	5.8	2.7	0.4	5.0	0.2	0.4	0.2	0.8	0.9

deeper water. This implies that the coastline of Hai Hau Beach is only supplied with sediment from the Red River to a limited degree. The limited sediment supply is expected to contribute to the sediment deficit and associated erosion along the Hai Hau coastline. In this study, the considered domain was expanded over the Ba Lat Mouth when running the wave propagation model to examine the effects of the river mouth and its protruding topography. The results of the wave simulations show that the headland of the Ba Lat Estuary produces significant diffractive and refractive effects on the waves approaching from the north, resulting in an alongshore variation of wave heights and angles in the nearshore zone of Hai Hau Beach. Wave height and angle along the 7-m depth contour increase from the Ha Lan Estuary (north) to the Lach Giang Estuary (south). Thus, when waves come from the northern sector, a corresponding increase appears of about 0.2–0.4 m in height and 10–15° in angle (Figure 16). Consequently, a gradient occurs in the LST when waves are coming from these directions. Thus, the Ba Lat Estuary does not only provide limited sediment for Hai Hau Beach, but it also produces gradients in the LST, causing the serious erosion at the Hai Hau coastline.

Several previous studies pointed out the existing high sediment transport alongshore and cross-shore. Pruszak *et al.* (2002) stated that the material originating from the Red River system is very mobile. About 70% of the mainly clayey material being discharged remains suspended, passes the intertidal plain, and goes offshore to deepwater areas (depths of 2 m to 30 m). The severe beach erosion suggests that relatively high sediment movement (longshore and cross-shore transport) should exist. Donnelly *et al.* (2004), by comparing the equilibrium beach profile behind the dikes and in the surf zone based on samples taken at Hai Hau Beach, found that 60–70% of the material mobilized by gradients in LST was transported to deep water. Do *et al.* (2007), using the method by McLaren and Bowles (1985) to analyze and relate grain-size trends with the net transport paths, showed that the dominant transport direction is perpendicular to the depth contours to a depth of about 25 m. Sediments are transported alongshore in a southwestward direction in coastal waters shallower than 5 m. Again, in this study, calculated results of LST and shoreline change show that fine sediment lost in the offshore direction represents a large ratio (about 60%) of the total sediment transport. Annual sediment transport in the southward, northward, and offshore directions is on the average about 220×10^3 m^3/y, 40×10^3 m^3/y, and 750×10^3 m^3/y, respectively. The net sediment transport is in the southward direction, being on the average 180×10^3 m^3/y.

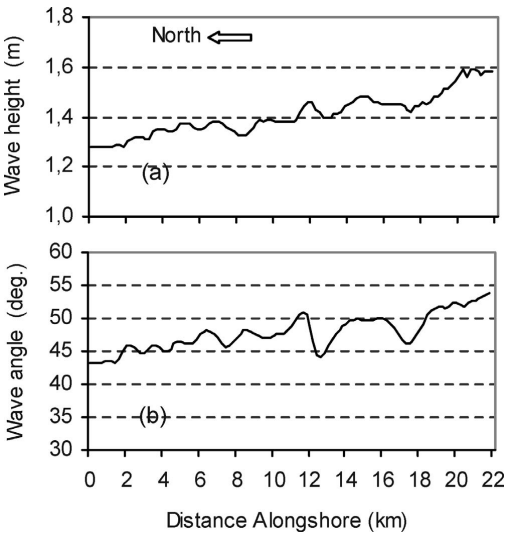

Figure 16. Distribution of wave height and angle along the 7-m depth contour for waves coming from the NE, H_s = 3.3 m, and T_p = 6 s. (a) Wave height, (b) wave angle.

CONCLUSIONS

(1) The shoreline change model successfully simulated the shoreline evolution at Hai Hau Beach, including the dike-seawall boundary condition, offshore sediment losses, and the complex morphology around the Ba Lat Mouth. The overall magnitude and trend of the simulated shoreline evolution was in good agreement with the measurements, both for the calibration and validation period. The calculated results used to establish a sediment budget showed that the net sediment transport is in the southward direction and that a large amount of fine sediment is transported offshore into deep water.

(2) Gradients in the LST and fine sediment lost into deep water are the major causes of the severe erosion at Hai Hau Beach. Gradients in the LST are generated by diffractive and refractive effects of the headland of the Ba Lat Estuary on the waves coming from the north; thus, the erosion rate of the Hai Hau shoreline is believed to have a strong relationship with the deposition rate at the Ba Lat Estuary.

(3) Incoming wave energy in the winter is much higher than in summer, resulting in a net sediment transport in the southward direction. Gradients in the LST rate are significant when the waves are coming from the north. Thus, the severe erosion at Hai Hau Beach occurs mainly in winter.

ACKNOWLEDGMENTS

The authors are grateful to Prof. Zbigniew Pruszak, Dr. Rafal Ostrowski, Dr. Grzegorz Rozynski, Dr. Shigeru Kato, Prof. Do Ngoc Quynh, Prof. Tran Gia Lich, Dr. Nguyen Thi Viet Lien, Dr. Dinh Van Manh, and Dr. Phan Ngoc Vinh for general discussions and comments on the paper; to Dr. Bas Van Maren for providing reprints of his papers; to Prof. Guohong Fang for providing tidal data; and to MS Nguyen Van Moi and MS Nguyen Thi Kim Nga for providing wind, wave, and shoreline data. This study was financed by a grant from SIDA.

LITERATURE CITED

Bijker, E.W., 1971. Longshore transport computations. *Journal of Waterways,* 97(4), 687–701.

Dean, R.G., 1977. Equilibrium Beach Profiles: U.S. Atlantic and Gulf Coasts. Newark, Delaware: University of Delaware, Department of Civil Engineering, Ocean Engineering Report No. 12, 45p.

Do, M.D.; Mai, T.N.; Chu, V.N.; Tran, N.; Dao, M.T.; Van Weering, Tj., C.E., and Van Den Bergh, G.D., 2007. Sediment distribution and transport at the nearshore zone of the Red River delta, Northern Vietnam. *Journal of Asian Earth Sciences,* 29(4), 558–565.

Donnelly, C.; Hung, N.M.; Larson, M., and Hanson, H., 2004. One-line modelling of complex beach conditions: an application to coastal erosion at Hai Hau beach in the Red River Delta, Vietnam. *In: Proceedings of the 29th Conference of Coastal Engineering* (Lisbon, Portugal), pp. 2449–2461.

Guohong, F.; Yue-Kuen, K.; Kejun, Y., and Yaohua, Z., 1999. Numerical simulation of principal tidal constituents in the South China Sea, Gulf of Tonkin and Gulf of Thailand. *Continental Shelf Research Journal,* 19(7), 845–869.

Hanson, H., 1987. GENESIS: A Generalized Shoreline Change Numerical Model for Engineering Use. Lund, Sweden: Lund University, PhD dissertation, 206p.

Hanson, H., 1989. GENESIS—A generalized shoreline change numerical model. *Journal of Coastal Research,* 5(1), 1–27.

Hanson, H. and Kraus, N.C., 1989. GENESIS: Generalized Model for Simulating Shoreline Change, Report 1, Technical Reference. Washington: Department of the Army, U.S. Army Corps of Engineers, 185p.

Häglund, M. and Svensson, P., 2002. Coastal Erosion at Hai Hau Beach in Red River Delta, Vietnam. Lund, Sweden: Lund University, Master's thesis, 80p.

Huan, N.N., 1996. Vietnam Coastal Zone Vulnerability Assessment. Hanoi, Vietnam: Center for Consultancy and Technical Support of Meteorology, Hydrology and Environment, Report of Vietnam VA Project, 5p.

Hung, N.M.; Hanson, H., and Dien, D.C., 2006. Simulation of shoreline evolution at Hai Hau beach, Red River Delta with the GENESIS model. *In: Proceedings of the First Scientific Workshop on "Coastline Evolution"* (Thinh Long, Vietnam), pp. 97–107.

Hung, N.M.; Moi, N.V.; Them, N.Q.; Dat, N.T.; Donnelly, C., and Grahn, L., 2006. Field measurements on nearshore processes in the Red River Delta coastal zone. *In: Proceedings of the First Scientific Workshop on "Coastline Evolution"* (Thinh Long, Vietnam), pp. 29–42.

Lam, N.X.; Ha, L.T.; Bon, T.V., and Phan, N.V., 2005. Report of the Current State of the Sea Dikes in Hai Hau District. Nam Dinh, Vietnam: Department of Natural Resources and Environment, Technical Report of CCP-2005 Project, 65p.

Mase, H., 2001. Multi-directional random wave transformation model based on energy balance equation. *Coastal Engineering Journal,* 43(4), 317–337.

McLaren, P. and Bowles, D., 1985. The effects of sediment transport on grain-size distributions. *Journal of Sedimentary Petrology,* 55(4), 457–470.

Ninh, P.V.; Quynh, D.N., and Viet Lien, N.T., 2001. The Scientific Foundation and Technical Parameters in the Coastal Zone of Vietnam for Nearshore Designed Constructions. Hanoi, Vietnam: Institute of Mechanics, NCST, Final Report of the National Marine Project, 99p.

Pruszak, Z., 1998. Coastal Processes in the Red River Delta with Emphasis on Erosion Problems. Gdansk, Poland: Institute of Hydroengineering, Polish Academy of Science, Internal Report, 18p.

Pruszak, Z.; Szmytkiewicz, M.; Hung, N.M., and Ninh, P.V., 2002. Coastal processes in the Red River Delta area, Vietnam. *Coastal Engineering Journal,* 44(2), 97–126.

Quynh Le, T.P.; Garnier, J.; Gilles, B.; Sylvain, T., and Minh, C.V., 2007. The changing flow regime and sediment load of the Red River, Viet Nam. *Journal of Hydrology,* 334(2), 199–214.

Saito, Y., 2001. Deltas in Southeast and East Asia: their evolution and current problems. *In: Proceedings of APN/SURVAS/LOICZ Joint Conference on Coastal Impacts of Climate Change and Adaptation in the Asia-Pacific Region, APN* (Kobe, Japan), pp. 185–191.

Sjödahl, M. and Kalantari, Z., 2005. Nearshore Hydrodynamics at Hai Hau Beach, Vietnam: Field Measurements and Wave Modeling. Lund, Sweden: Lund University, Master's thesis, 83p.

Smith, J.M.; Sherlock, A.R., and Resio, D.T., 2001. *STWAVE: Steady-State Spectral Wave Model, User's Guide for STWAVE Version 3.0.* Vicksburg, Mississippi: U.S. Army Corps of Engineers, 66p.

Sundstrom, A. and Sodervall, E., 2004. The Impact of Typhoon on the Vietnamese Coastline—A Case Study of Hai Hau and Ly Hoa Beach. Lund, Sweden: Lund University, Master's thesis, 70p.

Thanh, T.D.; Saito, Y.; Dinh, V.H.; Nguyen, H.C., and Do, D.C., 2005. Coastal erosion in Red River Delta: current status and response. *In: Proceedings of an International Conference on Geological Evolution and Human Impact* (Beijing, China), pp. 98–106.

USACE (U.S. Army Corps of Engineers), 1984. *Shore Protection Manual (SPM).* Washington: U.S. Government Printing Office, 1088p.

USACE, 2002. *Coastal Engineering Manual (CEM), Part II, Chapter 2.* Washington: U.S. Government Printing Office, 77p.

Van Maren, D.S., 2004. Morphodynamics of a Cyclic Prograding Delta: The Red River, Vietnam. Utrecht, the Netherlands: Utrecht University, PhD dissertation, 167p.

Van Maren, D.S. and Hoekstra, P., 2004. Seasonal variation of hydrodynamics and sediment dynamics in a shallow subtropical estuary: the Ba Lat River, Vietnam. *Estuary, Coastal and Shelf Sciences,* 60(3), 529–540.

Mouth, T.T.; Kant, G.; Huan, N.N., and Pruszak, Z., 1996. Sea dike erosion and coastal retreat at Nam Ha province, Vietnam. *In: Proceedings of the 25th Conference of Coastal Engineering* (Orlando, Florida, ASCE), pp. 2820–2828.

Wijdeven, B., 2002. Coastal Erosion on a Densely Populated Delta Coast, the Interactions between Man and Nature: A Case Study of Nam Dinh Province, Red River Delta, Vietnam. Delft, the Netherlands: Delft University of Technology, Master's thesis, 163p.

Paper VI

Modeling regional sediment transport and shoreline response in the vicinity of tidal inlets on the Long Island coast, United States

Hoan, L.X., Hanson, H., Larson, M., Nam, P.T., 2010.

Submitted to: *Coastal Engineering* (under review).

Modeling regional sediment transport and shoreline response in the vicinity of tidal inlets on the Long Island coast, United States

Le Xuan Hoan[a,b], Hans Hanson[a], Magnus Larson[a], Pham Thanh Nam[a,b]

[a] *Water Resources Engineering, Lund University, Box 118, 22100 Lund, Sweden.*
[b] *Institute of Mechanics, Vietnamese Academy of Science and Technology, 264 Doi Can, Hanoi, Vietnam.*

Abstract

A new numerical model was developed to simulate regional sediment transport and shoreline response in the vicinity of tidal inlets based on the one-line theory combined with the reservoir concept for volumetric evolution of inlet shoals. Sand bypassing onshore and sheltering effects on wave action from the inlet bar and shoals were taken into account. The model was applied to unique field data from the south coast of Long Island, United States, including inlet opening and closure. The simulation area extended from Montauk Point to Fire Island inlet, including Shinnecock and Moriches Inlets (Fig. 1). A 20-year time series of hindcast wave data at three stations along the coast were used as input data to the model. The capacity of the inlet shoals and bars to store sand was estimated based on measured cross-sectional areas of the inlets as well as from comprehensive surveys of the inlet area. Several types of sediment sources and sinks were represented, including beach fills, groin systems, jetty blocking, inlet bypassing, and flood shoal and ebb shoal feeding. The model simulations were validated against annual net longshore transport rates reported in the literature, measured shorelines, and recorded sediment volumes in the flood and ebb shoal complexes. Overall, the model simulations were in good agreement with the measured data.

Keywords: *Numerical modeling, sediment transport, shoreline response, tidal inlet, inlet shoal.*

1. Introduction

Morphology change and shoreline response in the vicinity of tidal inlets are controlled by both dynamic and static factors. Dynamic factors include net longshore transport rate, tidal prism, and wave regime, whereas properties of structures, angle of ebb jet related to the local shoreline, general offshore and nearshore bathymetry, size and shape of the back bay, sediment grain size, and artificial beach fills are static factors (Carr and Kraus, 2001). The dynamic factors can play a role in regional coastal processes, whereas the static factors often act at the scale of the local processes. Engineering activities around tidal inlets, such as creation and maintenance of navigation channels, require comprehensive knowledge of regional and local processes as well as the interactions between them. Regional sediment transport and shoreline evolution models that include local processes at tidal inlets are to a large degree lacking at present.

Kraus (2000, 2002) introduced a mathematical aggregate model of volume change and sand bypassing at tidal inlets, based on a reservoir analogy approach. In this model, the ebb shoal, bypassing bar, and attachment bar were included, but the flood shoal and main channel were neglected. Larson *et al.* (2002a) introduced a numerical model to simulate sediment transport and coastal evolution at regional scale, named Cascade. This model can simultaneously simulate different spatial and temporal processes at scales from regional to local. Regional sediment transport and shoreline change extending hundreds of kilometers and covering several inlets were represented. The model also includes inlet phenomena such as inlet creation, ebb shoal development, and bypassing bars between beaches and inlets. Larson *et al.* (2006) further developed the inlet reservoir model to include flood shoal development, based on the model introduced by Kraus (2002). This model was then included in Cascade after which the sediment transport and shoreline response in the vicinity of Shinnecock Inlet and Moriches Inlet on the south coast of Long Island, United States, were simulated. However, in these simulations the shoreline change downdrift the inlets were not well reproduced. The reasons for this discrepancy between calculations and measurements are attributed to sand moving onshore from the attachment bars, as well as the sheltering effects on wave action from the inlet shoals and bars. These processes have not been included in any previous model. Thus, in order to develop a general model for regional coastal evolution with regard to the effects of inlets, sand bypassing onshore from the attachment bars and the sheltering effects of the inlet morphological elements on the downdrift shoreline were described in the present model.

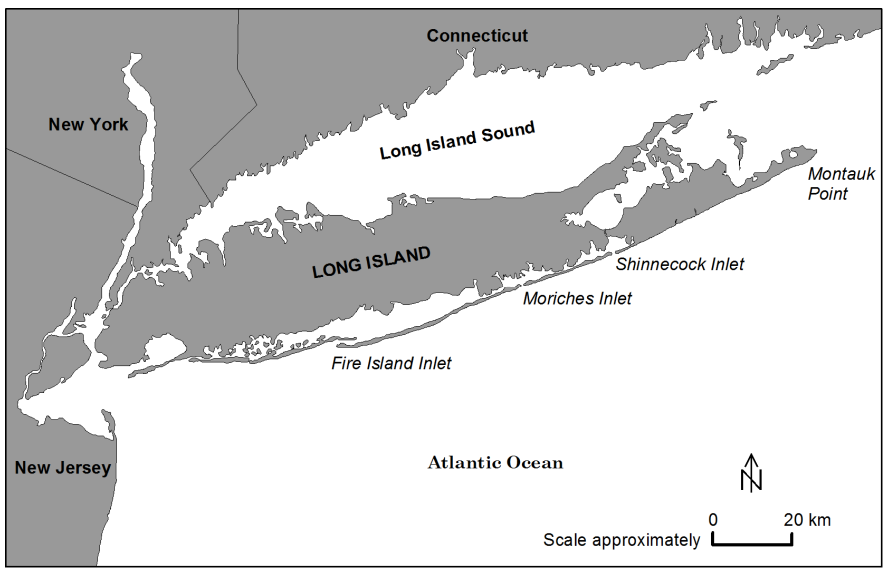

Fig. 1. Study site and locations of the inlets on the south Long Island coast, New York.

In this study, a new numerical model of regional sediment transport and shoreline change, combined with the inlet reservoir model, is introduced. The shoreline change model was based on one-line theory following basic formulations and algorithms developed by Hanson (1987). The predictive formula for longshore transport rate as modified by Larson *et al.* (2002a) to include shoreline characteristics at the regional scale was employed. Measured data by Gaudiano and Kana (2001) were used to model the onshore movement of a portion of the attachment bar volumes. Sheltering effects on the wave action from the inlet shoals and bars were represented by an attenuation coefficient affecting the breaking wave height in the sheltered area. Distances from the centerline of the inlets to the attachment bars were calculated using the empirical formulas introduced by Carr and Kraus (2001). The model was employed to simulate the coastal evolution of the Long Island coast covering the inlets at Shinnecock and Moriches. Measured shorelines in 1983, net longshore transport rates estimated by Rosati *et al.* (1999), and measured volumes of the flood and ebb shoal complexes (the ebb shoal complex includes ebb shoal, bypassing bar, and attachment bar) were used to validate the model.

2. Methodology

The model development focused on simulating regional sediment transport and local shoreline response in vicinities of the tidal inlet as well as development of the tidal shoal volumes. Regional sediment transport and shoreline evolution was simulated based on the shoreline change model developed by Hanson (1987). The inlet reservoir model based on a reservoir analogy approach developed by Kraus (2000, 2002) was employed. For this model, relationships between tidal morphological units and pathway of sand bypassing must be specified. The basics of the model components are described below with some of the components were developed as a part of this study, whereas other components were based on previous work.

2.1 Shoreline change model

The shoreline change modeling is based on the one-line theory (Pelnard-Considere, 1956), employing algorithms for the numerical solution developed by Hanson (1987). Conservation of sediment volume yields the fundamental equation to be solved for obtaining the shoreline change. Employing a local coordinate system, where the *y*-axis points offshore and the *x*-axis is oriented parallel to the trend of the shoreline, this equation is expressed as,

$$\frac{\partial y}{\partial t} + \frac{1}{(D_B + D_C)}\left[\frac{\partial Q}{\partial x} + q\right] = 0 \tag{1}$$

where: x = longshore coordinate; y = cross-shore shoreline position; t = time; D_B = average berm elevation; D_C = depth of closure; Q = longshore sand transport rate; q = source or sink of sand.

The empirical predictive formula for the total longshore sand transport developed by Hanson *et al.* (2006) was used,

$$Q = \frac{\varepsilon}{8(\rho_s/\rho - 1)(1-p)w_s} H_b^2 C_{gb} \cos\alpha_0 \left[K_1 \left(a_1 \sin\alpha_0 + \overline{V_{ex}} \right) - K_2 a_2 \right] \tag{2}$$

in which, $a_1 = \frac{5}{32}\frac{\pi\chi}{C_f}\sqrt{g}A^{\frac{3}{2}}$; $a_2 = \frac{\pi}{C_f\chi^2}\sqrt{gd_b}\frac{\partial H_b}{\partial x}$ and $A = 2.25\left(\frac{w_s^2}{g}\right)^{\frac{1}{3}}$

where: H = wave height; d = water depth; C_g = wave group celerity; b = subscript denoting breaking wave condition; K_1, K_2 = empirical coefficients (treated as calibration parameters); ρ_s = density of sand; ρ = density of water; p = porosity of sand on the bed; w_s = fall velocity; $\overline{V_{ex}}$ = external surf-zone average longshore current velocity generated by tide or/and wind; A = shape parameter; χ = breaker index; g = acceleration due to gravity; C_f = bottom friction coefficient; ε = transport coefficient expressing efficiency of the waves keeping sand grains in suspension, which can be estimated through physical parameters as (Bayram *et al.*, 2007), $\varepsilon = \left(4.0 + 9.0\frac{H_b}{w_s T_p}\right)\times 10^{-5}$; T_p = peak wave period; and α_0 = angle of breaking waves to the local shoreline orientation given by,

$$\alpha_0 = \alpha_b - \arctan\left(\partial y/\partial x\right) \tag{3}$$

The effect of a regional shoreline shape enters in Eq. (3) by assuming that the local shoreline evolves with respect to the regional shoreline (Larson *et al.*, 2002a), yielding a new expression for α_0,

$$\alpha_0 = \alpha_{br} + \alpha_b - \arctan\left(\partial y/\partial x\right) \tag{4}$$

where $\alpha_{br} = \arctan\left(\partial y_r/\partial x\right)$ and y_r denotes the regional shoreline, which is taken to be constant in time.

2.2 Tidal prism and equilibrium volume of ebb shoal complex

Jarret (1976) summarized the state of knowledge on the relationship between cross-sectional area and tidal prism for inlets in the United States. Separate relationships were developed for the Atlantic, Gulf, and Pacific Ocean coasts classified according to whether the inlets have two, one, or no jetties. The relationship for the Atlantic Ocean coast and inlets with two jetties is (Militello and Kraus, 2001),

$$A_c = 14.74\times 10^{-5} P^{0.95} \tag{5}$$

where A_c = minimum cross-sectional area of the entrance channel below mean sea level (in m^2), and P = spring tidal prism (in m^3).

Walton and Adams (1976) developed predictive empirical formulas for the equilibrium volume of an ebb tidal shoal depending on the tidal prism and the amount of wave exposure of the coasts classified into groups of highly exposed, moderately exposed, and mildly exposed coasts. The formula for moderately exposed coasts is most applicable to the inlets along the southern shore of Long Island (Millitello and Kraus, 2001), and thus it was used in this study,

$$V_E = 6.44 \times 10^{-3} \times P^{1.23} \tag{6}$$

where V_E = volume of ebb shoal complex at equilibrium (in m^3).

2.3 Inlet Reservoir Model

Larson *et al.* (2006) refined the inlet reservoir model by Kraus (2002) through the introduction of the flood shoal and associated coupling coefficients, which analytically describe the transfer of sediment between the morphological units. The inlet morphology is schematically divided into distinct morphology units including ebb shoal, bypassing bars, attachment bars, and flood shoal (Fig. 2). Each morphological unit is assumed to have a certain equilibrium volume for fixed hydrodynamic and sediment conditions.

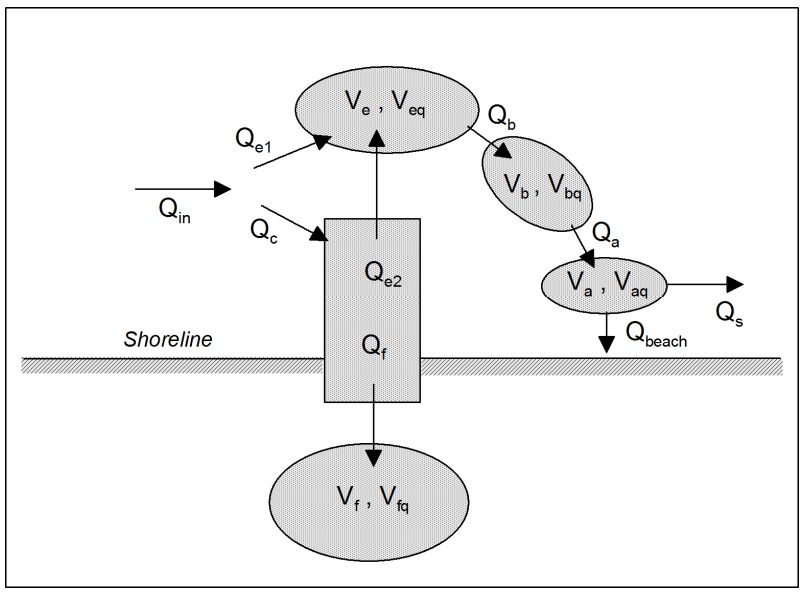

Fig. 2. Definition sketch for inlet morphological units with sediment transport occurring from the left-hand side (after Larson *et al.*, 2002a).

In order explain the inlet model employed in the present study, the simple case of sediment being transported from left-to-right is considered here, where Q_{in} is the incoming sediment transport rate around the jetty (if such a structure is present). The transport Q_{in} is split into one portion that goes to the ebb shoal, Q_{e1}, and one portion that goes into the channel, Q_c. Once in the channel, the sediment might be transported to the ebb shoal, Q_{e2} or to the flood shoal, Q_f. Sediment at a rate Q_b is leaving the ebb shoal and feeding the bypassing bar. The volume of the ebb and flood shoal at any given time is V_e and V_f, respectively, with the corresponding equilibrium values of V_{eq} and V_{fq}.

The mass conservation equation of sediment for the ebb shoal is,

$$\frac{dV_e}{dt} = Q_{e1} + Q_{e2} - Q_b \tag{7}$$

and for the flood shoal,

$$\frac{dV_f}{dt} = Q_f \tag{8}$$

Transport out of the ebb shoal is,

$$Q_b = \frac{V_e}{V_{eq}}\left(Q_{e1} + Q_{e2}\right) \tag{9}$$

Transport rates between elements are defined through the coupling coefficients,

$$Q_{e1} = \delta Q_{in} \;;\; Q_c = (1-\delta)Q_{in} \tag{10}$$

$$Q_{e2} = \beta\left(1-\delta\right)Q_{in} \;;\; Q_f = \left(1-\beta\right)\left(1-\delta\right)Q_{in} \tag{11}$$

where δ and β are coupling coefficients defined as follows (Larson *et al.*, 2006),

$$\delta = \frac{V_e + V_f}{V_{eq} + V_{fq}}\,,\; \beta = \frac{1 - V_e/V_{eq}}{2 - V_e/V_{eq} - V_f/V_{fq}} \tag{12}$$

Sediment at rate Q_a is leaving the bypassing bar and feeding the attachment bar. The volume of the bypassing and attachment bars at any given time is V_b and V_a, respectively, with the corresponding equilibrium values V_{bq} and V_{aq}.

The sediment volume conservation equation for the bypassing bar is,

$$\frac{dV_b}{dt} = Q_b - Q_a \tag{13}$$

whereas the transport from the bypassing bar is given by,

$$Q_a = \frac{V_b}{V_{bq}} Q_b \tag{14}$$

The transport out from the attachment bar and further along the shore, Q_s, is:

$$Q_s = \frac{V_a}{V_{aq}} Q_a \tag{15}$$

In the area of the bypassing and attachment bars, incident wave energy greatly exceeds ebb-directed tidal energy, allowing a portion of the ebb shoal to migrate towards the shore under accretionary wave conditions (Kana *et al.*, 1999; Rosati *et al.*, 1999; Gaudiano and Kana, 2001). Thus, shoal bypassing is a natural form of beach nourishment (Gaudiano and Kana, 2001). This process is believed to contribute partly in the generation of a salient-type feature commonly observed on beaches downdrift inlets. In order to describe the process of onshore sand transport from the attachment bar to the shoreline in the numerical model, a macroscopic approach is taken where it is assumed that a certain fraction of the transport supplying the attachment bar volume is transferred to the beach at each calculation time step. Thus, sediment moves at a rate Q_{beach} from the attachment bar to the shoreline, expressed through a fraction, γ, of the total net sand transport being supplied to the attachment bar at any given time,

$$Q_{beach} = \gamma\left(Q_a - Q_s\right) = \gamma Q_a \left(1 - \frac{V_a}{V_{aq}}\right) \tag{16}$$

The sediment volume conservation equation for the attachment bar is:

$$\frac{dV_a}{dt} = Q_a - Q_s - Q_{beach} = \left(1-\gamma\right)\left(Q_a - Q_s\right) \tag{17}$$

Larson *et al.* (2002a) introduced a nonlinear relationship for releasing sediment from the ebb shoals when the inlet cross-sectional area is decreasing or closes completely. Thus, the above equations, (9), (14), (15) and (16) were changed to a nonlinear form, that is, $Q_{out} = Q_{in}(V/V_q)^n$, where Q_{out} and Q_{in} are sediment transport rates going out and entering a morphological unit, respectively, V and V_q are the volumes at a given time and at equilibrium of the unit, and n is an empirical power. By specifying a value of $n < 1$ for situations where sediment is released back to the beach, the release will be slower than for the linear model. Larson *et al.* (2002a) suggested a value of n between 0.1 and 0.2 when the shoal experienced reduction in volume.

2.4 Distance to attachment bars

According to Hicks and Hume (1996) and Carr and Kraus (2001), the tidal prism is expected to control the size and location of the ebb shoal. Carr and Kraus (2001) developed an empirical relationship between tidal prism and the distance from the

centerline of the inlet to the downdrift and updrift attachment bars by examining 108 tidal inlets in the United States. The inlets were classified according to whether the inlets had two, one or no jetties. For inlets with two jetties, the empirical relationships governing distance to the attachment bar was found to be,

$$\text{for downdrift attachment bars: } Wd = 0.50 \times P^{0.451} \tag{18}$$

$$\text{for updrift attachment bars: } Wu = 0.16 \times P^{0.495} \tag{19}$$

where Wd and Wu = distance from centerline of the inlet to the downdrift and updrift attachment points where the ebb shoal complex attaches to the shoreline (in m), respectively.

The angle between the orientation of the ebb jet and the shoreline affects the size and shape of the delta (Hicks and Hume, 1996); thus, the above relationships could be modified for improved predictability by including the ebb jet angle. If the ebb jet is perpendicular to the local shoreline trend, the morphological asymmetry is mainly controlled by the magnitude and direction of net longshore transport, as well as wave refraction and diffraction over the bathymetry and ebb shoal. Thus, a straight channel is expected to promote morphological symmetry and a reduced distance to the downdrift attachment point (Carr and Kraus, 2001). However, if the ebb jet angle becomes more acute, the tidal and wave energy oppose each other less. An ebb jet flow more parallel to the wave crests implies that the waves can more efficiently return shoreward sand deposited from the ebb jet (Hicks and Hume, 1996), but at a location further downdrift. Thus, a more acute ebb jet angle is expected to promote more sand being transferred to the downdrift beach and a longer distance to the attachment bar. These effects are believed to act at Shinnecock Inlet as well as at Moriches Inlet (Carr and Kraus, 2001), where the ebb shoal is attached to the updrift shoreline close to the jetty with an extended distance to the downdrift attachment bar. Thus, Eqs. (18) and (19) were modified by including the angle between the ebb jet and the local shoreline, ψ, expressed as,

$$\text{for downdrift attachment bars: } Wd = 0.50 \times P^{0.451}(1 + \cos\psi) \tag{20}$$

$$\text{for updrift attachment bars: } Wu = 0.16 \times P^{0.495}(1 - \cos\psi) \tag{21}$$

For the case where the ebb jet is perpendicular to the shoreline, ψ takes on a value of 90 deg, implying no asymmetry due to ebb jet orientation.

2.5 Wave sheltering effects from attachment bar

Beach erosion typically occurs along the shoreline on both sides of the attachment bar, whereas accretion occurs in its lee (Dean and Walton, 1975; Williams and Kana, 1987; Gaudiano and Kana, 2001) (see Figs. 3 and 4). The sheltered area behind the bar is gradually filled in, and finally the shoal attaches to the shore resulting in alongshore spreading of the bar in both directions from the point of attachment (Gaudiano and Kana, 2001). Thus, there are two mechanisms that cause sediment to gradually feed sand to the area behind the bar. The first mechanism is the onshore bypassing process of sand from the attachment bar due to landward flow associated with the waves (Williams and Kana, 1987;

FitzGerald *et al.,* 2000). The second mechanism is due to the sheltering from the wave activity provided by the bar, which produces a zone of low energy in which alongshore currents can deposit transported material (Dean and Walton, 1975). The onshore bypassing process is described through the coefficient, γ, which represents the fraction of the transport supplied to the attachment bar build-up that is transferred to the shore (see Eq. (16)). The decrease in wave energy in the lee of the bar is expressed through a reduction in breaking wave height. In the numerical model, a calibration parameter for reduction of the breaking wave height in the lee of the bar was introduced. In principal, the value of this parameter depends on the size and shape of the bar, which are different on the downdrift and updrift sides of the inlet due to asymmetry in inlet morphology. The breaking wave height in the lee of the bar was multiplied by a spatially varying attenuation parameter, η, and thus, H_b in Eq. (2) was replaced with ηH_b, where $0 \le \eta \le 1$. The value of η is less than 1.0 behind the bars, and equals 1.0 outside the sheltered areas. In principal, η has a minimum value at the centre point of the sheltered area, and its value increases towards both sides of the bar. As a simplification for this study, the values of η within the sheltered areas were obtained by linearly interpolating between a minimum value at the centre point of the respective sheltered area and 1.0 in areas not sheltered by the bar. The minimum values inside the bars were determined through a calibration procedure.

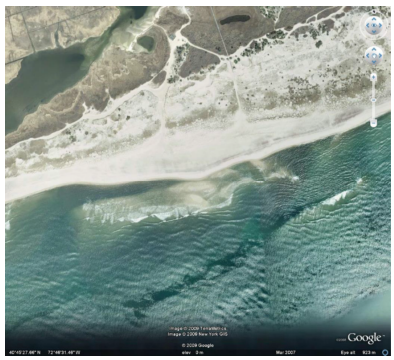

Fig. 3. Onshore migration of sediment from attachment bar at Moriches Inlet.

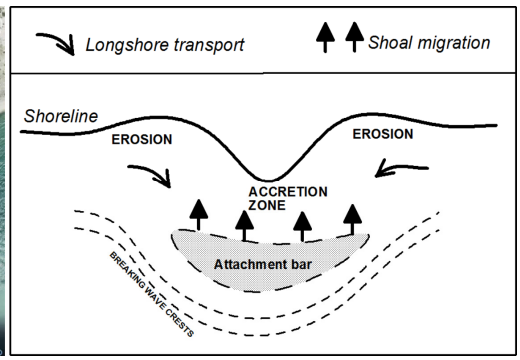

Fig. 4. Depiction of sand movement (after Kana *et al.*, 1985).

3. Study area and model setup

The Long Island coast, New York, was selected as a suitable location for validating the capability of the model to simulate regional sediment transport and development of tidal inlet shoal volumes. The study area extended from Fire Island Inlet to Montauk Point because the most available information originated from this coastal stretch (Larson *et al.*, 2002a). The stretch includes many coastal features and processes such as sediment transport and evolution at regional scale, the cross-sectional areas of the inlets varied

substantially with time including opening and closure of the inlets, substantial shoreline response in vicinities of the jettied inlets, large amount of beach fill volumes placed at several locations along the coast (Larson *et al.*, 2002a), and a system of groins constructed to protect the beach.

Two types of simulations were performed with the new numerical model for the study area: (1) simulating the overall annual net longshore transport and regional shoreline evolution; and (2) simulating shoreline response in vicinities of the inlets and the tidal inlet shoal development in connection with varying cross-sectional area of the inlets. The objectives of these simulations were to validate the capability of the model to simulate shoreline response in the vicinity of the inlets and tidal inlet shoal development at local scale in combination with longshore sediment transport and shoreline evolution at regional scale.

The Long Island shoreline has a length of about 135 km and it is oriented in a direction of about 67.5 deg northeast. A model coordinate system was defined with a similar orientation for the *x*-axis. The lateral boundary conditions for the modeling consisted of "no shoreline change" specified based on shoreline measurements covering a period from 1830 to 1995 (Larson *et al.*, 2002a). Suitable locations for such a boundary condition were identified approximately 10 km west of Montauk Point and 15 km east of Fire Island Inlet.

Hindcast wave data (a 20-years time series at an interval of 3 hours from 1976 to 1995) from three WIS Stations along the coast was used as input data for the modeling. The spatial step was set at 100 m, and the input wave parameters were linearly interpolated based on the three stations corresponding to this spatial interval. The time step was set at 3 hours, coinciding with the interval of measured wave data. Following Larson *et al.* (2002a), the depth of closure was chosen to 8 m and the representative median grain size 0.3 mm. The regional shoreline shape was determined from spatial filtering of the shoreline measured in 1870 when no inlets existed using a window length of 7 km (Larson *et al.,* 2002a).

Measurements of inlet cross-sectional areas at Shinnecock and Moriches Inlets were performed at several occasions between 1931 and 1998, which includes the closure and subsequent opening of Moriches Inlet in the 1950's. These data were used to calculate the equilibrium volumes of the ebb shoal complexes, from which the equilibrium volumes of the individual morphological units at the inlets could be estimated (Larson *et al.*, 2002a). Equilibrium volume of the flood shoals were set to 4.10^6 m^3 for both inlets (Larson *et al.*, 2006).

Several structures were included in the simulations. Jetty lengths on each side of the inlets and the time of construction were specified according to information from the literature. The lengths of the east and west jetties at Moriches Inlet are 258 m and 445 m, respectively, and the jetties were constructed in 1953 (Vogel and Kana, 1984). For Shinnecock Inlet, the lengths of the east and west jetties are 280 m and 450 m, respectively, with construction carried out in 1953 (Smith *et al.*, 1999). Changes in the jetty lengths were not modeled, but they were kept constant during the simulation time

after completion. The 15 groins comprising the Westhampton groin field were constructed in three phases, from March 1965 to October 1966, from 1969 to 1970, and in 1998 (Rosati *et al.*, 1999). These groins were included in the model at the proper times and the lengths and locations of the groins were specified based on available data.

Dredged material has typically been placed along adjacent beaches or within nearshore areas east and west of the inlets (Smith *et al.*, 1999). These beach fill volumes were included in the model as source terms in the sediment conservation equation that vary in time and space. A total volume of about 800,000 m^3 was placed west of Shinnecock Inlet between 1949 to 1983, and another 1,115,000 m^3 was put in this area between 1983 and 1995 (Larson *et al.*, 2002a). From 1955 to 1969, a total volume of about 661,000 m^3 was placed east of the inlet. Total quantities placed at Moriches Inlet between 1953 to 1996 were approximately 2.5 million cubic meters in which about 1.3 million cubic meters (52%) and 0.75 million cubic meters (30%) were placed to the east and west of the inlet, respectively (Smith *et al.*, 1999). Smaller beach fills have been placed at other locations, but they were neglected in the present modeling study.

In order to employ Eqs. (20) and (21), the angle between the ebb jet and the local shoreline must be specified. At Shinnecock Inlet, after completion of the jetties, the inlet opening rotated to conform to the jetty orientation which were in a north-south direction (Smith *et al.*, 1999), and at Moriches Inlet, the channel was oriented slightly east of north entering the inlet (Psuty *et al.*, 2005). The ebb jets are generally oriented parallel to the jetties. Based on satellite images, the angle between the ebb jet and local shoreline at Shinnecock and Moriches Inlet were set to 60 deg and 67 deg, respectively.

The equilibrium volumes, V_{eq}, V_{bq} and V_{aq}, of each morphology unit must be specified in Eqs. (7) to (17). Limited information exists on the equilibrium size of the individual morphological units described in the reservoir model. To simplify, the units are determined as being a constant fraction of the volume of the ebb shoal complex, which in turn is a function of inlet cross-sectional area (tidal prism). Militello and Kraus (2001) estimated sand bypassing to the attachment bar at a rate of about 19,000 m^3/yr for Shinnecock Inlet. The rate of ebb shoal growth, which is estimated to 117,000 m^3/yr (Williams *et al.*, 1998), implies that the ratio between the attachment bar and the ebb volume growth is 0.16. The ratio between bypassing bar and the ebb shoal volume is assumed to be 0.25 following Larson *et al.* (2002a). In the present study, the same ratios were employed for the both inlets.

To employ Eqs. (16) and (17), the fraction of the transport causing deposition on the attachment bar transferred to the shore at any given time must be specified. Gaudiano and Kana (2001) analyzed nine tidal inlets in South Carolina on the Atlantic Coast, which revealed that only a small fraction of the entire ebb shoal complex are transferred to the shore during bypassing events. The mean volume percentage is about 3.1. Taking into consideration the ratio between the attachment bar and the ebb shoal complex volume, the sand volume percentage transferred to the shore is about 20.0. Thus, the coefficient γ in the Eqs. (16) and (17) was set to 0.20.

The length of the attachment bars must be specified when modeling the alongshore distribution of the onshore sand transport from the attachment bar. This term could be expressed through the distances from inlet to the attachment bars, which is a function of the tidal prism. The assumption is made here that the length of the attachment bar corresponds to half the distance from the inlet to the attachment bar center.

4. Results and discussion

4.1. Shoreline evolution

The model was first run for the period 1933 to 1983 to compare with the measured shoreline in 1983. The simulated and measured shorelines, as well as the initial shoreline, are plotted in Fig. 5, in which Fig. 5a gives an overview and Fig. 5b and 5c the details at Shinnecock and Moriches Inlet, respectively. The shoreline plots provide a view "standing on shore" looking towards the ocean with Montauk Point on the left side and Fire Island Inlet on the right side. The transport coefficients were chosen based on the best fit between simulated and measured shorelines to be $K_1 = 0.15$ and $K_2 = 0.04$, respectively. The value of the transport coefficient was held constant for the entire study domain. The wave height attenuation coefficient was set to $\eta = 0.85$, implying that the breaking wave height at centre point of the lee of the attachment bars decreases 15% compared to the height outside the sheltered areas. This value was held constant during the entire simulation time, as well as for the downdrift and updrift bars. In general, η depends on the size and shape of the attachment bar, the incident wave energy relative to the tidal energy, and the wave refraction and diffraction around the bar. Ebb shoal volumes vary over time and differ between downdrift and updrift sides due to the morphological asymmetry of tidal inlet. However, for long-term simulation performed here, the attenuation coefficient is regarded as an average value.

The simulated shoreline is overall in good agreement with the measured shoreline, particularly on the updrift side of the jetties and in the downdrift area where the salient-type feature appears. However, at Shinnecock Inlet, on both sides of this feature, the shoreline retreat was overestimated by the model, and south of the downdrift attachment bar at Moriches Inlet, the simulated shoreline retreat was underestimated. The reason for this discrepancy may be due to several factors, at regional and local scale, that were not included in the model. Overwash by storm waves could produce shoreward displacement of the shoreline, which may have been the case west of Moriches Inlet. During storm surge, waves may overtop the island, and overwash of sediment occurs. This sediment is deposited on the back of the island and it is lost from the nearshore system or transported back at a low rate by wind (Larson *et al.*, 2002b). Large storm events have contributed to significant alteration of the Fire Island shoreline. These storms generally cause rapid beach erosion, dune displacement, and coastal flooding (Psuty *et al.*, 2005).

A local transport process, not described in the model, is a part of the transport system that is formed when sediment moves around the inlet, being bypassed through the shoals and bars (Kana *et al.*, 1999). In this system, a portion of the bypassing sand cycles back to the inlet (Williams and Kana, 1987; Kana *et al.*, 1999) due to flood tidal currents and wave

refraction around the ebb shoal. This process is expected to produce erosion in the area close to the jetties. In addition, there are a number of other factors expected to cause the difference between the modeled and measured shorelines that were not included the model, such as wind-blown sand, inlet channel dredging, and sea level rise.

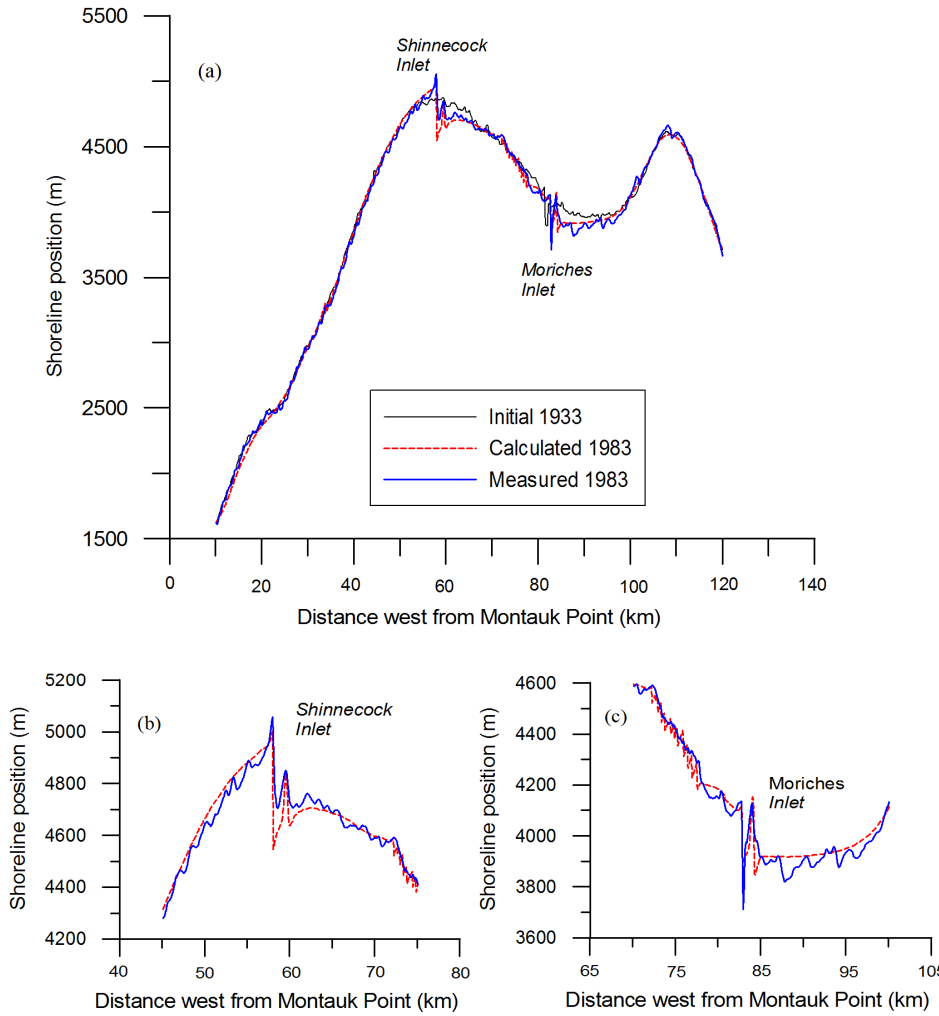

Fig. 5. Comparison between the measured and simulated shoreline in 1983 (a): Overview and detail from (b) Shinnecock Inlet and (c) Moriches Inlet.

4.2 Longshore transport rate

The simulated net transport rate together with the derived transport data reported by Rosati *et al.* (1999) is plotted in Fig. 6. The simulated annual net longshore transport rates were in good agreement with the analyzed data, except at Montauk Point where the rate was underestimated. The data from Rosati *et al.* (1999), for Montauk Point, included several important sinks and sources not described in the model, such as offshore losses due to sea level rise (76,000 m^3/yr), beach fill placement (from zero to 170,000 m^3/yr), and bluff erosion (from 33,000 to 203,000 m^3/yr). This will affect net transport rates and cause a difference between the modeled and analyzed results at Montauk Point.

The net annual longshore transport rate exhibits an increasing trend from Montauk Point to Fire Island Inlet. Since the tidal inlets act as sinks to the longshore transport as they evolve towards their equilibrium state, the net transport rate decreases significantly across the inlets. The average annual longshore net transport rate obtained in this study is 108,000 m^3/yr.

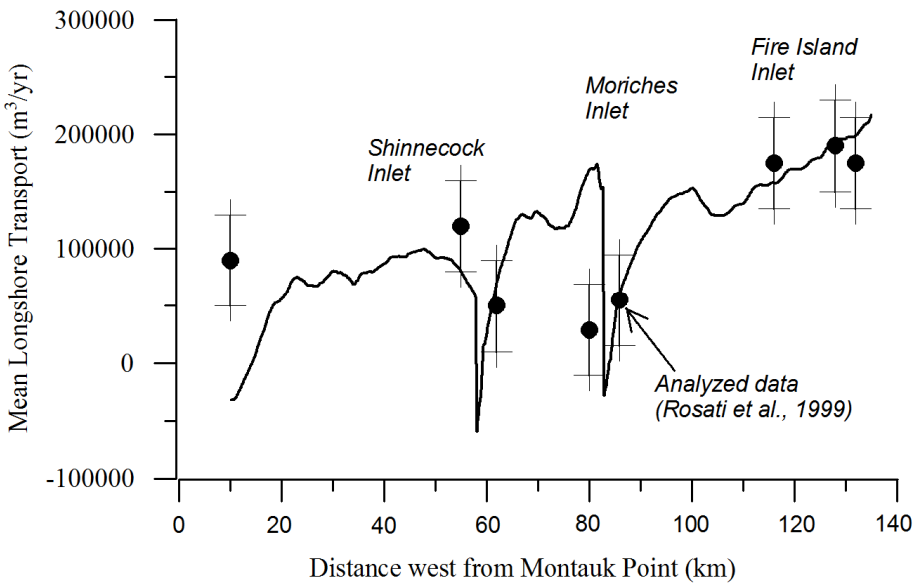

Fig. 6. Comparison between annual net transport rate and estimated data from measurements.

4.3 Flood and ebb shoal growth

The model was also run for the period 1933 to 2000 to compare with the measurements of ebb and flood shoal volume growth. Comparison between the calculated and measured ebb and flood shoal volumes are plotted in Figs. 7 and 8, respectively, where the total volume

of the ebb shoal complex is displayed. Overall, the calculated and measured data are in good agreement, although specific individual points show more discrepancy.

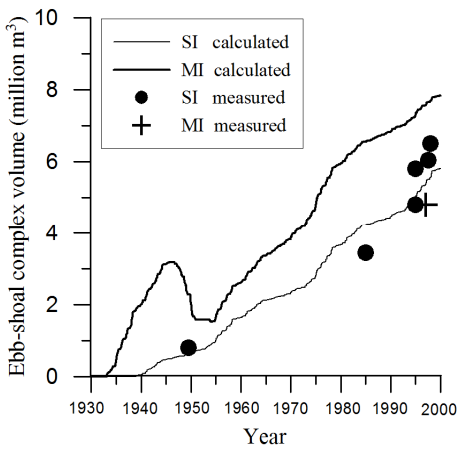

Fig. 7. Comparison between the measured and calculated volume of ebb-shoal complex (SI = Shinnecock Inlet, MI = Moriches Inlet).

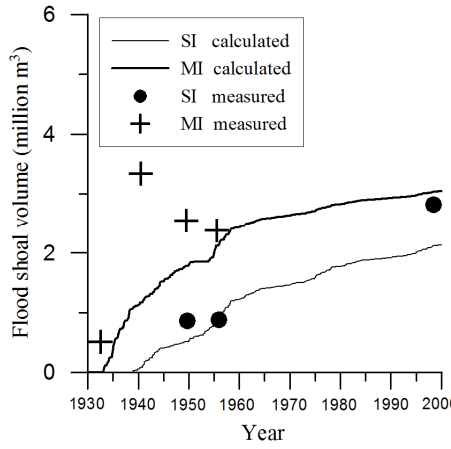

Fig. 8. Comparison between the measured and calculated volume of flood shoal (SI = Shinnecock Inlet, MI = Moriches Inlet).

5. Conclusions

A new numerical model of regional sediment transport and shoreline change combined with the inlet reservoir model was developed and successfully applied to simulate the evolution of the south shore of the Long Island coast, New York. The model was employed to simulate the period from 1933 to 2000, which included inlet opening and closure. The simulations covered a stretch of coastline from Montauk Point to Fire Island Inlet that includes two tidal inlets and other complex conditions involving a wide range of structures and activities such as jetties, groins, and beach fill. Model calculations were compared with measured shoreline evolution, annual net longshore transport rates reported in the previous literatures, and measured flood shoal and ebb shoal complex volumes. The simulated shoreline agreed well with the measured shoreline, including the accumulation updrift the inlets, the overall erosion downdrift the inlets, and the formation of salient-type features downdrift the inlets. The annual net longshore transport rates were overall in good agreement with the reported data, showing an increase in transport rate going west from Montauk Point. The growth of the flood and ebb shoal complexes at the inlets was also well predicted.

In order to realistically simulate the erosion and development of the salient-type feature downdrift the inlets, the predictive formula for the longshore transport rate was modified by introducing an attenuation coefficient for breaking wave height in the lee domain of the

attachment bars. Also, sand bypassing from the bar to the shore was included in the inlet reservoir model. This modeling approach was indirectly validated through the improved agreement between the simulated and measured shoreline change downdrift of the inlet, in comparison with the previous model by Larson *et al.* (2002a), which failed to capture the details of the shoreline response downdrift the inlets.

The empirical formulas for calculating the distance from centerline of an inlet to the attachment bars based on the tidal prism, developed by Carr and Kraus (2001), were modified by including the angle between ebb jet and the local shoreline trend. The average calculated distances from the inlet to updrift and downdrift attachment bars are, respectively, 252 m and 1150 m for Shinnecock Inlet, and 310 m and 1073 m for Moriches Inlet. These values are close to reported field data, implying that the updrift attachment bars are close to the jetties at both inlets, but the downdrift attachment bars extend to about 1200 m at Shinnecock Inlet (Williams *et al.*, 1998) and approximately 1100 m at Moriches Inlet (Psuty *et al.*, 2005). The calculated results show that the empirical formulas proposed, Eqs. (20) and (21), which include the angle between the ebb jet and the local shoreline, work reasonably well for the study site.

Application of the model to the Long Island coast shows the capability of the model to simulate regional sediment transport and shoreline evolution for complex conditions. Thus, a simulation domain may extend over hundreds of kilometers and cover several inlets including opening and/or closure, development of flood shoal and ebb shoal complexes, different shore protection measures, and shoreline response in the vicinity of inlets.

Acknowledgements

This work was partly funded by the Swedish International Development Cooperation Agency (Sida/SAREC) in the framework of the Project VS/RDE/03 “The evolution and sustainable management in the coastal areas of Vietnam” (LXH and PTN), and partly by Coastal Morphology Modeling and Management (Cascade) work unit, System-wide Water Resources Program conducted at the U.S. Army Engineer Research and Development Center (ML and HH). Support from Sida/SAREC project SWE-2007-123 is also appreciated.

References

Bayram, A., Larson, M., and Hanson, H. (2007). A new formula for the total longshore sediment transport rate. Coastal Engineering, 54, 700-710.

Carr, E.E., and Kraus, N.C. (2001). Morphologic Asymmetries at Entrances to Tidal Inlet. Coastal and Hydraulics Engineering technical Note IV-33, U.S. Army Engineer Research and Development Centre, Vicksburg, MS.

Dean, R.D., and Walton, T.L. (1975). Sediment transport processes in the vicinity of inlets with special reference to sand transport. Estuary Research, Volume II, Geology and Engineering, L.E. Cronin, ed., Academy Press, New York, 129-149.

FitzGerald, D.M., Kraus, N.C., and Hands, E.B. (2000). Natural Mechanisms of Sediment Bypassing at tidal Inlets. Coastal and Hydraulics Engineering Technical Note ERDC/CHL CHETN-IV-30, U.S. Army Engineering Research and Development Centre, Vicksburg, MS.

Gaudiano, D.J., and Kana T.W. (2001). Shoal bypassing in mixed energy inlets: Geomorphic variables and empirical predictions for nine south Carolina Inlets. Journal of Coastal Research, 17(2) 280-291.

Hanson, H. (1987). GENESIS: A generalized shoreline change numerical model for engineering use. Lund, Sweden: Department of Water Resources Engineering, Lund University, Ph.D. thesis, 206p.

Hanson, H., Larson, M., Kraus, N.C., and Gravens, M.B. (2006). Shoreline response to detached breakwaters and tidal current: Comparison of numerical and physical models. Proceeding of the 30th Coastal Engineering Conference, World Scientific, pp. 3357-3369.

Hicks, D.M., and Hume, T.M. (1996). Morphology and size of ebb tidal deltas at natural inlets on open-sea and pocked-bay coasts, North Island, New Zealand. Journal of Coastal Research, 12(1), 47-63.

Jarrett, J.T. (1976). Tidal prism – inlet area relationships. U.S. Army Engineer Waterways Experiment Station, Vickburg, MS, 60p.

Kana, T.W. (1995). A mesoscale sediment budge for Long Island, New York. Marine Geology, 126(1995) 87-110.

Kana, T.W., Hayter, E.J., and Work, P.A. (1999). Mesoscale sediment transport at southeastern U.S. tidal inlets: Conceptual model applicable to mixed energy settings. Journal of Coastal Research, 15(2), 303-313.

Kraus, N.C. (2000). Reservoir model of ebb-tidal shoal evolution and sand bypassing. Journal of Waterway, Port, Coastal, and Ocean Engineering, 126(3), 305-313.

Kraus, N.C. (2002). Reservoir model for calculating natural sand bypassing and change in volume of ebb-tidal shoals, part I: Description. Coastal and Hydraulics Engineering Technical Note ERDC/CHL CHETN-IV-39, U.S. Army Engineering Research and Development Centre, Vicksburg, MS.

Larson, M., Kraus, N.C., and Connell, K.L. (2006). Modeling sediment storage and transfer for simulating regional coastal evolution. Proceeding of the 30th Coastal Engineering Conference (California, USA), World Scientific, pp. 3924-3936.

Larson, M., Kraus, N.C., and Hanson, H. (2002a). Simulation of regional longshore sediment transport and coastal evolution- the Cascade model. Proceeding of the 28th Coastal Engineering Conference. World Scientific Press, 2002.

Larson, M.; Rosati, J.D. and Kraus, N.C. (2002b). Overview of regional coastal processes and controls. Coastal and Hydraulics Engineering Technical Note CHETN XIV-4, U.S. Army Engineer Research and Development Center, Vicksburg, MS.

Militello, A., and Kraus, N.C. (2001). Shinnecock Inlet, New York, site investigation, Report 4, Evaluation of flood and ebb shoal sediment source alternatives for the west of Shinnecock Interim Project, new York, Technical Report CHL-98-32, U.S. Army Corps of Engineers, Engineer Research and Development Centre, Vicksburg, MS.

Pelnard-Considere, R. (1956). Essai de theorie de l'evolution des forms de rivage en plage de sable et de galets. 4th Journees de l'Hydraulique, Les Energies de la mer, Question III, Rapport No. 1, pp. 289-298 (in French).

Psuty, N.P., Grace, M., and Pace, J.P. (2005). The coastal geomorphology of Fire Island, A portrait of continuity and change. Technical Report NPS/NER/NRTR-2005/021. U.S. Department of the Interior, National Park Service, Northeast Region, Boston, Massachusetts.

Rosati, J.D., Gravens, M.B., and Smith, W.G. (1999). Regional sediment budget for Fire Island to Montauk Point, New York, USA. Proceeding of Coastal Sediment Conference -1999. pp.803-817.

Smith, W.G., Watson, K., Rahoy, D., Rasmussen, C., and Headland, J.R. (1999). Historic geomorphology and dynamics of Fire Island, Moriches and Shinnecock Inlets, New York. Proceedings of Coastal Sediment'99, ASCE, 1597-1612.

Vogel, M.J., and Kana, T.W. (1984). Sedimentation patterns in a tidal inlet system, Moriches inlet, New York. Proceeding of the 19th Coastal Engineering Conference. World Scientific. pp. 3017-3033.

Walton, T.L., and Adams, W.D. (1976). Capacity of inlet outer bars to store sand. Proceeding of Coastal Engineering-1976, pp. 1919-1937

Williams, G.L., Morang, A., and Lillycrop, L. (1998). Shinnecock Inlet, New York, site investigation, Report 2, Evaluation of sand bypass options. Technical Report CHL-98-32, U.S. Army Corps of Engineers, Waterways Experiment Station, Vicksburg, MS.

Williams, M.L., and Kana, T.W. (1987). Inlet shoal attachment and erosion at Isle of Palms, South Carolina: A replay. Proceedings of Coastal Sediment'87, (Columbia, SC), 1174-1187.